OPTICAL FIBRE SENSORS FOR THE OPTIMIZATION OF PLASMA PROCESSING

A THESIS SUBMITTED IN ACCORDANCE
WITH THE REQUIREMENTS OF
THE UNIVERSITY OF LIVERPOOL
FOR THE DEGREE OF DOCTOR OF PHILOSOPHY
BY

IMAN IBRAHIM KHANDAKER
AUGUST 1993.

CONTENTS

ACKNOWLEDGEMENTS ii

ABSTRACT iii

CHAPTER 1 1

1.1 PROBLEMS WITH PLASMA PROCESSING 2
1.2 OPTICAL SENSORS AS A SOLUTION 4
1.3 PERFORMANCE OF THE OPTICAL SENSORS 5

CHAPTER 2 7

2.1 INTRODUCTION TO PLASMA PROCESSING 8
2.2 THE LIMITATIONS OF SOLVENT ETCHING 9
2.3 DRY ETCHING TECHNIQUES 12
2.3.1 INTRODUCTION 12
2.3.2 ETCHING MECHANISMS 12
2.3.3 REVIEW OF DRY ETCHING 15
2.4 PLASMA DIAGNOSTIC TECHNIQUES 18
2.4.1 INTRODUCTION 18
2.4.2 REVIEW OF PLASMA DIAGNOSTIC TECHNIQUES 19
2.5 MONITORING THE THICKNESS OF THIN FILMS 23
2.5.1 INTRODUCTION 23
2.5.2 ELECTRICAL FILM MONITORING TECHNIQUES 25
2.5.3 MECHANICAL FILM MONITORING TECHNIQUES 25
2.5.4 OPTICAL FILM MONITORING TECHNIQUES 26
2.5.5 LIMITATIONS OF OPTICAL FILM MONITORING 29
2.6 VACUUM PUMP MONITORING. 30
2.7 NOVEL OPTICAL SENSORS IN PROCESS CONTROL 31

CHAPTER 3 32

3.1 INTRODUCTION TO OPTICAL FIBRE SENSING 33
3.2 OPTICAL FIBRE SENSOR COMPONENTS 34
3.2.1 OPTICAL SOURCES 35
3.2.2 OPTICAL DETECTORS 39

3.2.3 OPTICAL FIBRES 42
3.3 OPTICAL MODULATION TECHNIQUES 45
3.3.1 INTENSITY MODULATION 46
3.3.2 POLARIZATION MODULATION 47
3.3.3 PHASE MODULATION 49
3.3.4 WAVELENGTH MODULATION 50
3.3.5 CHOICE OF MODULATION PRINCIPLE 51

CHAPTER 4 53
4.1 INTRODUCTION TO COLOUR 54
4.1.1 THE RGB COLOUR CUBE 54
4.1.2 THE Yxy COLOUR SYSTEM (CIE 1931) 55
4.1.3 THE L*a*b* COLOUR SYSTEM (CIE 1976) 58
4.2 CHROMATIC SENSING SYSTEMS 58
4.2.1 HUMAN COLOUR PERCEPTION 58
4.2.2 ARTIFICIAL COLOUR DETECTION 60
4.2.3 CHROMATIC RESPONSE TO WAVELENGTH SHIFTS 64
4.2.4 CHROMATIC RESPONSE TO SOURCE MIXING. 65
4.2.5 CHROMATIC RESPONSE TO MULTIPLE SOURCES. 68

CHAPTER 5 70
5.1 INTRODUCTION 71
5.2 OPTICAL DIAGNOSTICS 72
5.2.1 CHROMATIC PLASMA MONITOR 72
5.2.2 CHROMATIC FILM-THICKNESS MONITOR 77
5.2.3 CHROMATIC OIL MONITOR 86
5.3 PLASMA PROCESSING SYSTEMS 87
5.3.1 DC PLASMA NITRIDING SYSTEM 87

CHAPTER 6 93
6.1 INTRODUCTION 94
6.2 MONITORING DC NITRIDING PLASMAS 95
6.2.1 PERFORMANCE IN DC PLASMA MONITORING 96
6.2.2 DISCUSSION 100
6.2.3 CONCLUSION 102
6.3 MONITORING RF ETCHING PLASMAS 103
6.3.1 PERFORMANCE OF THE RF PLASMA MONITOR 104
6.3.2 DISCUSSION 109
6.3.3 CONCLUSION 113

6.4 MONITORING ETCHING ENDPOINTS........114
6.4.1 MONITORING ETCH ENDPOINTS........115
6.4.2 DISCUSSION........119

CHAPTER 7........122
7.1 THIN FILM MONITORING........123
7.1.1 COMMERCIAL THIN FILM MONITORING........123
7.2 THE INITIAL THIN-FILM SENSOR........125
7.2.1. PERFORMANCE OF FILM THICKNESS SENSOR........127
7.2.2. DISCUSSION........128
7.3 ON-LINE MEASUREMENT OF SiO_2 DEPOSITION........130
7.3.1. PERFORMANCE OF ON-LINE THICKNESS SENSOR........131
7.3.2. DISCUSSION........133
7.4 ON-LINE MEASUREMENT OF Si_3N_4 ETCHING........135
7.4.1. PERFORMANCE OF ON-LINE THICKNESS SENSOR........136
7.4.2. DISCUSSION........139
7.5 THE LED BASED THIN-FILM MONITOR........141

CHAPTER 8........143
8.1 INTRODUCTION........144
8.2 SENSOR DESIGN........145
8.3 PERFORMANCE OF THE OIL SENSOR........148
8.3.1 SENSITIVITY TO OIL CONDITION........148
8.3.2 STABILITY OF OIL CHROMATICITY........152
8.3.3 REPEATABILITY OF OIL CHROMATICITY........154
8.3.4 LINEARITY OF OIL CHROMATICITY........156
8.4 DISCUSSION........158
8.4.1 DISCUSSION ON SENSOR SENSITIVITY........158
8.4.2 DISCUSSION ON SENSOR LINEARITY........159
8.5 CONCLUSIONS........161

CHAPTER 9........163
9.1 PERFORMANCE OF THE OPTICAL SENSORS........164
9.2 SUGGESTIONS FOR FUTURE WORK........168

REFERENCES........171

APPENDIX........177

This thesis is dedicated to my parents,
for their enduring support.

........I apologise that this communication is so long, but I have not the ability to make it shorter.

Blaise Pascal 1657.

ACKNOWLEDGEMENTS

I wish to express my gratitude to Professor Gordon Jones for his constant encouragement and guidance and for the benefit of his experience throughout the course of this research. I am also indebted to Dr. Paul Russell for his advice and supervision over the period of this project.

Particular thanks are due to Dr. Euripedes Glavas and Mr. David Alston as this project could not have been completed without their technical expertise. The software and hardware skills of Mr. Jim Wilkinson, Mr. Robert Smith and Mr. Saad Ahmed were also much appreciated. In addition I would like to thank them and other colleagues including: Dr Philip Henderson, Dr Api Vourdas, Mr. Jamal Chaaroui, Mr. Jim Humphries, Mr. Neil Pilling, Mr. John Walker and Mr. Ian West for the help they have volunteered over the years.

Amongst the University technical support staff I am particularly grateful to Mr. Alan Edwards for the design and construction of the PCB layouts for the sensor prototypes. I would also like to thank Mr. Paul Hale and Mr. John Roberts for their willingness to construct and modify mechanical assemblies at short notice.

Finally I would like to acknowledge the financial and technical assistance of Chell Instruments and the DTI as well as the technical assistance of GEC-MMT Caswell, Lucas Engineering and Systems. Particular thanks are due to Mr. John Cockrill, Dr. Paul Huggett, Mr. Phil Baker for their technical help.

ABSTRACT

This thesis describes the design and performance of three novel optical fibre sensors, invented to overcome three problems in the plasma processing industry, related to the real-time monitoring of:
(i) physical and chemical characteristics of a processing plasma,
(ii) thickness of dielectric films during their plasma processing,
(iii) condition of the pump oils necessary to maintain a vacuum.
Sensors are available to monitor plasma characteristics and film thickness but their prohibitive cost limits applications. No published accounts of an oil condition monitor were found. Common industrial practice is to rely on experts capable of judging these characteristics purely by visual inspection of plasma, film and oil colours. Initially this seems an ideal solution but its subjectivity makes it difficult to achieve reproducible results and describing it as 'low cost' ignores the need to employ experts. Human experts are also unable to continuously monitor colour over long periods. The limitations of visual inspection prompted the development of an artificial colour sensor based on the same trichromatic principles as the human eye. This sensor consisted of three photodiodes with overlapping spectral responses in the red, green and blue regions. The resulting detector photocurrents were processed to yield colour values. Artificial colour sensing is shown to exhibit sufficient sensitivity and stability to monitor commercial plasma processing; whilst retaining the typical advantages of optical sensing, such as being non-invasive and immune to electrical noise.

CHAPTER 1
INTRODUCTION

1.1 PROBLEMS WITH PLASMA PROCESSING

The drive towards ever increasing complexity in integrated circuits is forcing the semiconductor industry to tighten its production tolerances (Elliot 1982). Plasma etching techniques currently dominate integrated circuit fabrication; but the speed at which these techniques evolved has outpaced theoretical understanding of plasmas to such an extent that process control has become a 'black art' in which optimum parameters are discovered empirically and repeatability is difficult to obtain (Mayer et al 1988).

Simply reading the discharge power, gas pressure, gas mixture and flow rates entering the plasma off the appropriate meters is not sufficient to ensure repeatability in plasma processing since these parameters can interact in a complex manner to give an unstable equilibrium (Mayer et al 1988). A more reliable method is to monitor the physical and chemical characteristics of the plasma but this is a complex and expensive task commonly requiring optical or mass spectrometry. The ability of expert operators to detect irregularities in processing plasmas simply by observing their colours raises the possibility of mimicking their methods and avoiding the problems associated with the optical processes discussed above.

Another method of overcoming problems of repeatability is to monitor the product rather than the processing agent. The dielectric thin films which are etched or deposited by plasmas have distinctive interference colours related to their thickness.

Expert operators can accurately gauge film thickness simply by observing these colours but unfortunately this can only be done after processing since the plasma emission obscures the colours whilst processing is in progress. On-line monitoring of film thickness is also a complex and expensive task commonly requiring interferometers or ellipsometers [Heavens 1955]. An ideal solution would be to replace these instruments with an electronic colour sensor immune to background light.

Plasma processing systems must be pumped down to a low pressure and any fluctuations in the effectiveness of pumping may be manifested as fluctuations in product quality. Hence it is important to ensure that the vacuum pumps used in the system are maintained at optimum efficiency. The condition of the pump oil is a critical factor in pump efficiency, and is normally judged by visual inspection of oil colour. Visual inspection is time consuming and intermittent so an electronic colour sensor would also be valuable for this application.

Chapter 2 of this thesis provides a brief overview of the plasma etching systems currently employed in industry. It also discusses some of the problems encountered during processing and the diagnostic tools designed to overcome them. Whilst these traditional diagnostic tools often provide good results their cost and complexity frequently limit them to research rather than commercial applications.

1.2 OPTICAL SENSORS AS A SOLUTION

Throughout the previous section it was emphasized that the complex sensors designed for the three process monitoring applications were often avoided in favour of visual inspection of the sample colour. This observation inspired the development of an electronic colour sensor operating on chromatic principles similar to those underlying human colour vision.

Implementation of an electronic colour sensor required the use of a range of optical components: sources of sufficient power and spectral bandwidth to illuminate a sample; detectors with the appropriate sensitivity and spectral profiles to record sample colour; and optical fibres to channel light to and from the sample shielded from external noise. Chapter 3 contrasts the characteristics of a range of sources, detectors and fibres and evaluates their suitability for use in a commercial colour sensor. In addition the chapter compares the characteristics of traditional optical sensing techniques and highlights the advantages of colour measurement systems.

Chapter 4 of this thesis introduces human colour perception and various formal concepts of colour. Particular emphasis was placed on the standard agreed by the International Commission on Illumination (CIE) in 1931, which defines colour in terms of the responses of three standard photodetectors with overlapping spectral profiles. To construct an electronic colour sensor a photodiode triplet was selected (Jones et al 1989), which matched these standard photodetectors as closely as possible. Disparities in spectral response between these standard detectors and

commercially available photodiodes resulted in slight differences between the CIE standard colour and the output from the sensor which was termed chromaticity. Finally these formal concepts of chromaticity were used to derive the variation of chromaticity as a function of spectral mixing.

The system design of the sensors is described in chapter 5. Although each sensor consists of three photodiodes with a current to voltage converter and subsequent gain stages, slight modifications were made to tailor each to their application. This chapter also describes the construction of a DC plasma nitriding chamber and a RIE plasma etching chamber on which the sensor designs were tested.

1.3 PERFORMANCE OF THE OPTICAL SENSORS

The performance of an optical fibre chromatic sensor designed to measure plasma colour is described in Chapter 6. Initial tests on a DC plasma nitriding chamber showed that the sensor was capable of detecting and discriminating between the spectral shifts in plasma emission caused by changes in discharge power and gas mixture. More detailed experiments carried out on a reactive ion etching (RIE) chamber demonstrate the ability of the sensor to discriminate between the spectral shifts in plasma emission caused by changes in discharge power and gas mixture, gas pressure and gas flow rates. Further experiments on this chamber showed the sensor capable of detecting the end of an etching process by detecting changes in plasma mixture.

Chapter 7 of this thesis describes the performance of a novel thin film monitor based on chromatic sensing. Initially an off-line

sensor was tested on a set of semiconductor thin film samples. When this sensor proved capable of matching the sensitivity of the best expert observers attempts were made to modify the sensor so it could discard background plasma emission enabling its use during plasma processing. The incorporation of a chopped light source and a phase-locked signal recovery system enabled the chromatic sensor to discard all background illumination not at the chopping frequency. As a result the sensor was shown to monitor film thickness, on-line with no loss in performance. Despite this performance the high cost of including the commercial signal recovery system increased the sensor cost significantly. A simpler signal recovery system was constructed employing signal subtraction and this was shown to demonstrate similar performance to the commercial system at greatly reduced cost.

A novel chromatic fibre sensor was developed for the on-line monitoring of the condition of vacuum pump oils. A description of its design and performance will be found in chapter 8. The sensor is shown to exhibit sufficient sensitivity to the chromatic difference between pure and impure oils whilst also showing the stability and repeatability required for use in an industrial environment.

CHAPTER 2
PLASMA PROCESSING

2.1 INTRODUCTION TO PLASMA PROCESSING

The ever increasing demand for faster and more complex integrated circuits is forcing the semiconductor industry to investigate methods of improving its product quality. One of the 'simplest' methods of increasing the speed and component density of an integrated circuit is to reduce the linear dimensions of the circuit; this option has the added advantages of increasing reliability and reducing power consumption. Inevitably such increases in component density require improvements in semiconductor fabrication techniques. Component densities greater than 10^6 devices/cm^2 can be achieved using current fabrication techniques, but in this fast changing industry improvements are constantly being sought.

Fundamental to the fabrication of integrated circuits is the etching of well-defined patterns in thin-films of various masking materials; commonly silicon and its oxides and nitrides although occasionally metals (Al,W), III-V semiconductors (GaAs,InP) and various polymers are also used. Originally patterns of circuitry were etched through a mask using 'wet' chemical solutions but the promise of smaller device structures and improved etch anisotropy has led to a gradual shift towards 'dry' plasma etching techniques (Elliot 1982).

2.2 THE LIMITATIONS OF SOLVENT ETCHING

In the past, device structures were etched using a chemically reactive solvent capable of dissolving the substrate but unable to attack a masking material (Elliot 1982). Silicon nitride is a substrate commonly incorporated into silicon devices and figure 2.1a shows the layer structure of a device prior to etching.

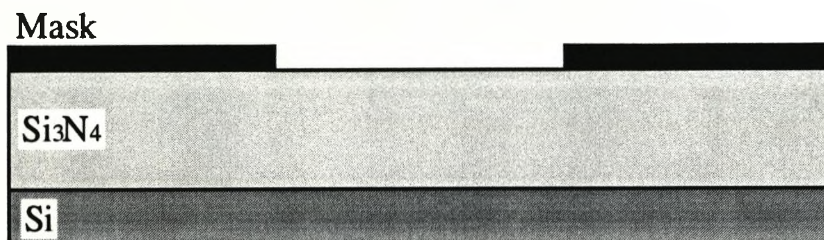

Figure 2.1a The layer structure of an unetched wafer.

Traditional solvent etching of silicon nitride is expensive and requires highly corrosive, boiling (430K) phosphoric acid to achieve a significant etch rate. Since the substrate is an isotropic material, chemical attack occurs isotropically i.e the etch rates parallel (R_X) and perpendicular (R_Y) to the sample surface are equal. Isotropic etching causes an undercut of the masking layer illustrated in figure 2.1b which leads to distortion of the desired etching pattern and places a lower limit on the device dimensions attainable (Coburn 1986).

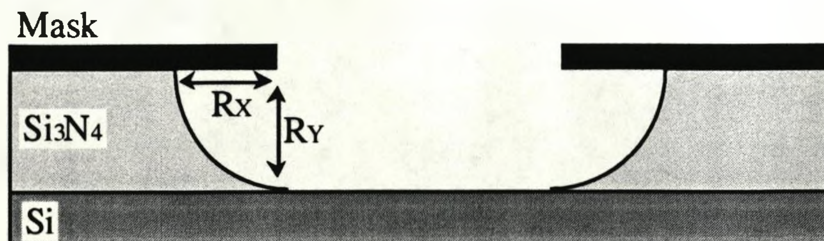

Figure 2.1b Mask undercut due to isotropic etching.

If the characteristic device dimensions are orders of magnitude larger than the mask undercut, the problem is minimal and can be overcome by introducing appropriate compensation to the masking layer. However device densities have increased to a point where the lateral dimensions of a device (the mask spacing s) and the layer to be etched are comparable in thickness (d); at this point the effects of mask undercut become critical (figure 2.1c).

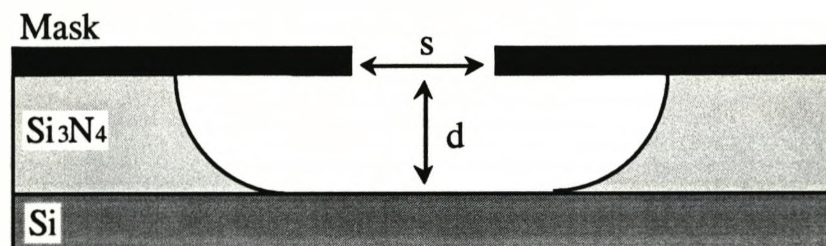

Fig 2.1c Mask undercut significantly affecting device dimensions.

Perfect reproduction of the mask pattern could be achieved by a completely anisotropic etch (figure 2.1d) but in practice no etching methods have complete anisotropy.

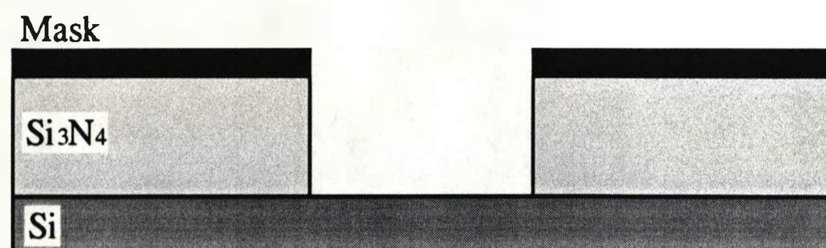

Fig 2.1d An ideal etching profile.

Etch directionality δ, (Zarowin 1983) is defined as the ratio R_X/R_Y and ranges from zero for a completely anisotropic etch to unity for a completely isotropic etch. Other sources (Mogab 1983) prefer to describe etching in terms of the *degree of anisotropy* A_f,

which is defined as $A_f = 1-\delta$. The amount of compensation required for a given degree of anisotropy may be calculated by considering the equidistant pattern of lines and spaces shown in figure 2.1e

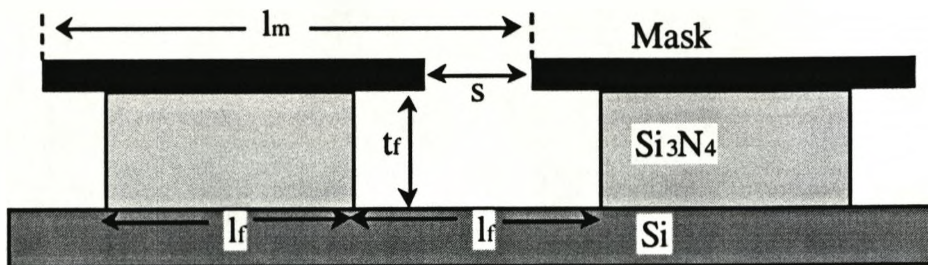

Fig 2.1e An idealized profile of edge undercut.

A mask spacing s ($s = 2l_f - l_m$ as illustrated in figure 2.1e) is enlarged to an etched feature of length l_f by undercut; these variables are related by

$$s = l_f\,(1-\delta\ 2t_f / l_f) \qquad \text{Equation 2.1}$$

where t_f is the film thickness. This demonstrates that the mask spacing is related to the feature length by two factors; the etch directionality δ and the aspect ratio t_f/l_f; either of which must be minimized to keep undercut enlargement to a minimum. Aspect ratio can determine the electrical characteristics of a device so it is difficult to minimize in practical VLSI manufacturing. Consequently as feature sizes decrease higher degrees of etch anisotropy are required.

Anisotropy in solvent etching can occur if the solvent attack is concentrated along the mask/film interface. However this 'mask lifting' as it is known, is an extreme form of undercut which results in large areas of mask flaking off the film and exposing it to direct attack. The anisotropic etch should be directed perpendicular to the mask/film interface rather than parallel to it.

This can be achieved by dry etching techniques which have the added advantage of etch rates far higher than the 50Å/min typical of the solvent etching of silicon nitride (Fonash 1985).

2.3 DRY ETCHING TECHNIQUES

2.3.1 INTRODUCTION

Dry etching techniques were first exploited by the semiconductor industry in the 1960s when 'plasma ashing' was used to remove organic photoresists by subjecting them to an oxygen discharge (Irving 1968). Electron impact dissociation of oxygen molecules generated highly reactive atomic oxygen which oxidized the organic photoresist to carbon dioxide and water. Since then plasma etching has been adapted to use a wide range of gas mixtures, operating pressures and electrode configurations; many of which are known by different names despite their basic similarity. These processes have largely replaced solvent etching since they employ a variety of etching mechanisms (Fonash 1985), some of which can result in a very directional etch.

2.3.2 ETCHING MECHANISMS

There are four main etching mechanisms:

Physical Etching: in which etching is effected by the impact of ions accelerated in a potential gradient. Since this gradient can be highly directional the resulting etch can also be highly directional. To preserve the etch anisotropy chemically inert ions are chosen. On impact atoms of the substrate can be physically displaced; a process known as sputtering; this is not a very selective process since all atoms respond similarly to impacts.

Quantitative analysis of physical (or sputter) etching would be very difficult if it was necessary to consider the interatomic potential function in detail, but a good agreement with experiment can be obtained by regarding the impact as a binary collision. Sigmund (1969) found the sputtering yield S was proportional to the ion impact energy (determined by the nuclear stopping power E) for impact energies up to 1keV:

$$S = \frac{3\alpha}{4\pi^2} \frac{4m_i m_t}{(m_i+m_t)^2} \frac{E}{U} \qquad \text{Equation 2.2}$$

where m_i & m_t are masses of the ions and the target atoms respectively, α a function of the ratio of these masses and U the surface binding energy of the substrate. As the ion impact energies exceed 1keV the yield saturates since the excess energy simply heats the target; further increases in ion energy eventually result in a reduction in yield as ion implantation becomes the dominant effect.

Chemical Etching: in which etching is effected by chemical reactions between the substrate and active radicals generated within the plasma. It is important that the reaction by-products are volatile so that they can be removed to expose more of the substrate to the plasma. The process is analogous to solvent etching and produces selective but isotropic etching; with some exceptions where reactions occur along crystallographic planes.

Chemical-Physical Etching: where the two processes are combined in an effort to obtain the advantages of both. Most dry etching techniques combine the two in some degree. Chemical weakening of bonds can enhance the rate and selectivity of

sputtering. Sputter damage can enhance chemical reaction rates and ion impacts can provide the activation energy required for chemical etching. It has been demonstrated that the etching of silicon by an ion-assisted XeF_2 etch occurs at a far greater rate than the sum of the etch rates obtained when each process is used separately. Controllable etch rates in excess of 500Å/min can be achieved (Coburn 1986).

Photochemical Etching: where photons, generated either within the plasma or externally introduced, initiate the etching of organic photoresists. This method is both selective and directional.

Dry etching plasmas are normally driven using radio frequency generators. If DC generators were used insulating materials could not be etched since they would accumulate a large surface charge from contact charging so repelling further attack from ions and perhaps extinguishing the plasma. To sustain a continuous discharge excitation frequencies in excess of 100kHz are required; in practice 13.56MHz is used most often since this frequency is allotted by international communication authorities as a band where significant radiation is permitted. The RF power is coupled to the driven electrode via a matching network and blocking capacitor so that the output impedance of the generator (typically 50Ω) can be matched to the plasma impedance (typically a few ohms). This maximizes the power dissipated within the plasma and protects the generator from overload (Fonash 1985).

2.3.3 REVIEW OF DRY ETCHING

There are numerous electrode configurations associated with dry etching. Table 2.1 summarizes the characteristics of three of the commonest methods currently in commercial use.

System Characteristics	Plasma Etching	Plasma Effluent Etching	RIE Etching
Etching Mechanism	Chemical	Chemical	Physical/ Chemical
Electrode Arrangement	Planar Diode	External Electrodes	Planar Diode
Pressure Range	10^{-1} to 10^{1}T	10^{-1} to 1T	10^{-3} to 10^{-1}T
Sample Location	On Grounded Electrode	Downstream of plasma	On Driven Electrode
Power	RF	RF	RF

Table 2.1 Comparison between dry etching methods.

Plasma Etch: although plasma etching is commonly used to describe all dry etching processes the term is also used to describe more specific processes where the sample is placed on the grounded electrode. This implies that plasma etching is a purely chemical process where the sole function of the plasma is to provide reactive chemical species. However, the plasma potential can be considerable, so physical etching mechanisms such as ion bombardment can also occur. To maximize the etch rate these systems operate at relatively high pressures of 10^{-1} to 10T, even so the etch rates are relatively low. The reduced mean free path

and low potential gradient above the grounded electrode also lead to low etch anisotropy.

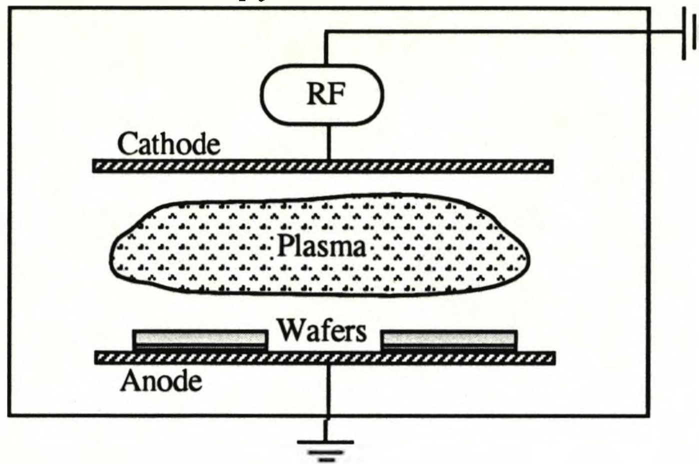

Figure 2.3 A schematic diagram of a plasma etch system.

Plasma Effluent Etching. is a process which isolates the sample from the plasma by placing it downstream of the electrodes. This reduces irradiation and ion impact damage at the cost of reducing the etch rate and anisotropy. A modification of this process enhances the etch rate and anisotropy by employing a laser to initiate photochemical reactions.

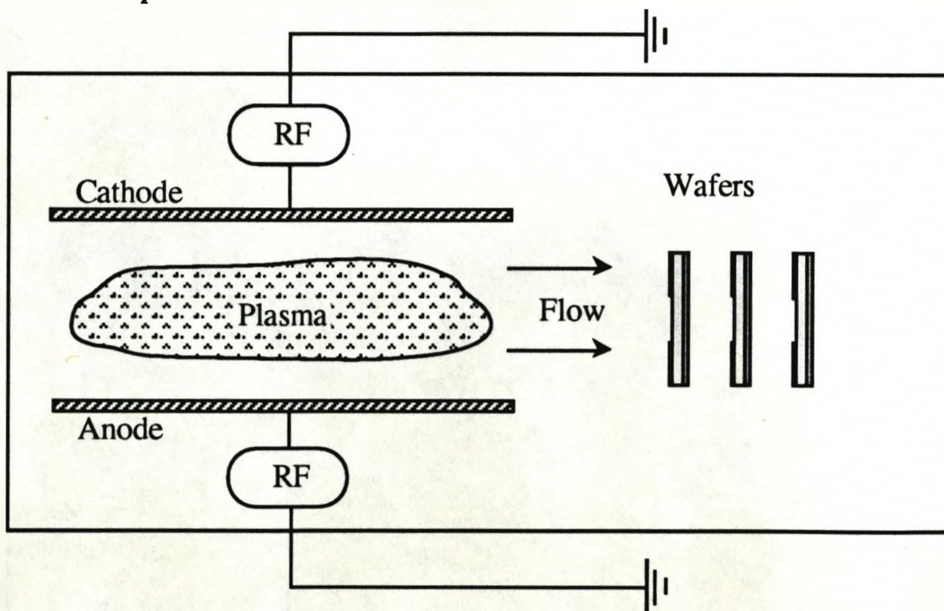

Figure 2.4 Sample position in a plasma effluent etch system.

3. Reactive Ion Etching (RIE): is a process which achieves selective and isotropic etching by using a combination of ion impact and chemical reactions; it occurs when the sample is placed on the driven RF electrode. This electrode receives an excess diffusion current of electrons (because their mobility is higher than that of ions) which generates a negative bias that rises until the electron and ion currents are in balance. The negative bias between plasma and sample ensures that higher potential gradients exist in RIE systems than in plasma etch systems, which in combination with the lower process pressures (10^{-3} to 10^{-1}T) lead to improved etching anisotropy. Disadvantages of RIE include increased rates of surface contamination and damage (Semura & Satoh 1984). Figure 2.5 is a schematic diagram of an RIE system.

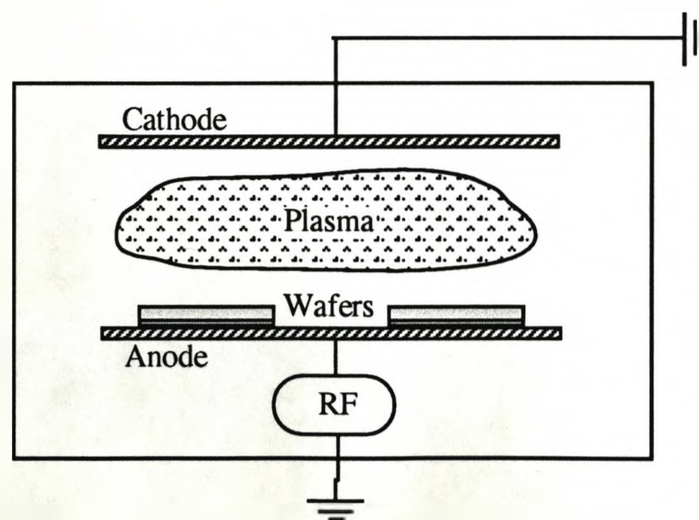

Figure 2.5 A schematic diagram of an RIE system.

2.4 PLASMA DIAGNOSTIC TECHNIQUES

2.4.1 INTRODUCTION

Being a market-driven fabrication process the application of plasma processing has outpaced understanding of the fundamental plasma phase and surface chemistry involved (Mayer et al 1988). The degree of uncertainty is such that attaining the correct settings for process parameters like power, pressure, flow rate and gas composition has become a black art and once an 'optimum' is achieved the settings are left unchanged for all subsequent processing. Common industrial practice is to establish a 'repeatable' etch or deposition rate and vary the process time to obtain various degrees of etching or deposition.

Unfortunately the process parameters within the operators control only influence the plasma chemistry in an indirect manner, e.g. if the density of a free radical is to be increased this cannot always be achieved by simply increasing the partial pressure of the neutral gas since the degree of ionization may be dependent upon many other factors. Allied to these problems the plasma chemistry can be very sensitive to changes in temperature, humidity and even previous processes run on the chamber. Such sensitivity causes wide variations in the rates of etching and deposition, encouraging the development of a wide range of plasma sensors.

The primary function of many plasma sensors is the detection of an etching endpoint. At the endpoint the rate of etchant depletion suddenly decreases as does the rate of substrate sputtering. The resulting large changes in plasma chemistry are detectable to a wide variety of sensors. The detection of this

endpoint permits the etch to stopped before mask undercut or substrate damage can occur. Small changes in plasma process parameters cause changes of degree, not of kind and are therefore more difficult to detect. The monitoring of these changes would be a valuable secondary function of a plasma sensor.

2.4.2 REVIEW OF PLASMA DIAGNOSTIC TECHNIQUES

1. Electrostatic probes: were developed by Langmuir (Chen 1965) in 1924, to study plasma characteristics; in consequence these probes are often known as Langmuir probes. They consist of a small metal electrode (usually a wire probe) attached to a power supply and a current collector linked to a detection circuit. The probe is immersed in the plasma and the bias potential generated between it and the plasma drives a current. In principle it is possible to calculate the densities and energies of the charged particles in the plasma from this current, permitting both endpoint detection and plasma monitoring. In practice however, only limited confidence can be placed on these calculations since the probe distorts the plasma by drawing current from it. The effective collection area of the probe is actually the area of the sheath, which can vary with the bias. Further difficulties arise from currents generated by impact heating and impact generated secondary ionization.

2. Mass spectrometry: is a technique for analyzing the concentration of species in the plasma. Neutral molecules are ionized and accelerated by an electric field whilst being subjected to a perpendicular magnetic field. The magnetic field causes them

to describe circular orbits, the radii of which are dependent on the ionic mass and charge. Although mass spectrometry provides detailed chemical information, this is difficult to interpret since the ions can recombine or undergo further reactions in the time taken to travel downstream (Mogab et al 1978). This problem can be minimized by reducing the distance between the plasma and detector; in the limit the detector orifice can be drilled through the grounded electrode but this is an invasive solution. Further difficulties in interpretation are caused by the quadrupole detector which can fragment molecules during ionization; leading to the detection of species not present in the plasma. Despite being a useful research tool the bulk, expense and invasive nature of mass spectrometers limit their applicability in industrial plasma processing environments. In addition mass spectrometers are limited to providing chemical information on plasma and cannot monitor its physical parameters.

3. Electrical characteristics of plasmas: such as its capacitance and resistance change as the plasma process parameters are altered. Attempts have been made to use this for the detection of etching endpoints and plasma monitoring (Mlnyko 1985). Plasma impedance changes are measured by detecting the phase-shift on RF input voltage. These measurements are limited by the deviation of RF fields from the pure sinusoid, which makes it difficult to assign an exact phase to the signal.

4. Optical Diagnostic Methods: comprise a wide range of non-invasive techniques, largely based on changes in plasma absorption and emission. Endpoints and other major changes in

plasma chemistry can be detected by the appearance or disappearance of characteristic spectral lines. Changes in plasma parameters cause small shifts in plasma equilibrium which are manifested as changes over the spectral continuum. This flexibility, coupled with their non-invasive nature make optical sensors a good choice for plasma monitoring.

Atoms in a plasma have stable electronic configurations only when their electrons occupy one of a number of quantized energy states $E_1, E_2 \ldots E_n$. When an electron in the ground state E_1 receives energy $E_n - E_1$; from a photon of frequency $f=(E_n-E_1)/h$; it is raised to the higher energy level E_n (Rae 1986). The stable atom (X) is said to be excited (X*),

$$X + hf \Leftrightarrow X^* \Leftrightarrow X^+ + e \qquad \text{Equation 2.3}$$

this process of excitation gives the plasma a characteristic absorption line at that frequency. Ionization is an extreme form of excitation where an electron (e) absorbs enough kinetic energy to escape the attraction of the nucleus, leaving behind a positive ion (X^+). Excitation can also be achieved by electron impacts (when the electron energy $eV=E_n-E_1$) and thermal collisions (when the ion kinetic energy $kT=E_n-E_1$). Relaxation is the inverse of the excitation processes described above, where an electron in an excited state E_n spontaneously decays to a lower energy level E_1. The release of the excess energy is in the form of a photon of frequency $f=(E_n-E_1)/h$, giving the characteristic emission line at that frequency. Recombination is the inverse of ionization where a free electron and an ion coalesce resulting in the emission of light, since the binary process is forbidden by the conservation laws the process normally involves three body collisions. (Hancock 1991)

Every photon emitted at a certain frequency corresponds to a relaxation or recombination, so the total number of such events can be estimated from the number of photons emitted by the plasma. Since each atom is capable of emitting at many frequencies the most accurate estimate of the ion density can be obtained by restricting the photodetector sensitivity to the bandgap frequency of a single transition. This is done by placing an interference filter in front of the photodetector. With such a setup the optical intensity is a measure of the population of excited species in the plasma, although factors such as self-absorption may distort the linearity of this relationship. Such spectral lines are commonly used in the plasma processing industry to measure reactants and trace contaminants down to one part in 10^6 (Robinson 1991).

Although widely used in industry optical plasma diagnostics have their limitations (Hancock 1991). Observations limited to monitoring single spectral lines require a whole range of specially tailored interference filters if they are applied to a wide range of processes. In practice such monitoring is conducted using expensive and complex variable wavelength monochromators such as prisms, gratings or etalons which can scan across an entire emission spectrum. This approach permits the observation of a wide range of phenomena but records an excessive amount of data which is difficult to interpret and increases the response time of the sensor.

2.5 MONITORING THE THICKNESS OF THIN FILMS

2.5.1 INTRODUCTION

One of the objectives of plasma deposition is the fabrication of dielectric films with uniformly good electrical characteristics. Of particular interest is the consistency of capacitance ($C=\varepsilon_0 A/d$) and resistance ($R=\rho d/A$) between dielectric films deposited in different batches (A is the area of probe contact, ε_0 the permittivity of free space and ρ the resistivity and d the film thickness). Since both the capacitance and resistance of a film are dependent on its thickness, the control of this parameter assumes great importance when circuits with reproducible characteristics are required.

Lack of process repeatability has encouraged the development of many methods of film thickness monitoring, some of which are outlined below. It should be noted that the optical measurement techniques described in table 2.2 (Heavens 1955) are significantly superior to other methods in terms of sensitivity.

Method	Measurand	Range	Accuracy
Electrical	Thickness(d)	>100Å	d=+/-10%
Mechanical	Thickness(d)	>100Å	d=+/-5%
Ellipsometry	Thickness(d), Ref.Index(n)	20-5000Å	d=+/-0.2% n=+/-0.0005%,
Interferometry	Thickness(d), Ref.Index(n)	20-5000Å	d=+/-0.2% n=+/-0.003%,

Table 2.2 Methods used for monitoring thin film thickness.

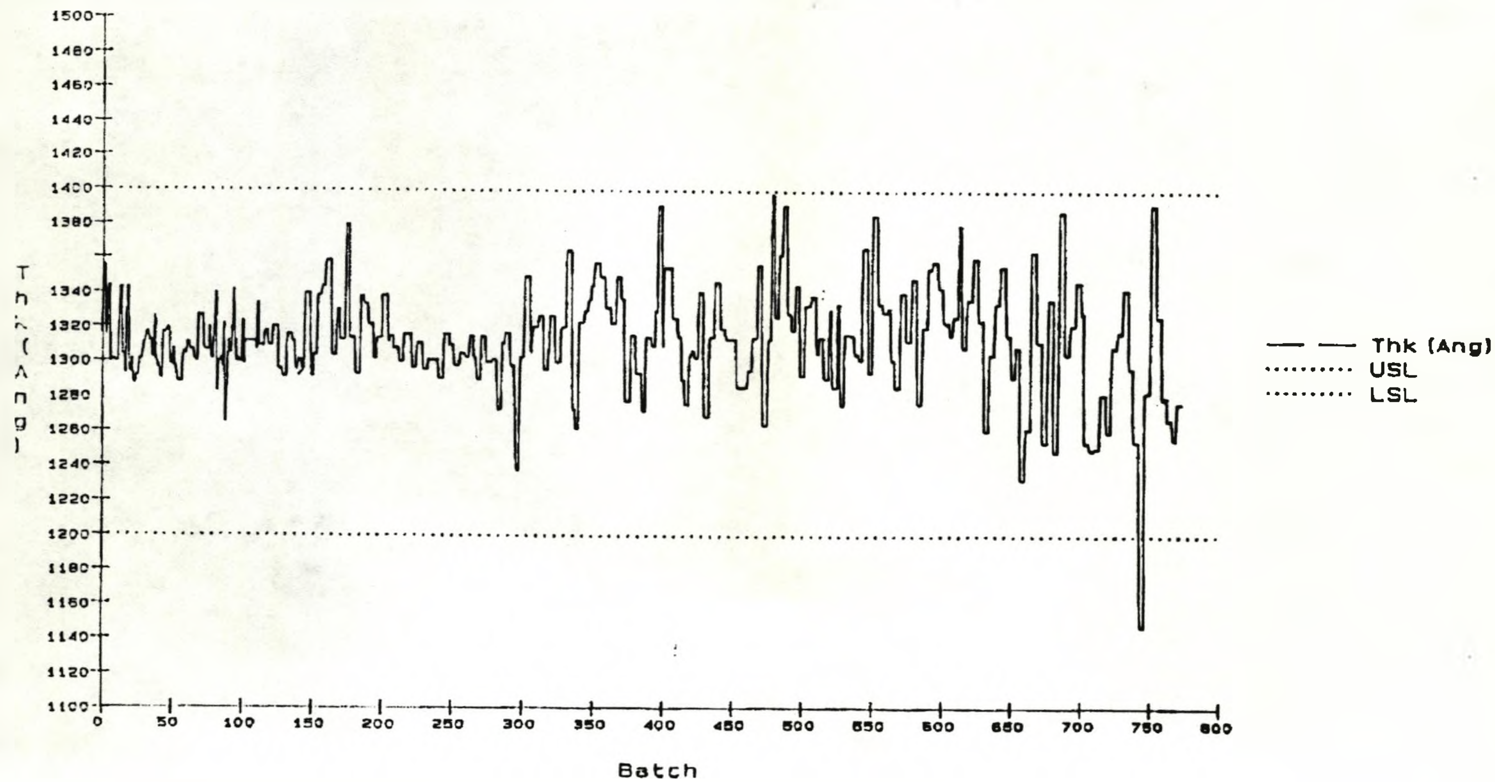

Figure 2.6 Variations in film thickness of silicon nitridebetween 'identical' batches.

Figure 2.6 demonstrates the difficulty in obtaining consistent film thicknesses between runs, despite maintaining all measured plasma parameters at constant levels and running the process for the same duration. The two dotted lines on figure 2.6 (upper specified limit or USL & lower specified limit or LSL) represent the extreme acceptable film thicknesses; these extreme values are approached quite often and was exceeded in the case of batch 746, ruining it.

2.5.2 ELECTRICAL FILM MONITORING TECHNIQUES

Electrical characteristics can be measured directly using long established techniques (Bar 1940) involving the contact of electrical probes with the wafer surface. Whilst these techniques demonstrate good accuracy they are difficult to extend to the two-dimensional mapping of electrical characteristics across the wafer surface. Their chief disadvantage is that they cannot be used during plasma processing since the introduction of electrical probes would severely distort the plasma. Considerable commercial interest has been focused on online wafer monitoring since such a system could ensure higher yields by stopping a process at the optimum time.

2.5.3 MECHANICAL FILM MONITORING TECHNIQUES

Film thickness can be monitored during deposition by simply weighing the sample at the onset and recording the increment in mass (Δm) as a function of time. The film thickness d

of a parallel sided film of area A and density ρ is given by $d=\Delta m/\rho A$. The sensitivity of this technique is surprising; even simple microbalances capable of measuring to 10^{-7}gm can record the formation of monomolecular layers (Clegg & Crook 1952). One difficulty of this method is that the average density of a thin film is known to be less than that of the bulk material due to its structural granularity, so the density is itself a function of film thickness (Clegg & Crook1952). Furthermore this method cannot be adapted to yield the thickness profile across a wafer.

2.5.4 OPTICAL FILM MONITORING TECHNIQUES

The capacitance of a dielectric film is dependent on its chemical composition (via ε_0) and its thickness (d). Both these characteristics can be monitored by optical means; the chemical composition can be obtained from the refractive index and the film thickness can be gauged from the phase change induced by the film.

Consider a uniform thin film of silicon nitride deposited on a silicon substrate and immersed in air as shown in figure 2.7. Light from a broadband source at angle ϕ_0 illuminates the film. The reflection and transmission coefficients r_1 and t_1 refer to waves travelling from air to silicon nitride whilst r_1' and t_1' refer to waves travelling from silicon nitride to air. Waves travelling from silicon nitride to silicon are represented by r_2 and t_2 whilst waves travelling in the opposite direction are represented by r_2' and t_2'.

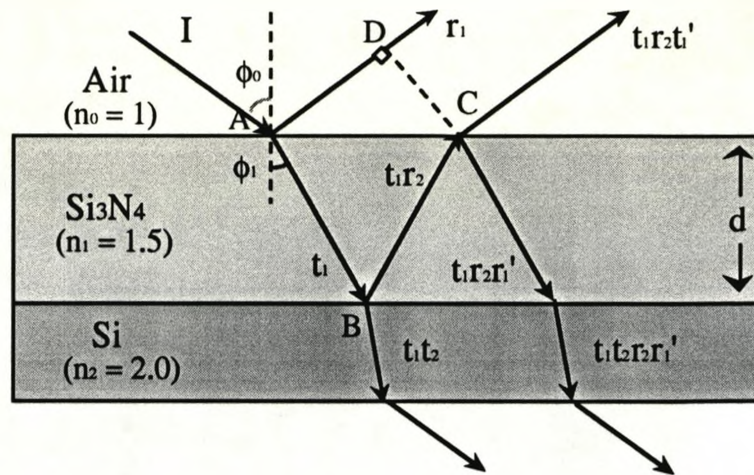

Figure 2.7 Reflections within a uniform thin film.

The optical path difference (Δ) between the first two waves leaving the front face of the film (r_1 and $r_2\, t_1 t_1'$) is given by:

$\Delta = n_1\, [\, AB + BC\,] - n_0\, AD$ since $AB = BC = d/\cos\phi_1$

so $\Delta = (2n_1 d/\cos\phi_1) - n_0\, AD$

but $AD = AC \sin\phi_0 = (n_1/n_0)\, AC \sin\phi_1$ *and* $AC = 2d \tan\phi_1$

$\Delta = (2n_1 d/\cos\phi_1)\,(1 - \sin^2\phi_1) = 2n_1 d \cos\phi_1$

This path difference corresponds to a phase difference δ of:

$$\delta = (2\pi/\lambda)\,\Delta = (4\pi/\lambda)\, n_1 d \cos\phi_1 \qquad \text{Equation 2.4}$$

The overall reflected amplitude is the sum of a series of waves each separated by this phase difference:

$$R = r_1 + t_1 t_1' r_2\, e^{-i\delta} + t_1 t_1' r_1 r_2^2\, e^{-2i\delta} + ...$$

or $R = r_1 + (\, t_1 t_1' r_2\, e^{-i\delta} / 1 + r_1 r_2\, e^{-i\delta}\,)$

and since $t_1 t_1' = 1 - r_1^2$ *(conservation of energy)*

$$R = (\, r_1 + r_2\, e^{-i\delta} / 1 + r_1 r_2\, e^{-i\delta}\,) \qquad \text{Equation 2.5}$$

The reflected intensity can be found by multiplying equation 2.5 with its complex conjugate:

$$n_1 RR^* = \frac{n_1 (r_1^2 + 2r_1r_2 \cos\delta + r_2^2)}{(1+ 2r_1r_2 \cos\delta + r_1^2 r_2^2)} \qquad \text{Equation 2.6}$$

If the film is absorbing then n_0 can be replaced by a complex quantity $n = n_0 + i\alpha$ (where α represents the absorption coefficient). It can be shown (Heavens 1965) that this variation of reflected intensity approximates to:

$$R = \left(\frac{n_1 - n_0}{n_1 + n_0} \right)^2 e^{-i(4\pi\, nd \cos\phi/\lambda)} \qquad \text{Equation 2.7}$$

which is a sinusoidal function of thickness when absorption is insignificant and an exponentially decaying sinusoid when absorption is significant. Such variation in reflectance will be observed in chapter 7.

Intensity based film thickness sensors have been developed to exploit this variation (Keenan et al 1991). However as well as suffering from ambiguity due to the oscillating signal the sensors require a high degree of stabilization (section 3.3.1) which reduces their practicality.

Commercial instruments used for film thickness monitoring are predominantly based on the two most sensitive techniques, ellipsometry and interferometry.

Ellipsometry : is an optical reflectance technique which measures changes in polarization rather than changes in intensity (section 3.3.2). It does not require absolute intensity measurements, but relies on the measurement of a series of angles at which the reflected intensity goes through turning points. The advantages of ellipsometry include the high resolution of thickness and

refractive index and its immunity to intensity fluctuations (Heavens 1955). A major disadvantage of ellipsometry is its cost, an automated ellipsometer requires a laser and a polarizer rotated by a synchronous motor. A further disadvantage is the complexity of a single measurement, which requires a sequence of mechanical rotations of the analyzer, after which the angles obtained must be processed by a computer or an operator familiar with a nomogram (thickness/refractive index contour chart).

Interferometry: is a sensitive method of measuring film thickness and refractive index which relies on recording the phase of a light wave reflected from the film surface. An increment Δd in film thickness results in an increment in optical phase $\Delta\delta$ given by

$$\Delta\delta = \Delta d\,(2\pi n/\lambda) \qquad \text{Equation 2.8}$$

This increment in phase results in a shift of interference fringes generated by an interferometer as described in the following chapter. The advantages of interferometry are its extreme sensitivity, lack of moving components and simplicity in analyzing data; its main disadvantages are high cost and a sensitivity to external disturbances.

2.5.5 LIMITATIONS OF OPTICAL FILM MONITORING

The complexity and expense of both these optical film monitoring techniques has limited their applications mainly to the field of research. Commercial semiconductor foundries often measure film thickness by visual inspection. Experts can judge film thickness to within 50Å simply by observing the interference colours generated by the thin film; although they measure the

overall optical path length (nt) rather the separate refractive index (n) and thickness (t), this proves adequate for most purposes since the refractive index does not vary greatly in a well defined process. The major disadvantage of visual inspection is that it cannot be used during plasma processing since background plasma emission makes accurate judgment of hue impossible.

2.6 VACUUM PUMP MONITORING

Good quality plasma etching occurs when operating at low pressure (approx. 1Torr), since at higher pressures the etch anisotropy is reduced. As a result the maintenance of low pressure within a plasma etching system is vital. These pressures are maintained by using a wide variety of vacuum pumps that include rotary pumps, Roots blowers and turbopumps, and any loss of efficiency in these pumps would result in a reduced etch quality. The condition of lubrication oil is critical to the functioning of vacuum pumps to such an extent that it is replaced at regular intervals that are considerably shorter than the true ‘lifetime’ of the oil (Baker 1990).

At present these pumps are periodically inspected by a human expert familiar with the colour of pure and impure oils. A commercial semiconductor foundry can contain several hundred pumps using several thousand litres of oil, making visual inspection a time consuming task. Since the prices of these oils range from £10-£500 per litre (Edwards 1990) significant losses occur if these oils are replaced before they become unusable, hence there is considerable commercial interest in an automated oil quality monitor. Indeed the applications of such a sensor would

have general applications in monitoring oil lubricated engines and would not be limited to the semiconductor industry.

2.7 NOVEL OPTICAL SENSORS IN PROCESS CONTROL

This chapter provides a brief survey of the designs and the modes of operation employed by modern etching systems. Three problems characteristic of plasma etching systems (plasma, thin-film and oil condition monitoring) were described, along with a summary of the diagnostic methods currently used to monitor them. Some of the limitations of these diagnostic methods were highlighted, and chromatic modulation was proposed as a general purpose diagnostic method. This choice was inspired by the observation that human colour vision is capable of discriminating between good and bad process conditions in all three cases.

CHAPTER 3
OPTICAL FIBRE SENSORS

3.1 INTRODUCTION TO OPTICAL FIBRE SENSING

Modern sensor technology is predominantly based upon electronic signals and modulators. Obviously this simplifies the signal acquisition techniques required, but there are situations in which alternative sensor technologies are preferable. Because of the volume mass production of electrical components, new technologies such as optical fibre sensing are unlikely to establish themselves on grounds of cost, they are most likely to appear in niche markets where the disadvantages of electrical sensors are prohibitive (Pitt 1985).

Amongst the disadvantages of electronic sensors are their inherent sensitivity to electromagnetic interference and hazards related to electrical sparking. These problems rule out the use of electronic sensors in industrial situations where strong electromagnetic fields or explosive chemicals are commonplace. Since powerful RF generators and highly reactive gases are essential components of a semiconductor processing facility, such a hostile environment would appear to provide an ideal niche for the application of optical fibre sensors (Giallorenzi et al 1982).

The original concept of optical confinement within a dielectric waveguide dates back to Hondros and Debye in 1910, but their theoretical analysis failed to arouse interest possibly due to the lack of convenient sources and detectors. In addition their waveguide design relied on reflections at the glass-air interface, so it suffered from severe losses when this surface became contaminated. Optical waveguides were revived by the invention of clad waveguides for endoscopy (Hopkins & Kapany 1954). The

cladding is an outer coating of low index glass which replaces air as the second medium; since this interface is within a solid it is protected from contamination. Clad waveguides inspired Kao and Hockham (1966) at STL in their attempts to exploit the vast bandwidths of optical systems in telecommunications. Their experiments triggered the explosion of interest in optical fibre communications; shaping the modern communication industry.

Optical fibre sensors are instruments which use the waveguiding properties of optical fibres to couple light from a source into a transducer. The light is then modulated by the action of physical or chemical influences on the transducer. This modulated signal is then monitored by a photodetector. Perhaps the recent explosive growth in optical fibre sensor applications is indebted to improvements in optical components, resulting from research efforts in the communications industry.

3.2 OPTICAL FIBRE SENSOR COMPONENTS

The telecommunications industry has created a range of relatively inexpensive, low loss optical fibres (Li 1980) whilst replacing cumbersome discharge lamps and photomultipliers by compact LEDs and photodiodes. Meaningful comparisons between measurements can only be made with sources and detectors that maintain a stable output regardless of ageing and fluctuations in environmental conditions. High sensor resolution is dependent on the source and detector displaying good noise characteristics. Assuming increasing importance are commercial considerations such as compactness, reliability, ease of manufacturing and low

unit cost; which give solid state sources and detectors an increasing edge.

3.2.1 OPTICAL SOURCES

Optical sources provide the signal for subsequent modulation within the sensor, and should possess sufficient power to overcome losses due to fibre attenuation and coupling. High optical power should be coupled with high conversion efficiency to save power and simplify drive circuitry. A small emission angle is normally a desirable characteristic since it minimizes source-fibre coupling losses without resort to external collimation.

Emitter Response	**LEDs** (Hamamatsu 89)	**Laser Diodes** (Hamamatsu 89)	**Filament Lamps** (Lucas 90)
Optical Power	1 to 10mW	1 to 100mW	upto 1W
Drive Power	2 to 20mW	2 to 200mW	120W
Efficiency	50 to 80%	40 to 60%	upto 15%
Emission Angle	60° to 4°	>1°	upto 360°
Line-width	20 to 100nm	0.01nm	1000 to 5,000
Wavelengths	550 to 1500nm	680 to 1550nm	400 to 5,000nm
dL/dI	quasi-linear	linear	non-linear
dL/dT	0.1 to 0.5%/°C	1 to 5%/°C	not available
Thermal Range	-40 to +100°C	-40 to +60°C	not available
Cost	50p-£10	£10-£1000	£10-£1000

Table 3.1 A summary of the characteristics of optical sources.

For many sensor applications the precise source wavelength may not be critical but small linewidths are sometimes preferred, particularly in applications such as interferometry where coherence is important (Steel 1986).

The luminance (L) of an ideal source should be independent of fluctuations in drive current (dI) and temperature (dT); if not the dependence should be linear to simplify the implementation of compensation techniques. Optical sources can be classified into three major groups whose source characteristics are summarised in table 3.1.

(i) Wideband sources: such as incandescent lamps, produce thermal radiation which is generated by the resistive heating of a tungsten filament. Enough electrical energy is dissipated in the filament to raise its temperature to 3000K and in order to maintain thermal equilibrium with its surroundings the filament emits electromagnetic radiation. Gases heated to such a temperature would emit characteristic spectral lines but in a solid the interactions between atoms broadens the spectral output into a continuum typical of blackbody emission (Meyer-Arendt 1984). The power emitted per unit area per unit wavelength at wavelength λ, known as the spectral emissive power $E_\lambda(T)$ was quantified by Planck in 1900 and was the first great success of quantum theory (Reif 1955):

$$E_\lambda(T) = \frac{2\pi hc^2}{\lambda^5 \left(e^{hc/\lambda kT} - 1\right)} \qquad \text{Equation 3.1}$$

(where h is Planck's constant, T the thermodynamic temperature, k Boltzmann constant, c the speed of light and λ its wavelength)

The form of the power spectrum of a perfect (blackbody) emitter is illustrated in figure 3.1; subsequent measurements carried out on a real source show a broad similarity (fig.8.3). The advantages of such sources include their high power output, broad spectral range and moderate cost; their disadvantages include their non-directional emission, short lifetimes and potential drift problems (although this final problem has been reduced in the quoted a.c. driven lamp supplied by Lucas Applied Technology).

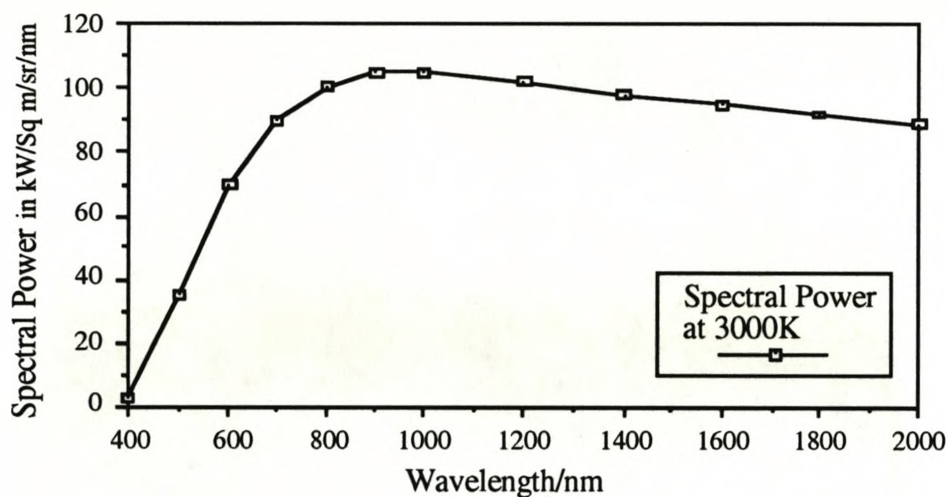

Figure 3.1 Power Spectrum of a Blackbody Emitter.

(ii) Light Emitting Diodes: radiate because of the recombination of electron-hole pairs in a forward biased p-n junction (Wilson & Hawkes 1983). Forward bias increases the migration of majority carriers from both sides of the junction (figure 3.2) cross the potential barrier (represented by the solid gradient in figure 3.3) where they are minority carriers, this is known as minority carrier injection. This occurs because forward bias creates a gradient between the Fermi levels (represented by the dashed gradient in figure 3.3) that opposes the potential barrier.

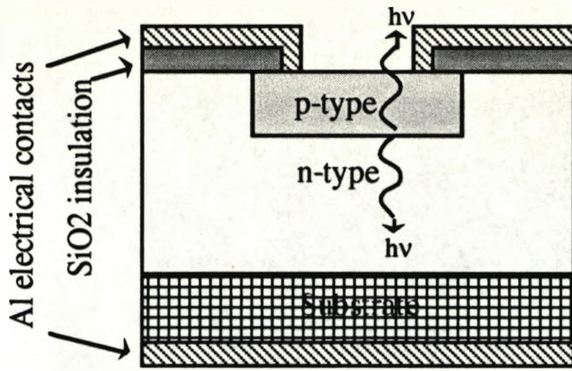

Figure 3.2 Construction of a p-n junction as used in an LED

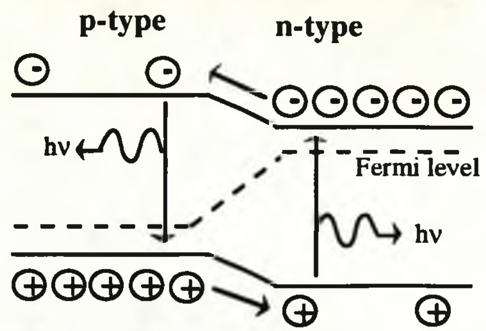

Figure 3.3 Radiative recombination in a p-n junction

Surplus minority carriers diffuse away from the junction and recombine with majority carriers emitting light in the process. The rate of radiative recombination is proportional to the rate of minority current injection; hence the intensity of emitted light is proportional to the flowing current (equation 3.3). The emitted wavelength is precisely determined by the energy gap between the conduction and valence bands of the material (equation 3.3), although thermal excitations broaden the spectral profile.

$$I = A\, i_0 \left[\exp\left(\frac{eV}{\beta kT}\right) - 1\right] \quad \text{Eqn 3.2} \qquad \& \qquad \lambda_g = \frac{hc}{E_g} \quad \text{Eqn. 3.3}$$

(where I is the emitted intensity, A is the photon conversion efficiency, e the electronic charge, i_0 the reverse saturation current, V the applied voltage, β a material constant, T the thermodynamic temperature, λ_g and E_g the wavelength and energies of the bandgap).

Advantages of LEDs include their small size, low cost, long lifetimes, and directional emission; their disadvantages include their low power output (the quoted Toshiba photodiode is an exception), narrow spectral range and drift problems. The

disadvantages may soon be reduced since there is potential for significant improvements in LED technology. (Berg & Dean 1976)

(iii) Lasers: radiate by stimulating emission in a medium capable of sustaining a population inversion (Maiman 1960). A wide range of material can lase but the only lasers inexpensive enough for use in commercial sensor applications are diode lasers. Their mode of operation is similar to that of LEDs; population inversion is achieved by increasing the doping and biasing to such an extent that the Fermi level is driven into the conduction band, facilitating minority carrier injection. Their advantages over LEDs are their exceptional directionality and coherence; their disadvantages include their short lifetimes, high cost, narrow spectral range and potential drift problems. Since the disadvantages of lasers outweigh their advantages when used as the source of a broadband colour sensor they have not been used in the work presented in this thesis.

3.2.2 OPTICAL DETECTORS

Optical detectors measure the intensity of the signal after modulation in the sensor and should demonstrate sufficient sensitivity for this purpose. Short response times are desirable for the observation of rapid processes although the achievement of adequate response is often at the cost of reduced sensitivity. A high spectral bandwidth is also desirable since it broadens the range of detectable sources. The detector photocurrent (I) should be a linear function of the incident luminance (L) to allow easy calibration. Ideally the detector photocurrent should be independent of temperature fluctuations (dT) but failing this a weak linear dependence simplifies the implementation of

compensation techniques. Optical detectors can be classified as photodiodes or photomultipliers; these are compared in table 3.2

Detector Response	**Photodiodes** (Hamamatsu 89)	**Photomultipliers** (Hamamatsu 89)
Wavelengths	200 to 1100nm	120 to 1000nm
Sensitivity	0.1 to 0.6A/W	0.2 to 0.9A/mW
Drive Power	none	25mW to 300mW
dI/dL	linear	quasi-linear
dI/dT	-0.1 to +0.5%/oC	-0.4 to +0.8%/oC
Thermal Range	-20 to +70oC	-50 to +50oC
Cost	£5 to £25	£400 to £2500

Table 3.2 Comparison of the two main types of photodetector.

(i) Photodiodes: convert photons into current by the photogeneration of electron-hole pairs in the depletion layer of a p-n junction (figure 3.4). Electron-hole recombination at a p-n junction forms a layer depleted of charge carriers. If an incoming photon is absorbed in this depletion layer an electron-hole pair (figure 3.5) is formed.

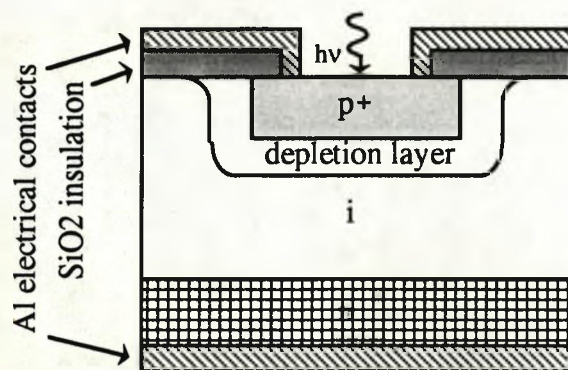

Figure 3.4 Construction of a p-i-n silicon photodiode

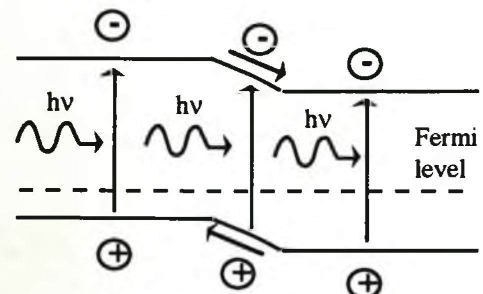

Figure 3.5 Generation of electron hole pairs in a p-n junction

Under the influence of the strong electric field gradient across the central depletion layer the electrons and holes diffuse into the n-

type and p-type regions respectively. This charge separation results in a photocurrrent, the value of which is given by (Wilson & Hawkes 1983):

$$I_p = I_0 \left[\exp\left(\frac{eV}{\gamma kT} \right) - 1 \right] \qquad \text{Eqn 3.4}$$

(where I_0 is the dark current, γ a quality factor, e the electronic charge, V the generated voltage and T the thermodynamic temperature). It should be noted that photodiodes are only capable of detecting photons with an energy greater than the energy difference between conduction and valence bands.

The main advantages of photodiodes include small size, low cost and low driving voltage requirements. Their disadvantage is the lack of sensitivity in comparison to photomultipliers, although this difference is gradually being eroded by newer solid-state devices such as avalanche photodiodes and phototransistors.

(ii) Photomutlipliers: which convert photons into a current by collecting photoelectrons displaced from a metal cathode. When radiation below a critical wavelength is incident on a metal surface electrons are emitted, a phenomenon known as the photoelectric effect (Wilson & Hawkes 1983). These photoelectrons are accelerated towards a series of electrodes maintained at successively higher potentials. Each electrode emits several secondary electrons for each incident electron. This 'chain reaction' serves to amplify the photocurrent greatly, resulting in extreme sensitivity to light; photomultipliers can detect single photons. Their disadvantages include bulk, high cost and high driving voltage requirements. As extreme sensitivity was not essential to the research presented in this thesis, these disadvantages discriminated against the use of photomultipliers.

3.2.3 OPTICAL FIBRES

An optical fibre is a dielectric waveguide which confines light by a series of total internal reflections (Senior 1985). In this research optical fibres serve to channel the reference signal from the source to the detector via an appropriate modulator. Many of the inherent advantages of optical sensing arise from the high degree of signal isolation that can be achieved using the transmission properties of optical fibres.

Geometric optics predicts that a ray of light travelling within the core of a step index fibre will undergo total internal reflection at the core-cladding interface if the angle θ is greater than the critical angle (θ_c defined as n_{core}/n_{clad}), the resulting ray is known as the guided ray. If this condition is not satisfied light leaks from the core into the cladding and the optical power in such 'leaky' waves is lost, both cases are illustrated in figure 3.6.

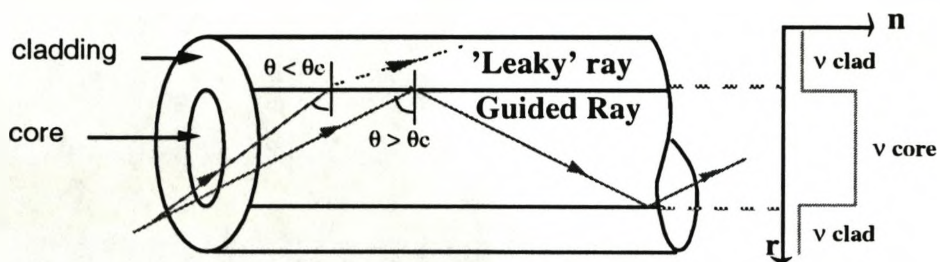

Figure 3.6: Confinement of light in a fibre according to ray theory.

It is apparent that light can only enter the fibre from a limited range of angles, sometimes known as the angle of acceptance θ_A, which correspond to those angles for which $\theta > \theta_c$:

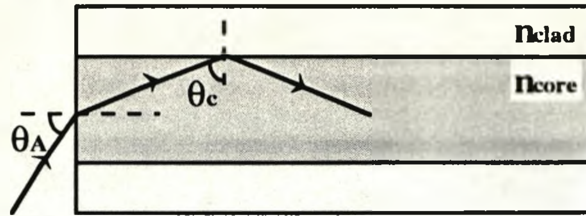

Figure 3.7: Fibre acceptance angle determining Numerical Aperture.

The angle of acceptance is often measured in terms of a numerical aperture NA (Senior 1985) defined as:

$$NA = n_{clad} \sin\theta A = n_{core} \sin\theta c$$

or

$$NA = n_{core}\sqrt{1 - \left(\frac{n_{clad}}{n_{core}}\right)^2} \approx \sqrt{2n\Delta n} \qquad \text{Equation 3.5}$$

(where n is the mean refractive index and Δn their difference)

Light propagating in graded index fibres (in which the core index decreases gradually rather than abruptly) follows a curved path; but as this can be approximated by a series of refractions ending in total internal reflection, the physical principles are the same. Graded index fibres are appropriate for communications purposes, but the extra cost of producing a graded index profile cannot be justified in the context of a chromatic sensor (Senior 1985).

Geometric optics is inadequate for modelling fibres which are so narrow that they can only support a single normal mode. Adequate modelling of such small ($<20\lambda$) monomode fibres requires the solution of Maxwell's relations in a cylindrical waveguide (Senior 1985). Monomode fibres have such a small core area that it is difficult to couple high intensities of incoherent light

into them. Hence they are not appropriate for chromatic sensor applications and were not used in this project.

For sensor applications it is desirable to maximize the optical power coupled into the fibre. Two characteristics that optimize coupled power, are large guiding area and large numerical aperture. The matching of fibre transmission spectra to source emission spectra, and low fibre attenuation are important in sensor applications even though the distances involved are small in comparison to communications applications. These and other relevant fibre characteristics are shown in table 3.3

Fibre Characteristic	Glass Fibre Bundles	Multimode HCS/Silica	Multimode Polymer
Guiding Area	10^{-2} cm^2	$5x10^{-4}$ cm^2	$5x10^{-3}$ cm^2
NA	0.05 to 0.2	0.2 to 0.4	0.3 to 0.5
Optimum	300-1500nm	300-1500nm	450-1200nm
Attenuation	5 to 20dB/km	0.1 to 0.5dB/km	<200dB/km
Core	nx100μm (n>50)	100 to 400μm	400μm to 1mm
Cladding	nx50μm	140 to 420μm	various
Thermal Range	<300°C	<140°C	<80°C
Cost	£20-100/m	£1 to £2/m	50p to £1/m

Table 3.3 The characteristics of various fibre types.

Since most materials have refractive indices of the same order of magnitude there is little scope of increasing NA by this route. The fibres used in this thesis are composed of glass, and not polymer which shows strong attenuation at short wavelengths; a disadvantage for chromatic sensing. NA can be increased by on-fibre collimation but such fibres are not commonly available.

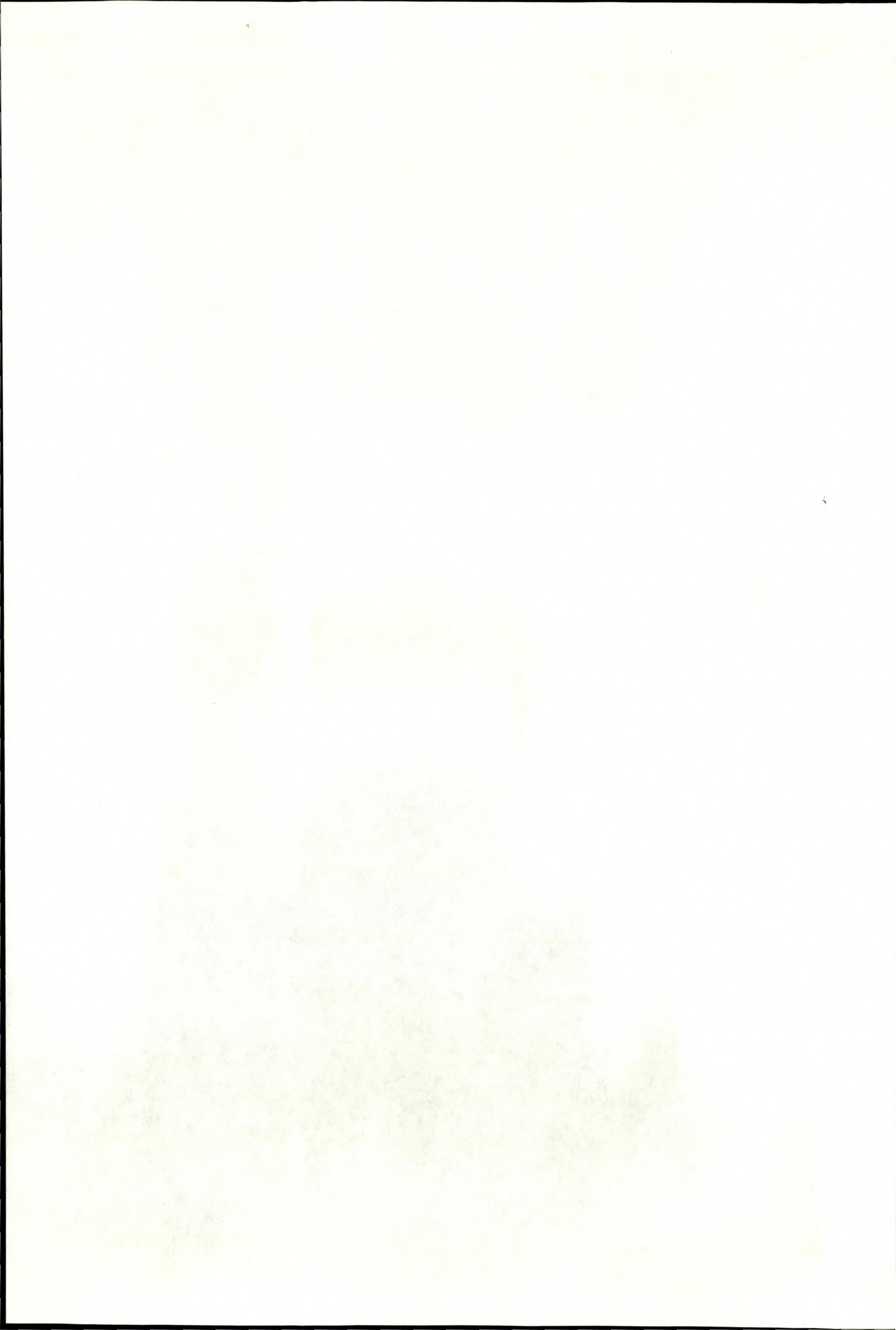

In principle the fibre radius can be increased greatly but mechanical constraints such as reduced flexibility and increased fragility make this impractical. Beyond a certain radius (>0.5μm) polymer fibres have better mechanical characteristics (Senior 1985) but their attenuation problems limit their use. The most effective method of increasing optical throughput is to bundle many small glass fibres into a large cylindrical ferrule and glue them together for mechanical support. A disadvantage of this solution is the high cost, but for short lengths this can be offset by simplification in the detection system due to the increased levels of signal obtained.

3.3 OPTICAL MODULATION TECHNIQUES

If a beam of light is to encode information relating to the state of a measurand, one of its parameters must be modulated by changes in that measurand. In common with all wave phenomena light shares three main parameters - amplitude, wavelength and phase. Additionally, being a transverse wave, it can also be characterized by its state of polarization. Not all these parameters can be used to monitor a given measurand. For instance electric fields leave the first three parameters largely unaffected whilst having a pronounced effect on the polarization (Yariv 1975). So the choice of modulation technique depends on the availability of appropriate modulators as well as considerations of sensitivity, repeatability, linearity etc. Extensive comparisons of the relative merits of these techniques are made in the literature (Pitt 1985). A review of these techniques aims to

show that chromatic modulation is an appropriate choice for plasma discharge and thin film monitoring.

3.3.1 INTENSITY MODULATION

The electric component of an electromagnetic wave can be represented by an oscillating electric field of amplitude E,

$$E = E_0 \cos(kz - \omega t) \qquad \text{Equation 3.6}$$

(E_0 is the maximum amplitude, k the wave number, ω the angular frequency and z the distance in the direction of propagation). The intensity of this wave is defined as the square of the amplitude: Absolute intensity sensing is the simplest and cheapest optical sensing technique since it is detected directly by all photodetectors. Most other sensing methods convert their signals into an intensity signal prior to detection. However the design simplicity of intensity based sensors places stringent demands on source, detector and connector stability since no self-referencing is possible. Even so monitoring the intensity of a specific line in an emission spectrum (Figure 3.8) is an accepted method of monitoring the population of excited species in a plasma (Hancock 1990) and has been considered as a method of thin film monitoring.

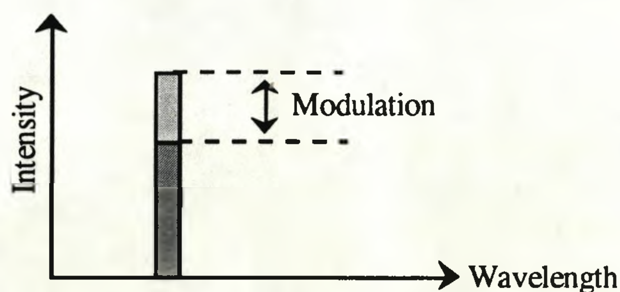

Figure 3.8 Stimulus for an intensity sensor

A major disadvantage of this approach is that the lack of self-referencing makes the design vulnerable to long term drift caused by external effects such as detector ageing or fibre bending. This problem can be minimized using a technique known as relative intensity monitoring which measures the ratio of intensities at two wavelengths $I_{\lambda_1}/I_{\lambda_2}$ (figure 3.9).

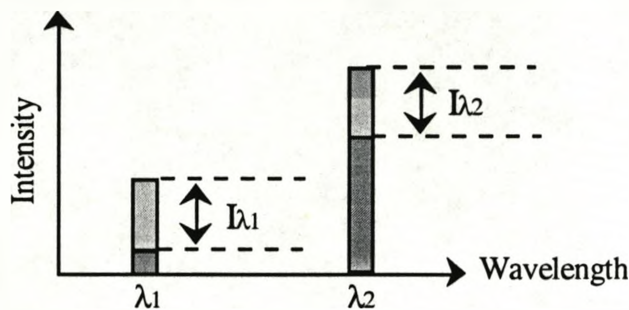

Figure 3.9 Stimulus for a relative intensity sensor

Although such wavelength referencing eliminates some optical variables, the filters at λ_1 and λ_2 discard a major proportion of the optical power (Dakin 1984).

3.3.2 POLARIZATION MODULATION

Since electromagnetic waves are transverse oscillations, the plane of oscillation of the electric field vector is free to rotate in two dimensions (x,y) perpendicular to the direction of propagation; this plane is known as the plane of polarization. Any plane of polarization can be reduced to two orthogonal components of the electric field vector:

$$E_x = E_o \cos(kz-\omega t)$$

$$E_y = E_o \cos(kz-\omega t+\varepsilon) \qquad \text{Equation 3.7}$$

where ε is the phase lead of E_x relative to E_y, the rotation of the plane of polarization is illustrated in figure 3.10

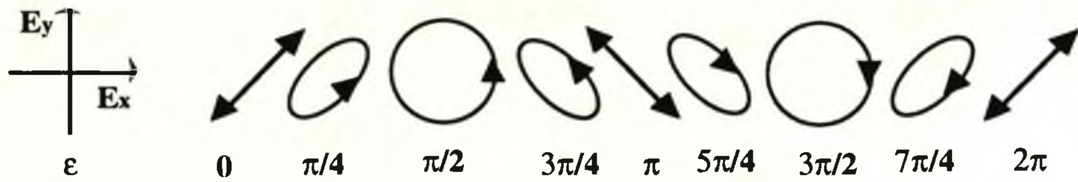

Figure 3.10 Electric field vector orientation of polarization states.

Polarimetry measures the changes in polarization state induced by a modulator (Spillman 1982). The optical signal is passed through a polarizer which preferentially transmits light with an electric field orientation parallel to an internal axis. The intensity of light transmitted by a polarizer depends on the component of the electric field parallel to that axis, so if the axis of the polarizer is parallel to E_x the intensity is $E_0^2 \cos^2 f(\varepsilon)$; where $f(\varepsilon)$ is a function of ε.

In the semiconductor industry a variant of polarimetry, known as ellipsometry, is used to measure the thickness and refractive index of deposited dielectric layers. The change in polarization can be expressed in terms of the ratio of two complex reflection coefficients r_p (for light polarized parallel to the plane of incidence) and r_n (for light polarized normal to the plane of incidence) where r represents the ratio of the reflected and incident electric fields. The complex quantity

$$r = r_p / r_n = \tan\psi \exp(i\Delta) \qquad \text{Equation 3.8}$$

defines two angles ψ and Δ which are measured during ellipsometry. The ratio r_p / r_n in equation 3.8 illustrates the self-referencing inherent in ellipsometry. An ellipsometer consists of two rotatable polarizers and a quarter-wave plate to compensate

for changes in phase due to reflection, the angles ψ and Δ are obtained by using polarimetric techniques described above. It can be shown that the appropriate substitution of these angles into the Fresnel relations (Azzam & Bashara 1971) can yield the film thickness and refractive index of the film.

3.3.3 PHASE MODULATION

Phase sensing or interferometry converts a relative phase difference between two light waves into an intensity signal. The two waves are superimposed so that phase differences between them cause varying degrees of constructive and destructive interference. Consider two linearly polarized waves of the same frequency, with a phase difference δ:

$$E_1 = E \cos (kz-\omega t)$$

$$E_2 = E \cos (kz-\omega t+\delta)$$

if these waves overlap the resultant intensity is given by the time averaged Poynting vector of summed amplitudes (Hecht 1975):

$$I = \langle E_1 + E_2 \rangle^2 = I_1 + I_2 + 2 E_1 E_2 \cos\delta \qquad \text{Equation 3.9}$$

Hence if the measurand generates a phase difference (see section 2.5.4) it can be monitored by observing the resultant fluctuations in intensity. The visibility V of these fringes is defined as:

$$V = \frac{I_{max} - I_{min}}{I_{max} + I_{min}} = \frac{2\sqrt{I_1 I_2}}{I_1 + I_2} \qquad \text{Equation 3.10}$$

LIVERPOOL UNIVERSITY LIBRARY

which reduces to unity if $I_1 = I_2$. Hence interferometry is independent of source fluctuations. The primary advantage of

interferometry is its extremely high sensitivity (Heavens 1955); a Michelson interferometer is capable of measuring the optical path length of semiconductor thin films to resolutions comparable to those obtained by ellipsometry, without the need for mechanical components. Its primary disadvantage is the sensitivity to external influences shown by the reference arm. The high cost and complexity of interferometry further limit its application in industrial environments.

3.3.4 WAVELENGTH MODULATION

Wavelength sensing is based on the measurement of wavelength shifts in the optical spectrum of the signal (figure 3.11), hence it is immune to intensity fluctuations (Hutley 1985). These wavelength shifts can be detected by spectrometry which is simple in principle but complex and expensive in practice; because of the need for a dispersive optical element to separate wavelengths and the consequent need for either a mechanical scanner or a CCD array. The dispersive element wastes optical power, mechanical scanners reduce sampling rate and CCD arrays add to the cost.

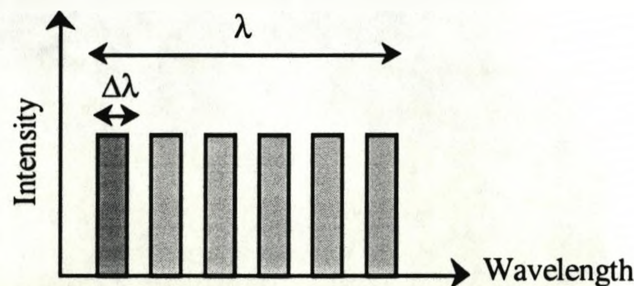

Figure 3.11 Stimulus for a wavelength sensor

These disadvantages are sometimes tolerated because a great deal of information can be obtained from a spectrum. In addition to its expense spectrometry requires the acquisition and processing of large amounts of data in order to extract a few relevant features; since it requires the sampling of $\Delta\lambda/\lambda$ intensity channels in parallel (where $\Delta\lambda$ is the wavelength resolution and λ the spectral range as shown in figure 3.11). This surfeit of information can require considerable expertise in interpretation.

In the plasma processing industry, spectrometry is used in areas where its high cost can be justified. Amongst its applications are the monitoring of the conditions of a processing plasma by the observation of it emission spectra (Robinson 1991) and the measurement of the thickness of dielectric thin films which can be derived from the reflectance spectra obtained on illumination with a broadband source (Heavens 1955). Although spectrometry gives good results in both these applications its cost places limits on its use and frequently visual observation of sample colour is used in its place.

3.3.5 CHOICE OF MODULATION PRINCIPLE

In the field of plasma processing human experts are often able to diagnose faults in a plasma system, simply by observing the colour of the glow discharge. Similarly wafer processing experts are capable of discriminating 100Å differences in the thickness of dielectric films simply by observing their interference colours. The ability of the human eye to resolve such differences using just three photodetectors, suggests that the use of spectrometers may be unnecessary for these purposes. Therefore large savings in cost and complexity could result from the

replacement of spectrometers with artificial 'eyes' capable of pseudo-colour monitoring.

Taking into account the characteristics of these sensing techniques, the alternative technique of chromatic modulation was proposed (Jones et al 1987). Chromatic sensing detects a change in a measurand not by detecting intensity changes at particular wavelengths in the manner of wavelength sensing, but by monitoring the sum of the contributions of changes over all wavelengths within a spectral power distribution. As such it is an integrated form of spectral monitoring as opposed to the differential (dispersive) nature of wavelength modulated systems. Since optical power is integrated rather than dispersed chromatic sensing is more appropriate than wavelength sensing in applications with low levels of illumination often encountered in plasma processing. Chromatic sensing can be implemented simply by measuring the intensity in three broad spectral regions; hence it retains the advantages of simplicity and low cost characteristic of intensity sensors. In addition it also provides a means of detecting overall shifts in spectral power distributions with the inherent self referencing, characteristic of wavelength modulation. These characteristics based on principles governing colour perception in the human eye; are discussed in the following chapter.

CHAPTER 4

CHROMATIC MODULATION

4.1 INTRODUCTION TO COLOUR

The perception of colour is not reliant on the detection of the details of a spectral power distribution. A colour can be specified by just three attributes of the spectral power distribution - hue, saturation and brightness (Billmeyer & Saltzmann 1966).

(i) Hue (Chroma): quantifies the characteristic described by adjectives like red, green and blue. The hue of a spectrum can be described by a single number; the dominant wavelength; which can be considered to be the weighted mean of the 'redness', 'greenness' and 'blueness' of the spectrum. The method of this calculation will be described in the following sections.

(ii) Saturation (Purity): quantifies the vividness of a colour. Low saturation is characterized by a spectral power distribution containing a high proportion of white light resulting in a pale colour, whereas high saturation is characterized a low proportion of white light which results in a vivid colour.

(iii) Brightness (Lightness): is the intensity of the spectrum.

4.1.1 THE RGB COLOUR CUBE

One of the strengths of colour sensing is that the hue, saturation and brightness need not be measured using three different sensors; they can be calculated from the outputs of three photodetectors with overlapping spectral responses. In fact the simplest method of specifying colour; the RGB cube (Billmeyer & Saltzmann 1966); plots the intensity of the spectrum in the red, green and blue regions as shown figure 4.1:

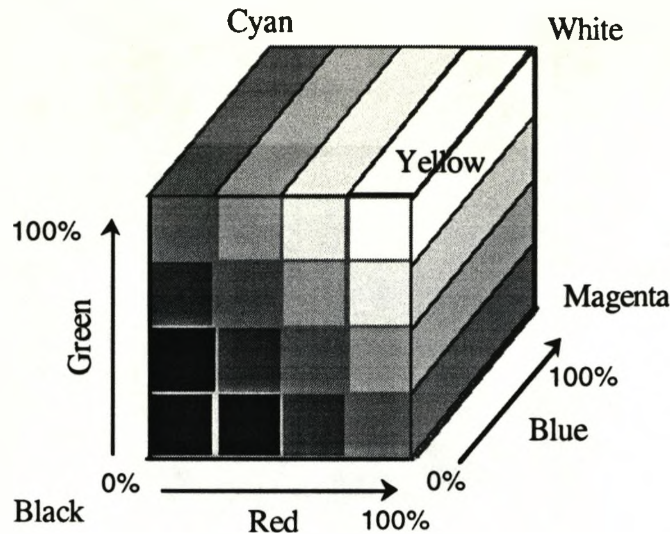

Figure 4.1 Chromatic representation on an RGB colour cube

The disadvantage of this method is that the hue, saturation and brightness are not readily apparent. A more satisfactory method of specifying colour would map these characteristics on three orthogonal axes.

4.1.2 THE Yxy COLOUR SYSTEM (CIE 1931)

In 1931 the *Commission International d'Eclairage* (CIE) agreed to define colour in terms of the responses obtained from three idealized photodetectors sensitive to stimuli in the red (X), green (Y), and blue (Z). The spectral responses of these photodetectors are illustrated in figure 4.2. From these photodetectors three spectral characteristics can be obtained: the brightness defined as Y, and two chromaticity coordinates x and y. If the intensities in the red, green and blue regions X,Y and Z are normalized so that $x+y+z=1$, three normalized chromatic coordinates x,y and z can be defined :

$$x = \frac{X}{X+Y+Z}, \quad y = \frac{Y}{X+Y+Z}, \quad z = \frac{Z}{X+Y+Z} \qquad \text{Equation 4.1}$$

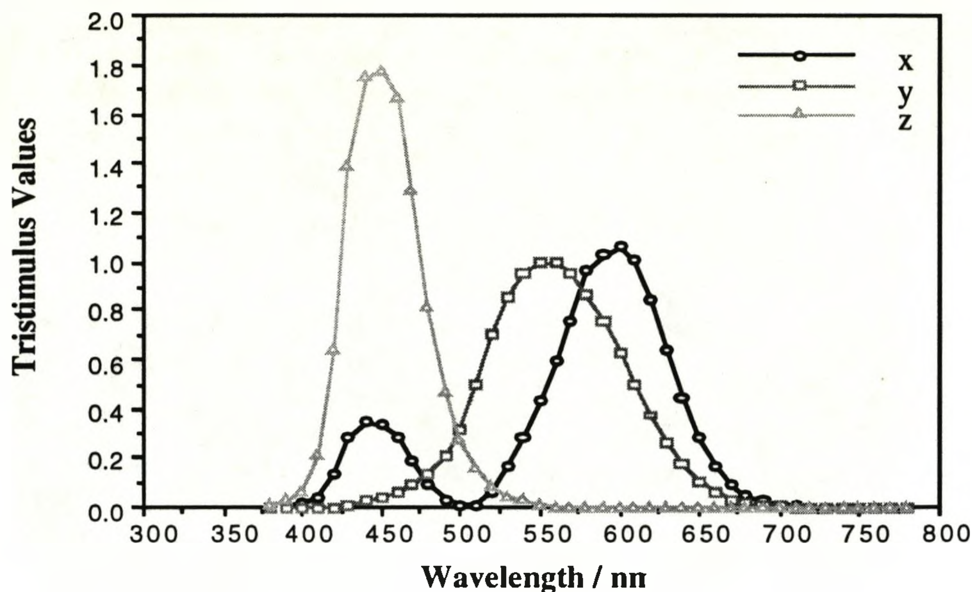

Figure 4.2 The spectral responses of the three definitive CIE detectors

Any two of these coordinates can be plotted against each other to construct a chromatic plane on which it is possible to map all possible hues and saturations:

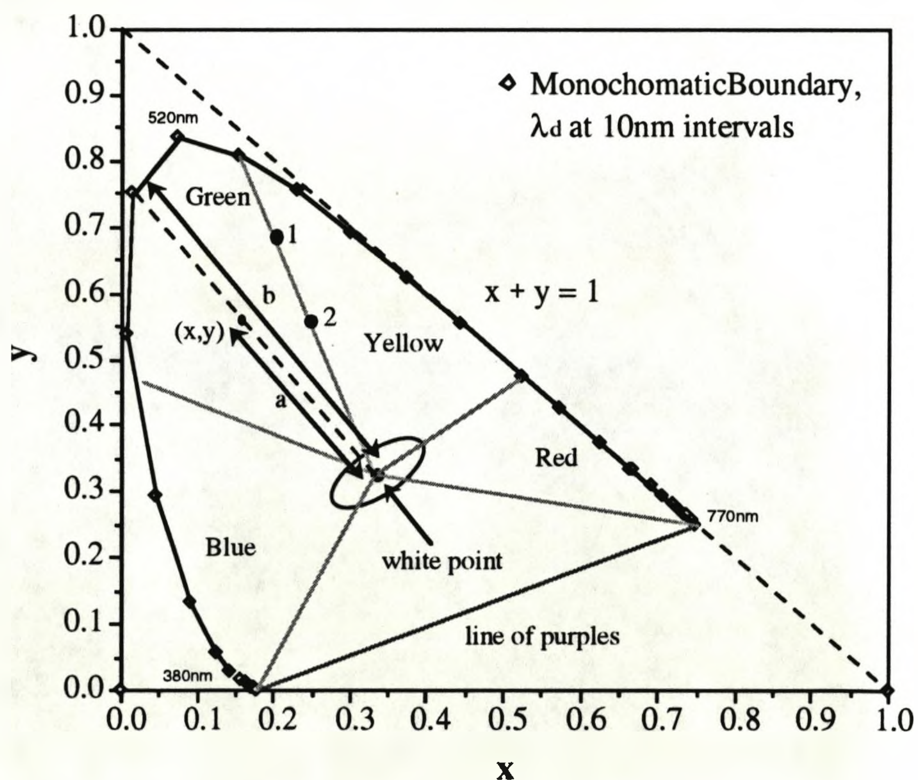

Figure 4.3 Chromatic representation on the Yxy (CIE) plane

Figure 4.3 shows the CIE chromatic plane with all possible colours at a given luminance lying within the curved boundary. Each point (x,y) within the boundary represents a unique colour although caution is required in the spectral interpretation of the chromatic plane since any colour may be generated by an infinite set of spectra, a phenomenon known as metamerism.

Visualization of the hue and saturation of a colour is easier in the CIE system than in the RGB system. A colour represented by a point (x,y) on the CIE chromatic plane has a hue determined by a dominant wavelength λ_d whilst its saturation is determined by its proximity to the monochromatic boundary. The dominant wavelength is defined by the intersection of a construction line with the chromatic boundary, this line is produced by the extension of a line connecting the achromatic point (1/3,1/3) to (x,y). If the distance between the white point and (x,y) is a and the distance between the white point and the monochromatic boundary is b, then the saturation is defined as the ratio a/b. A dominant wavelength does not exist if the construction line from the achromatic point to (x,y) intersects the 'line of purples'. In this case a complimentary dominant wavelength is derived by extending the construction line in the opposite direction, to intersect the monochromatic boundary.

Colours lying near the white light point are known as unsaturated colours because of the high proportion of white light they contain. The ellipse surrounding the white point on figure 4.3 contains a region of unsaturated colour. It is of note that lines of equal saturation, which are horseshoe-shaped at high saturations, reduce to the approximately elliptical curve illustrated on the figure.

4.1.3 THE L*a*b* COLOUR SYSTEM (CIE 1976)

The L*a*b colour colour system is a refinement of the Yxy system adopted to eliminate a lack of uniformity in the areas occupied by visible colours. For instance the interval between 500nm and 550nm occupies nearly a third of the chromatic plane whilst occupying only an eighth of the spectral range covered by the detector triplet. Another advantage of the L*a*b system is that the hue is uniquely defined in terms of an angle θ; eliminating the need for complimentary dominant wavelengths when analyzing colours on the 'line of purples'.

The main advantage of the L*a*b is that it represents hue and saturation as the an angle and radius respectively on a polar coordinate system, thus simplifying theoretical analysis of a locus of colours. A major problem with the L*a*b system is that the nonlinear normalization equations are more complex and require prior knowledge of the channel of minimum intensity (CIE 1976). These factors make a real time L*a*b based sensor more difficult to implement than one based on the Yxy system. In consequence this standard was not adopted for subsequent work.

4.2 CHROMATIC SENSING SYSTEMS

4.2.1 HUMAN COLOUR PERCEPTION

Human colour perception is achieved by a combination of physiological and neurological adaptations (Gregory 1986). Whilst the neural aspects of colour perception are not well understood (Land 1959) the physiological aspects are sufficiently well

documented to be of relevance to the design of artificial colour sensors.

Colour stimuli are detected by cone cells which are concentrated in the central region of the retina known as the fovea. Three types of cone have been identified, with spectral responses peaking at long L(λ), medium M(λ) and short S(λ) wavelengths; as illustrated in figure 4.4 (Gregory 1986). The labels red, green, and blue should be avoided since all three cones contribute to the perception of each colour.

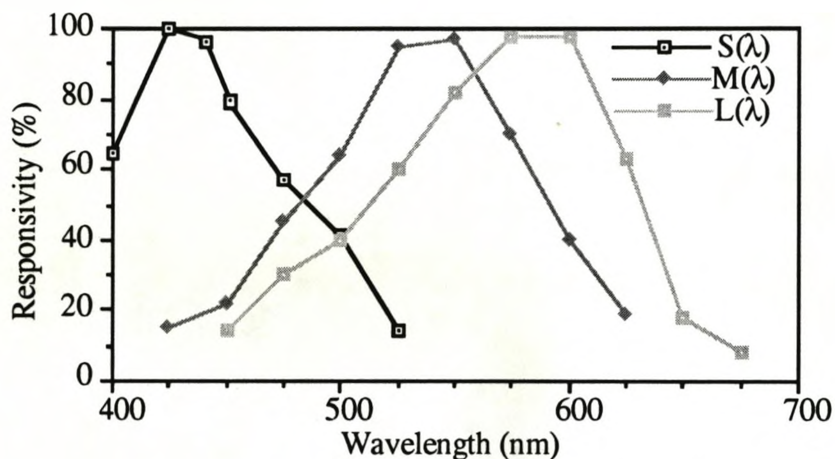

Figure 4.4 Spectral responses of cones in the human eye

Physiological tests show that the three cones allow the discrimination of three pairs of complementary colours (pairs of colours which, when mixed generate no colours other than themselves or white) red-green, blue-yellow and black-white. In order to explain the perception of six stimuli from three cones, the following neural processing scheme has been proposed (Overheim & Wagner 1982).

In the perception of the red-green complementary pair, a sensation of red is perceived if the sum of the contributions from the long and short wavelength cones exceed the contribution from

the medium wavelength cones, the reverse behaviour leads to the perception of green. The blue-yellow complementary pair is sensed in an identical manner. Perception of the black-white pair is slightly different, if the sum of the contributions of all three cones exceeds a lateral inhibition term X generated by neighbouring cones the white is sensed otherwise the sensation is black. These rules are summarized below:

$L(\lambda) + S(\lambda) - M(\lambda)$	> 0 QRED	< 0 QGREEN	(a)
$L(\lambda) + M(\lambda) - S(\lambda)$	> 0 QYELLOW	< 0 QBLUE	(b)
$L(\lambda) + M(\lambda) + S(\lambda) - X$	> 0 QWHITE	< 0 QBLACK	(c)

Equation 4.2

This scheme has been confirmed by the measurement of the frequency of nerve impulses carried by the bipolar nerve cells which link cones to the optic nerve (Overheim & Wagner 1982). Interestingly these equations explain the mechanism of red-green colour blindness. If the long wavelength cones are absent and replaced by medium wavelength cones equation 4.2a is always positive hence green stimuli are observed as red; the same substitution changes equation 4.2b into $2M(\lambda) - S(\lambda)$ which allows discrimination between blue and yellow. This form of limited colour measurement may have implications in the design of simplified colour measurement systems using only two detectors.

4.2.2 ARTIFICIAL COLOUR DETECTION

Artificial colour sensors operate in a manner analogous to that of the human eye so it is no surprise that their construction also mimics that of the human eye. The three types of cone cells are replaced by three photodetectors with overlapping spectral

responses but different peak sensitivities. The photocurrents generated by these detectors can then be processed to yield a value analogous to colour known as chromaticity.

Photodetectors with responses exactly matching those of the human eye are not commonly available but the chromatic principle can be applied to any three overlapping photodetectors and this flexibility can be useful in applications where spectral changes occur outside the visible range. Three photodiodes were chosen accordingly with spectral range slightly broader than the human eye; peaking in the blue (Hamamatsu G1961), red (Sharp PD1) and near infra-red (Sharp PD2), as shown in figure 4.5:

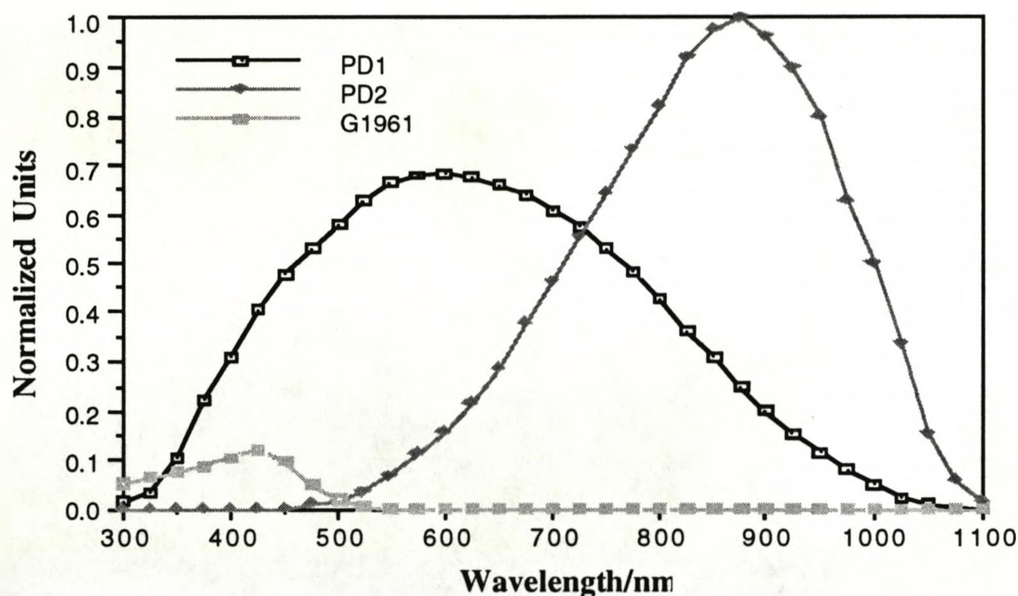

Figure 4.5 Spectral responses a PD1, PD2, G1961 photodiode triplet (Henderson 1990).

Since the derivation of colour from three cone responses involves unknown neural processing techniques further biological mimicry cannot be implemented. One implementable method is to use the spectral responses of the three photodetectors to define a chromatic plane analogous to the CIE chromatic plane. The shape of the monochromatic boundary is slightly different to that of the

CIE boundary reflecting the different shape of the detector responses. Also the dominant wavelengths on this boundary are slightly higher and broader in range, reflecting the higher and broader range of the photodiode triplet as compared to the standard CIE photodetectors, as shown in figure 4.6.

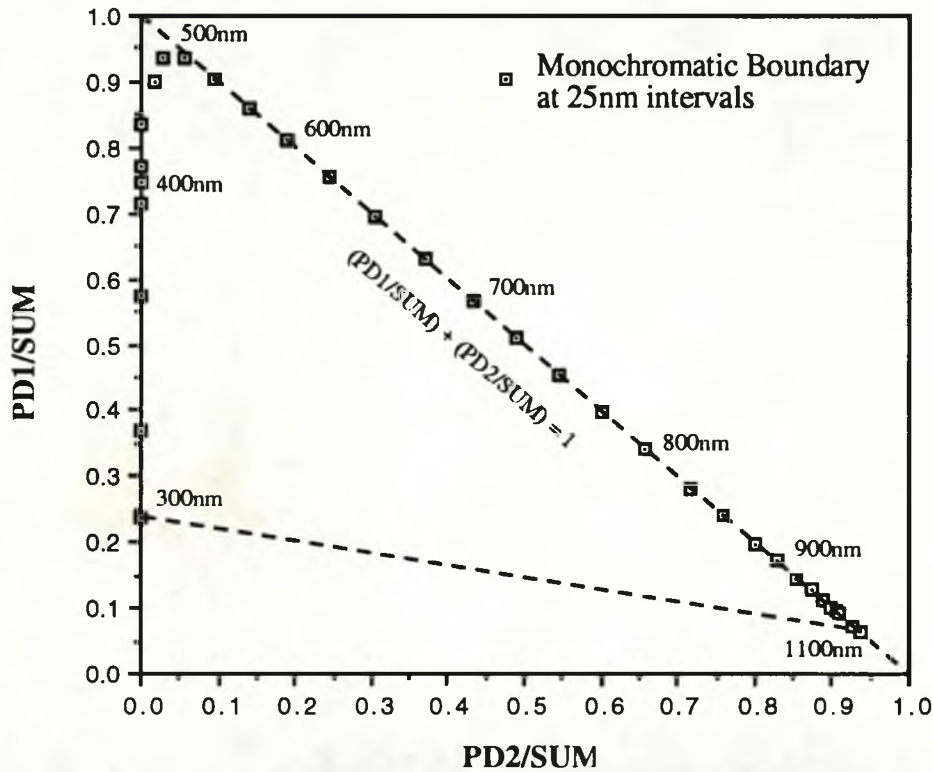

Figure 4.6 The chromatic plane defined by a photodiode triplet.

Some appreciation of this processing technique can be obtained by examining the mathematics relating chromaticity to the detector photocurrents. When addressing an optical signal with spectral power distribution P(λ) the output currents of photodetectors with spectral responses R(λ) will be:

$$I_x = K_x \int P(\lambda) R_x(\lambda)\, d\lambda$$

$$I_y = K_y \int P(\lambda) R_y(\lambda)\, d\lambda$$

$$I_z = K_z \int P(\lambda) R_z(\lambda)\, d\lambda \qquad \text{Equation 4.3}$$

where K_x, K_y and K_z are constants of proportionality and λ is the wavelength. Equations 4.3 may be normalized with respect to the effective optical power according to:

$$x=I_X/(I_X+I_y+I_Z)$$
$$y=I_y/(I_X+I_y+I_Z)$$
$$z=I_Z/(I_X+I_y+I_Z) \qquad \text{Equation 4.4}$$

If the parameters x,y,z are calculated from a standard set of idealized detectors, a plot of x against y results in the CIE diagram which forms the basis of colour science. Although many spectra can be mapped onto a single point on the chromatic plane the degree of degeneracy is less than that of intensity sensors where spectra map onto points restricted to a line. Hence chromatic analysis permits discrimination between spectra which could not be distinguished by measuring the intensity alone. The normalization of x,y and z has another important implication for optical sensing, namely that chromatic detection techniques are independent of intensity. The inherent intensity compensation renders the chromatic sensor immune to changes in source intensity and fluctuations in transmission along the optical path. In this thesis experimentally obtained equivalents to x,y and z are normally referred to as G1961/Sum, PD1/Sum and PD2/Sum respectively.

These advantages are still apparent if only two detectors are used to address the region of spectral overlap but in this case it is not possible to distinguish between colours of different saturation since the CIE or chromatic regions collapse to the line x+y=1. In

this simplified distimulus form (used in Chapter 8), equation 4.4 reduces to

$$x = I_x/(I_x+I_y) \qquad y = I_y/(I_x+I_y) \qquad \text{Equation 4.5}$$

4.2.3 CHROMATIC RESPONSE TO WAVELENGTH SHIFTS

Consider a monochromatic source the wavelength of which can be scanned across the entire range of the visible spectrum. As the source wavelength is scanned the chromaticity traces out the monochromatic boundary outlined in figure in 4.6. If a proportion of white light is mixed with the source; i.e. the saturation reduced; and the process repeated the outline of this boundary is distorted significantly. As the proportion of white light is increased these lines of equal saturation contract into a set of concentric ovals (figure 4.7) centred on the white point (Billmeyer & Saltzmann 1966).

There are several applications (thin film monitoring, fringe order measurements, photoelastic strain measurements) which show such large chromatic changes that practical measurements encounter several cycles of colour change. In such cases the sample chromaticity (x,y) on a tristimulus plot executes several circuits around the white point. As the optical path length through the sample increases the light saturation decreases resulting in the 'washing out' of sample colour; hence the circuit path of the sample chromaticity spirals towards the white point as shown in figure 4.7.

Using wavelength dependent methods it is not possible to distinguish between colours 1 and 2 which have the same dominant wavelength (520nm) but different saturations. Tristimulus representation permits discrimination between these

colours and so increases the range of a sensor beyond that determined by a single cycle thorough all possible wavelengths.

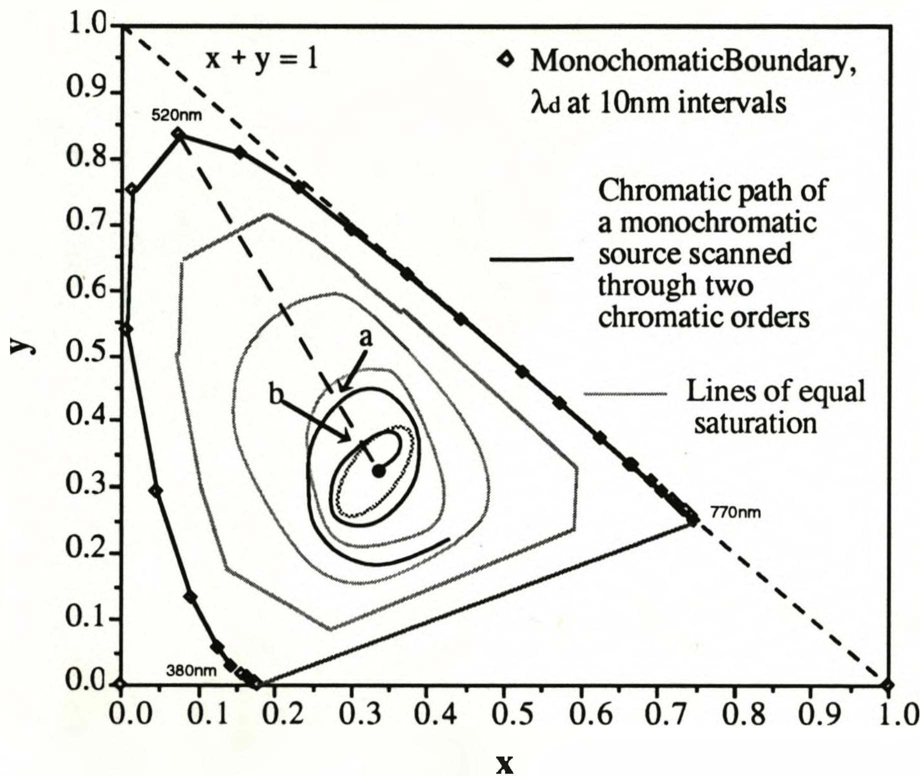

Figure 4.7 Shows the chromatic path of a source with changing saturation and wavelength.

4.2.4 CHROMATIC RESPONSE TO SOURCE MIXING.

When two lights with different dominant wavelengths are mixed the resulting mixture will have a dominant wavelength between those of its constituents. Unfortunately the variation of dominant wavelength with mixture is not in general a linear process. The resulting difficulty in calibration means that traditional forms of wavelength modulation do not easily yield the relative contributions of each constituent, to the composite dominant wavelength.

If however, the chromaticity of the constituents and the mixture are plotted on a tristimulus diagram a simple linear

relationship emerges. Suppose two colours C_1 and C_2 have chromatic coordinates $Y_1x_1y_1$ and $Y_2x_2y_2$ with tristimulus values $X_1Y_1Z_1$ and $X_2Y_2Z_2$ as defined by the Yxy (CIE 1931) system. On mixing a composite colour $C_3 = C_1 + C_2$ is formed with composite tristmulus values $X_3Y_3Z_3$ defined by

$$X_3 = X_1 + X_2 \qquad Y_3 = Y_1 + Y_2 \qquad Z_3 = Z_1 + Z_2 \qquad \text{Equation 4.6}$$

hence substituting these equations into equation 4.1 we have

$$x_3 = \frac{X_1 + X_2}{X_1 + X_2 + Y_1 + Y_2 + Z_1 + Z_2}$$
$$y_3 = \frac{Y_1 + Y_2}{X_1 + X_2 + Y_1 + Y_2 + Z_1 + Z_2} \qquad \text{Equation 4.7}$$

If we assume that the intensity of a given colour is proportional to the sum of its tristimulus values:

$$I_1 \propto X_1 + Y_1 + Z_1 \qquad \text{Equation 4.8}$$
$$I_2 \propto X_2 + Y_2 + Z_2$$

then substituting equations 4.8 into equations 4.1 & 4.7 we have

$$x_1 = \frac{X_1}{I_1}, \quad x_2 = \frac{X_2}{I_2}, \quad x_3 = \frac{X_1 + X_2}{I_1 + I_2}$$
$$y_1 = \frac{Y_1}{I_1}, \quad y_2 = \frac{Y_2}{I_2}, \quad y_3 = \frac{Y_1 + Y_2}{I_1 + I_2} \qquad \text{Equation 4.9}$$

so the composite coordinates x_3 and y_3 can be represented as

$$x_3 = x_1\left(\frac{I_1}{I_1 + I_2}\right) + x_2\left(\frac{I_2}{I_1 + I_2}\right)$$
$$y_3 = y_1\left(\frac{I_1}{I_1 + I_2}\right) + y_2\left(\frac{I_2}{I_1 + I_2}\right) \qquad \text{Equation 4.10}$$

which are parametric equations for a straight line, dependent on the intensities I_1 and I_2. Equations 4.10 show that the composite chromaticity C_3 (x_3,y_3) lies on a straight line connecting the two component chromaticities C_1 (x_1,y_1) and C_2 (x_2,y_2). As a result the relative contribution of each constituent chromaticity to the composite chromaticity can be obtained by using the ratios $x_1:x_2$ or $y_1:y_2$.

The ability of chromatic systems to determine the composition of a mixture of lights, merely by ratios of the constituent chromaticities, is particularly valuable in a field like plasma monitoring. For instance the rate of etching achieved by a plasma consisting of a mixture of CF_4 and oxygen is a sensitive function of the ratio of these two gases. Since the dominant wavelength and intensity are such complex functions of mixture, wavelength and intensity sensors are seldom useful. Commercial monitors are either slow, expensive and computer intensive spectrometers or line filter intensity monitors which are limited to monitoring the population of a single radical. A chromatic monitor would determine gas composition simply by dividing the chromatic separation between the pure gases (s_1) by the chromatic separation between the mixture and pure gas (s_2) as shown in chapter 6.

It should be noted that this linear chromatic variation is only valid when the two sources do not interact (Billmeyer & Saltzmann 1966). In a plasma some interactions between emitting species is inevitable but as subsequent results show the degree of interaction can be small enough to be neglected. This linearity also fails when absorption and scattering become significant, as is often the case in liquids and solids. In such cases the simple relationship

$C_3 = C_1 + C_2$ no longer holds and changes in hue are described by nonlinear (Kubelka-Munk) equations which can only be solved by approximation (Billmeyer & Saltzmann 1966). The effects of absorption and scattering are thought to be the cause of the nonlinear variation of oil chromaticity discussed in chapter 8.

4.2.5 CHROMATIC RESPONSE TO MULTIPLE SOURCES.

The real advantage of using chromatic analysis becomes apparent when observing more complex systems involving two or three parameters. For instance the etch rates of the plasmas described in chapter 6 were found to be dependent on three parameters; the gas mixture, the plasma power and the plasma pressure. Suppose that the 'normal' levels of these parameters are independently disturbed to the maximum possible extent and we get three colours corresponding to anomalous mixture (C_{mix}), anomalous power (C_{pow}), and anomalous pressure (C_{pres}). In a real process however, these disturbances would occur simultaneously to give a composite chromatic fault (C_{fault}) the nature of which would be difficult to determine.

The colours C_{mix}, C_{pow}, C_{pres} and their additive mixture C_{fault} are shown in figure 4.8. The purpose of the subsequent analysis is to calculate the intensity ratios I_{mix}/I_{pow} and I_{mix}/I_{pres} which will show the relative contributions of mixture, power and pressure to the overall fault. Let $C_{mix\text{-}pow} = C_{mix} + C_{pow}$ and $C_{mix\text{-}pres} = C_{mix} + C_{pres}$ as shown in figure 4.8. From equation 4.10 we have:

$$I_{mix}/I_{pow} = s_1/s_2 \qquad \& \qquad I_{mix}/I_{pres} = s_0/s_3 \qquad \text{Equation 4.11}$$

Applying the rules of additive colour mixing discussed in the previous section, $C_{mix-pow}$ must lie on the line connecting C_{pow} and C_{mix}. Similarly since $C_{fault} = C_{mix-pow} + C_{pres}$ it is apparent that $C_{mix-pow}$ also lies on the straight line connecting C_{fault} and C_{pres}. Therefore $C_{mix-pow}$ can be found by calculating the point of intersection of these two lines.

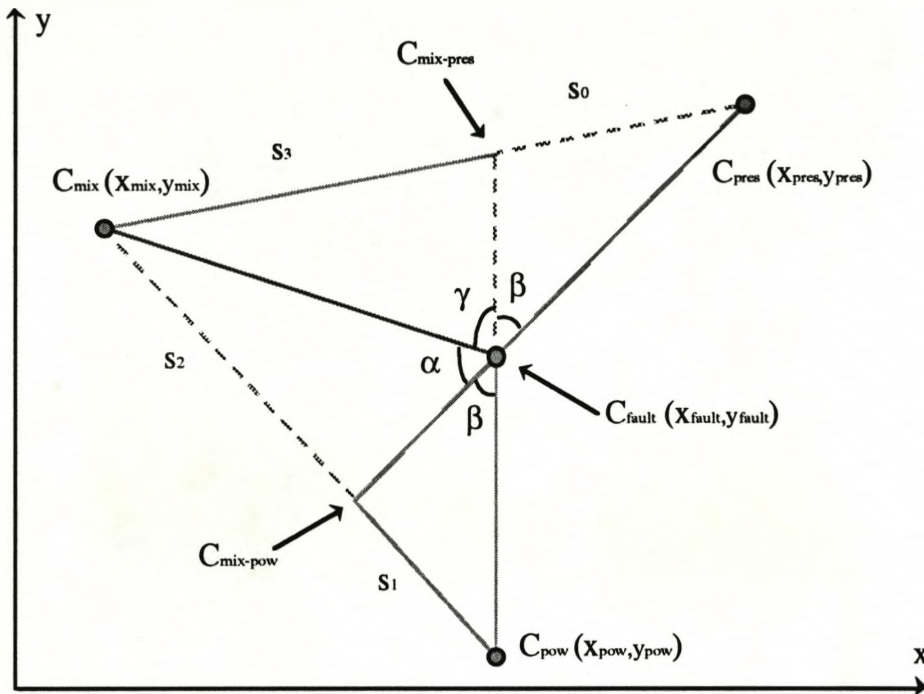

Figure 4.8 Chromatic shift resolved into components.

$$\frac{I_{mix}}{I_{pow}} = \frac{s_1}{s_2} = \frac{\sin\beta}{\sin\alpha}\sqrt{\frac{(x_{fault}-x_{pow})^2+(y_{fault}-y_{pow})^2}{(x_{mix}-x_{fault})^2+(y_{mix}-y_{fault})^2}}$$

$$\frac{I_{mix}}{I_{pres}} = \frac{s_0}{s_3} = \frac{\sin\beta}{\sin\gamma}\sqrt{\frac{(x_{fault}-x_{pres})^2+(y_{fault}-y_{pres})^2}{(x_{mix}-x_{fault})^2+(y_{mix}-y_{fault})^2}}$$

Equation 4.12

In this way it is possible to calculate the relative contributions of each source I_{mix} and I_{pow} to the composite chromaticity $C_{mix-pow}$. This process can be repeated and so the relative proportions of all three colours can be deduced from their individual chromaticities and the chromaticity of their mixture.

CHAPTER 5

EXPERIMENTAL APPARATUS

5.1 INTRODUCTION

The first section of this chapter describes the construction of the three novel chromatic sensors designed for use in the plasma processing industry. Each sensor is described in terms of its component sources, fibres, detectors and circuitry and their overall configuration. The similarities between the sensors have been stressed and the major differences between the sensors (largely related to the signal recovery systems) have been illustrated. The electronics of the plasma and thin film monitor are described in some detail but the oil monitor which, in electronic terms is very similar to the plasma monitor, is only discussed briefly. Discussion of the optical oil probe design is deferred to Chapter 8.

The second section describes the two plasma processing chambers monitored by the chromatic sensors and illustrates how the sensors are integrated to operate in a non-invasive manner. In each case it is significant that no alterations were required to accommodate the sensors since optical ports with 2 inch quartz windows were already fitted to accommodate spectrometers and ellipsometers.

5.2 OPTICAL DIAGNOSTICS

5.2.1 CHROMATIC PLASMA MONITOR

To implement a plasma monitor based on chromaticity, a three channel photodiode amplifier was constructed. Optical access to the plasma emission was obtained by engineering quartz windows into the chamber walls; this optical signal was coupled into a glass fibre clamped onto the window by an aluminium faceplate. Care was taken to ensure that the cone of acceptance of the fibre contained the bulk of the plasma. A schematic of the arrangement is shown in figure 5.1:

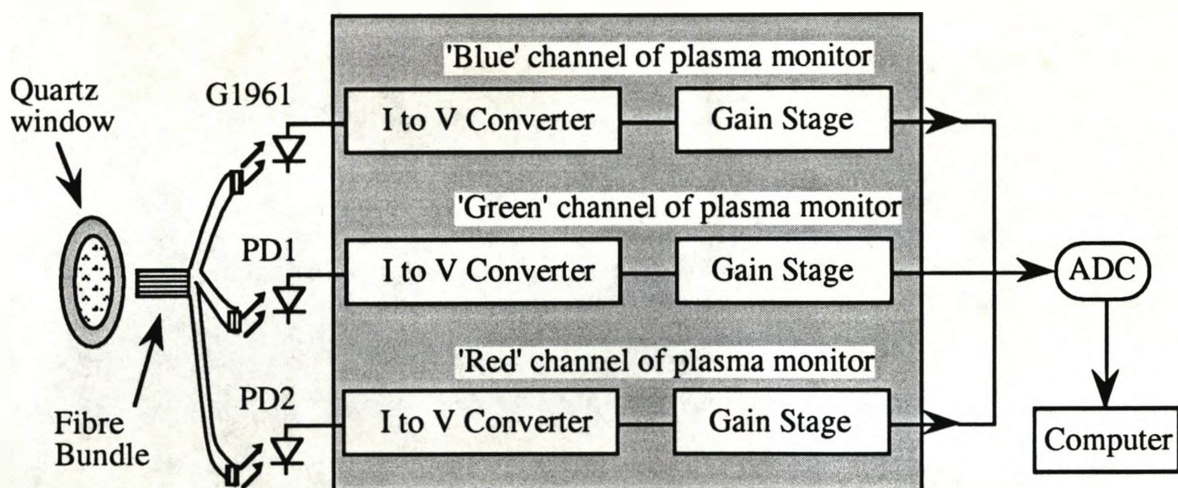

Figure 5.1 A schematic of the chromatic plasma monitor.

Optical fibres: were chosen to maximize the collection of light from the plasma, which was a relatively weak source. The largest diameter fibres available; 1mm polymer; were satisfactory for the infra-red and red channels but proved to have too great an attenuation in the blue region of the spectrum. The superior transmission characteristics of glass fibres (an order of magnitude

better in the blue) were somewhat offset by their smaller diameter (400μm) but they still delivered almost twice the optical power of the polymer fibres, as measured by the blue detector. To eliminate the effect of inhomogenous plasma emission all three fibres shared the same SMA input ferrule. Since it was possible to fit four fibres into the ferrule a four-tailed fibre bundle was constructed with one redundant fibre for use in case of damage.

A photodiode triplet: consisting of a Hamamatsu G1961(blue), a Sharp PD1(green to red) and a Sharp PD2(red to infra-red) was chosen for a combination of good responsivity, noise characteristics and spectral range. The Sharp PD1 and PD2 are packaged as a double layer photodiode (PD150 in figure 5.2) consisting two overlaid p-n junctions sharing an n doped region:

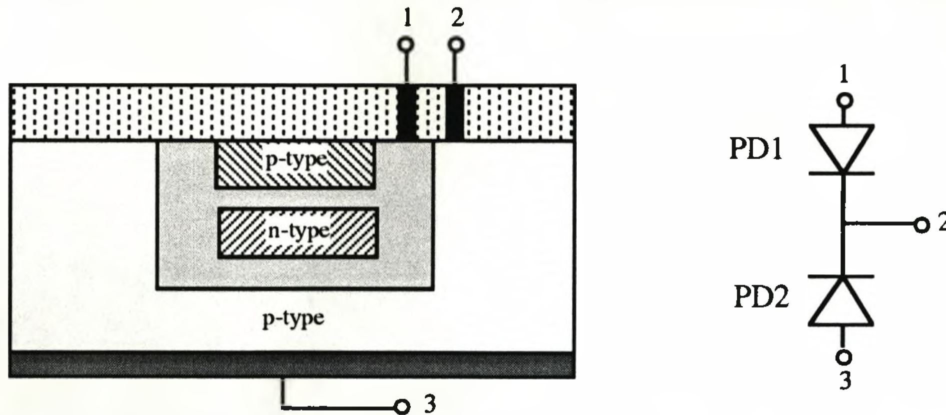

Figure 5.2 Construction of the PD150 Double layer photodiode.

This construction induces a difference in the spectral responses of the two photodiodes since the light incident on the second is filtered on passing through the first. To allow significant illumination of the second photodiode the first has to be thinner than a typical single layer photodiode; this characteristic combined with the large area of the PD150 limit the bandwidth to 2KHz. This

limit was not considered a handicap since sampling rates of 1Hz were thought adequate for closed-loop control of plasmas. The convenience of recording a distimulus value using a single photodiode and fibre which influenced the original choice of the Sharp PD150 (Moghishi 1989) is of less significance in a tristimulus system which needs a third photodiode and hence a second fibre. However the photodiode was maintained to ensure sensor compatibility with commercial chromatic sensors based on the PD150 (Lucas).

Detection Circuitry: converted the incident optical signal into an output voltage in the range 0-10V. The detector photocurrents were converted into voltages and amplified by an initial gain stage. The design shown in figure 5.3 was based on the 'low-level light sensor' circuit recommended in the Hamamatsu catalog (1989) and the components were also chosen according to those recommendations.

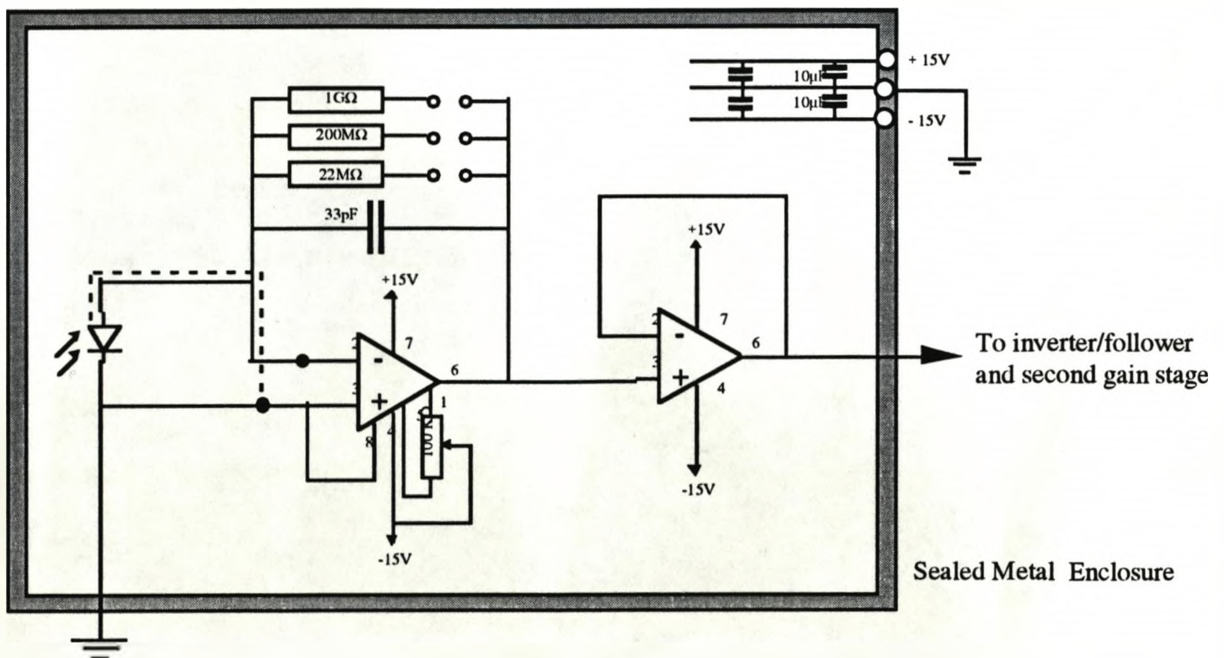

Figure 5.3 Circuit diagram of the low level light sensor

A Burr-Brown OPA-111 precision FET amplifier was chosen for this stage because of its exceptional noise characteristics. Standard feedback resistors (22-200MΩ) with a 0.25W dissipation and 5% tolerance were used to provide gain on the red and infra-red channels. Due to a combination of low plasma emission and poor detector sensitivity in the blue, that channel required a higher gain which was provided by a specialist (Eltec 1-5GΩ) metal-glaze resistor with a 5% tolerance. Specifying such large gains reduced the amplifier bandwidth to 5Hz but since the specified sampling rate was 1Hz the design proved satisfactory.

The amplified output from this gain stage was passed through an inverter/follower circuit and a second switchable gain stage (figure 5.4), allowing the external selection of an additional gain factor (1-100) by means of a panel mounted rotary switch.

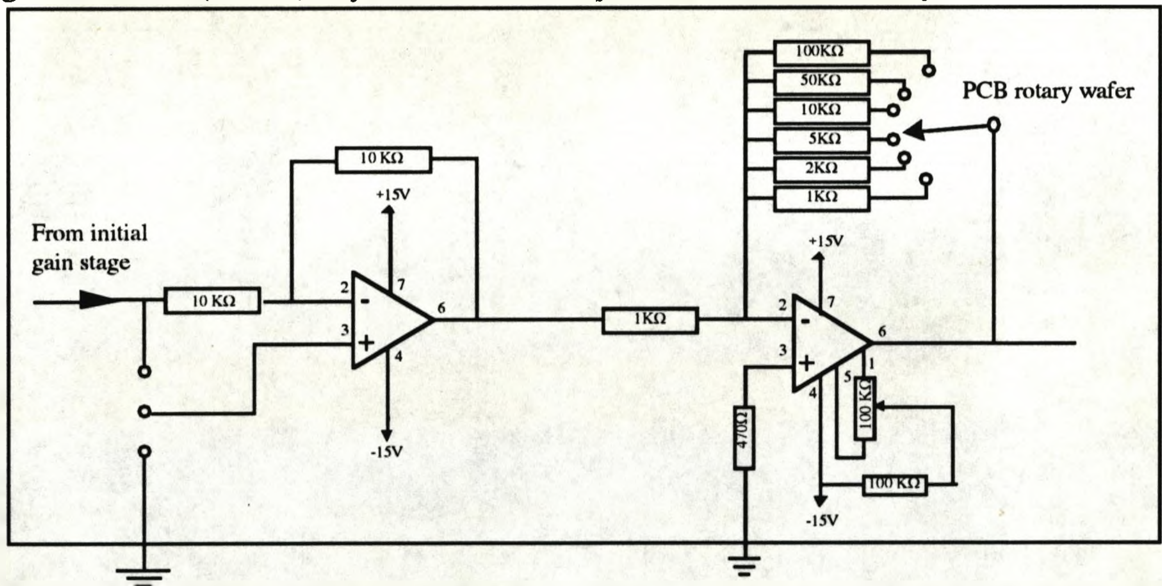

Figure 5.4 Inverter/follower circuit and second switchable gain stage.

Again following Hamamatsu recommendations the amplified signal was fed into a biasing circuit (figure 5.5) which allowed the dark current to be offset. The degree of this bias could be externally

controlled by varying the resistance of a 10 turn potentiometer mounted on the front panel of the monitor.

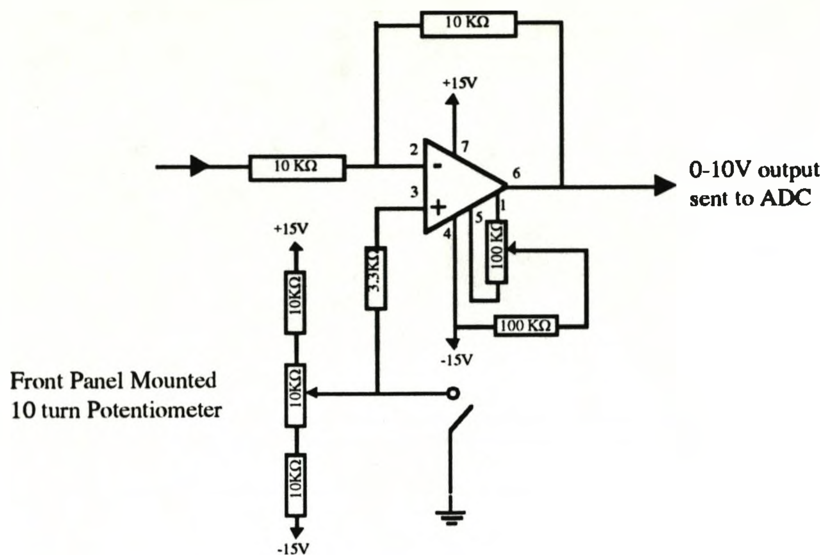

Figure 5.5 Dark current biasing circuit.

The system performance is characterised is table 5.1

Plasma Monitor Feature	Plasma Monitor Response
Range	0-10V
Electrical Noise	+/- 0.6mV
Long Term Drift	+/- 0.2mV/hour
Temperature Sensitivity	- 1.1mV/K
Bandwidth	5Hz

Table 5.1 Summary of the the plasma monitor performance.

The use of high feedback resistances in the gain stage required a number of design precautions. Radio frequency pickup was minimized by enclosing the initial gain stage in a metal shield, which was itself enclosed in the metal instrument casing. Another precaution against pickup was the use of guarded wiring between the photodiodes and the feedback resistors and capacitor.

5.2.2 CHROMATIC FILM-THICKNESS MONITOR

Although it shares many features with the plasma monitor the chromatic film-thickness monitor differs in a crucial respect. It relies on the modulation of an external source and as a result it must incorporate some form of signal recovery to prevent changes in the background plasma illumination adding a spurious and variable offset to the modulated signal. Details of the signal recovery methods are given after a brief overview of the system setup and components.

Optical access to the semiconductor wafer was obtained from a quartz window machined into the upper (grounded) electrode of the chamber, approximately 10cm above the wafer which rested on the powered electrode. This arrangement is shown in figure 5.6:

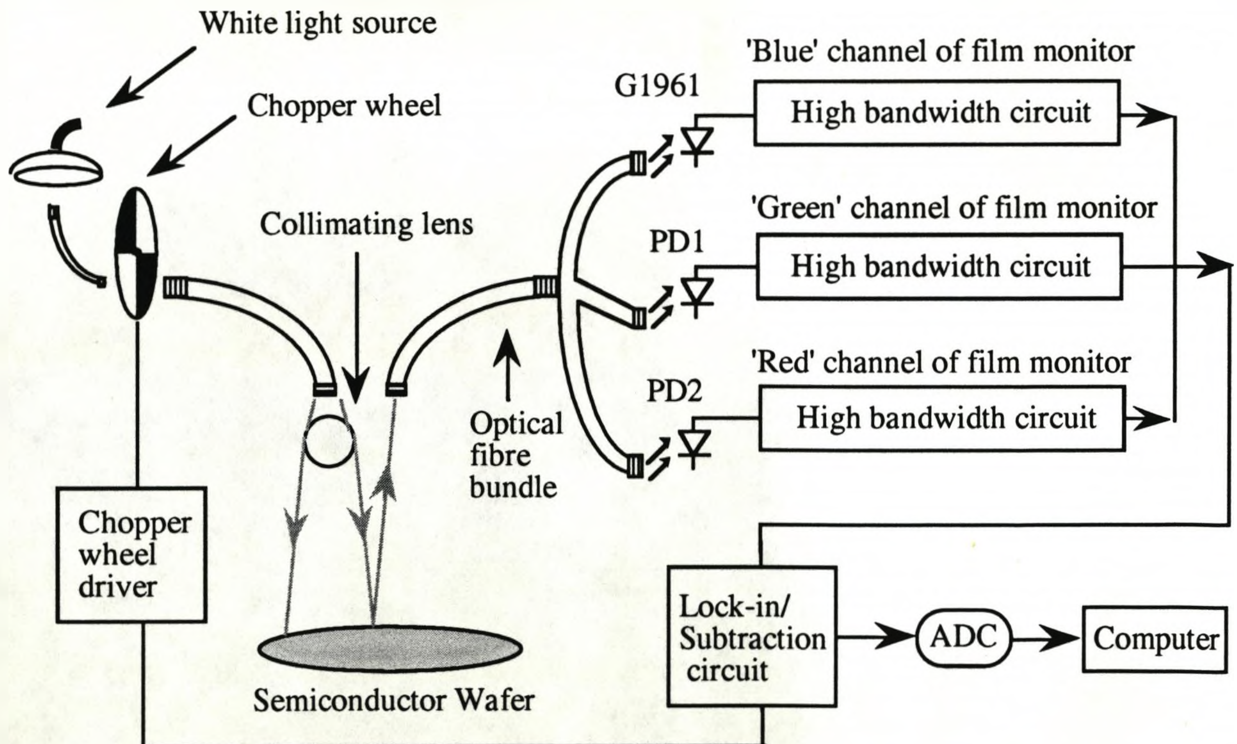

Figure 5.6 A schematic of the chromatic film-thickness monitor.

Illumination from a stabilized white light source was channelled onto the wafer surface using a fibre bundle clamped onto the window by an aluminium plate. Normal reflection off the wafer surface was captured by a three-tailed fibre bundle situated adjacent to the illuminating bundle. Each tail carried the reflected optical signal to one photodiode of a triplet.

The optical sources: selected for the sensor were a white light source designed specifically for chromatic sensing (Lucas) and an ultrabright LED. The emitter in the white light source was a standard tungsten halogen lamp with modifications in its drive circuitry serving to improve both its lifetime and noise characteristics. Short term stability was maintained by precisely controlling the constancy of the drive current. Long term drift was reduced by using an alternating current to drive the lamp, which also extended the lifetime of the lamp filament. A further improvement in filament lifetime was achieved by ensuring a gradual increase in drive current on activation, which minimized the thermal stresses accompanying a surge current in a cold filament .

From the onset of the project the advantages of using LED sources were appreciated; particularly since the signal recovery system requires rapid pulsing of the source. However no LEDs of sufficient power were commercially available until the end of the project. When the 15cd Toshiba HLMP 8100 became available it was used to develop a single channel(intensity) thin-film monitor to demonstrate the viability of an LED based chromatic sensor.

Optical fibres: were chosen to maximize the illumination of the wafer and the collection of the reflected signal. Light from the

source was guided onto the quartz window by an 8mm fibre bundle with a core consisting of numerous, randomly arranged 50μm glass fibres. The collecting fibre also consisted of numerous, randomly arranged 50μm glass fibres; these were terminated by a single SMA ferrule at one end and four SMA ferrules at the other. These somewhat expensive components were used in anticipation of difficulties related to the low levels of reflected signal. Every effort was made to maximize optical efficiency since the 1kHz bandwidth required by this sensor restricted the available gain. Furthermore the high market value of a successful thin-film monitor makes such components more suitable here than in the plasma monitor. A final optical modification was the inclusion of a collimating sphere to ensure the illumination of the wafer only and not the surrounding electrode.

The photodiode triplet: was identical to the one used for the chromatic plasma monitor. Its broad spectral response, good responsivity and low noise were key factors as was the need to ensure sensor compatibility with commercial chromatic sensors based on the PD150 (Lucas).

The signal recovery system: was designed to prevent changes in the background plasma emission adding noise to the chromatic signal reflected from the semiconductor wafer. The thin film monitor detected the chromatic signal using similar circuitry to the 'low-level light sensor' used in the plasma monitor. Subsequent signal recovery from the output of this stage was achieved by applying two distinct techniques both of which relied on the source, and hence signal, being pulsed at a precise

frequency to differentiate it from broadband noise and constant background illumination. These techniques were subtraction and lock-in amplification.

(i) Lock-in amplification: is the elimination of signals not at a defined frequency, using a voltage multiplier in series with a low pass filter. Consider a system (figure 5.7) which measures the amplitude of an optical signal beam (a_s) chopped at a precise frequency (ω_s): whilst also generating an optical reference beam with an amplitude (a_r) chopped at a precise frequency (ω_r). These beams are detected by two photodiodes P_s and P_r and the output photocurrents are converted into voltages V_s and V_r.

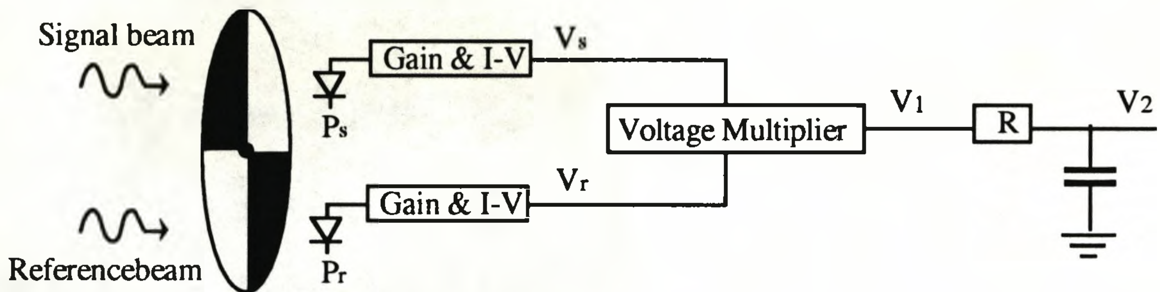

Figure 5.7 Schematic of a lock-in amplifier

When these voltages are fed into a voltage multiplier and then into a low pass filter the resulting voltage outputs V1 and V2 can be calculated from the sinusoidal signal and reference voltages

$$V_s = a_s \cos(\omega_s t + \phi_s)$$

and

$$V_r = a_r \cos(\omega_r t + \phi_r)$$

The voltage V_1 after the multiplier circuit is then:

$$V_1 = V_s V_r$$

$= a_s\, a_r \cos(\omega_s t + \phi_s) \cos(\omega_r t + \phi_r)$ Equations 5.1

$= (1/2)\, a_s a_r [\cos\{(\omega_s + \omega_r)t + (\phi_s + \phi_r)\} + \cos\{(\omega_s - \omega_r)t + (\phi_s - \phi_r)\}]$

which shows that the output of the multiplier circuit consists of a high frequency ($\omega_s + \omega_r$) beat superposed on a low frequency ($\omega_s - \omega_r$) beat both with an amplitude $a_s a_r/2$. When this signal passes through a low pass filter with a frequency response:

$$\left|\frac{V_2}{V_1}\right| = \frac{1}{\sqrt{1 + \left(\frac{\omega_s}{\omega_0}\right)^2}}$$ Equation 5.2

(where $\omega_0 = 1/\sqrt{RC}$ is the resonant frequency)

high frequency components ($\omega_s + \omega_r >> \omega_0$) are strongly attenuated so that component of the beat in equation 5.2 can be ignored:

$$V_2 = \frac{\frac{1}{2} a_s\ a_r}{\sqrt{1 + \left(\frac{\omega_s}{\omega_0}\right)^2}} \cos\left[(\omega_s - \omega_r)t + (\phi_s - \phi_r)\right]$$ Equation 5.3

Thus V_2 has a Lorentzian dependence on signal frequency assuming the reference frequency is kept constant. The peak value of V_2 is $a_s a_r/2$ and occurs when the signal frequency equals the reference frequency; incoming signals at all other frequencies are strongly attenuated. The full width at half maximum is ω_0. Although this may resemble the response of an ordinary bandpass filter there is a significant difference, when $\omega_s = \omega_r$ the time dependence disappears and V_2 becomes a constant DC signal:

$$V_2 = (1/2)\, a_s\, a_r \cos(\phi_s - \phi_r)$$ Equations 5.4

The ϕ_s-ϕ_r term is minimized by chopping the source and reference by the same wheel and residual differences by a phase shifter incorporated into the lock-in amplifier. Phase noise is still present in such a system but it is so small that it had no measurable effect on performance.

A lock-in amplifier operating in this mode was used in conjunction with the 'low-level light sensor' circuitry which provided the input signal V_s. The reference signal was generated by an LED built into the chopper wheel housing supplied with the lock-in amplifier. Only two input channels were available which posed a minor difficulty since three intensity signals were required to record colour. To overcome this two pairs from the three intensity signals (G1961,PD1,PD2) were divided (using an analogue divider) to generate two hue values (G1961/PD1 & PD1/PD2). Each hue was then used as an input signal. The output (V_2) from the lock-in amplifier was recorded onto a PC via a 12-bit ADC.

Good results (described in chapter 7) were achieved with this design but the high cost of the dual channel lock-in amplifier motivated an attempt to incorporate the signal recovery system into the circuit design.

(ii) Signal Subtraction: is perhaps the most obvious way of removing quasi-static background noise from a pulsed signal. In theory this can be implemented (figure 5.8) by simply measuring the noise with the signal off and then subtracting this stored value from the total signal and noise. However the practical implementation of this method required a significant redesign in

the sensor circuitry and for this reason its construction was deferred until the lock-in based sensor was successfully tested.

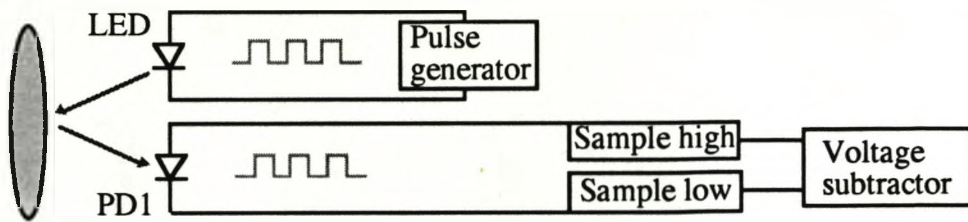

Figure 5.8. A schematic of the signal subtraction system.

The original 'low level light sensor' could have been used as the initial stage for this sensor design, but since it was designed for low bandwidth (5Hz) applications the range of available chopping frequencies would be very limited.

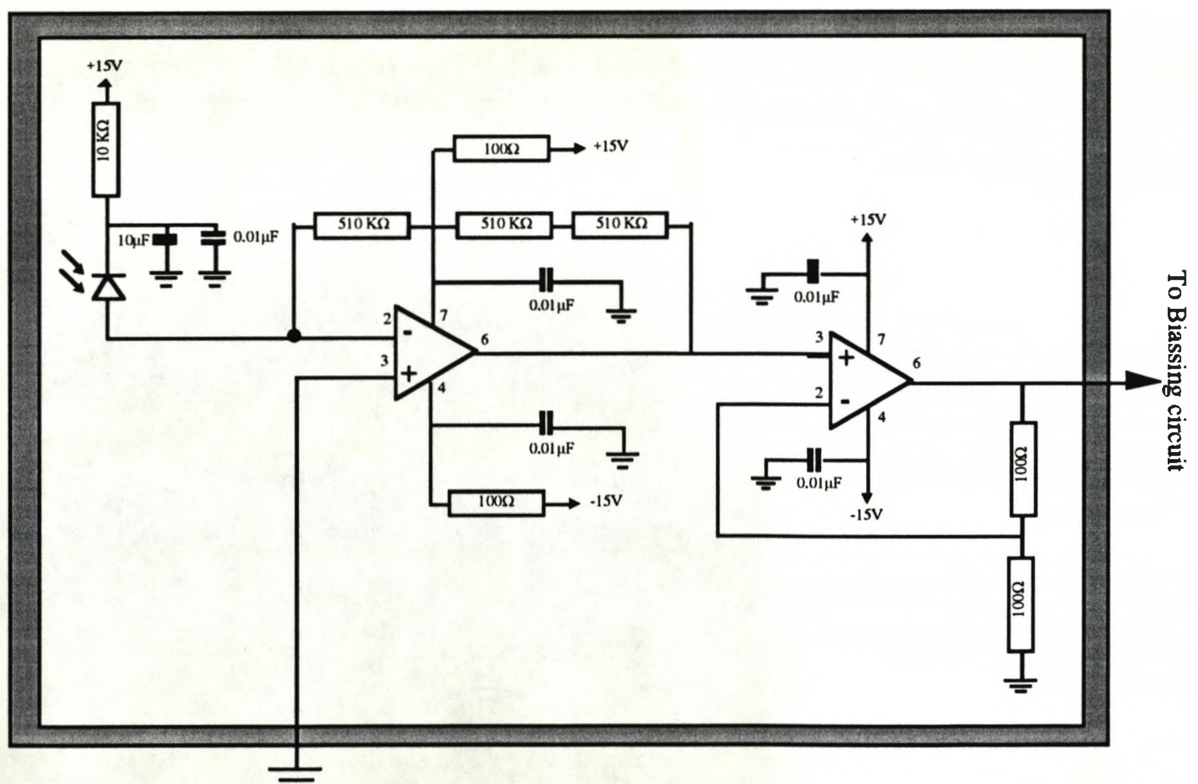

Figure 5.9 High bandwidth optical detection system.

The 1kHz chopping frequency which proved noise free on our plasma chamber might not be suitable for all plasma chambers so

a slightly different 'high bandwidth light sensor' design was chosen from the Hamamatsu catalogue with the intention of making a broader range of reference frequencies available. The circuit diagram of this sensor is shown in figure 5.9. The output of this stage was fed into a standard Hamamatsu biasing circuit, shown in figure 5.10, to eliminate photodiode dark current:

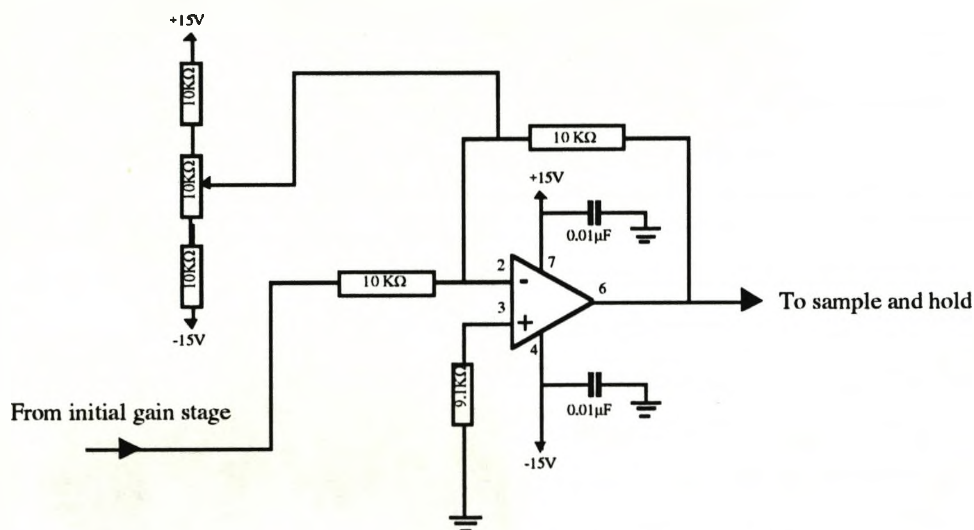

Figure 5.10 Dark current biasing circuit.

Having zeroed the dark current the biasing circuit channelled the signal to a pair of sample and hold circuits. One sample and hold circuit was triggered to sample when the reference pulse from the chopper was high implying that the white light source was unobstructed. The value stored in this circuit is the sum of the signal and the background plasma emission. The other sample and hold circuit was triggered to sample when the reference pulse from the chopper was low implying that the white light source was obstructed. The value stored in this circuit is solely due to background plasma emission. When the latter value is subtracted from the former using a

difference amplifier the resultant value is just the signal from the wafer without the background plasma emission.

The full chromatic thin-film sensor illustrated in figure 5.11, required three channels each consisting of the above circuits linked in sequence. As well as being cheaper to implement than the lock-in amplifier this system has the added advantage of being able to monitor the background emission as well, so it could be used both as a thin film monitor and as a plasma monitor.

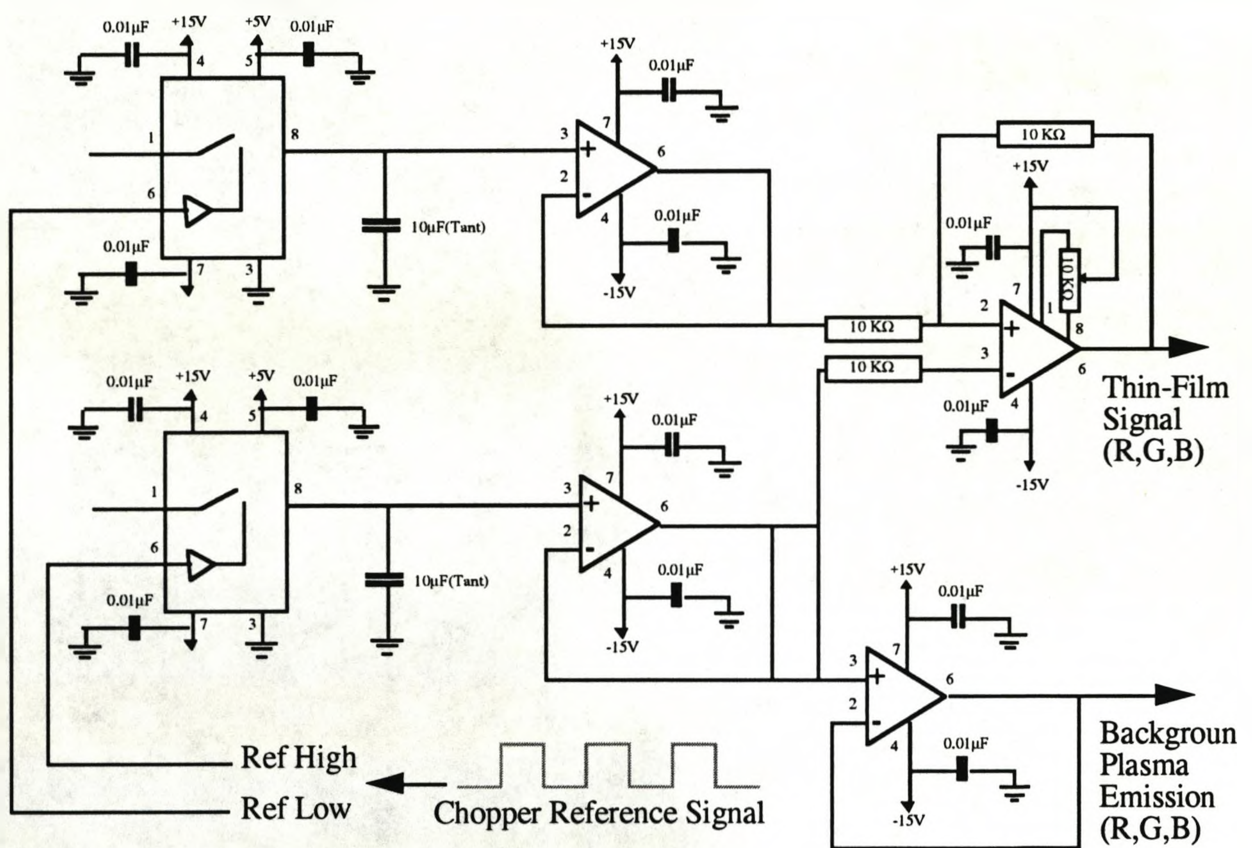

Figure 5.11 Circuit diagram of the subtraction circuit.

This subtraction based thin film monitor would be a self contained electronic sensor but for the use of a tungsten halogen source and a mechanical chopper. Ideally both these components should be replaced by a electronically pulsed LEDs. A sufficiently powerful LED was found but it was only available at red

wavelengths, although the manufacturers plan to supply amber and green LEDs of comparable power in the near future. With this in mind a single channel prototype of a pulsed LED driver circuit was constructed and the pulsed signals were used to drive the sample and hold circuits in the same way as the pulsed signals from the mechanical chopper. This source, in conjunction with the subtraction circuitry, formed an intensity sensor which was tested as a single channel prototype of an LED based chromatic sensor.
The system performance is characterised is table 5.2

Film Monitor Feature	Film Monitor Response
Range	0-10V
Circuit Noise	+/- 0.8mV
Source Noise [White Light:LED]	+/- 1.1mV : +/- 1.7mV
Circuit Drift	+/- 0.2mV/hour
Source Drift	+/- 0.2mV/hour : +/-2.1mV/hour
Thermal Sensitivity of Circuit	-0.7mV/K
Thermal Sensitivity of Source	+0.4mV/K : +1.8mV/K
Bandwidth	5kHz : 5kHz

Table 5.2. Summary of the film monitor performance.

5.2.3 CHROMATIC OIL MONITOR

The chromatic oil monitor is a simplified form of the plasma monitor which uses just the Sharp PD150 and two of the three available channels. In this reduced form the chromatic sensor measures a single hue PD1/PD2. Lacking the Hamamatsu G1961, it is in effect 'colour blind' in the blue region of the spectrum. This insensitivity in the blue is relatively unimportant since the oils examined showed very little transmission in the blue; because of

this 1mm polymer fibre was considered but 400μm glass fibre was eventually chosen since it displayed better resistance to the relatively high temperatures that might be encountered in an oil pump. The light source was the same stabilized tungsten-halogen lamp used in the chromatic film thickness monitor. The detection circuitry was identical to that used in the chromatic plasma monitor, although the high source brightness and very short optical path length permitted the use of very much lower (22MΩ) feedback resistors. A detailed description of probe design is given in chapter 8.

5.3 PLASMA PROCESSING SYSTEMS

5.3.1 DC PLASMA NITRIDING SYSTEM

Initial testing of the chromatic plasma sensor was carried out on a high current DC plasma nitriding chamber illustrated in figure 5.12. The main chamber was a 24 litre stainless steel cylinder which acted as the anode; safety considerations dictated that the chamber be grounded. An axial spindle acted as the cathode, on which the titanium samples were supported. Power to hold the cathode at a negative potential was obtained from a switched-mode power supply capable of generating up to 3KV at 150mA although working plasmas could be generated with 0.8KV at 15mA. A 5H inductor was connected in series with the power supply to store enough energy to sustain the high transient-current arcing that occurred at points of contamination.

Gas pressures were measured using an MKS 310 Baratron capacitance manometer which measures pressures up to

1333.22Pa (1Torr), an MKS 220 Baratron for pressures up to atmospheric and an ion gauge for pump-down pressures around 10^{-4} Pa. An MKS 270 gauge head unit was used as a driver for both the Baratron and an MKS 252 exhaust flow controller; this unit also provided a digital pressure readout. Flow rates were measured and regulated using MKS 1259 mass flow controllers which operated by recording the amount of energy required to sustain a fixed thermal gradient along the gas lines.

Chromatic characteristics of the emission spectrum were measured by recording the output voltages of three photodiodes on a PC via a 12-bit ADC card. These photodiodes were selected for their sensitivity and coverage of the appropriate spectral range. A combination of these diodes have been shown to discriminate 0.04nm spectral shifts (Morse 1992). Plasma spectra were obtained by the concurrent use of a Hilger-Watts 0000 spectrograph modified into a spectrometer by the addition of a stepper-motor driven exit slit which illuminated a photomultiplier. Spectral resolutions of 0.1nm were obtained but the slow scan rate of this instrument dictated a four minute scan periodicity. A Keithley Instruments 417 picoammeter was used to measure the photomultiplier output currents; these values were logged on a PC via an ADC card. Both sets of optical data were obtained through a set of glass fibre bundles with high transmission in the visible and near ultra-violet.

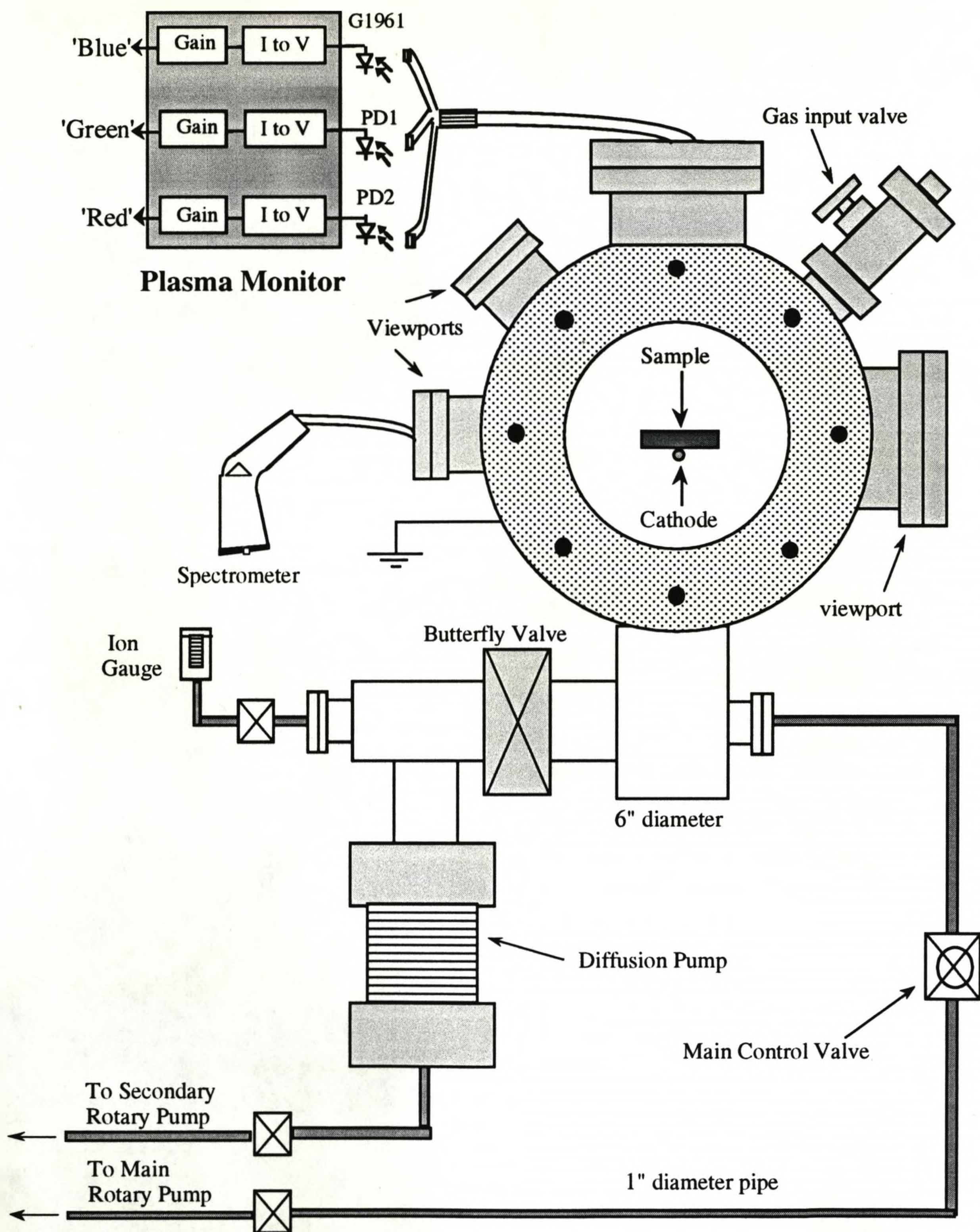

Figure 5.12 The DC plasma nitriding chamber

5.3.2 RF PLASMA ETCHING SYSTEM

A parallel-plate etching system was the subject of the majority of the experimental work presented in this thesis. Both the plasma and film-thickness sensors were used to monitor the etching characteristics of this system. Originally the system was used for commercial etching of silicon nitride and so it was considerably larger than required and came complete with integrated power supply, gas flow controllers and pressure monitors.

The etching chamber was a cylindrical stainless steel cavity with an electrode radius of 48 cm and an electrode separation of 20 cm. An anodized aluminium electrode at the base of the chamber functioned as the driven electrode whilst the rest of the chamber formed the grounded electrode. Semiconductor samples were placed on this electrode for subsequent etching. The chromatic thin film sensor was used to monitor this process through an integral two inch quartz window whose aperture permitted a line of sight normal to the electrode surface. Three further quartz windows were available giving lines of sight parallel to the electrode surface and were thus ideal optical ports for the chromatic plasma monitor. The ports were located at the '3, 6 and 9 o'clock positions'; only the last of these was used and the others were sealed to minimise background light.

As a commercial system (Leybold-Heraeus) the RF power supply was suitable for etching as many as fifty wafers at a time and so the peak power output was in the region of 3KW. The high cost of wafers limited their use to just one at a time so a lower

power range (0-300W) was selected and even then the power applied rarely exceeded 70W. Fluctuations in plasma composition result in fluctuations in plasma impedance (Semura & Satoh 1984); the resulting changes in the impedance matching mean that the ratio between the RF power absorbed by the plasma to that reflected back to the power supply can vary. To counteract this the power supply was fitted with a capacitative 'auto-tuning' system whose impedance was varied to smooth out fluctuations in plasma impedance. The effectiveness of the auto-tuning was checked by a Bird 210 RF power meter which was capable of measuring both power components.

Gas pressures were measured using capacitance manometers which measures pressures up to 1Torr, an MKS 220 Baratron for pressures up to atmospheric and an ion gauge for pump-down pressures around 10^{-4} Pa. An MKS 270 gauge head unit was used as a driver for both the Baratron and an MKS 252 exhaust flow controller; this unit also provided a digital pressure readout. Flow rates were measured and regulated using MKS 1259 mass flow controllers which operated by recording the amount of energy required to sustain a fixed thermal gradient along the gas lines.

Chromatic characteristics of the plasma emission were measured by recording the output voltages from the plasma monitor on a PC via a 12-bit ADC card. These photodiodes were selected for their sensitivity and coverage of the appropriate spectral range. The RIE parallel-plate etching system and associated optical sensors are illustrated in figure 5.13.

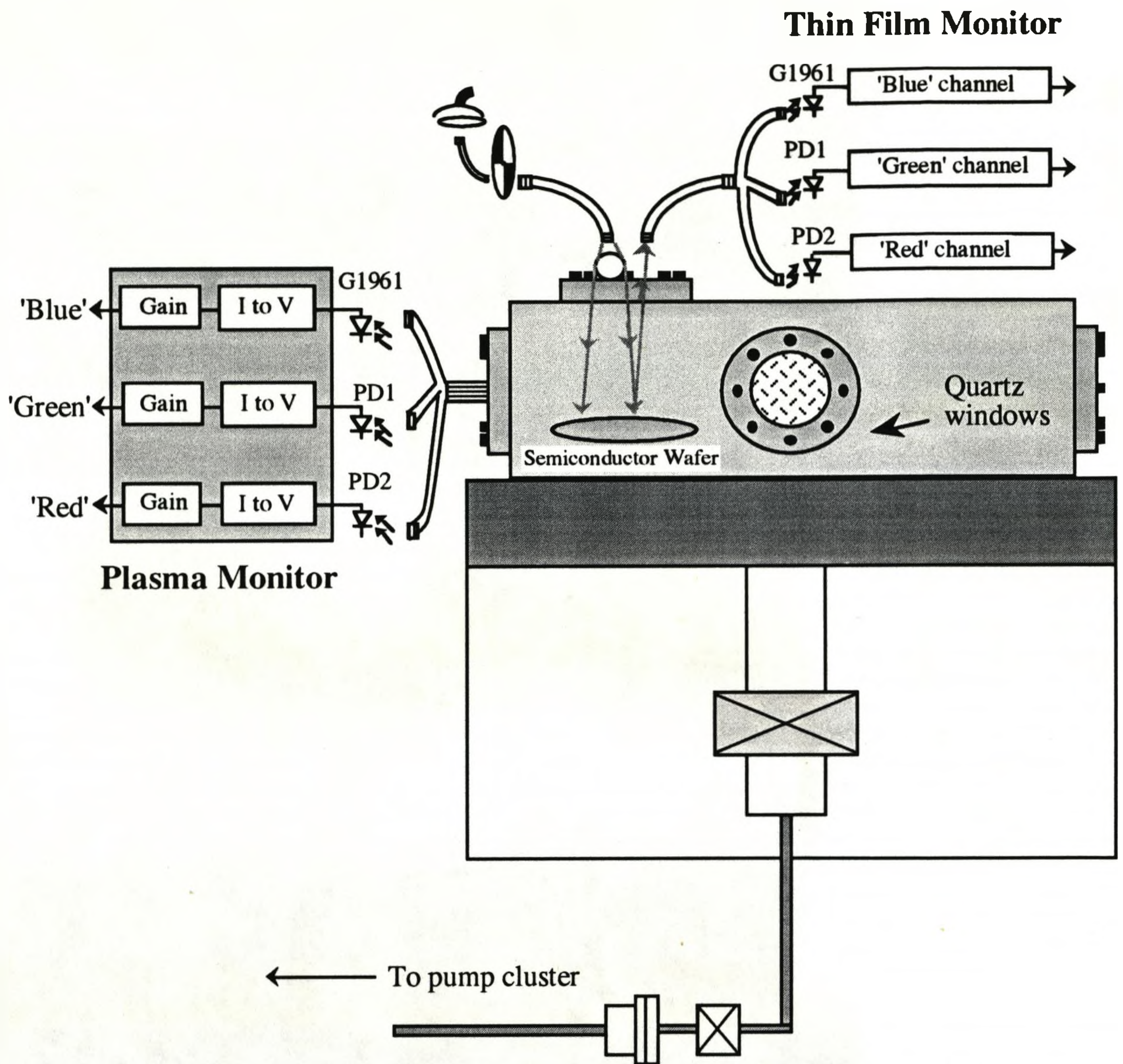

Figure 5.13 The RIE etching system and chromatic sensors

CHAPTER 6

CHROMATIC PLASMA MONITORING

6.1 INTRODUCTION

This chapter deals with the performance of the chromatic plasma monitor described in section 5.2. Initially the sensor was used to observe plasma chromaticity as a function of the plasma composition and discharge power in a DC nitriding plasma. When this sensor demonstrated the capability to discriminate between chromatic changes caused by fluctuations in plasma composition and power, an industrial semiconductor etching chamber was installed to test its performance in an area of immediate commercial interest to the project sponsors. The ability of the chromatic sensor to detect and discriminate between the chromatic changes caused by fluctuations in the plasma composition, discharge power and plasma pressure of a CF_4/O_2 semiconductor etching plasma was then determined. Finally the sensor was used to monitor chromatic changes accompanying the etching process itself. The emphasis on this experiment was placed on the detection of the etching endpoint so that the etch could be stopped at the optimum time without the excessive over-etching or undercutting described in section 2.2.

Sensor performance was judged with reference to its sensitivity to chromatic changes caused by changes in the variable parameter. The chromatic noise levels that limited sensor resolution were also investigated. This performance was compared to 'intensity' monitoring, where intensity is assumed to be proportional to the sum of the photodiode output voltages G1961+PD1+PD2. The chromatic data obtained is displayed on a chromatic plane, as discussed in section 4.2. This form of

presentation is shown to assist in the analysis of the chromatic data by yielding a set of 'contour maps' corresponding to the levels of various plasma parameters.

In each of the following experiments the emitted light was collected by a four tailed 1mm glass fibre bundle which channelled light onto three photodiodes G1961, PD1 and PD2 which were a part of the chromatic sensor described in section 5.2. The output from this sensor was stored on an IBM/PC via an analogue to digital card (ADC). The ADC used for these experiments had a 12-bit voltage resolution corresponding to 1/4096 or a 0.025% level of digitization noise. The fibre bundle was aligned so as to maximize the light intercepted from the plasma; it was then clamped to a quartz window on the chamber by an aluminium plate in order to ensure mechanical stability.

6.2 MONITORING DC NITRIDING PLASMAS

During a DC nitriding process, knowledge of plasma composition is particularly important for the detection of leaks (Hancock 1991). A typical leakage condition might be the gradual introduction of atmospheric nitrogen into the process chamber so this event was staged to test the chromatic monitor. Another critical variable is power discharged in a plasma, since this can determine the rate at which nitride deposition occurs. Both these parameters can be monitored by a few human experts who can observe and interpret the plasma colour (Hancock 1991). In consequence these processes were chosen as an initial test for the chromatic plasma monitor.

Variations in plasma mixture and power were investigated in an effort to determine whether chromatic techniques were capable of distinguishing between the spectral changes caused by varying either parameter. If such discrimination is possible then a significant advantage over intensity sensing will have been demonstrated. Conventional spectra were examined (Morse 1992) to ensure that the three photodiodes had spectral responses appropriate to the changes in plasma emission.

6.2.1 PERFORMANCE IN DC PLASMA MONITORING

Plasma composition: Pure hydrogen was introduced into the process chamber at a pressure of 1 Torr and a 20W plasma discharge initiated, the flow rate was kept at 40sccm (standard cubic centimetres per minute). Nitrogen was then introduced into the chamber in a sequence of controlled releases in which its flow rate was ramped by 10sccm with a corresponding decrease in hydrogen flow; thus increasing the relative concentration of nitrogen in steps of 20%. Each new plasma mix was maintained for one minute to allow the conditions to settle.

Large spectral changes were expected in the red region of the spectrum (Morse 1992) where the chromatic sensor should be sensitive. Visual inspection revealed that as the nitrogen concentration in the H_2/N_2 plasma was increased, its hue changed markedly from light blue to vivid pink. The intensity of the plasma emission also appeared to decrease as a function of hydrogen concentration. The observations relating to hue were confirmed by the chromatic sensor which showed the increase in the 'blue' component of chromaticity as function of increasing hydrogen concentration:

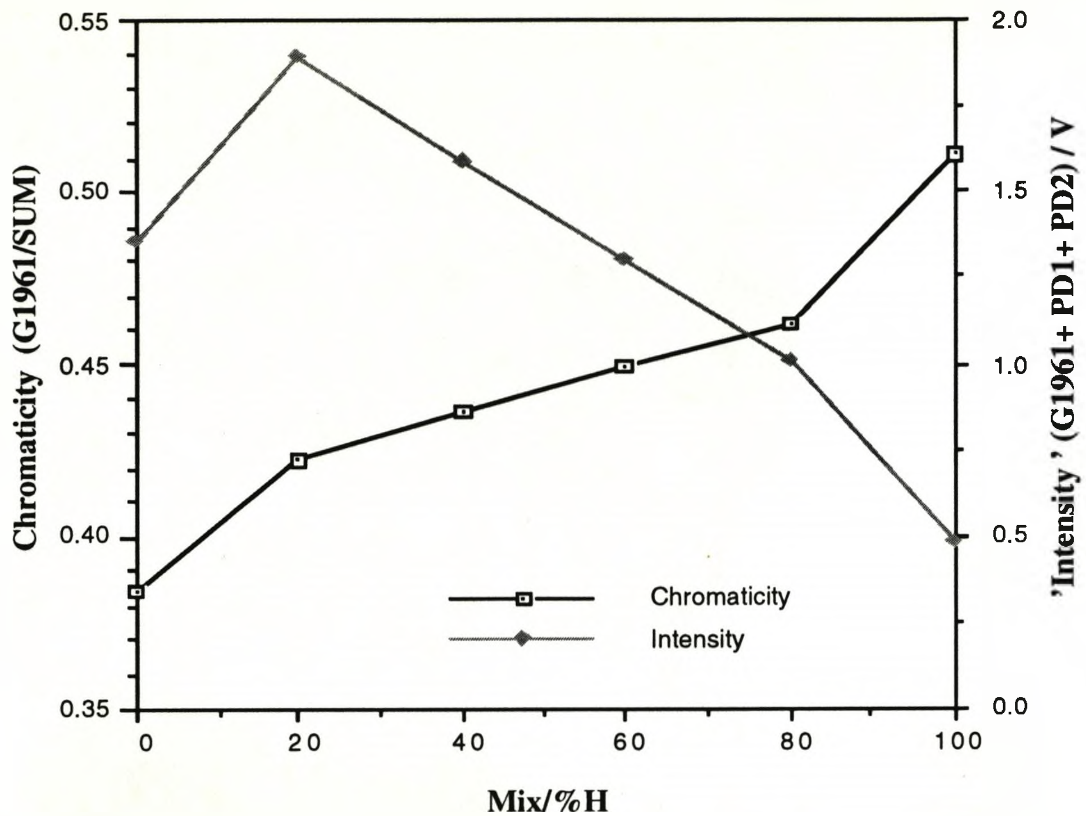

Figure 6.1 The change in plasma chromaticity and intensity as a function of increasing hydrogen concentration.

The intensity response of the chromatic sensor was somewhat unexpected in that its dependence on increasing hydrogen concentration showed an initial increase followed by a decrease, as illustrated in figure 6.1. This behaviour was not detected by the eye but since the experimental procedure did not allow continuous inspection it may be explained by the inconsistencies in the dark adaptation of the human eye when subjected to fluctuations in background illumination.

Chromatic monitoring of plasma composition shows better linearity than intensity monitoring when studying changes in a

mixture of hydrogen and nitrogen. The chromaticities of pure nitrogen or hydrogen do not lie on the same straight line occupied

by the chromaticities of their mixtures, the significance of this is discussed in the following section. Chromatic sensitivity to mixture as calculated from the linear region is 0.05 for an 80% change of hydrogen in nitrogen, the chromatic noise component of 0.00025 on the 0.05 modulation corresponds to an ability to resolve (ratio of noise to modulation depth, Eckman 1966) 1% changes in the composition of a hydrogen/nitrogen mixture.

Discharge power: Nitrogen was introduced into the plasma chamber at a flow rate of 40sccm. The power deposited by a constant current arc was ramped from 20W to 40W in 5W steps by appropriate increases in the arc voltage. The chromaticity of pure nitrogen was recorded with discharge powers of 20W and 40 W; each new power level was maintained for one minute to allow the conditions to settle.

As before significant spectral changes were expected in the red region of the spectrum although the differences in spectral profile between pure nitrogen plasmas at 20W and 40W should be less marked than for varying plasma compositions (Morse 1992). Perhaps because changes in power did not result in the creation of new spectral lines, visual detection proved difficult; it was thought that the pink emission became visibly redder but this was difficult to confirm due to the changes in emission intensity.

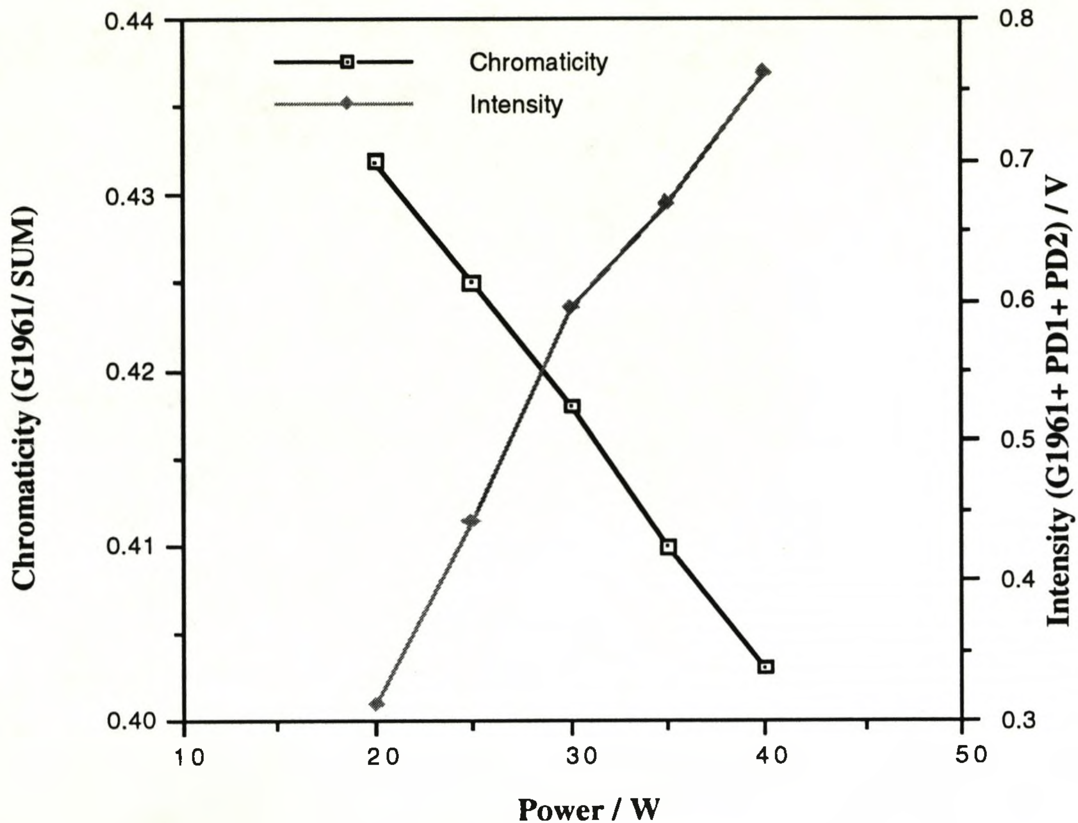

Figure 6.2 The change in chromaticity as a function of increasing power with the change in plasma intensity for comparison.

It is significant that the decrease in the 'blue' component of chromaticity is apparent from the output of the chromatic sensor (figure 6.2), demonstrating its advantage over an inexperienced observer. Figure 6.2 shows the intensity response of the chromatic sensor, the approximately linear increase with power is consistent with the published spectra (Morse 1992).

Chromatic monitoring of discharge power shows good linearity when analyzing changes in a mixture of hydrogen and nitrogen. The chromatic sensitivity to power is 0.0016 per Watt. The chromatic noise component of 0.00025 corresponds to a resolution of 0.3W, considerably better than any observer tested.

6.2.2 DISCUSSION

A linear chromatic response to a change in plasma parameter has two implications; that the conditions for additive colour mixing are satisfied and that the shift in the plasma emission spectrum has a linear relationship with the varied parameter. Additive colour mixing is only valid if the plasma has minimal self-absorption and scattering. Linearity between a parameter and its resultant spectral shift may not be valid if a new emitting species is created in the plasma, or if excited species interact with each other (Billmeyer & Saltzmann 1966).

One possible mechanism for the observed linear chromatic response to power, is a shift in the black body radiation generated by electrical heating of the plasma. An increase in temperature is known to cause a linear decrease in the wavelength of the black body emission peak (Wiens displacement law). Although the peak wavelength shows a linear downshift with temperature, the accompanying change in spectral profile causes the chromaticity of black body radiation to describe a curve on the chromatic plane (Billmeyer & Saltzmann 1966). However the curvature is only noticeable over a large temperature range so the linear results are still consistent with this explanation. Attempts were made to confirm this idea by recording the plasma temperature using a thermocouple, but they proved unsuccessful because of repeated arcing, despite attempts to sheath the junction in quartz.

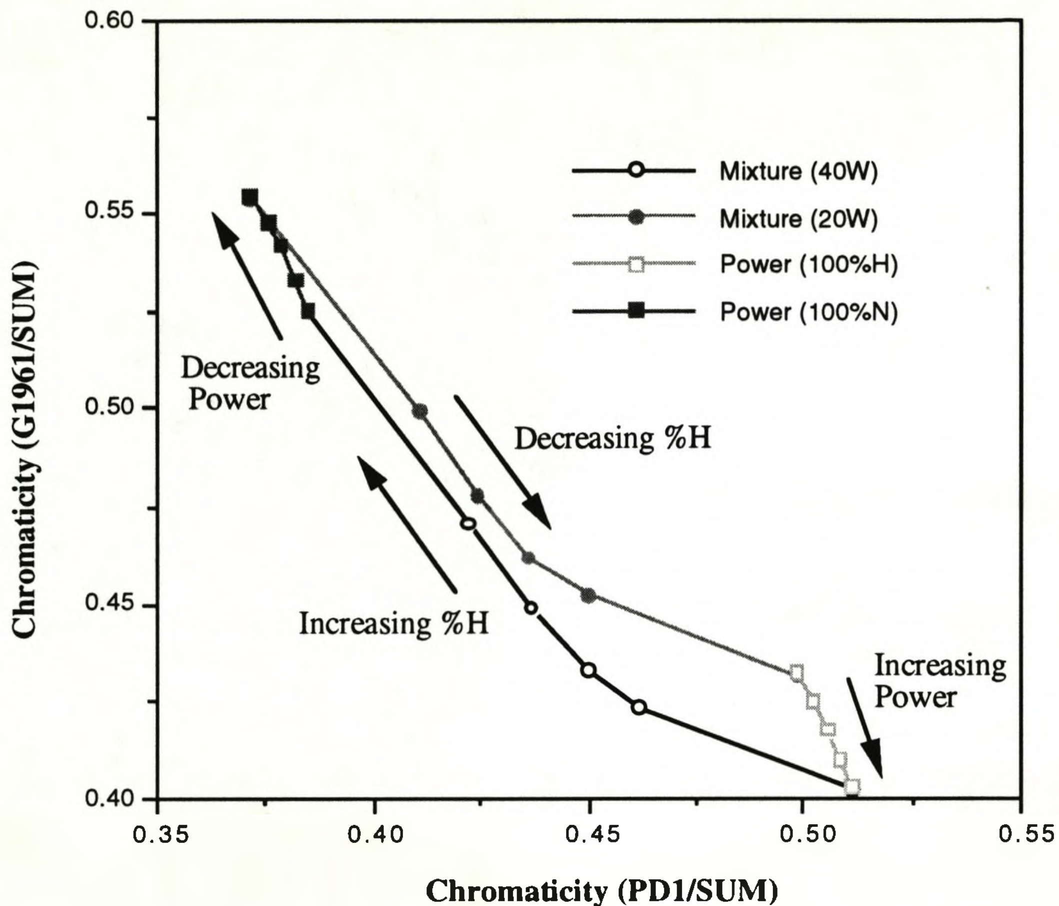

Figure 6.3 Summary of experimental data on a chromatic plane

The linearity of chromatic response to changes in gas mixture holds over the range 20%H/80%N to 80%H/20%N but significant deviations are observed for the pure gases. Figure 6.1 illustrates the anomalous changes in intensity and chromaticity that occur at the transition between pure gas and mixture. These changes indicate that the pure hydrogen and pure nitrogen plasmas interact to generate a plasma mixture with a spectrum that is not simply the sum of its constituents. It has been shown (Morse 1992) that $N\text{-}H^{+}$ emission lines form a significant part of the emission continuum of a nitrogen/hydrogen plasma; since these lines depend on the existence of both gases this may explain the chromatic deviation shown by the pure gas plasmas.

The chromatic responses to power and gas mixture trace out a contour map of the parameter value on the chromatic plane. If these contour lines were orthogonal it would be possible to measure both parameters independently simply by using the contour lines as a set of coordinate axes. Figure 6.3 illustrates the chromatic power and mixture responses; which have gradients -2.31 and -1.23 respectively when measured over their linear regions. The lack of orthogonality means that it is not possible to deduce the absolute power and mixture from an absolute chromaticity. However changes in both power and mixture would result in a chromatic shift with a gradient that is the weighted mean of the two extreme gradients. The value of the weightings might then yield the relative contributions of power and mixture fluctuations.

6.2.3 CONCLUSION

The chromatic sensor has been demonstrated to function as a real-time plasma diagnostic tool. Changes in plasma power and gas mixture have been shown to generate chromatic shifts of differing gradients. This result confirms that the chromatic sensor has the capability of discriminating between those changes in optical emission due to power fluctuations and those due to mixture fluctuations; which is beyond the capacity of intensity sensors. In addition the chromatic sensor can also monitor intensity, which is simply the sum of its three channels. This flexibility is achieved at little extra cost.

These experiments have also demonstrated the advantages of the chromatic sensor over the inexperienced human observer. The peak in intensity shown in figure 6.1 was not seen by any

observer. The significant chromatic shift shown in figure 6.2 was unnoticed visually, probably because it occurred smoothly over a broad spectral region. However, the chromatic sensor was able to detect this shift and exploit it to measure discharge power.

6.3 MONITORING RF ETCHING PLASMAS

Having demonstrated the use of chromatic sensing in plasma nitriding, commercial considerations resulted in attention being focused on semiconductor etching plasmas. Etching semiconductor wafers to fine tolerances normally requires the control and monitoring of four plasma characteristics: plasma composition, discharge power, plasma pressure and gas flow rate. Changes in the plasma composition cause discrete spectral changes, such as the appearance or disappearance of emission lines characteristic of the material causing the changes. These large spectral changes confined to specific wavelengths are easily detected by monitoring spectral lines. However changes in power, pressure and flow rate normally result in smaller spectral changes spread across the continuum of the spectrum (Kawata et al 1987).

These changes in the plasma emission continuum are normally measured using spectrometry. During this phase of experimentation a spectrometer was not available but the spectral changes in CF_4/O_2 plasmas have been reported in the literature (Kawata et al 1987). These reports raised expectations that the chromatic sensor would be capable of detecting the accompanying chromaticity and intensity changes. The following experiments are intended to investigate the possibility of using a chromatic sensor to measure both discrete and continuum changes.

6.3.1 PERFORMANCE OF THE RF PLASMA MONITOR

Plasma composition: An industry standard mixture of etchants comprising 91.5% CF_4 and 8.5% O_2 was introduced into the process chamber at a pressure of 70 mTorr. A plasma was then initiated using 60W of RF electrical power at 13.56 MHz, whilst the gas flow rate was maintained at 40sccm. Nitrogen was then introduced into the chamber in a sequence of controlled releases in which its flow rate was ramped by 2sccm thus increasing the relative concentration of nitrogen to CF_4/O_2 in steps of 5%. Each new plasma mix was maintained for one minute to allow the conditions to settle.

Visual inspection of the plasma revealed little since the plasma retained a pale pink colour throughout the experiment; changes in the intensity of the plasma emission were also too small to detect visually. Some observers claimed to see a slight reddening with increasing CF_4/O_2 concentration and the accompanying increase in intensity however there was little consensus between them. The chromatic plasma monitor succeeded in detecting both the chromatic and intensity changes resulting from the alteration in plasma composition, the sensor output is shown in figure 6.4.

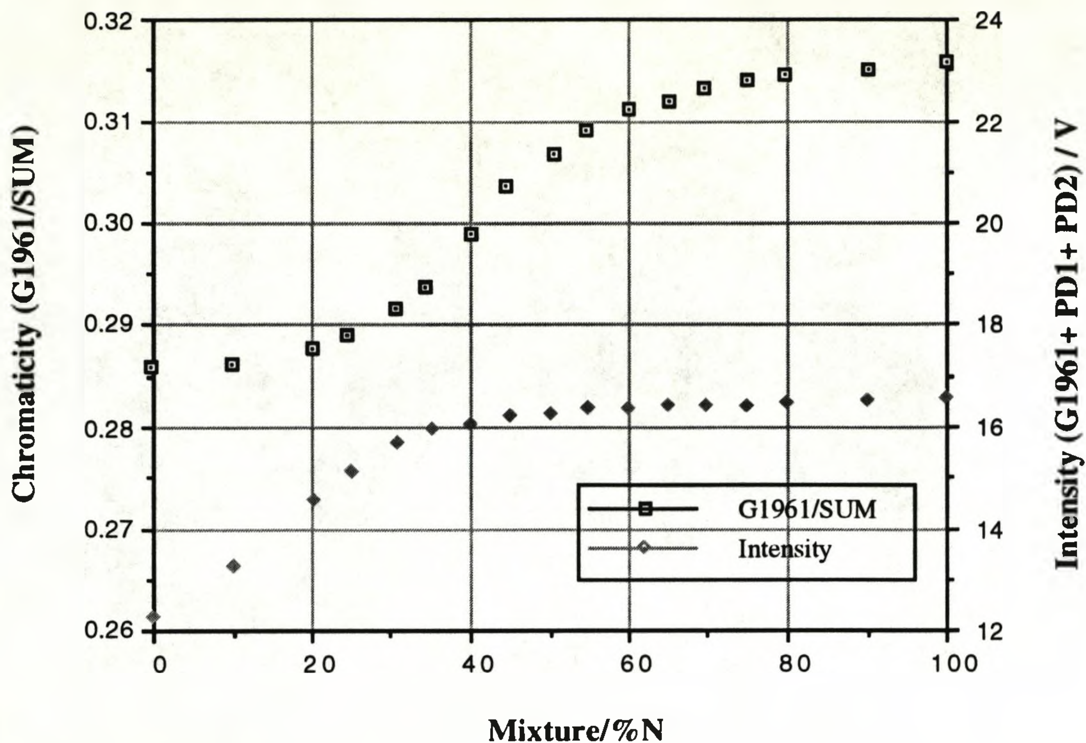

Figure 6.4 The change in plasma chromaticity and intensity as a function of increasing CF_4/O_2 concentration.

Compared to the equivalent experiment with the H_2/N_2 plasma, changes in the CF_4/O_2 fraction relative to the N_2 fraction result in a more limited linear region. Initial introduction of up to 20% nitrogen into a CF_4/O_2 plasma, gives little chromatic response. However, increasing the concentration of the introduced gas further results in a linear change in chromaticity, which eventually saturates as the gas concentration exceeds 80%. The significance of this saturation in chromatic response is discussed in the following section.

This nonlinear response makes the calculation of chromatic sensitivity somewhat arbitrary. The average sensitivity to mixture was calculated over the linear range yielding an overall chromatic change of 0.03 for a 1% change of nitrogen in CF_4/O_2.

The chromatic noise component of 0.00025 corresponds to an ability to resolve 1.7% of change of nitrogen in CF_4/O_2. The intensity response of the chromatic sensor to increasing CF_4/O_2 concentration has a somewhat higher (0.1%) noise component than the chromaticity and saturates in only one direction.

Discharge power: An industry standard mixture of etchants comprising 91.5% CF_4 and 8.5% O_2 was introduced into the process chamber at a pressure of 70mTorr. A plasma was then initiated using 50W of RF electrical power at 13.56 MHz, whilst the gas flow rate was maintained at 40sccm. The power deposited in the plasma was increased from 50W to 90W in steps of 2W. Each new power level was maintained for one minute to allow the conditions to settle.

As before visual inspection of the plasma resulted in conflicting opinions. Some observers thought that the pale pink colour of the plasma became deeper red as the power was increased but again there was little consistency between them or even between the same observer at different times. Intensity observations were somewhat more clear cut with most observers being able to distinguish between the highest and lowest power levels but showing little discrimination in the mid range. The chromatic plasma monitor was capable of detecting both the chromatic and intensity changes resulting from the increments in plasma power, the sensor output is shown in figure 6.5:

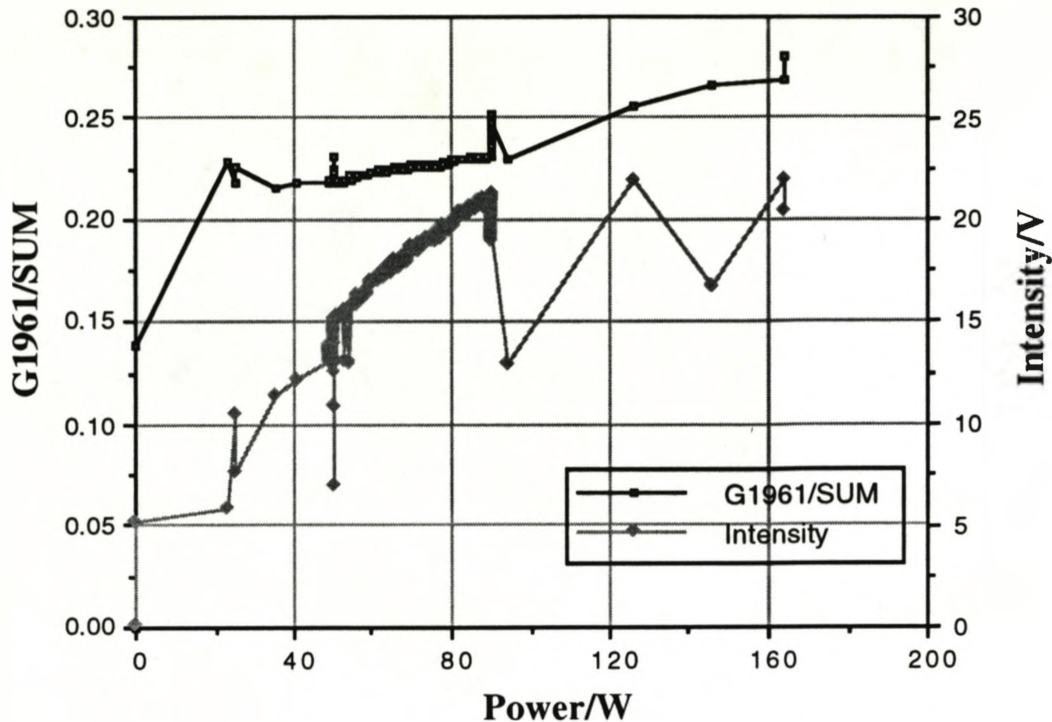

Figure 6.5 The change in chromaticity as a function of increasing power with the change in plasma intensity for comparison.

The chromatic response of the CF_4/O_2 plasma to fluctuations in discharge power has the approximately linear form that characterized the behaviour of the H_2/N_2 plasma. The intensity response of the chromatic sensor to power fluctuations in the plasma, mirrors the linearity of the chromatic response. The chromatic sensitivity to power was calculated over the linear range, yielding an overall chromatic change of 0.0005 per Watt (0.02/40). The chromatic noise component of 0.00025 yields a sensor resolution of 2W.

Plasma pressure: An industry standard mixture of etchants comprising 91.5% CF_4 and 8.5% O_2 was introduced into the process chamber at a pressure of 70mTorr. A plasma was then initiated using 50W of RF electrical power at 13.56 MHz, whilst the gas flow

rate was maintained at 40sccm. The pressure at which the CF_4/O_2 plasma was maintained was decreased from 70mTorr to 40mTorr in steps of 2mTorr.

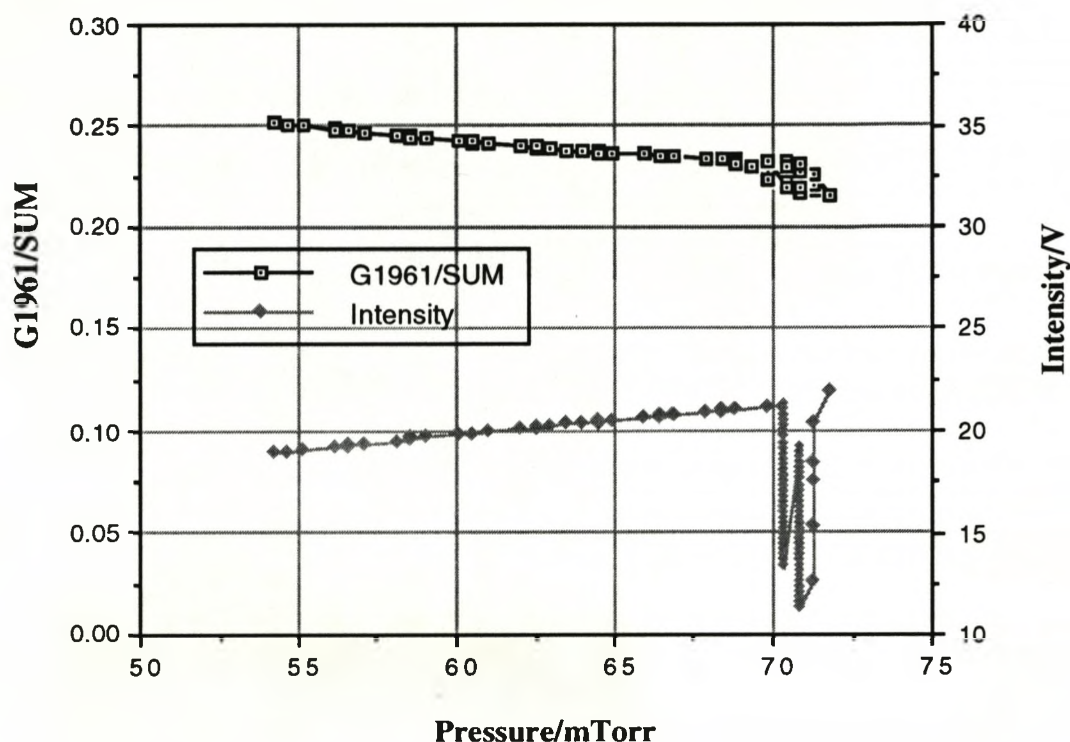

Figure 6.6 The change in chromaticity as a function of increasing pressure with the change in plasma intensity for comparison.

Each new pressure level was maintained for one minute to allow the conditions to settle. Visual inspection of the plasma was inconclusive with regard to both plasma colour and intensity but the chromatic plasma monitor was capable of detecting both the chromatic and intensity changes resulting from the changes in plasma pressure, the sensor output is shown above in figure 6.6.

The chromatic response of the CF_4/O_2 plasma to fluctuations in pressure shows strong linearity. The intensity response of the chromatic sensor to plasma pressure fluctuations, shows a

linearity similar to that of the chromatic response. The chromatic sensitivity to pressure was calculated over the entire range yielding an overall chromatic change of 0.03 for 1 mTorr. The chromatic noise component of 0.00025 yields a sensor resolution of 1.7mTorr.

6.3.2 DISCUSSION

The conditions necessary for linear chromatic response to a change in plasma parameter; the validity of additive colour mixing and the linearity between spectral shift and plasma variable; were refered to in section 6.2.2. Additive colour mixing is only valid if the plasma has minimal self-absorption and scattering. Linearity between a parameter and its resultant spectral shift may not be valid if a new emitting species is created in the plasma, or if excited species interact (Billmeyer & Saltzmann 1966).

The nonlinear dependence of chromaticity on mixture indicates that the pure CF_4/O_2 and pure nitrogen plasmas interact to generate a plasma mixture with a spectrum that is not simply the sum of its constituents. It has been shown that a significant part of the emission continuum in a $CF_4/O_2/N_2$ plasma are generated by interactions between fluorine and oxygen radicals attacking the nitrogen molecule (Cockrill 1990). Since such form of chemical attack can only occur when both gases coexist in the plasma this may explain the chromatic deviation from linearity (figure 6.4) shown by the pure gas plasmas when compared to the chromaticity shown by their mixtures. If this inference is correct it would demonstrate the usefulness of a chromatic sensor for deducing qualitative trends in spectra without requiring complete spectral information.

The linear chromatic response to power observed in H_2/N_2 plasmas is repeated in $CF_4/O_2/N_2$ plasmas. This was expected since the probable explanation; a shift in black body radiation generated by electrical heating of the plasma; is a physical effect independent of the chemical constitution of the plasma. Increases in temperature are known to cause linear decreases in the wavelength of the black body emission peak (Wiens displacement law). This downshift (or blueshift) in plasma spectral profile translates to an increase in G1961/Sum with increasing temperature and hence increasing discharge power; this variation is exactly what is shown in figure 6.5. Direct confirmation of this idea; by using a thermocouple to record plasma temperature; was not possible due to insulation difficulties. Figure 6.5 also serves to illustrate the self referencing advantages of a chromatic sensor. When the power was at 70W a plasma instability (created by the onset of rapid power changes) caused a 100% fluctuation in intensity which was accompanied by 10% chromatic fluctuation.

The linearity of the chromatic response to pressure is also striking. Aside from some plasma instabilities generated at 70mTorr figure 6.6 illustrates this chromatic linearity. In contrast much larger fluctuations are suffered by the intensity and since the modulus of the chromatic and intensity gradients are very similar, this difference is not due to any pronounced differences between chromatic and intensity sensitivity. Without spectral information the origin of this linearity is difficult to isolate but the implication is that pressure changes in this range simply rescale and/or skew a spectrum without giving rise to any new features. The introduction of extra molecules into a plasma would be expected to increase the overall plasma intensity (rescaling)

merely by increasing the number of emitters. Skewing a spectrum would require differential changes in intensity across all emitting lines; such differential changes are characteristic of equlibrium chemistry (Fonash1985). If changes in plasma pressure result in a surfeit of some ions the equilibrium will be shifted resulting in a skew in the observed plasma spectrum. The confirmation of this idea must await a spectrometric study.

A major strength of chromatic monitoring is its capacity to distinguish between changes caused by different variables, the basis of which was discussed in section 4.2.5. Changes in two variables should manifest themselves as two straight lines of chromaticity with different gradients. Indeed if the variables are varied in a cyclic manner these lines of chromaticity should describe a ‘parallelogram of colours’; by analogy with parallelograms of force it should then be possible to resolve a chromatic change into its components.

The power in a CF_4/O_2 plasma was ramped from 54mTorr to 70 mTorr and back again in increments of 2mTorr. Alternating between the increases and decreases in pressure the discharge power was ramped from 50W to 90W and back again in 2W increments. The chromatic changes in the resulting plasma emission were all linear as shown in figure 6.7. In the case of pressure changes the chromatic gradients were identical for high and low power plasmas. However the power changes at low and high pressures showed a marked difference in gradient. This difference means that discrimination between power and pressure effects are easy in high pressure plasmas and become more difficult as the pressure falls:

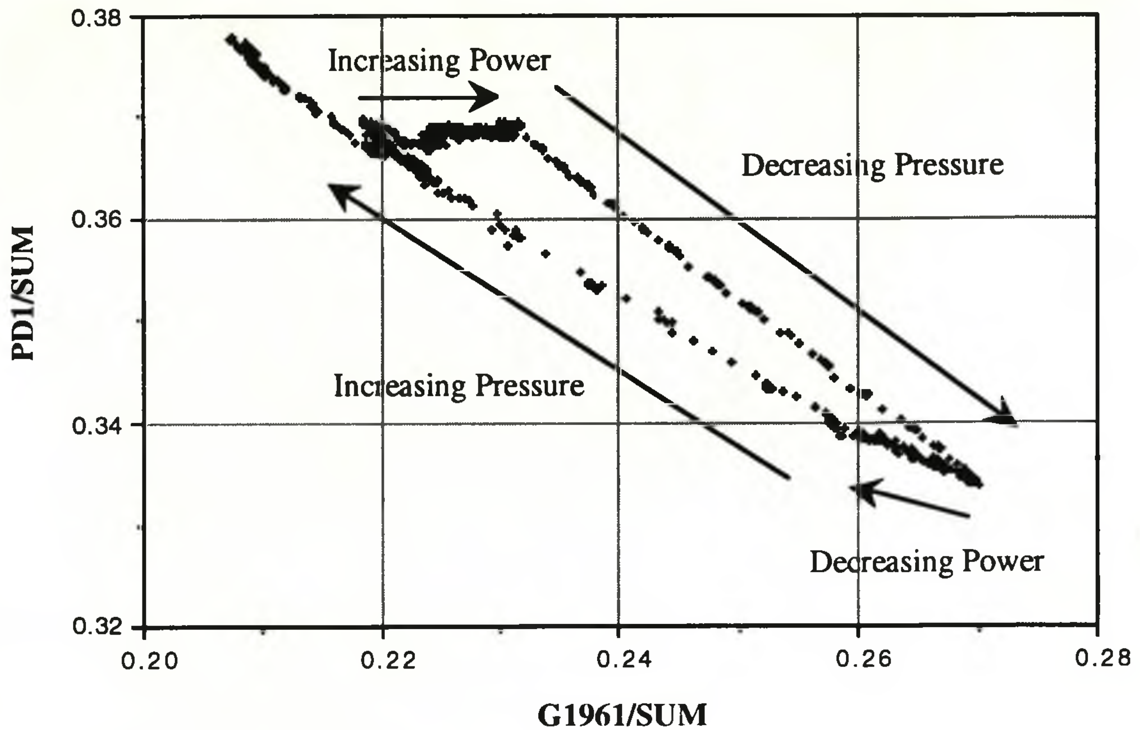

Figure 6.7 Power and pressure changes on a chromatic plane

The power in a CF_4/O_2 plasma was ramped from 60W to 100W and back again in increments of 2W. Alternating between the increases and decreases in power the plasma composition was ramped from 100% CF_4/O_2 to 100% nitrogen and back again in 5% increments. The breakdown of chromatic linearity as a function of mixture, discussed in the previous section, is apparent in figure 6.8. In the case of mixture changes the chromatic gradients were identical for high and low power plasmas. As before the power changes at low and high mixtures are linear and show a marked difference in chromatic gradient making interpretation difficult. This interpretation is made more difficult by the characteristic departures from chromatic linearity at low gas concentrations.

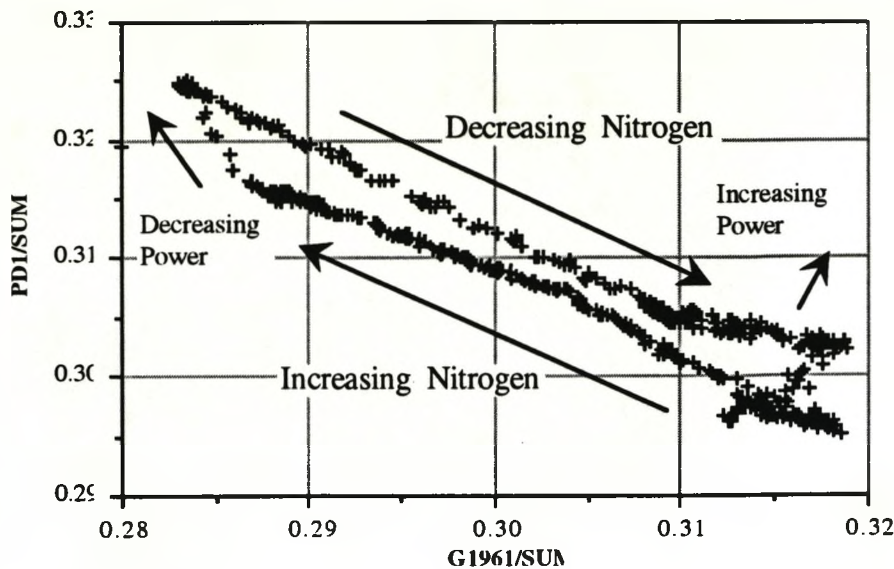

Figure 6.8 Power and mixture changes on a chromatic plane

6.3.3 CONCLUSION

The viability of real-time plasma diagnosis by chromatic techniques has been demonstrated. Power and pressure changes were shown to cause linear shifts in chromaticity. Changes in chromaticity were found to be linear for mixture changes in the range 80%H_2-20%N_2 to 20%H_2-80%N_2, but significant deviations were observed outside this range. Changes in plasma power, pressure and composition have been shown to generate chromatic shifts of differing gradients. This raised the possibility of using chromatic monitoring to distinguish between changes caused by these variables. ,

Changes in two variables manifested themselves as two straight lines of chromaticity with different gradients. The theory for resolving composite chromatic changes (section 4.2.5) caused by composite changes in variables, predicts that this can be accomplished by resolving the total chromatic change into two chromatic vectors. Although the interpretation is slightly more

difficult than this, chromatic monitoring was found to be significantly superior to intensity sensing.

When used in conjunction, the three photodiodes are capable of measuring the hue and saturation of a plasma emission spectrum, in addition to the intensity measured by traditional photodiode sensors. Hue and saturation can be mapped onto a chromatic plane, each point of which corresponds to a set of spectra. Although many spectra can be mapped onto a single point on the chromatic plane the degree of degeneracy is less than that of intensity sensors where spectra map onto points restricted to a line. Chromatic sensing is shown to retain the cost and sampling rate advantages of intensity sensors whilst demonstrating an ability to detect spectral shifts; more often associated with spectrometry.

6.4 MONITORING ETCHING ENDPOINTS

The preceding bare chamber observations serve to illustrate the principle of chromatic plasma monitoring. However a major market for such sensors is in the detection of etching endpoints; an application in which spectrometers are currently used (Cockrill 1990), despite the complexity and expense. The detection of this endpoint allows the etch to be stopped before mask undercut or substrate damage can occur as discussed in section 2.2.

At the endpoint the rate of etchant depletion suddenly decreases as does the rate of substrate sputtering causing large changes in plasma composition. Since changes in composition also cause changes in plasma pressure and discharge power (Lochte-Holtgreven 1968), the results in the previous section indicate that

the chromatic sensing of such endpoints is viable. This possibility was investigated in a series of experiments conducted using the same chromatic plasma sensor described above.

Initially the semiconductor etching facilities required were not available in the laboratory so the chromatic plasma monitor was installed on a commercial semiconductor plasma etch chamber (μP800) at GEC-MMT Caswell. At this site a spectrometer was also available to monitor changes at precise wavelengths. The μP800 was a plasma etch chamber operating primarily on chemical etching but recently interest has turned to RIE chambers relying on physical-chemical etching (section 2.3). In response to this the etching experiments were repeated on a newly installed RIE chamber. The objective of both experiments was to confirm that the chromatic plasma monitor was capable of detecting etch endpoints in addition to recording changes in plasma parameters.

6.4.1 MONITORING ETCH ENDPOINTS

Plasma Etching: The etching gas used in the μP800 was an industry standard mixture of 91.5% CF_4 and 8.5% O_2. This etchant was introduced into the chamber at a rate of 70 sccm until the pressure reached 300mT. A plasma was initiated with 30W of RF energy and the emission spectrum was recorded with no sample in the chamber. This procedure was repeated with a 5 inch silicon wafer (coated with 2400Å of silicon nitride) present in the chamber. The silicon nitride layer was etched under these conditions and an emission spectrum was acquired during this etch. To highlight the differences between the spectra the second spectrum was subtracted from the first as shown in figure 6.9.

μp800 etching spectra recorded using a SOFIE SD20
Parameter: $CF_4/8.5\%O_2$, 70sccm, 200mT, 25W

3/ 5/90 10:10:21

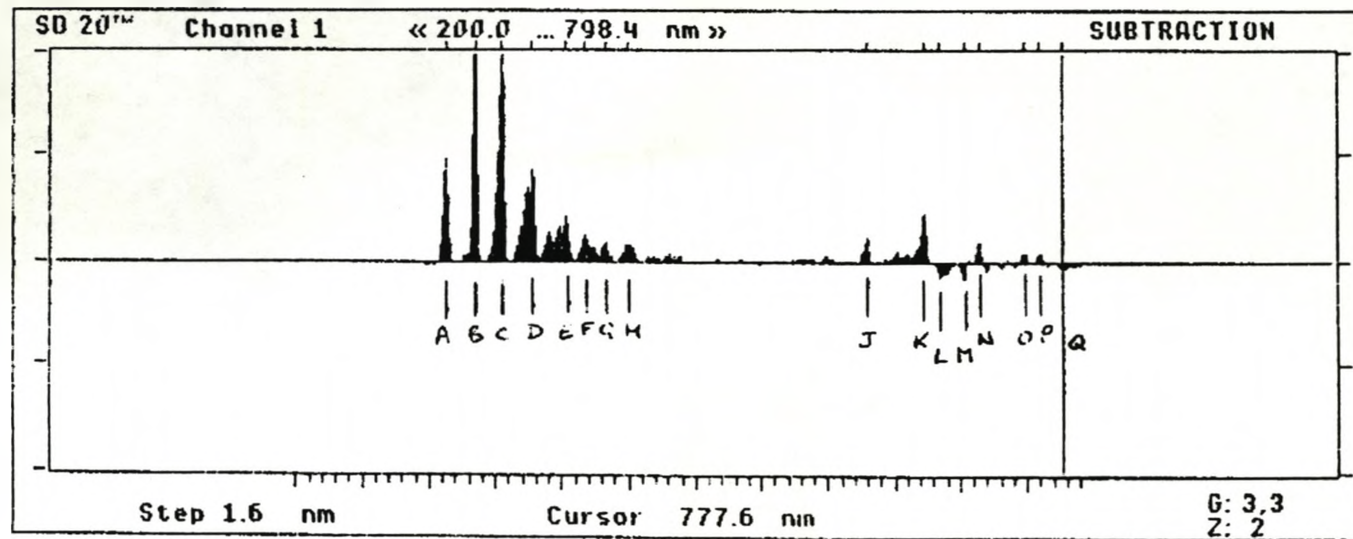

Figure 6.9 Subtraction spectrum of an etching plasma
Lines A to M are from CF_4 whilst N to Q are unique to oxygen

Seventeen spectral lines (A-Q) characteristic of CF_4/O_2, (Mogab 1978) are shown. No change in Si or N_2 lines were noticed.

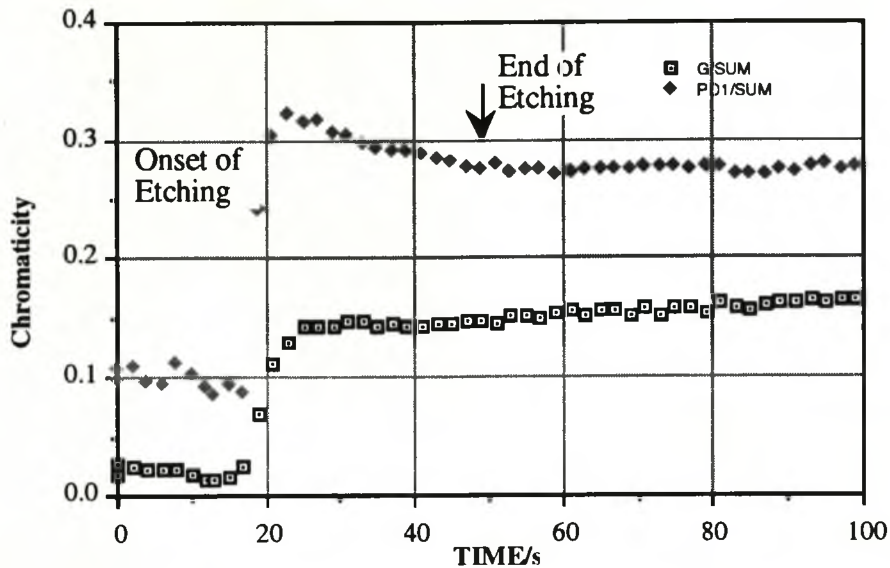

Figure 6.10 Chromatic changes during a plasma etch process

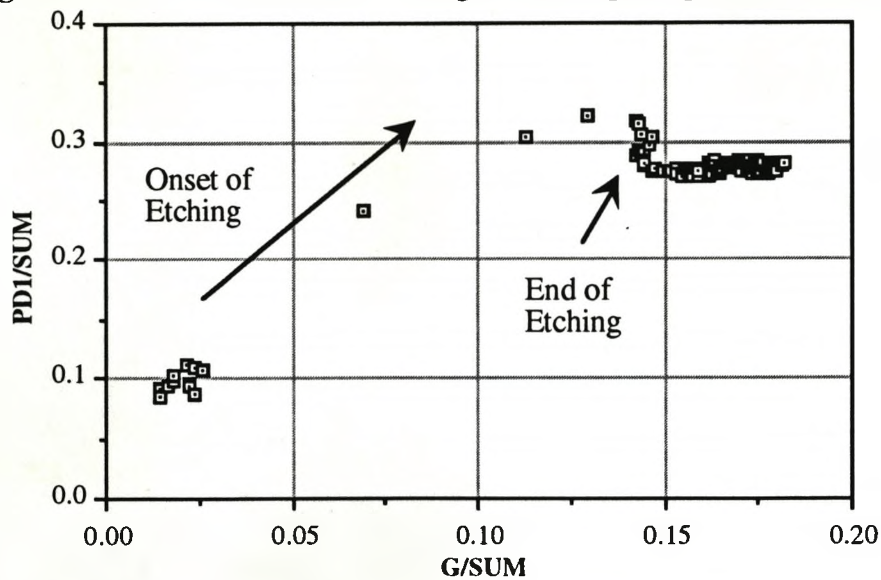

Figure 6.11 A plasma etch represented on a chromatic plane

The chromatic changes accompanying these spectral changes are shown in figure 6.10. The 'blue' chromaticity represented G/Sum shows a sharp upward change at the onset of etching but barely shows any change at the end of etching (which was also monitored by spectroscopy). The 'red' chromaticity shows a sharp increase on

the onset of etching but in contrast to the 'blue' it shows a small (0.004) decrease at the end of etching. Allied to a chromatic noise of 0.00025, this means that an endpoint can be detected to within 1 part in 8. Figure 6.11 displays these traces on a chromatic plane, the end of etching being represented by a curved line of chromaticity.

RIE Etching: The etching gas used in the RIE chamber was an industry standard mixture of 91.5% CF_4 and 8.5% O_2. This etchant was introduced into the chamber at a rate of 40sccm until the pressure reached 70mT and plasma was initiated with 60W discharge of RF energy. The substrate was a 3 inch gallium arsenide wafer coated with 2400Å of silicon. During the etch process the silicon nitride layer was etched whilst the gallium arsenide layer was left intact.

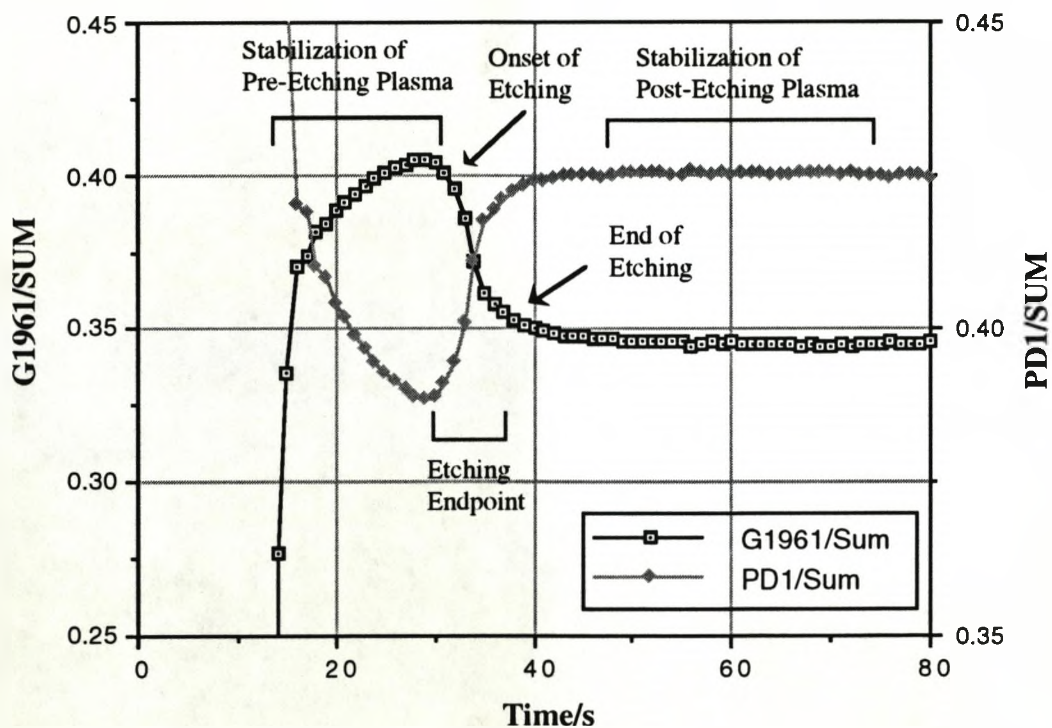

Figure 6.12 Chromatic changes during an RIE etch process

The chromatic changes accompanying the end of etching are shown in figure 6.12. Both the 'blue' chromaticity represented G/Sum and the 'red' chromaticity represented by PD1/Sum show a sharp change at the onset of etching and a sharper change at the end of etching. These changes are significantly clearer than those shown by the plasma etching system. When this data is plotted on a chromatic plane as shown in figure 6.13 a straight line connects the initial plasma chromaticity with the final plasma chromaticity.

The chromatic change on etching is approximately 0.075, allied to a chromatic noise of 0.00025, this means that an endpoint can be detected to within 1 part in 150.

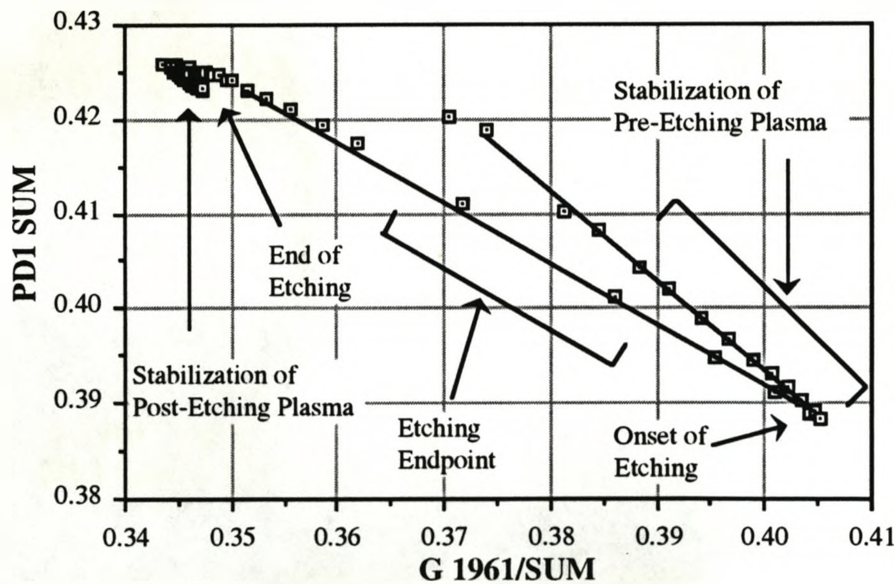

Figure 6.13 An RIE etch represented on a chromatic plane

6.4.2 DISCUSSION

In the following experiments the etched substrate consists of an unpatterned silicon nitride layer covering a relatively impervious layer of gallium arsenide or silicon, whilst the etching gas was a mixture of CF_4 and oxygen. During the etching process

the CF_4/O_2 plasma attacks the silicon nitride to release the gases fluorine, oxygen, nitrogen and $SiOF_2$ (LFE 1975):

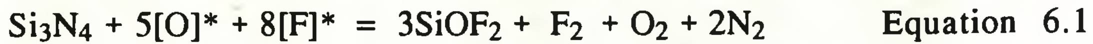

$$Si_3N_4 + 5[O]^* + 8[F]^* = 3SiOF_2 + F_2 + O_2 + 2N_2 \qquad \text{Equation 6.1}$$

These gases partially dissociate under electron impact ionization thus changing the composition of the plasma; on recombination they emit at characteristic wavelengths as described in section 2.4.2. The resulting levels of optical emission from the plasma only lasts as long as the silicon nitride is etched. Once the etching is complete the supply of these gases ceases, resulting in the abrupt change in plasma emission detected in the above experiments. It is notable that the spectral changes accompanying the plasma etch (figure 6.9) showed only the depletion of the CF_4/O_2plasma with little trace of the evolved nitrogen or silicon oxyfluoride, it is possible that these lines were masked in the plasma continuum but no convincing explanation can be given for this observation.

Despite the similarities in substrate and etchant, the plasma and RIE etching endpoints appear to have little in common. The absolute chromaticities are different and even the shape of the chromatic traces on the chromatic plane appear different. However it should be noted that these chromaticities are very different to those obtained by the simple changes in plasma parameters studied in the previous sections. On the chromatic plane neither endpoint trace is monotonic, unlike the traces obtained changing single plasma parameters, both the endpoint traces show a maximum and a minimum value.

During the large changes in plasma composition occurring at an endpoint the pressure and power deposited in a plasma change

significantly too (Sugano 1985). The dissociation of etchant and substrate result in the evolution of new material which can cause transient changes in pressure; whilst the evolution of new material changes the electrical impedance of the plasma also altering the electrical power absorbed by it. It is interesting to speculate whether the chromatic maxima and minima observed correspond to a competition between these three changes in plasma parameters. However this cannot be answered until spectrometers with bandwidths comparable to the chromatic sensors become available.

CHAPTER 7
CHROMATIC THIN-FILM MONITORING

7.1 THIN FILM MONITORING

During the design of the chromatic plasma monitor it was noticed that the hues of semiconductor thin films showed a pronounced dependence on their thickness. Indeed the expert operators (Huggett 1992) informed us that they judged the thickness of thin films purely from their hue and that skilled operators could judge thickness to within 50Å by this method. Since such fine tolerances in film thickness are critical in determining the quality of the finished IC, these discussions prompted a series of experiments to determine whether the chromatic sensing could be applied to the measurement of film thickness. Initially the objective was to automate the process of off-line visual inspection by using the chomatic plasma monitor to measure the film chromaticity. When the viability of this approach was confirmed, an attempt was made to modify the bandwidth the chromatic sensor to allow thickness measurements during processing.

7.1.1 COMMERCIAL THIN FILM MONITORING

When exceptionally fine tolerances are required, thin films are measured using ellipsometric or interferometric means (Chapter 4). However in most cases these methods prove prohibitively costly and time consuming so visual inspection is relied upon instead. The standardized visual inspection technique requires the thin film to be illuminated, normal to its surface, by a specified tungsten filament lamp. The perceived hue of the film is then compared to a list of hues on standard calibration chart

shown in Table 7.1 (Applied Materials 1967). When a colour match is found the appropriate film thickness can be read off the chart.

CHROMATIC FRINGE ORDER	SILICON NITRIDE THICKNESS ( )	SILICON NITRIDE FILM COLOUR
First	0-200	Silicon
First	200-400	Brown
First	400-550	Golden- Brown
First	550-730	Red
First	730-770	Deep Blue
First	770-930	Blue
First	930-1000	Pale Blue
First	1000-1100	Very Pale Blue
First	1100-1200	Silicon
First	1200-1300	Light Yellow
First	1300-1500	Yellow
First	1500-1800	Orange Red
First	1800-1900	Red
First	1900-2100	Dark Red
Second	2100-2300	Blue
Second	2300-2500	Blue-Green
Second	2500-2800	Light-Green
Second	2800-3000	Orange-Yellow
Second	3000-3300	Red

Table 7.1 Calibration chart of film hue against film thickness

Although very simple this process encounters some problems. It can be seen that a given hue can occur more that once in the chart. This recurrence (which is a result of changes in film thickness corresponding to an integral number of wavelengths) can create uncertainty as to which chromatic fringe

order is being observed. In practice this is not a serious limitation since coarse estimates of film thickness (based on etch/deposition time) are almost always sufficiently accurate to define fringe order; the hue is then used to accurately determine film thickness within the defined fringe order.

A more serious limitation is subjectivity of the method and the resulting difficulty in ensuring repeatable results. By replacing the unknown and variable detectors in individual human eyes with a standard photodetector triplet, it was hoped to improve repeatability whilst replacing the vague descriptive calibration chart with a quantitative one relating film thickness to detector photocurrents.

7.2 THE INITIAL THIN-FILM SENSOR

In order to test the feasibility of a chromatic thin film sensor, twelve test samples were obtained from GEC MMT at Caswell. Each sample consisted of a 2 inch silicon wafer with a silicon oxide thin film, thermally deposited for good uniformity. The silicon oxide films varied in thickness from 50Å to 2400Å, spanning a range of great commercial interest.

The light source for these experiments was a stabilized tungsten filament lamp [Lucas 00513]. Each sample was illuminated normal to the surface by a 5mm glass fibre bundle placed at the focus of the source collimator. The reflected light was collected by a four tailed 1mm glass fibre bundle which channelled light onto three photodiodes G1961, PD1 and PD2. To reduce spurious reflections the samples were placed on a matt black ceramic tile 10cm away from the source and receiver fibres.

The distance between wafer and fibres was chosen to allow the illumination of most of the wafer area (eliminating local non-uniformities in thickness) whilst minimizing spurious surface reflections from the supporting tile.

During attempts to optimize the setup it was found that the normal orientation of the source and receiver fibres resulted in significant optical losses. This was because the fibres were not observing identical regions on the wafer. The best optical efficiency was obtained by inclining each fibre at an angle of 15 degrees to the normal so that both the 'cones of acceptance' converged, thus observing identical regions of the wafer. Most of the initial experiments were conducted with this geometry although a single test was also performed (with an inclination of 60 degrees to the normal) to determine the viability of oblique measurements.

Each silicon wafer was placed over a circular template scored onto the ceramic tile, ensuring that each measurement was taken with a consistent position. The white light source was left on for 30 minutes to allow the filament to reach thermal equilibrium and hence a constant chromaticity. Finally the entire assembly was isolated from background light by enclosing it in a matt black plastic box.

The film chromaticity could have been recorded simply by monitoring the individual intensities and normalizing. However because of the limited number of available data acquisition channels the wafer chromaticity was recorded in terms of two hues i.e the ratios G1961/PD1 and PD1/PD2. The chromaticities x and y were extracted from these hues as discussed in Chapter 4.

In order to reduce random errors each measurement was taken twice and then averaged. The repeated readings were taken once in order of ascending thickness and once in order of descending thickness to examine systematic errors within the sensor. Both sets of readings proved identical to within the optical noise limits of the system, demonstrating its good stability. Digitization errors of 0.00025 introduced by the 12-bit ADC were undetectable .

7.2.1. PERFORMANCE OF FILM THICKNESS SENSOR

The sensitivity can be gauged from figure 7.1 which shows an objective thickness calibration chart capable of replacing the subjective chart described in section 7.1.1. It consists of two hues plotted as a function of film thickness.

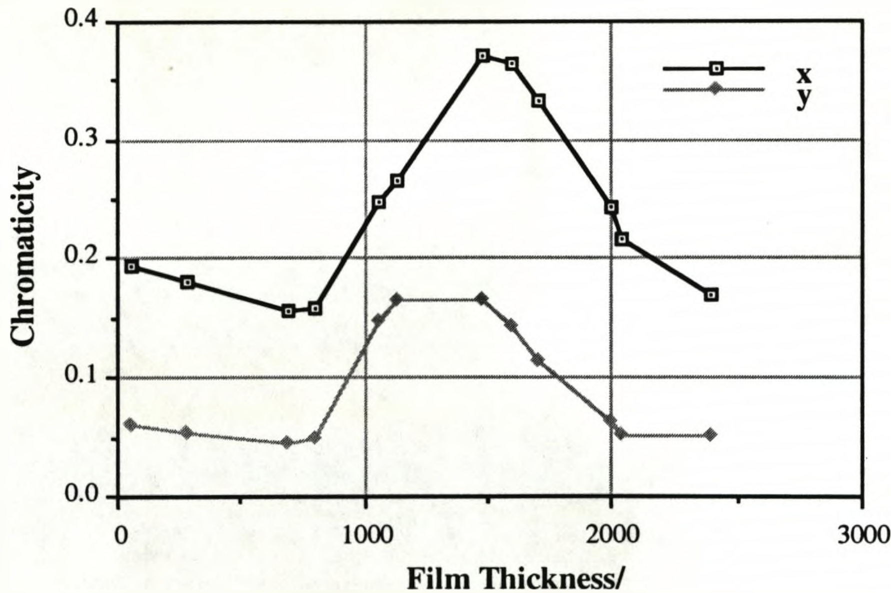

Figure 7.1 Chromatic calibration of oxide film thickness

Over the first 800Å the chromaticity changes by approximately 0.05 and since the chromatic noise of the system is 0.00025, this translates to a sensitivity of 1 part in 200 or 4Å. Over the second

800Å the chromaticity changes by approximately 0.2, resulting in a sensitivity of 1Å.

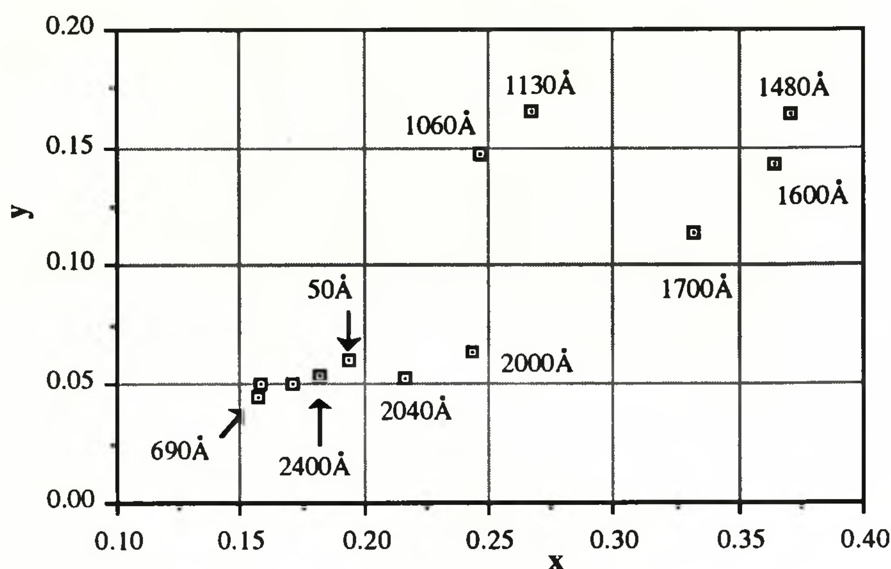

Figure 7.2 Film thicknesses on the chromatic plane

Figure 7.2 displays the same information on a tristimulus graph with the two chromaticities x and y plotted against each other. With this representation it is possible to see that the film chromaticities appear to describe an ellipse. Levels of chromatic drift were monitored over periods of 8 hours. Typically the observed levels were approximately 0.3% indicating that the stability was sufficient to make 15Å resolution a practical possibility.

7.2.2. DISCUSSION.

Thin film theory, outlined in section 2.5.4, predicts that the reflectance for monochromatic wavelengths is a sinusoidal function of film thickness (equation 2.7). The normalized chromaticity curves, shown in figure 7.1, are oscillatory functions of film thickness. However, they appear to be slightly skewed

when compared to pure sinusoids, perhaps suggesting a superposition of many slightly different sinusoids. The superposition would be consistent with the assertion made in section 4.2.3, that broadband changes in spectra can be represented by a shift in a single dominant wavelength. A possible explanation for the deviation from sinusoidal behaviour is that the wafers were externally calibrated, several months previously and at unknown times. They may have absorbed water vapour in proportion to their exposure to the atmosphere, significantly affecting their optical characteristics (Francis 1992). Noise and drift are not thought to be a factor in the 'distortion' since they are barely visible on the scale of the graph.

When the chromaticities are plotted against each other as shown in figure 7.2, they trace out an approximately oval shape. This shape is characteristic of large changes in hue with approximately constant saturation (figure 4.3). It should be noted that the locus of chromaticities is not smooth; the smaller thicknesses (0-690Å) appear to show a linear change in chromaticity whilst the larger thicknesses trace out the oval. A possible explanation is that for small thickness the intrinsic colour of the material has a significant effect on overall colour, whilst for larger thicknesses the interference colour becomes dominant.

This experiment demonstrates the possibility of measuring film thickness to angstrom precision by chromatic means. As a result an effort was made to design a sensor of equal sensitivity capable of operating during a plasma etching or deposition process.

7.3 ON-LINE MEASUREMENT OF SiO_2 DEPOSITION

Having demonstrated the possibility of replacing visual inspection by a chromatic detector the next step was to examine the advantages obtained by doing this. The resolution and repeatability (both 20Å) are slightly superior to those obtained by a skilled observer but automation may have another more significant advantage. All the tests conducted so far have been off-line tests where measurements are taken after the end of processing. Although such measurements are satisfactory for the purposes of quality control, measurements taken during processing (on-line tests) would be far more attractive since they would offer the possibility of controlling a manufacturing process to optimize yield.

Visual inspection of a wafer during processing is out of the question since the processing plasma emits such a bright light that no human operator could accurately judge the colour of a sample. Background light would have the same effect on the chromatic sensor described above, but well established techniques exist to recover signal buried in high background noise.

One of the best known signal recovery techniques is lock-in amplification or phase sensitive detection. In this method the signal is chopped at a precise frequency and then mixed with a reference frequency. The resulting resonant peak serves as a band-pass filter (Section 5.2.2) so any background noise not at the chopping frequency is strongly attenuated.

In order to incorporate this signal recovery into the thin film sensor two modifications had to be made to the experimental

setup described in section 5.2.1. Firstly a chopper wheel was placed between the lamp filament and the source fibre; a chopping frequency of 1kHz was selected since it was sufficiently high to avoid interference from the harmonics of mains and three phase ripple whilst being sufficiently low to avoid being affected by the relatively low bandwidth of the photodiodes. Secondly the voltage representing the sum of the film and background hues were fed in to a Bentham 214 lock-in amplifier and mixed with the 1kHz reference pulse used to drive the chopper wheel. The resulting DC voltage represents the hue of the film only and this voltage was stored in a computer via an ADC.

For the on-line monitoring of thin film deposition, the optics were fitted to a silicon oxide deposition chamber by kind permission of the departmental semiconductor group. Since the chamber consisted of a glass cylinder 20cm in diameter, the fibre to substrate distance had to be increased. This would have resulted in increased optical losses. To compensate for these losses the original 1mm receiver fibre was replaced by a specially prepared 3mm fibre bundle. Constraints of space forced the adoption of a 45 degree angle for the fibres with respect the substrate.

7.3.1. PERFORMANCE OF ON-LINE THICKNESS SENSOR

This equipment was used to monitor the progress of several oxide deposition runs each lasting approximately twenty minutes. During this period approximately 2000Å of silicon oxide were deposited on the wafer surface. The exact thickness of the deposited film was found by interrupting the run on five occasions

and removing the wafer to perform ellipsometry; the results are shown in figure 7.3:

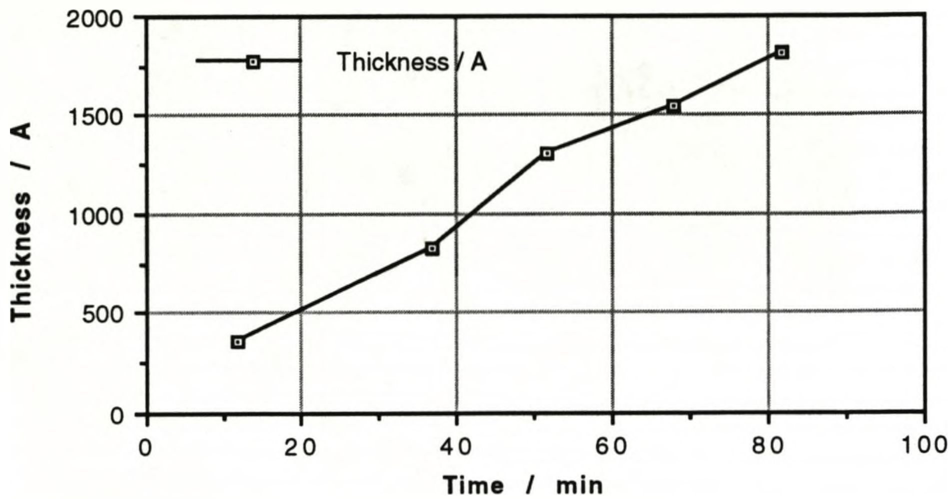

Figure 7.3 Ellipsometric film thickness as a function of time.

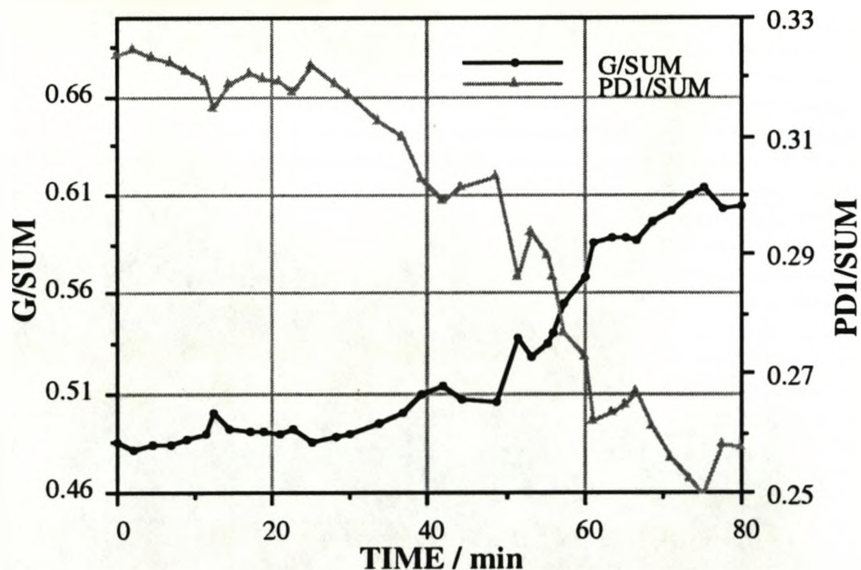

Figure 7.4. Film chromaticity as a function of deposition time

Whilst deposition occurred two chromatic characteristics of the wafer were recorded as a function of time; the evolution of these chromaticities is shown in figure 7.4. These curves also appear to be periodic, although the thickness deposited was only sufficient

to illustrate a quarter cycle. Figure 7.5 shows this data plotted on a chromatic plane.

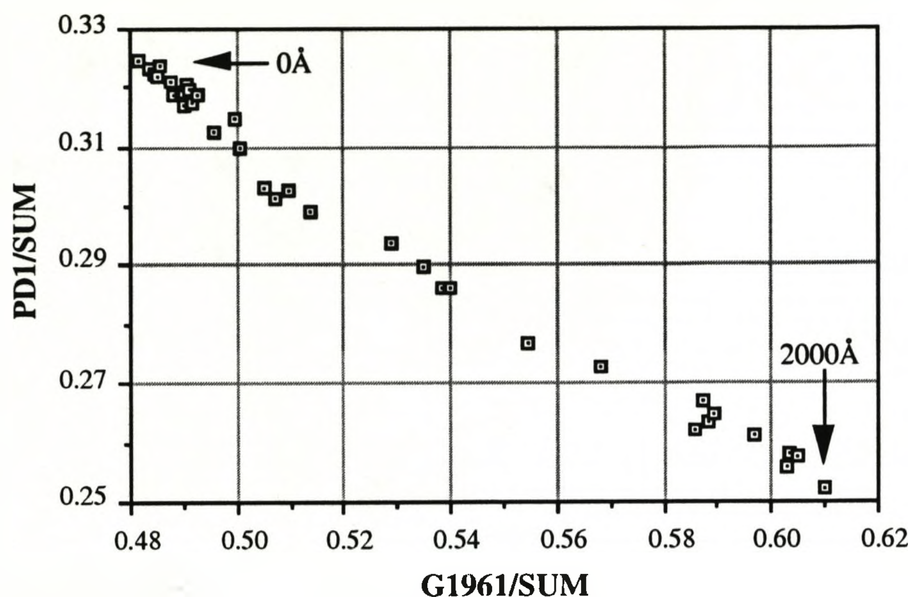

Figure 7.5 Film thickness plotted on a chromatic plane.

7.3.2. DISCUSSION

One of the problems encountered during these experiments was the difficulty in obtaining on-line calibration for the sensor, since no such equipment was available. To overcome this a 20 minute calibration run was interrupted at 5 minute intervals and the wafer removed to enable the measurement of film thickness by ellipsometry. The resultant plot of film thickness against time was shown in figure 7.3. Since the plot is approximately linear it would have been possible to calibrate the hue curves by interpolation. However some work performed in the department (Ahmed 1994) offered the opportunity to calibrate the sensor using neural networks. The neural network was trained to match the chromatic responses of the film sensor to the film thicknesses obtained from ellipsometry. The actual film thicknesses and the values calculated by the neural network showed excellent

agreement, proving capable of measuring film thicknesses to within 20Å as illustrated in figure 7.6:

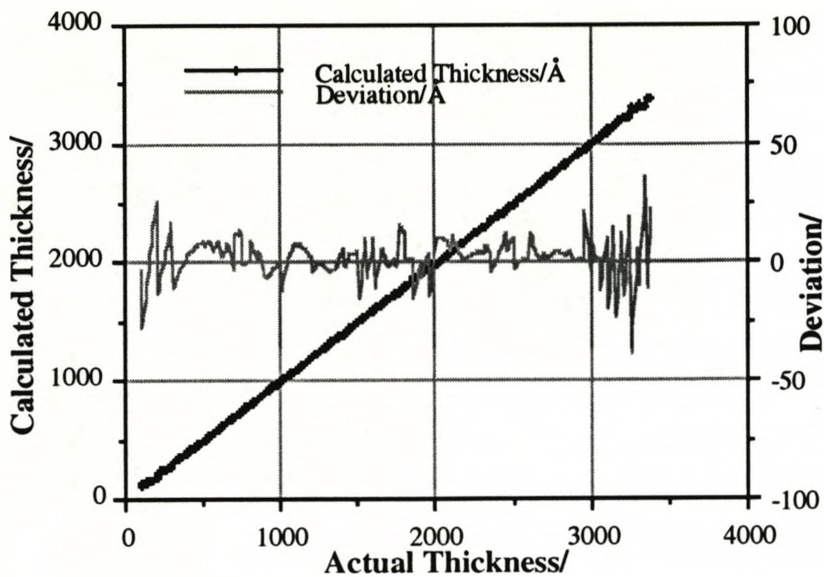

Figure 7.6 Neural network calibration of the thin film sensor

It is of note that the trace on the chromatic plane (figure 7.4) is almost linear, in marked contrast to the oval shape observed previously. The reason is that in this case the optical access to the wafer surface was at approximately 45 degrees in contrast to the right angles used previously. This difference in angle results in a difference in 'phase lag' between the chromaticities- in figure 7.1 the chromatic peaks are almost in phase whilst in figure 7.3 they are exactly out of phase. This change in shape from linear to elliptical in response to a phase shift is analogous to the behaviour of Lissajous figures (Hecht 1975).

7.4 ON-LINE MEASUREMENT OF Si_3N_4 ETCHING

The successful demonstration of on-line thin film monitoring encouraged the construction of a dedicated system for monitoring an accessible RIE system. Although the sensor is primarily intended to monitor film deposition (since these are difficult to monitor by plasma measurements); film etching can be regarded as a time reversed deposition process, so for the purpose of testing sensor performance this distinction is unimportant. Etching endpoints can be detected by plasma measurements but the film monitor can yield the instantaneous etch rate which is not easy to obtain by other means. An advantage of using the RIE chamber was the availability of plasma monitoring as an independent method of corroborating endpoints determined by the film sensor.

Because the RIE chamber was commissioned with the film sensor in mind, a 2 inch quartz window was available allowing convenient observation of the wafer surface. The source and receiver fibre bundles accessed this window by using fibre connectors drilled into an aluminium faceplate. This arrangement allowed the fibres to be orientated normal to the wafer surface and kept the wafer - fibre distance down to 12cm. A schematic of this arrangement was shown in figure 5.13.

Whilst waiting for the installation of the RIE etching chamber an attempt was made to redesign the film monitor with the aim of reducing its cost. Since approximately half the cost of the monitor was due to the use of a commercial lock-in amplifier, the attempt concentrated on eliminating it and incorporating a signal recovery system into the detection electronics instead. The first intention was to construct a basic lock-in amplifier, however before this somewhat ambitious step was taken it was decided

that a simpler circuit should be tested. This circuit measures the total optical intensity arriving from both wafer and plasma when the reference pulse is switched on but measures only the plasma intensity when the reference pulse is switched off. These two intensities are recorded as voltages on sample and hold circuits and the latter is subtracted from the former; this difference represents the intensity arriving from the wafer. The light from the source was chopped at the reference frequency.

If the optical emissions from the plasma oscillate at the reference frequency it is possible that this background noise could leak into the signal. The plasma emissions were observed in the frequency domain using an oscilloscope and the frequency of 1KHz appeared free of plasma oscillations. So this frequency was chosen for the reference pulse. The ability of the new design to discard background light levels was tested by adding a strong continuous beam of white light to the chopped white light arriving from an identical source. Without the signal recovery system in operation the continuous beam increased the photodetector voltage output (αintensity) by 120% (1.2V +/- 4mV); with the signal recovery system in operation no appreciable difference (+/-4mV) was observed between measurements taken with the continuous beam switched on and with it switched off.

7.4.1. PERFORMANCE OF ON-LINE THICKNESS SENSOR

This equipment was used to monitor the progress of several nitride etching runs each lasting approximately six minutes. During this period approximately 2400Å of silicon nitride were etched off the wafer surface. Unfortunately no silicon nitride

wafers with calibrated thickness were available, so it was necessary to produce them. A batch of 3 inch GaAs wafers with 2400Å of nitride was available, and a reproducible etch rate of 400Å/min was established to allow calibration. A silicon nitride wafer was etched for a period of 30 seconds whilst its chromaticity was recorded using the thin film sensor. After this period the wafer was removed from the chamber and the nitride film thickness was measured using ellipsometry. This process was repeated increasing the etch time of the wafers by 30 seconds each time until the sixth minute by which time the nitride layer had been completely removed. The resulting calibration plot of film chromaticity and film thickness as functions of etch time is shown in figure 7.7

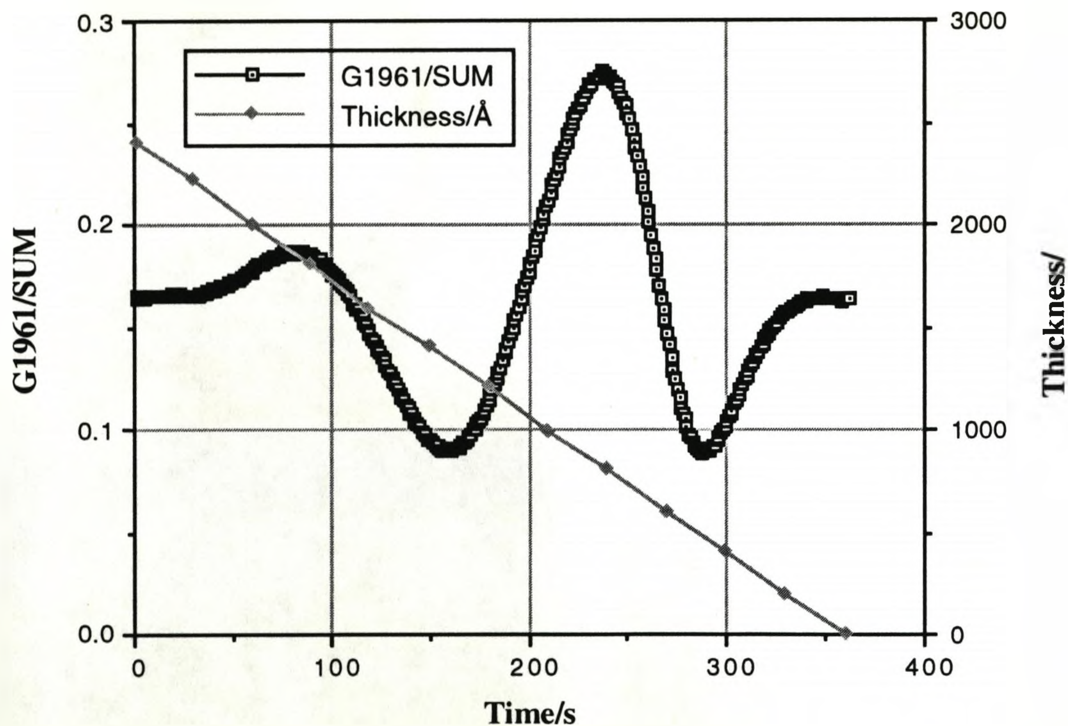

Figure 7.7 Calibration of film chromaticity and film thickness

Whilst etching occurred two chromaticity characteristics of the wafer were recorded as a function of time; the evolution of these chromaticities is shown in figure 7.8.

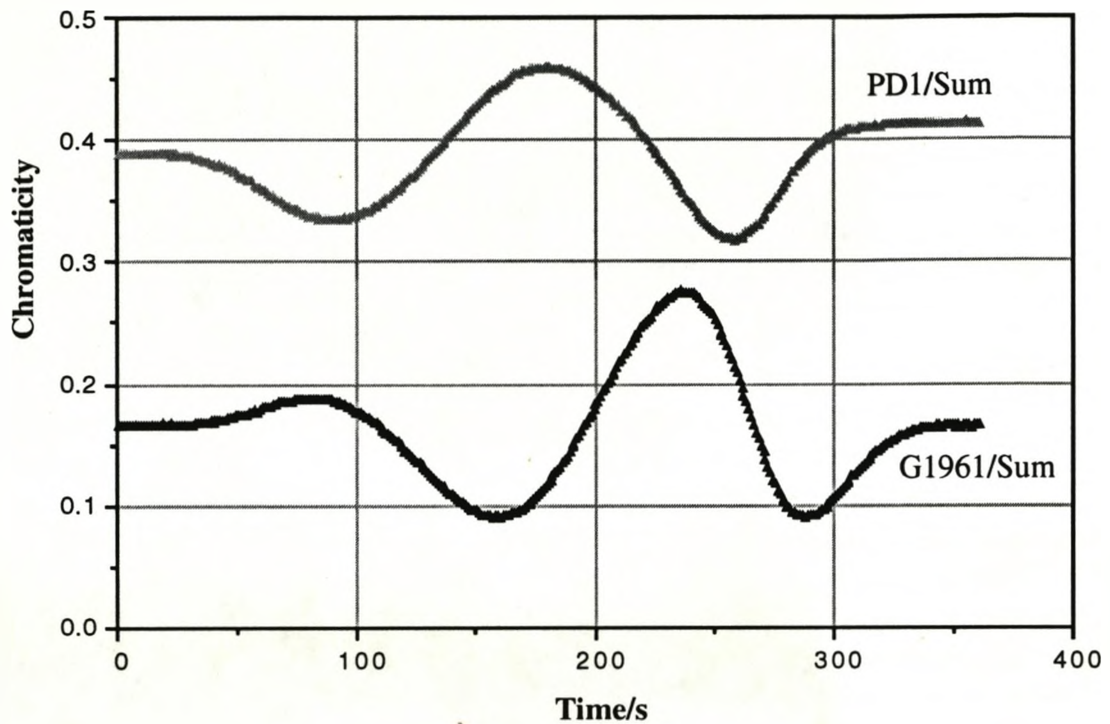

Figure 7.8 Film chromaticities as a function of time

To check repeatability, such curves were recorded for 10 etching runs and the average chromaticities calculated for one second intervals. The averaged data was then placed in a look-up table (LUT) which linked chromaticity to film thickness assuming a linear etch rate. The experimentally measured film thickness from a single run was then plotted against the average value from the LUT. The resulting graph is shown in figure 7.9.

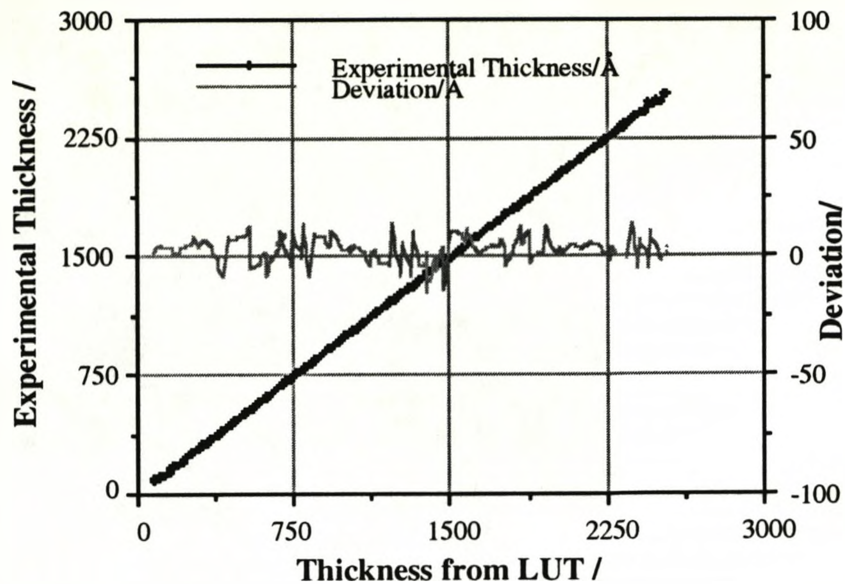

Figure 7.9 Repeatability of the thin film sensor

7.4.2. DISCUSSION.

The oscillatory behaviour of the film thickness curves shown in figures 7.7 & 7.8 are similar those previously shown in figures 7.1 & 7.4. However, they are much closer to the sinusoids predicted in equation 2.7 than either of the two previous results; showing no clipping or spurious peaks. Since the later experiments (at high sampling rates) show the closest agreement with theory there is some justification for dismissing the distortions on the previous results as artefacts due to inadequate sampling. It should be noted that the positive and negative gradients are different. This skew may be a result of the asymmetric spectral profile of the source since it disappears when an LED is used (Francis 1992).

The repeatability experiments described above yield the straight line in shown figure 7.9. The 20Å repeatability obtained compares well to the 50Å claimed by expert observers.

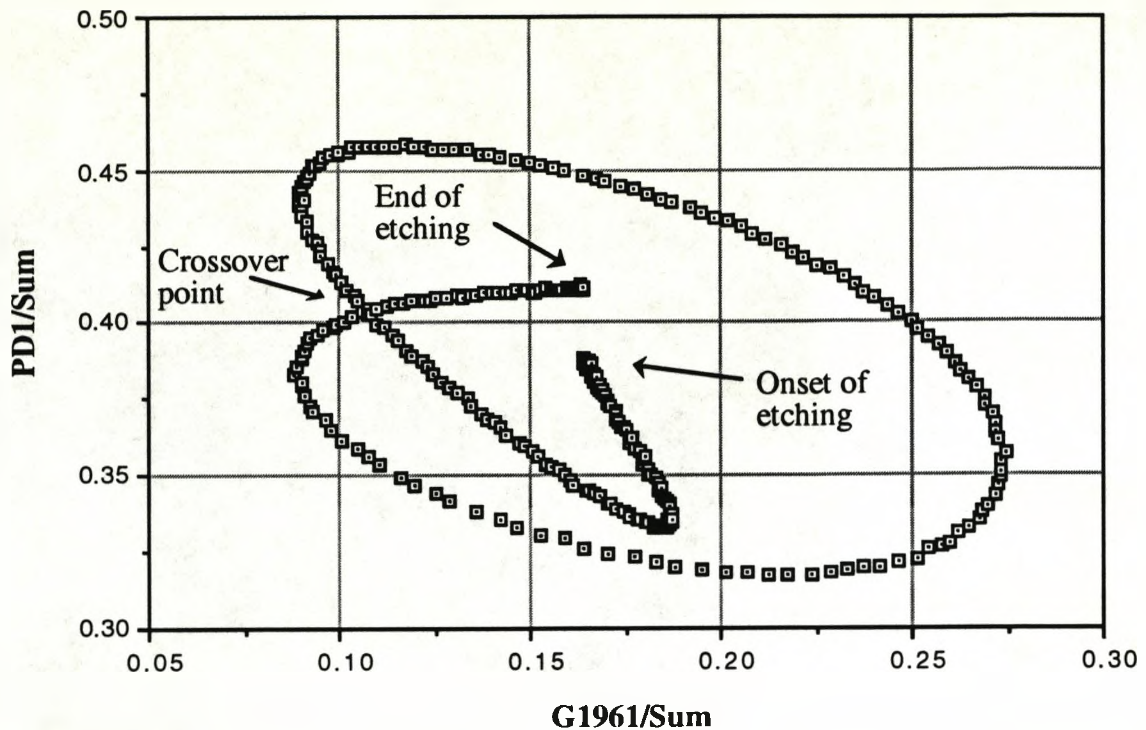

Figure 7.10 Film chromaticity plotted on a chromatic plane.

When the chromaticities are plotted against each other as shown in figure 7.10 they trace out an approximately oval spiral. This shape is characteristic of large changes in hue with approximately constant saturation (figure 4.3). It is notable that the saturation of the film chromaticity increases as the film thickness increases; in accordance with the theory discussed in section 2.5.4. However there is an anomaly for very small thicknesses. Instead of continuing to increase the saturation shows a sudden reduction at very small thicknesses causing the chromatic trace to cross over itself in a manner not predicted by simple theory. A possible explanation is that for small thicknesses the intrinsic colour of the material has a significant effect on overall colour, whilst for larger thicknesses the interference colour becomes dominant. This effect makes interpretation slightly more difficult since at the point of crossover there are two possible thicknesses. However since

etching is a progressive process an examination of the etching history allows the selection of the correct thickness.

7.5 THE LED BASED THIN-FILM MONITOR

The success of the above tests led to a serious appraisal of the sensor costs. The original system consisted of approximately £100 worth of electronics, a £1000 white light source and a £2000 lock-in amplifier. Replacement of the lock-in amplifier by a signal recovery circuit eliminated a major part of the cost whilst barely increasing the cost of the electronics. Logically the next step was to replace the white light source and mechanical chopper by a solid state source that could be chopped simply by pulsing the drive current.

However at the beginning of this project the brightest room temperature LEDs available (500mcd) were far too dim to use with practical (10cm) path lengths. Toward the end of the project a new family of LEDs (InGaAsP) became available offering an order of magnitude improvement in brightness (10cd) for a low price (£10). These LEDs were available at only one specific wavelength (670nm) so it was not possible to construct a chromatic sensor from them. Nevertheless a single channel system was built in anticipation of amber and green LEDs which will shortly become available.

The semiconductor group in the department expressed interest in applying this sensor for the monitoring of oxide deposition processes. In response, a prototype system was constructed for extensive testing by the group. The published results were promising (Francis1992), confirming oscillatory

variations in intensity similar to the oscillatory variations in chromaticity described in this chapter.

CHAPTER 8

CHROMATIC OIL MONITORING

8.1 INTRODUCTION

One of the major factors determining the performance and longevity of industrial machinery is the quality of its lubricating oil. Since the degradation of machine oil is a slow process, commonly taking months, it has become standard practice to replace the oil at regular intervals regardless of its condition. Obviously this procedure fails to allow for varying machine loads and so might lead to oil being replaced when still in good condition or more seriously lead to a delay in replacing poor quality oil.

The colour of pure oil normally ranges from clear yellow to deep amber, the impure oils are of a much deeper shade ranging from dark brown to black. As a result oil changes are frequently decided by an expert observer; however visual inspection constitutes an inefficient use of manpower and at best gives only a qualitative indication of oil condition. In an industrial environment, where any down-time may prove costly, an automatic oil-diagnostic system has obvious attractions.

Although a sensor to detect the oil content in water based on laser diffractometry has been reported (Snell & Pitt 1983) there is little indication in the literature of a general oil condition monitor. The advantages of optical sensing discussed in chapter 3 are relevant in a harsh environment such as an engine sump, particularly when the engine is used in the plasma processing industry where strong electromagnetic interference is prevalent.

A novel optical fibre sensor has been developed for the on-line monitoring of oil quality within industrial equipment. The monitoring is based on chromatic modulation because of the inherent self-referencing demonstrated by this technique. Initially

the sensor was designed for use on the vacuum pumps used to evacuate plasma chambers. Since the control of plasma pressure has a critical effect on plasma processes (Chapter 6) and the processed material has a very high value, this niche appeared an ideal one. Of equal importance is that semiconductor foundries normally have many clusters of distributed pumps (Cockrill 1990) which are inconvenient to inspect. Furthermore some silicone oils (e.g. Fomblin) used in the semiconductor industry can cost several hundred pounds *per litre,* and since a pump may require several litres a practical sensor could recover its cost very rapidly.

8.2 SENSOR DESIGN

Preliminary experiments conducted with a simple transmissive system were satisfactory but since the degree of access to the oil sump can vary greatly from machine to machine, the probe was redesigned to operate in a reflective mode so as to be minimally invasive. A reflective probe eliminates the need for two access ports to the sump as well as avoiding the need to bridge the oil sump. Two forms of reflective probes were constructed: one using total internal reflection in a prism, and the other using a spherical lens and plane mirror combination.

The prismatic approach was an attempt to avoid the corrosion problems suffered by silvered surfaces. An equilateral prism was drilled longitudinally to provide a path of entry for the oil. Optical access to the oil was obtained by butting the emitter and receiver fibre to the side of the prism. Collimating lenses were used to reduce the divergence of the input and output beams. This prototype is shown in figure 8.1

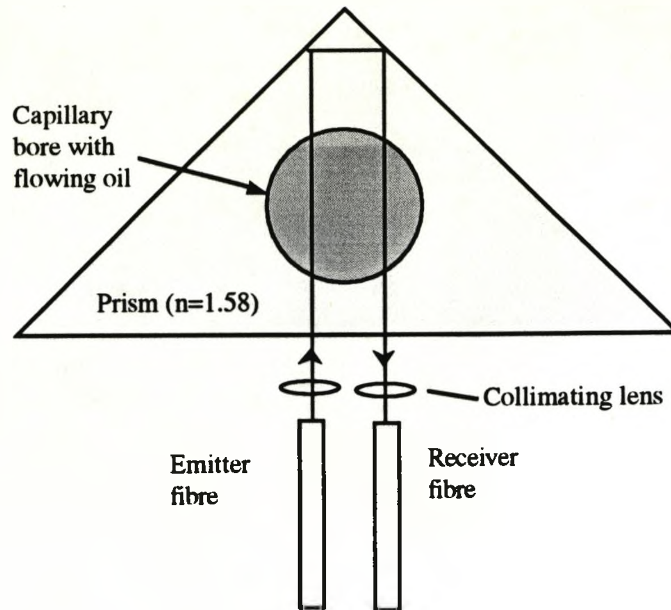

Figure 8.1 Schematic of the prototype oil probe.

The performance of this design was similar to that of the spherical lens and plane mirror assembly described below; however it was rejected because of its high cost and fragility when compared to the following design.

In the probe incorporating the plane mirror a collimating lens was used in order to reduce optical losses due to beam divergence. The lens should have as short a focal length as possible so as to reduce the probe length. The oil cavity should be illuminated by collimated light in order to eliminate variations in chromatic aberration caused by changes in the refractive index of the oil. This is best achieved by placing the emitter fibre at the focus of a biconvex lens; the emergent light is then parallel. A probe was made to this design and engineered to survive industrial conditions as illustrated in figure 8.2.

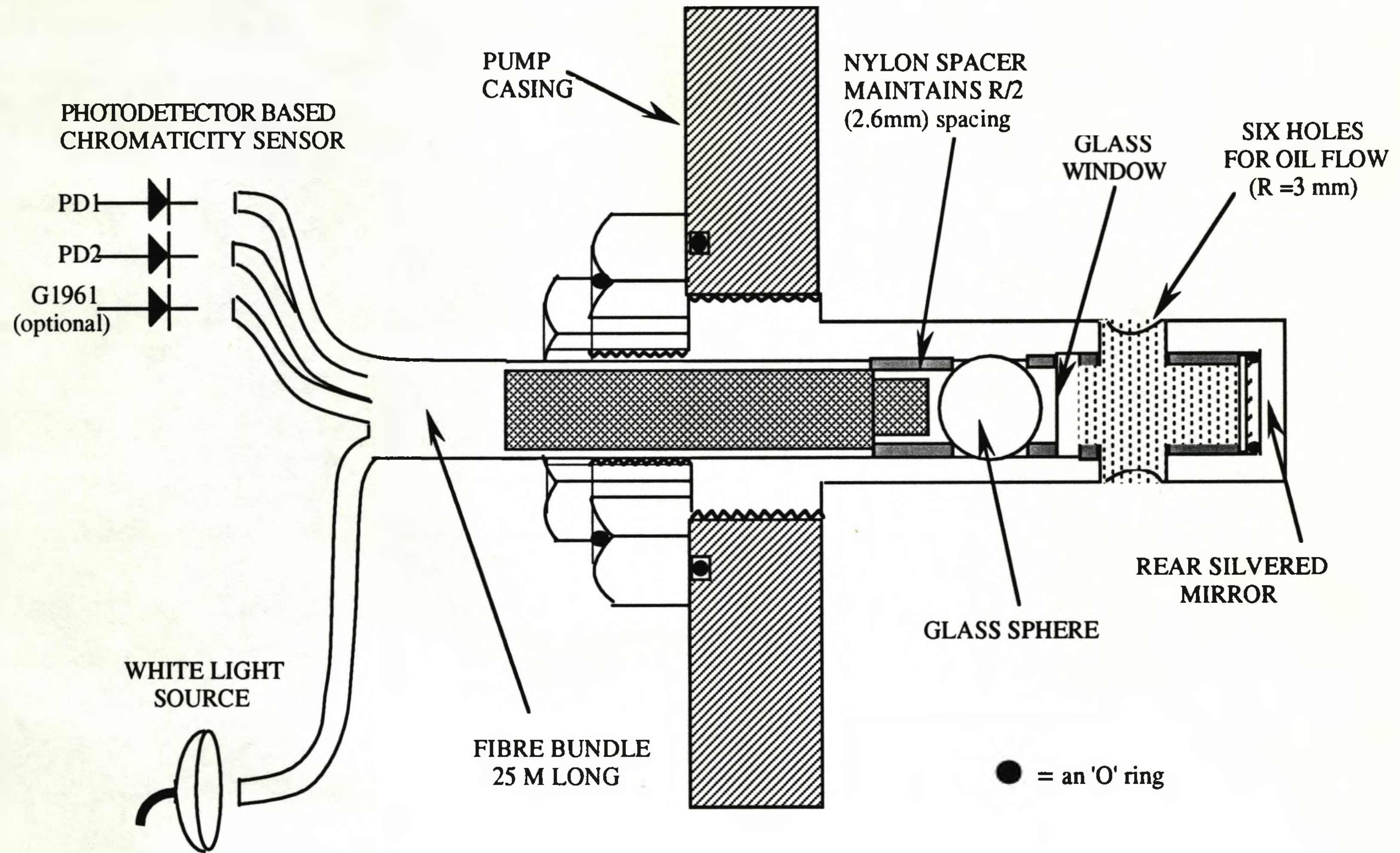

Figure 8.2 Schematic of the oil condition probe

The optical sensor shown above was encapsulated in a 3/8" BSP machine screw for protection and ease of access. Separation between the optical components was maintained by annular nylon spacers. Six holes each with a 3mm radius were drilled into the optical cavity, these were sufficiently large to provide good drainage for the optical cell without weakening the cell. A glass sphere of radius 5mm was placed 2.5mm from the fibre bundle and a glass window was placed between the sphere and the plane mirror to create the optical cell. A cavity length of 6mm was chosen for signal to noise considerations as described in the following section.

8.3 PERFORMANCE OF THE OIL SENSOR

The components of this design were sufficiently inexpensive and robust for a practical sensor; so the probe was fitted to the oil sump of an AEI Metrovac Type GS 10 rotary pump to investigate the sensor performance in an industrial environment.

8.3.1 SENSITIVITY TO OIL CONDITION.

Although the difference in hue between pure and impure oils is sometimes apparent to the naked eye, the eye is known to be very sensitive in discriminating between hues; hence it was necessary to ensure that a combination of commercially available photodetectors would be capable of discriminating between the pure and impure oil samples. Transmission spectra of three commercially significant oil samples; Edwards 17, Edwards 15 and Crylin 87 were recorded (figures 8.3a-c) whilst within the probe.

Figure 8.3a Transmission spectra of pure and impure Edwards 17.

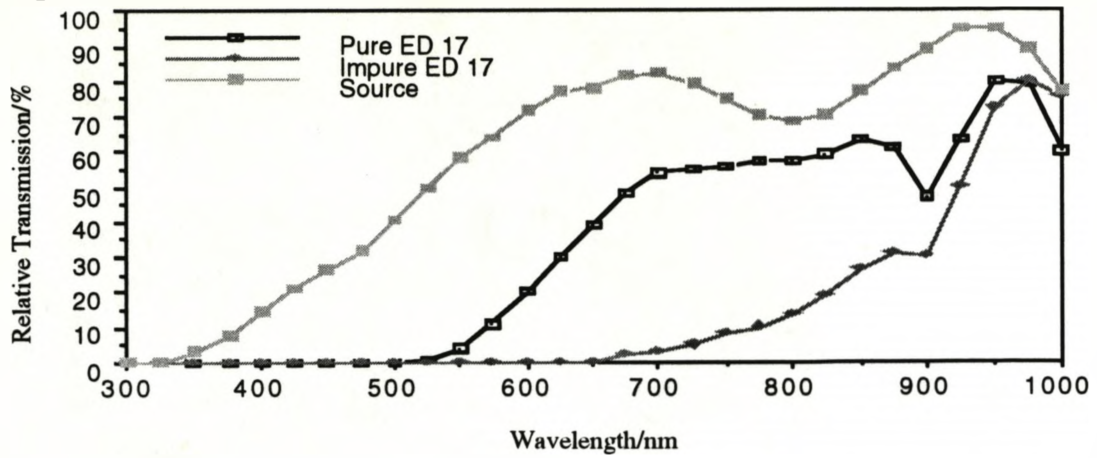

Figure 8.3b Transmission spectra of pure and impure Edwards 15.

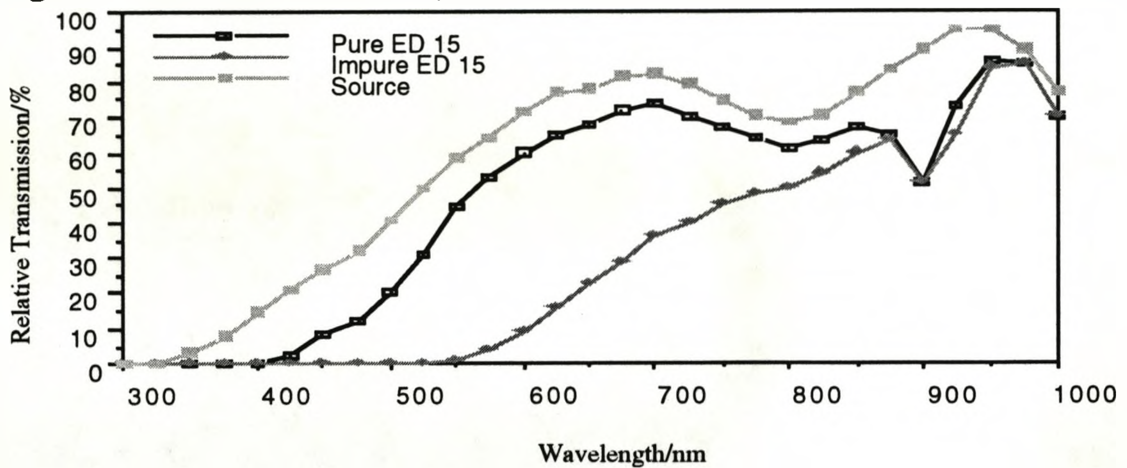

Figure 8.3c Transmission spectra of pure and impure Crylin 87.

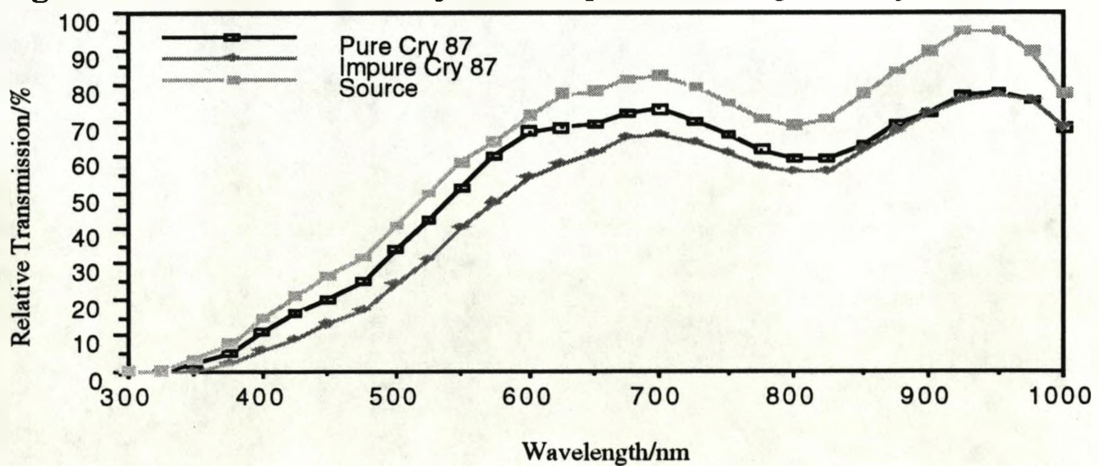

The spectrum of the standard Lucas source was also recorded and is shown for comparison. On examination of these spectra the decision was taken to ignore the 'blue' photodiode and concentrate on the red and infra-red photodiodes. These spectra were digitized to allow a computer program (Russell et al 1990) to calculate the distimulus chromaticity. These values were then compared with the experimental chromaticity as shown in section 8.3.4. Pure and impure samples of three industrial pump oils were examined for their chromatic modulation depth, a parameter defined by:

$$\frac{\text{Chromaticity of pure sample} - \text{Chromaticity of impure sample}}{\text{Chromaticity of pure sample}} \times 100\ \%$$

Equation 8.1

(Impure oil being defined as the lowest quality for acceptable use) The three oils recommended as being of particular commercial interest were Edwards 15, Edwards 17 and Crylin 87; the chromaticities of pure and impure samples of these oils are shown in figure 8.4. Edwards 15 shows a chromatic modulation depth approximately 20% of signal, Edwards 17 shows a modulation depth 20% of signal but Crylin 87 shows a modulation depth of only 5%, although this is not surprising as both pure and impure Crylin 87 are clear to the eye. These experimental values correlate well with the computer predictions of a 22% modulation depth for Edwards 15, 24% for Edwards 17 and 7% for Crylin 87. These computer predictions were based on the iterative solution of the colour equations (4.3 & 4.4) using digitized spectra of the source, oil samples and photodiodes (Russell et al 1990).

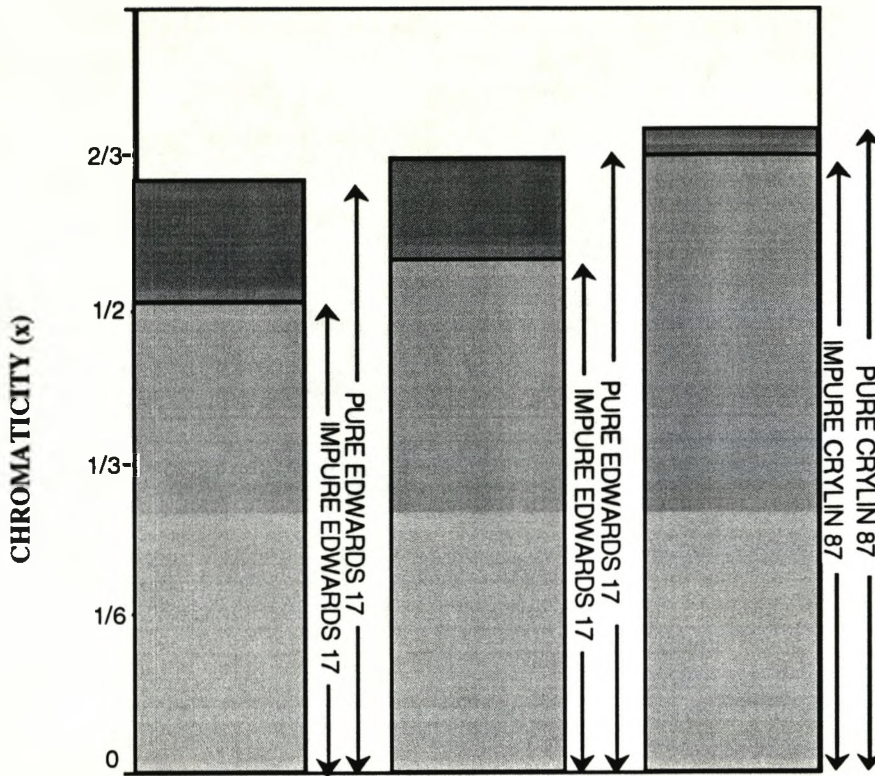

Figure 8.4 Comparison of the modulation for the three oils.

Chromatic noise levels of approximately 0.1% were encountered for the chromatic changes in the two Edwards oils. This information allows the calculation of sensor sensitivity, which is defined as the ratio of noise to modulation depth (Eckman 1966). The sensitivity of the sensor to oil purity was approximately 0.001/0.2 or one part of impure oil in 200 parts of pure oil when applied to the Edwards oils. Higher noise levels of approximately 0.005 for Crylin 87 resulted in a lower sensitivity of 0.005/0.05 or one part of impure oil in ten parts of pure oil. Both these levels of sensitivity are better than those of most human inspectors (Cockrill 1990).

The choice of a 6mm cavity length for the oil probe is justified in figure 8.5, which illustrates the variation of sensor

sensitivity with cavity length using Edwards 17 as the test oil. This graph shows sensitivity (defined as chromatic modulation depth/chromatic noise) reaching a maximum for cavity lengths of approximately 6mm.

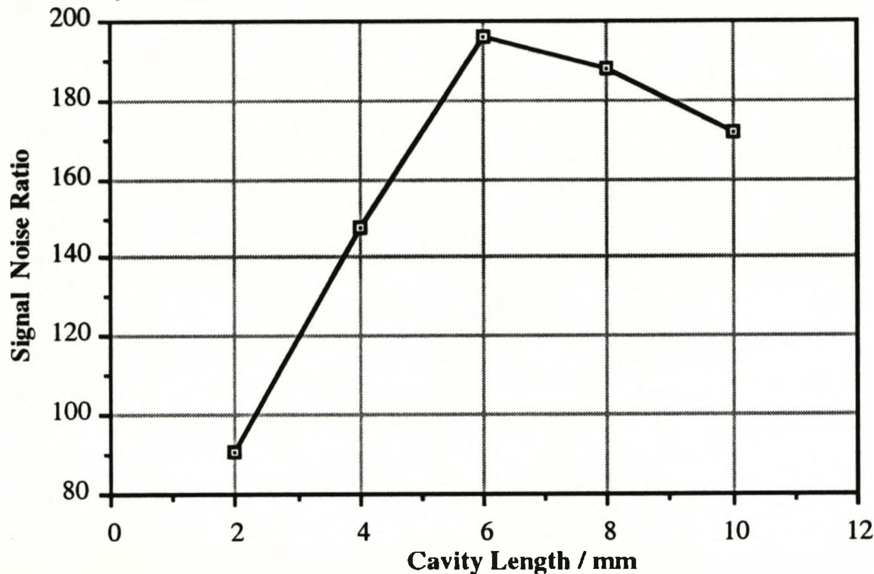

Figure 8.5 Sensor sensitivity as a function of cavity length

Shorter cavity lengths reduce the modulation depth since insufficient spectral absorption occurs for large chromatic changes. Longer cavity lengths result in so much spectral absorption that noise becomes increasingly significant and serves to reduce the sensitivity. The optimum cavity length is specific to each oil. On learning that Edwards17 was the oil of greatest commercial interest to the project sponsor (Baker 1990) the 6mm cavity length was chosen for the probe and all subsequent investigation were conducted using it as the sample oil.

8.3.2 STABILITY OF OIL CHROMATICITY.

Having established that it is possible to detect the difference between pure and impure oils, the next step was to examine the stability of the colour output. The chromatic stability of the white

light source used to illuminate the oil is a critical factor determining the overall chromatic stability of the instrument. To minimize this limitation a specially designed, stabilized white light source (Lucas OSL-00513) with a chromatic drift of approximately 0.001 and chromatic noise of 0.0005 was used.

In order to test the temperature stability of the probe, the sensor head was heated from room temperature to 120 ^{o}C whilst inside the pump containing pure Edwards 17. The temperature change caused a 0.5% chromatic drift on a 20% modulation depth whereas the intensity shows a fivefold drift over a comparable modulation depth.

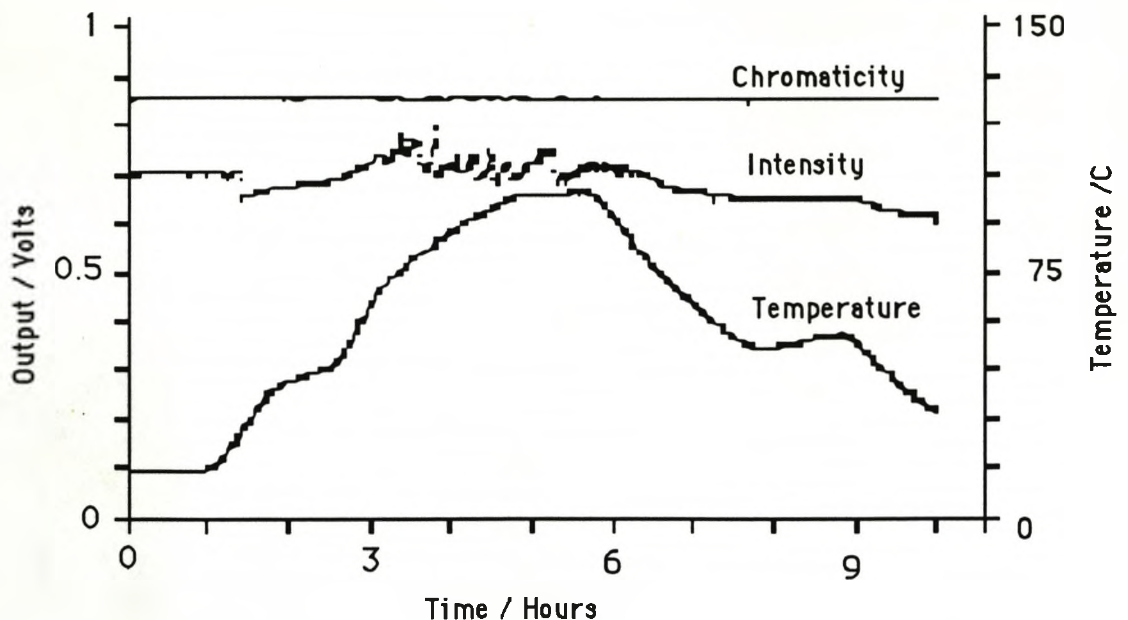

Figure 8.6 Comparative temperature stability of oil sensors.

Figure 8.6 shows the light intensity fluctuating strongly as the temperature rises whilst the colour remains remarkably constant,

vindicating the preference for a chromatic sensor over an intensity sensor.

A further noise component may arise from mechanical changes in the probe. Chromaticity values from a probe in an operational (and hence vibrating) pump were compared to the values from the pump when switched off and no measurable differences were observed. Other factors causing discrepancies in oil chromaticity were related to the initial setup of the sensor and are dealt with in the following section.

8.3.3 REPEATABILITY OF OIL CHROMATICITY.

The repeatability of the chromatic signal obtained from Edwards 17 was checked by filling and draining the probe in two cycles as illustrated in figure 8.7. Oil colour showed a repeatability within 1% of the modulation depth, the air colour showed a far poorer repeatability of the order of 2%. The implications of this for the system viability as an oil level monitor are not as serious as they first appear since the chromaticity of air is so much greater than that of the oil a 2% drift would not result in confusion between the two.

This chromatic instability might be caused by the formation of oil films which exhibit thin film interference, so giving rise to large chromatic changes. These effects are most pronounced when observing the edges of an oil meniscus where light and dark interference fringes are visible to the naked eye. Since these films were created at an oil/air interface the additional chromatic instability created by them is only apparent when the oil drains from the probe, once drainage is complete the oil film would be too thin to significantly affect the chromaticity.

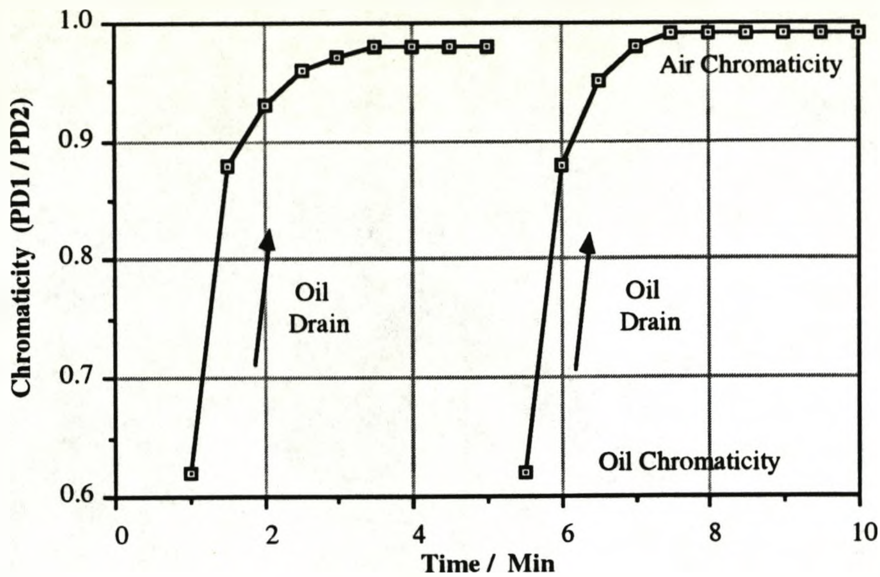

Figure 8.7 The repeatability of air and oil chromaticities.

The effect of rotating the fibre bundle within the probe head was also examined. Initially a segmented fibre bundle (in which the fibres were arranged in quadrants) was employed in the arrangement shown in figure 8.2.. The bundle was rotated through a complete circle and the percentage of chromatic (PD1/PD2) change was recorded as shown on figure 8.8:

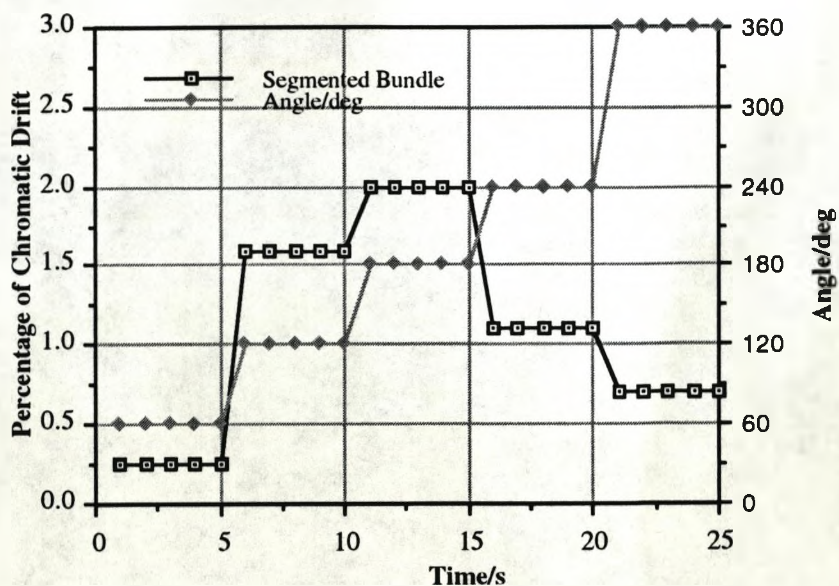

Figure 8.8 Chromatic instability caused by fibre rotation.

The changes were large (2%) and demonstrated that the system lacked rotational symmetry. When the segmented bundle was replaced by a randomised fibre bundle this source of chromatic variation was reduced to a level below that of source noise and was therefore undetectable.

8.3.4 LINEARITY OF OIL CHROMATICITY

The linearity of chromatic response was checked by immersing the sensor in various mixtures of Edwards 17 oil. If pure oil is represented as 100% purity and impure oil by 0% purity, mixtures of 0%, 20%, 50%, 80% and 100% purity were created and the resulting chromatic outputs recorded. Subsequently mixtures of 33% and 66% were also used in order to highlight the emerging nonlinearity of response. Figure 8.9 is a graph showing the variation of chromatic output from Edwards 17 oil as a function of purity. The line labelled experimental chromaticity displays values obtained using the distimulus sensor whereas the line labelled theoretical chromaticity displays values calculated from oil spectra. They demonstrate that the chromatic variation displays a pronounced sigmoid characteristic, as predicted by theory (equation 8.4).

The integrals in equation 8.4 were solved using an iterative procedure implemented in a computer programme (Morse 1992). This programme was fed the digitized spectral responses of the white light source, oil samples and photodiode pair. It then numerically integrated the product of these spectra with respect to wavelength giving a chromaticity value. This procedure

assumes additive colour mixing (Billmeyer & Saltzmann 1966) which may account for the discrepancy between the two curves.

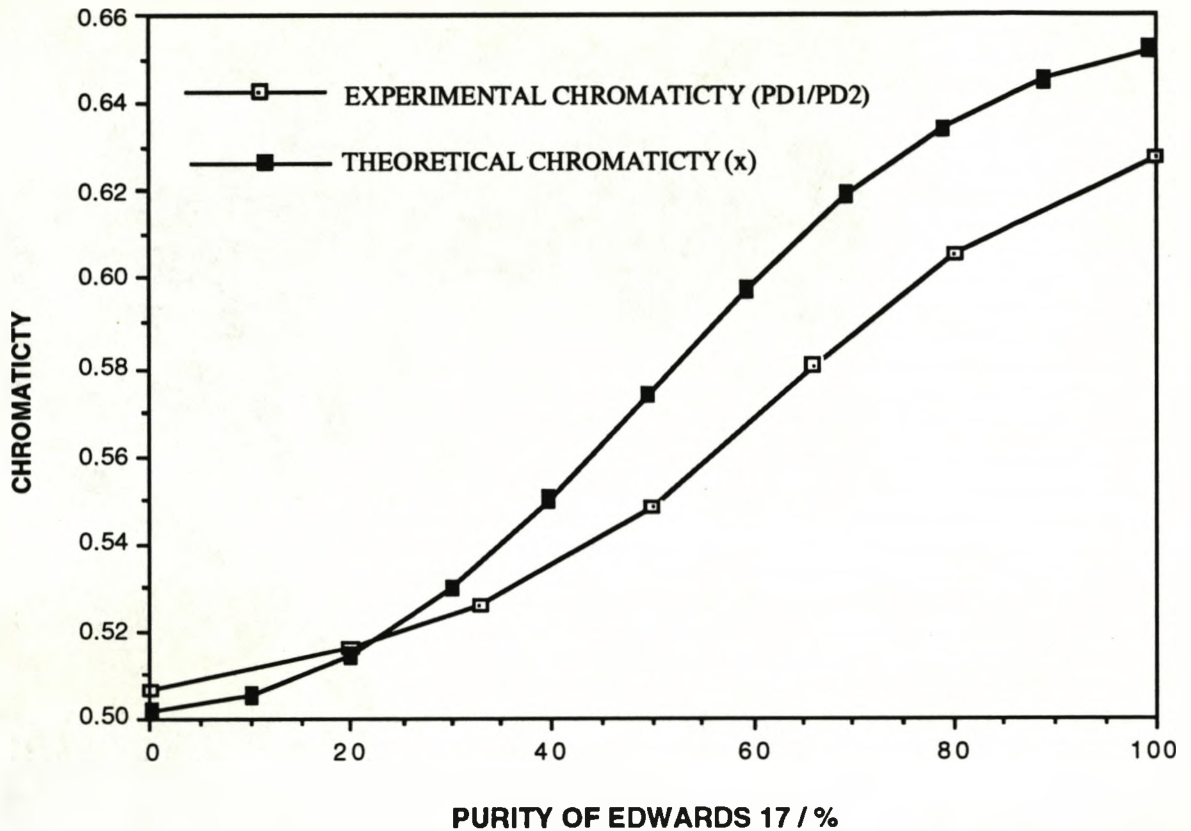

Figure 8.9 Chromaticity of Edwards 17 as a function of purity.

The nonlinearity of the sensor response results in a threshold purity of approximately 20% and a saturation level of 80% beyond which the sensitivity is low. This 'clipping' of the chromatic curve for extreme values of purity limits the range of maximum sensitivity to the central 60% of the oil purity range.

8.4 DISCUSSION

8.4.1 DISCUSSION ON SENSOR SENSITIVITY.

The sensitivity of the oil monitor is dependent on its modulation depth and noise levels. Precautions against noise have been described in chapter 5 so in this section the emphasis will be on improving the modulation depth. Crylin 87 gave particular problems with regard to modulation depth since its greatest spectral change occurred in the green/yellow region of the spectrum (figure 8.3c) rather than the red region where the photodiode triplet had its maximum sensitivity. On figure 8.10 this spectral mismatch between detector and modulator is represented by a sensor response (line of chromatic shift) with a large angle of convergence (ϕ) between the distimulus line and the line of chromatic shift. Selection of photodetectors with appropriate spectral responses reduces this, thus increasing sensor resolution by a factor proportional to cos ϕ.

Even for Crylin 87 the modulation depth and precision obtained are superior to human inspection (Cockrill 1990) and sufficient to trigger an alarm signal when oil quality becomes unacceptable. However guided by software simulations (Russell 1990) it was possible to find a photodetector pair (Hamamatsu GM5 and G1742) that gave a 12% modulation depth for Crylin 87, with a commensurate improvement in sensitivity. This improvement was because the Hamamatsu detector pair were a better spectral match for Crylin 87. However as this oil is a relatively specialist oil no attempt was made to construct a specific sensor for it.

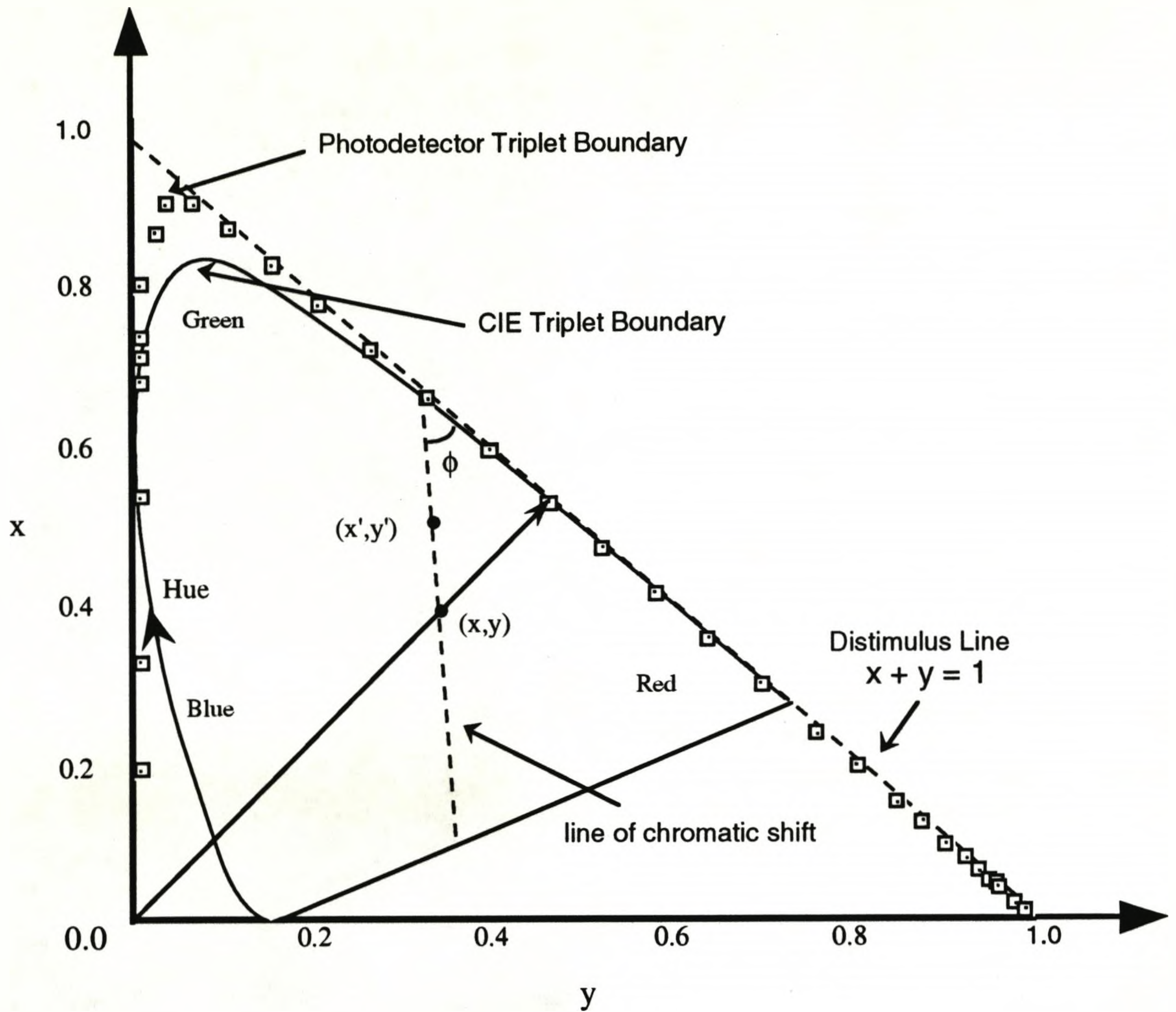

Figure 8.10 Schematic of a sensor response on a CIE diagram.

8.4.2 DISCUSSION ON SENSOR LINEARITY.

Pure and impure oils have different chromaticities and on progressive mixing or progressive degradation of pure oil the chromaticity varies as a smooth function of oil purity. The nonlinearity of this variation is thought to be due to the effects of absorption and scattering (section 4.2.4). The chromatic response of the distimulus system can be estimated by approximating the spectral profiles of the photodetectors to Gaussian curves (with

height A & width λ_p, Moghishi 1990), when the spectral sensitivity of the photodiodes, R_x and R_y (equation 4.3) become:

$$R_x(\lambda) = A_x e^{-bx(\lambda-\lambda_{p1})^2}$$
$$R_y(\lambda) = A_y e^{-by(\lambda-\lambda_{p2})^2} \qquad \text{Equation 8.2}$$

and upon substitution of these spectral profiles, first into equation 4.3 and subsequently into equation 4.5, we have

$$x = \frac{K_x \int P(\lambda)\, A_x e^{-bx(\lambda-\lambda_{p1})^2}\, d\lambda}{K_x \int P(\lambda)\, A_x e^{-bx(\lambda-\lambda_{p1})^2}\, d\lambda + K_y \int P(\lambda)\, A_y e^{-by(\lambda-\lambda_{p2})^2}\, d\lambda} \qquad \text{Eq. 8.3}$$

As a further approximation, equation 8.3 can be simplified by characterising the spectrum $P(\lambda)$ by a single dominant wavelength (λ_d) in the region of spectral overlap:

$$x = (\text{Constant}) \frac{K_x A_x e^{-bx(\lambda_d-\lambda_{p1})^2}}{K_x A_x e^{-bx(\lambda_d-\lambda_{p1})^2} + K_y A_y e^{-by(\lambda_d-\lambda_{p2})^2}} \qquad \text{Eq. 8.4}$$

Appropriate values of responsivity(R), dominant wavelength(λ_d), detector bandwidth(λ_p) and electronic gain (K) were substituted into equation 8.4 to yield the theoretical curve shown in figure 8.9. This analysis of the chromatic variation as a function of wavelength λ_d yields a sigmoid curve. Equation 8.4 only expresses the variation of chromaticity with a monochromatic signal but because broad spectral signals can be represented by changes in a single dominant wavelength as defined by the CIE colour system (Jones et al 1987); changes in this wavelength are equivalent to a monochromatic wavelength shift. Since the dominant wavelength

λ_d is a function of the oil purity (equation 8.4), the oil chromaticity is also a function oil purity as shown in figure 8.9.

Despite the approximations made in equations 8.2 and 8.4, the final equation shows a reasonable fit to the data considering that factors such as differential absorption and scattering have been ignored. In order to account for effects of differential absorption and scattering without access to the spectra of the mixtures, the equations for complex subtractive mixing would have to be applied. Since these equations commonly have no analytic solutions and demand considerable processing power (Billmeyer & Saltzmann 1966), the instrument was empirically calibrated.

It might be argued that for the purpose of instrument design a linear response characteristic would be preferable. However as the sensor described is intended as a warning system for an industrial end-user the low sensitivities for small deviations from complete oil purity might be seen as an advantage.

8.5 CONCLUSIONS

The on-line fibre optic oil condition monitor is capable of measuring the state of purity of machine oils in an industrial environment despite high temperatures and electromagnetic interference. The sensor is shown to exhibit long-term stability and is capable of operating up to a temperature of at least 120°C. Several industrial oils have been examined using the sensor; typical modulation depths of 20% were obtained with noise in the range of 0.1%. These levels of resolution and noise are sufficient for the sensor to predict the optimum time for a system oil

change. They also enable the sensor to monitor oil leaks within a system since it can distinguish between the chromaticity of oil and air.

A direct comparison of the oil sensor performance with that of competing sensors is not possible in this case since no published accounts of comparable sensors have been found. The novelty of the oil sensor is one of its major attractions. Another attraction is the wide range of possible applications; automotive, aerospace and marine applications suggest themselves. However the monitoring of transformer oils in electricity substations seems particularly attractive (Guruprasad 1993) since their isolation makes visual inspection more difficult than for the other cases were human observers are commonly available.

Possible applications are not limited to oil monitoring. There are doubtless many liquid phase processes in the chemical industry where the reaction kinetics can be monitored by absorption spectroscopy; but which are not monitored because of the high cost of this technique. Many of these could probably be monitored inexpensively by a suitably tailored chromatic sensor.

CHAPTER 9
CONCLUSIONS

9.1 PERFORMANCE OF THE OPTICAL SENSORS

A review of plasma processing techniques has highlighted some of the problems encountered by the semiconductor industry, in their attempts to ensure high product quality. Three process monitoring characteristics were considered; the condition of the processing plasma, the thickness of dielectric thin films and the condition of the vacuum pump oils. These characteristics were linked by the fact that human experts were capable of monitoring them by observing their colour. This connection encouraged the investigation of electronic colour sensing as a generic technology for the plasma processing industry.

Formal concepts of colour and chromaticity were introduced and the variation of colour was studied as a function of spectral mixing and spectral shifts. It was found that additive spectral mixing resulted in linear chromatic shifts with a characteristic gradient for each pair of spectra; this allowed the chromatic sensor to distinguish between spectral changes which appear identical to an intensity sensor. When the wavelength of the incoming spectrum shifted the chromaticity was found to trace out a curve the radius of which was proportional to the chromatic saturation; this allowed the chromatic sensor to distinguish between chromatic orders which appear identical to the eye. These advantages coupled to its insensitivity to intensity fluctuations and efficient use of optical power encouraged the development of electronic sensors designed to operate on chromatic principles.

Practical implementation of chromatic sensing has been described and the performance of the sensor was evaluated in

terms of sensitivity(%), stability(%) and repeatability(%). The commercial value of each sensor is best appreciated by direct comparison with competing technologies.

Semiconductor quality is known to depend on the physical and chemical condition of the processing plasma. Table 9.1 refers to the chromatic sensor when applied to plasma condition/endpoint monitoring and compares its performance to that of the two methods most commonly employed, optical spectrometry and visual inspection.

Sensor Parameter	Chromatic Sensing	Optical Spectrometry	Visual Inspection
Mixture Sensitivity	1.7% change in $CF_4/O_2:N_2$	1% change in $CF_4/O_2:N_2$	10% change in $CF_4/O_2:N_2$
Power Sensitivity	2W in CF_4/O_2	1W in CF_4/O_2	3W in CF_4/O_2
Pressure Sensitivity	1.7mTorr in CF_4/O_2	1mTorr in CF_4/O_2	5mTorr in CF_4/O_2
Optical Sensitivity	10nW	25μW	Variable
Noise	0.05%	0.01%	Variable
Bandwidth	5Hz(upto 5kHz)	10Hz	1Hz

Table 9.1 A comparison of plasma condition sensors.

This table shows that chromatic sensing demonstrates a sensitivity to plasma mixture, power and pressure that is comparable to that shown by optical spectroscopy and significantly superior to visual inspection. However the optical

sensitivity of the eye and chromatic sensor are significantly better than that of spectrometers since they require no dispersive elements. The chromatic plasma condition monitor can potentially have a far higher bandwidth than the alternatives, making it the preferred choice for on-line process control. It should be noted that the bandwidth of the most modern CCD based spectrometers can match those of the chromatic sensor but these are even more expensive than the spectrometer shown. Perhaps the most significant advantage of chromatic sensing is its relatively low cost of implementation.

Sensor Parameter	Chromatic Sensing	Optical Spectrometry	Visual Inspection
Thickness Sensitivity	2Å of Si_3N_4	2Å of Si_3N_4	15Å of Si_3N_4
Optical Sensitivity	10nW	25μW	Variable
Repeatability	20Å of Si_3N_4	20Å of Si_3N_4	50Å of Si_3N_4
Bandwidth	5Hz	10Hz	1Hz

Table 9.2 A comparison of film thickness sensors.

Constant thickness of dielectric films is one of the key quality parameters in semiconductor processing. The chromatic thin-film monitor is compared with the methods of optical spectrometry and visual inspection which are currently used in the semiconductor industry. This comparison is made in table 9.2, which illustrates that chromatic sensing and spectrometry share good sensitivity, stability and are capable of on-line application.

The good optical sensitivity of visual and chromatic systems is less significant in this application than in the plasma monitor since the source intensity can be increased arbitrarily; as a result the only advantage of visual inspection is that it is 'free' although the salary of an expert operator may be significant. The choice between the performance spectrometry and chromatic sensing is less clear cut; as before the most significant advantage of chromatic sensing is its relatively low cost of implementation.

Unlike the previous sensing applications the field of oil condition monitoring has not resulted in the development of specific sensors as can be seen from the lack of published material. Although oil degradation is of commercial significance it normally occurs so slowly that periodic visual checks are sufficient to ensure that adequate quality is maintained. The period between observations can be several weeks but the large number of pumps employed in a semiconductor processing foundry ensure that this can still be a time consuming operation.

Sensor Parameter	Chromatic Sensing	Visual Inspection
Impurity Sensitivity	0.1% of Edwards 17	5% of Edwards 17
Repeatability	0.1% of Edwards 17	3% of Edwards 17
Bandwidth	5 Hz	Weekly

Table 9.3 Performance of the chromatic oil condition sensor.

The performance of a chromatic oil condition monitor is compared to visual inspection in table 9.3. The chromatic oil monitor demonstrates significant advantages over visual inspection in the

areas of sensitivity, repeatability and bandwidth. These advantages in conjunction with the relatively low price indicate that the sensor is well suited to replacing visual inspection in applications where intermittent inspection may overlook critical faults.

9.2 SUGGESTIONS FOR FUTURE WORK

One notable advantage of chromatic modulation over spectrometry is the ease with which it can be adapted to spatial monitoring. The colour of each point on a plane can be measured simply by replacing the photodiode triplet by a trichromatic CCD array. Advances in CCD technology have reduced their cost to the point where the their application to industrial sensing has become viable. Recently it has been reported (Takikawa & Sakakibara 1991) that CCD arrays provide valuable spatial information when used to monitor flames used in industrial combustion chambers. This technique may provide valuable information (Ahmed 1994) when applied to plasma monitoring, since spatial information on the chromaticity of a plasma discharge may lead to better control of etching uniformity over a large electrode. Most plasma monitors cannot be easily modified to yield spatial information so this possibility is worthy of further research.

Spatial maps of film thickness would also be of great interest since nonuniform film thickness is a major problem in semiconductor manufacture. Currently uniformity is quantified by the thickness gradient between two points; this value is used to judge wafer quality and is sometimes used to judge the suitability of the plasma processing parameters being used. A CCD generated

contour map of film thickness would provide more detailed information on uniformity and might therefore result in improvements in process control. It might even be possible to provide a real time evolution of a film thickness contour and correlate this with changes in the spatial distribution of the processing plasma. But even if this is not possible the promise of improved wafer characterization is of sufficient interest to warrant further investigations.

Another area for future research is the selection of light sources. Advances in semiconductor sources are so rapid that they may soon replace tungsten filament lamp source used for the thin film and oil sensors. Ultrabright red LEDs are already available and their use has been described in chapter 7, but when ultrabright green and blue LEDs become available it may become possible to use a triplet of such LEDs as the source for a chromatic sensor. Their main advantage would be their low cost but since their emission linewidths are relatively narrow and fail to cover the entire visible spectrum their use in chromatic sensors must be viewed with caution.

One significant alteration should be made to the chromatic sensors described in this thesis before they become suitable for commercial production. The simple analogue circuitry described in chapter 5 should be replaced by more noise tolerant digital circuitry. Shortly after the completion of this thesis these modifications were made by Chell Instruments Ltd. (Edwards 1993) from whom a commercial chromatic plasma monitor is currently available for purchase.

REFERENCES

Adams C R:
'Applied Materials', *Solid State Electronics*, Vol 10. 1967 p.63.

Ahmed S U:
Intelligent Remote Chromatic Processing, *Ph.D Thesis, University of Liverpool 1994.*

Azzam R M & Bashara N M:
Ellipsometry and Polarized Light. *North Holland, Amsterdam 1971.*

Baker P:
Chell Instruments, Norfolk. Private Communication March 1990.

Bar W:
'Electrical characteristics of thin-films.' *Z.Phys,* Vol 115 pp658-667, 1940.

Beavan C M
Colour Measurement in Optical Metrology. *PhD Thesis, University of Liverpool 1989.*

Berg A A & Dean P J:
Light Emitting Diodes, Chapter 5, *Oxford University Pess, Oxford 1976.*

Billmeyer & Saltzmann:
Principles of Colour Technology, *John Wiley & Sons 1966.*

Chen F F:
Electric Probes, Chapter 4_Plasma Diagnostic Techniques, pp113-200. *Academic Press 1965.*

CIE 1931
International Commission on Illumination, *Proceedings of the Eighth Session, Cambridge. England. Bureau Central de la Paris 1931.*

CIE 1978 International Commission on Illumination, *Recommendations on Uniform Color Spaces, Supplement No.2 (TC-1.3, 1978) to CIE Publication No.15 (E-1.3.1, 1971), Bureau Central de la Paris 1978.*

Clegg P L & Crook A W:
Journal of Scientific Instruments , Vol 29 pp201 1952.

Coburn J W:
'Pattern Transfer', *Solid State Technology*, pp117-122, Jan. 1986.

Cockrill:
GEC - MMT Research Laboratories Caswell. Private Communication April 1990.

Dakin J P:
'Analogue and digital extrinsic optical fibre sensors based on spectral filtering techniques' *SPIE Vol.468, Fibre Optics '84 (SIRA), 1984.*

Eckman D P:
Industrial Instrumentation. *Wiley Eastern Ltd. 1966.*

Edwards
Product Catalogue 1990

Elliot D J:
Integrated Circuit Fabrication Technology, pp11-13 *McGraw Hill 1982.*

Fonash S J:
'Advances in Dry Etching Processes', *Solid State Technology*, pp150-158, Jan. 1985.

Francis J:
In-situ thickness measurement of SiO_2 during growth at low temperature,
M.Eng dissertation, University of Liverpool 1992.

Giallorenzi T D et al
'Optical Fibre Sensor Technology'. *IEEE Journal of Quantum Electronics,* 1982, QE-18 pp 626-665.

Gregory R L:
Eye and Brain *the psychology of seeing.* (3rd Edition) *Weidenfield & Nicholson 1986.*

Guruprasad K P:
Bangalore Central Power Research Institute. Private Communication January 1993.

Hancock G:
'Quantitative Optical Diagnostics in Plasma Chemistry'. pp 8/1-8/3 IEE Colloquium on *Plasma Chemistry, Sources and Diagnostics*, No.090 April 1991.

Heavens O S:
Optical Properties of Thin Solid Films, Chapter 5 pp102-103. *Dover Press 1955.*

Hecht E:
Optics *McGraw-Hill (Schaum)* p25 1975.

Henderson P J:
Chromatic Modulation Systems for Multiparamenter Measurement in Physically Demanding Environments, *PhD. Thesis, University of Liverpool 1990.*

Hondros D & Debye P:
'Electromagnetic waves along long cylinders of dielectric, *Annal. Physik*, 32(3), pp. 465-476, 1910.

Hopkins H H & Kapany N S:
'A flexible fibrescope, using static scanning', *Nature, London,* 173, pp. 39-41, 1954.

Huggett P G:
Private communication 1992

Hutley M C:
'Wavelength encoded optical sensors for the measurement of displacement', *Sensor Review*, Vol. 5, No.2, pp 64-68, 1985.

Irving S M:
Kodak Photoresist Seminar, Vol.68 pp26-29, May 1968.

Jones G R, Kwan S, Beavan C, Henderson P, Lewis E:
'Optical Fibre Based Sensing Using Chromatic Modulation'. *Optics & Laser Technology* Vol 19, No.6, 1987, pp 297-303.

Kao K C & Hockham G A:
'Dielectric-fibre surface waveguides for optical frequencies', *Proceedings of the IEEE,* 113, pp. 1151-1158, 1966.

Kawata H, Takao Y, Murata K and Nagami K :
'Optical Emission Spectroscopy of Plasmas Using a New Technique.' *Plasma Chemistry and Plasma Processing*, Vol.8, No.2, 1988.

Keenan W A, Keefer M E, Gise P E, Thornquist L A:
'Film Thickness Mapping of Advanced Wafer Production Processes' *Microelectronics Manufacturing Technology February 1991.*

LFE:
Corporation Technical Bulletin 8212-TA1, April 1975.

Land E H:
'Experiments in Colour Vision'. *Scientific American,* May 1959 Vol.200, pp84-89.

Li T:
'Structures, Parameters and Transmission Properties of Optical Fibers'. *Proceedings of the IEEE,* Vol.68, pp. 1175-1180, 1980.

Lochte-Holtgreven W:
'Plasma Diagnostics', *North-Holland Publishing Company, Amsterdam 1968.*

Lucas
Product Reference: OSL - 00513.

Maiman T H:
'Stimulated Optical Radiation in Ruby Masers', *Nature* 187, p193 1960.

Mayer T M, Ameen M S, Vitkavage DJ:
Surface Chemistry of Dry Etching Processes, Chapter 10, The Chemical Physics of Solid Surfaces and Heterogeneous Catalysis, Vol.5 Surface Properties of Electronic Materials, pp427-464. *Elsevier 1988.*

Meyer-Arendt J R:
Introduction to Classical and Modern Optics. *Prentice Hall Inc. 1984.*

Mogab C J, Adams A C, Flamm D L:
'Plasma Etching of Si and SiO_2 - The effect of oxygen additions to CF_4 plasmas.'
Journal of Applied Physics, Vol.49 No.7, pp3796-3803, July 1978

Mogab C J:
VLSI Technology, Chapter 8_Dry Etching pp303-345. McGraw-Hill 1983.

Moghishi M:
Optical Current and Voltage Sensors, *PhD. Thesis, University of Liverpool 1990.*

Morse K:
Chromatic Plasma Monitoring, *PhD. Thesis, University of Liverpool 1992.*

Overheim R D & Wagner D L:
Light and Colour. *Wiley, New York 1982.*

Pitt G D
'Optical-Fibre Sensors'. *IEE Proceedings*, Vol.132, Pt. J, No.4, 1985 pp 214-248.

Rae A I M:
Quantum Mechanics, Chapter 1 p3, *Adam Hilger 1986.*

Reif F:
Fundamentals of Statistical and Thermal Physics, pp373-388. *McGraw Hill 1965.*

Robinson J W:
Practical Handbook of Spectroscopy, *CRC Press, Inc 1991.*

Russell P C, Morse K, Khandaker I, Glavas E, Jones G R:
'Computer Aided Design of an Optical Fibre Sensor Based upon Chromatic Modulation', *Applied Optics and Opto-electronics*, Sept. 1990, Nottingham, 159-160.

Semura S & Saitoh H:
'Hydrogen mixing effects on reactive ion etching of GaAs in chlorine containg gases.'
Journal of Vacuum Science & Technology A, Vol.2 No.2, pp474-476, April 1984.

Senior J M:

Optical Fibre Communications, Principles and Practice, *Prentice Hall International 1985.*

Sigmund P:

'Theory of sputtering I. Sputtering yield of amorphous and polycrystalline targets.' *Physical Review,* 184, 383 1969.

Snell D & Pitt G D:

Proceedings of International Conference on Optical Techniques in Process Control, 1983, pp 27-41 (BHRA Fluid Engineering Publications, Cranfield, Beds, U.K. 1983).

Spillman W B:

'Multimode fibre optic pressure sensor based on the photoelastic effect', *Optics Letters,* Vol.7, pp. 388-390, 1982.

Steel W H:

Interferometry, *Cambrige University Press 1986.*

Sugano T:

Applications of Plasma Processes to VLSI Technology. *John Wiley and Sons 1985.*

Takikawa H & Sakakibara T:

'Radiative Aspects of Ablation Stabilized Arc in Polyethlyne Tubes', *Journal of Toyohashi University of Technology,* pp 11-32, May 1991.

Wilson J & Hawkes J F B:

Optoelectronics: An Introduction, *Prentice Hall International 1983.*

Yariv A:

Quantum Electronics, Section 14.8, *John Wiley*, 1975.

Zarowin C B:

Proc. 4th Symposium on Plasma Processing, Vol.83_10 pp11-30, The Electrochemical Society, Pennington, New Jersey 1983.

APPENDIX

Parts of this thesis have been accepted for publication elsewhere:

[1] **Chromatic monitoring of emissions from material processing plasmas for on-line diagnosis of irregularities** appeared in the *Proceedings of the Tenth International Conference on Gas Discharges and their Applications. Swansea 13-18 September 1992.* (From Chapter 6)

[2] **A fibre-optic oil condition monitor based on chromatic modulation** appeared in the May 1993 issue of *Measurement Science and Technology No.4 pp608-613.* (From Chapter 8)

[3] **Chromatic modulation as an on-line plasma monitoring technique** appeared in the January 1994 edition of *Vacuum Vol.45, No.1 pp109-113.* (From Chapter 6)

[4] **Chromatic monitoring for the processing of materials with plasmas** appeared in the March 1994 issue of *IEE Proceedings of Science & Measurement Technology, Vol 141, No.2, pp99-104.* (From Chapter 7)

[5] **Chromatic interferometry for an intelligent plasmas processing system** appeared in the May 1994 issue of *Measurement Science and Technology No.5 pp639-647.* (From Chapter 6 & Chapter 7)

[6] Also included is the sales brochure and price list for the **PlasmaChrom™** sensors developed in this thesis.

Proceedings of the Tenth International Conference on

GAS DISCHARGES AND THEIR APPLICATIONS

Swansea 13 - 18 September 1992

Editor: W. Terry Williams

Volume II

Organised in association with the:

Institution of Electrical Engineers
Institute of Physics
International Society for Optical Engineers
Society of Chemical Industry

Department of Physics
University College of Swansea
Swansea, Wales, U.K.

SWANSEA

CHROMATIC MONITORING OF EMISSIONS FROM MATERIAL PROCESSING PLASMAS FOR ON-LINE DIAGNOSIS OF IRREGULARITIES

P.C. Russell, I.I. Khandaker, E. Glavas, K. Morse, D. Alston, G.R. Jones.

Department of Electrical Engineering and Electronics, University of Liverpool, Brownlow Hill, PO Box 147, Liverpool, L69 3BX

1 Introduction

Plasma processes are now widely used in industry, especially for surface modification and for semiconductor processing. The complex nature of the plasma state makes it difficult to accurately predict the behaviour of a plasma processing system, leading to problems in setting up a stable process. All plasma systems have to be individually characterised to produce a system specific operating recipe. Having established a stable operating point, further problems arise due to variations between runs. Many semiconductor processes are sensitive to variations, leading to changes in the resulting device characteristics.

A number of techniques have been used to monitor and characterise plasmas. These conventional monitoring systems are either intrusive (eg the Langmuir probe) or rely on spectroscopic analysis of the plasma, either optical or mass spectrometry. The Langmuir probes can give useful information on the state of the plasma and have been successfully used in the transferral of processes between chambers [1]. However, because of their intrusive nature, Langmuir probes would not be acceptable as continuous monitors; the probe tends to cause a local disturbance in the plasma that affects uniformity across the processing system.

Optical and Mass spectrometry have both been used to provide information on plasma processes [2]; both techniques are non invasive and give information on the ionic content of the plasma. Both of these techniques can be used, on a run by run basis, and can indicate variations. However, the instruments required for these techniques are expensive and produce data that is not easily interpreted.

In this contribution a non-invasive monitoring system is described, based upon chromatic modulation. This system monitors the optical emissions of the plasma and produces rapid output indicating the current state of the plasma. The output from this system can be used to indicate variations from one run to another and to identify problems within a run.

2 Chromatic modulation based sensors

Chromatic modulation refers to the utilisation of polychromatic light for sensing changes within a physical system. Chromatic sensors are based on an array of photo detectors with overlapping wavelength dependent response's $c(\lambda)$. The output from each detector when used to monitor an optical signal having a spectral power distribution $P(\lambda)$ will be

$$V=\int_{\lambda} P(\lambda)\, C(\lambda)\, d\lambda$$

For many optical systems the monitoring system is optimised using three detectors with responses $c_x(\lambda)$, $c_y(\lambda)$ and $c_z(\lambda)$ giving three outputs

$$V_X=\int_{\lambda} P(\lambda)\, C_X(\lambda)\, d\lambda$$

$$V_Y=\int_{\lambda} P(\lambda)\, C_Y(\lambda)\, d\lambda$$

$$V_Z=\int_{\lambda} P(\lambda)\, C_Z(\lambda)\, d\lambda$$

These three outputs can be normalised according to

$$x = V_x (V_x + V_y + V_z)^{-1}$$

$$y = V_y (V_x + V_y + V_z)^{-1}$$

$$z = V_z (V_x + V_y + V_z)^{-1}$$

The resulting parameters' x, y and z form chromaticity co-ordinates which quantify the spectral signature P(λ). The state of any one of the chromaticity co-ordinates can be obtained from a knowledge of the other two, hence one of the terms is redundant. If the detector response's c_x, c_y and c_z were made to correspond to those of the cones in the human eye then the resulting x, y plot forms the CIE chromaticity diagram which is well known in the field of colour science [3]. In this representation, saturated or pure colours reside around the periphery of the chromaticity curve, whereas composite spectral signatures reside within the area enclosed by the chromaticity boundary.

These considerations have importance in relation to optical sensors. Firstly, there is the implication that even complicated spectral signals can be quantified in terms of only two parameters' x and y, any change in the spectral signature can therefore be quantified in terms of a change in these two parameters.

A property of the chromaticity co-ordinates x, y and z is that they are normalised with respect to the effective optical power content

$$V_x + V_y + V_z = \int_\lambda P(\lambda)\,(C_x(\lambda) + C_y(\lambda) + C_z(\lambda))\,d\lambda$$

As a result of this property a chromatic sensing system is less sensitive to changes in the intensity of the light brought about by changes in the transmissivity of the optical path. Hence changes in intensity due to a build up of deposit on a plasma chamber window would have little affect on the chromatic signal.

Chromatic sensors have been successfully developed for a number of industrial and medical monitoring applications [4,5]. In this work they have been developed specifically for monitoring plasma processes.

The sensitivity of the optical system is critically dependent on the choice of detectors used. A software package has been produced to aid in the development of the chromatic sensors.

3 Simulation software

A suite of programs have been produced, in 'C' and assembly language, for DOS workstations. These programs allow the user to specify an optical signal as input and choose from a selection of photo detectors. The software calculates the chromaticity co-ordinates of the optical signal using the selected photo detectors. The pure colour boundary for the detectors is displayed graphically and the position of the optical signal within this boundary is indicated.

The simulation software can be used to quantify the change in chromaticity co-ordinates observed when the spectral content of an optical signal changes. The sensitivity of the sensing system to this change can be maximised by selecting different

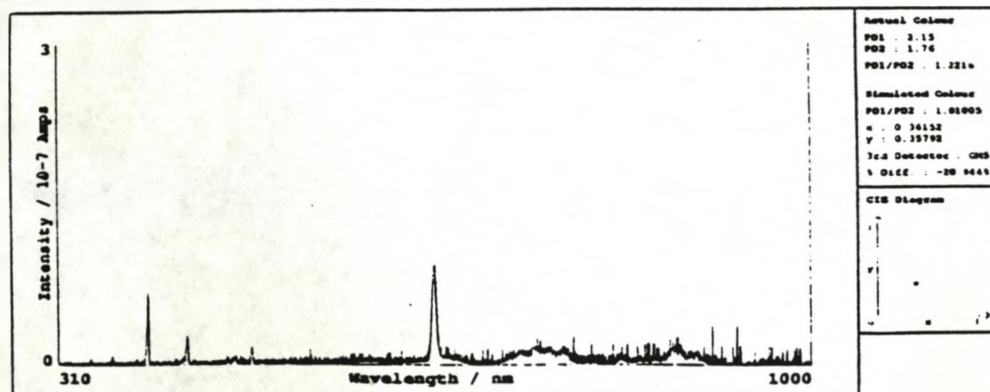

Figure 1 Demonstrates the use of simulation software in the development of chromatic sensors for plasma monitoring.

combinations of photo detectors and choosing the set giving the largest change in chromaticity co-ordinates.

An example of the use of this software in the development of sensors for plasma monitoring is shown in figure 1. The spectral emission of a plasma depends on a variety of parameters, especially the mixture of gases within the plasma. Any change in gas mixture, due to leakage or variation in the mass flow controller, will produce a noticeable change in chromaticity co-ordinates. The spectral emission of a plasma can be monitored using a spectrometer for a series of runs with different conditions. The spectra from each run can be input into the software package and the chromaticity co-ordinates calculated for a series of detector sets. The most sensitive detector set can then be used in a full chromatic monitoring system.

The chromatic monitor has successfully identified faults in these systems and has been used to give information about the state of the process.

When used to monitor the silicon oxidation chamber, a research system, the optical output varied cyclically with time. This cyclical variation proved to be the result of a power supply instability.

The chromatic monitor was used to observe variations in the optical emissions caused by varying the process parameters. These observations were performed both on the plasma nitriding system and on the RIE system. In both cases significant changes in optical emission were observed. Figure 2 shows the variation in chromaticity with pressure. Similar results could be plotted for variations with power and gas mixture.

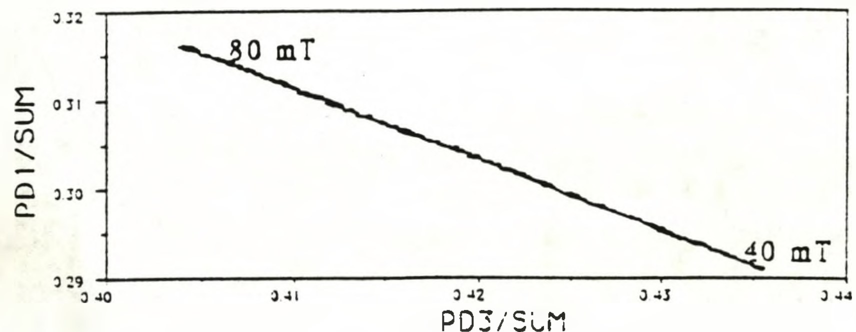

Figure 2 The variation in chromaticity with pressure.

4 Plasma monitoring

A sensor based on chromatic modulation has been developed for monitoring processing plasmas. The optical emission of the plasma is accessed through a quartz view port using an optical fibre, allowing the electronic instrumentation to be situated away from the processing chamber. The monitoring system is based on three photo detectors covering the visible spectrum and extending into the near infrared. This system has been used to monitor a number of semiconductor processing plasmas, including; a reactive ion etching process (RIE), a plasma nitriding process and a silicon thermal oxidation process.

When etching an insulating layer off a semiconductor substrate it is important to know when the etch has finished, thus preventing over-etching. The chromatic monitor shows a clear change when the end point of the etch is reached (figure 3). The data plotted in figure 3 also indicates that there is a significant delay after switching on the plasma before etching begins. This delay is the result of water condensing on the chamber walls whilst the chamber is open for sample loading. This effect can be removed by loading the sample through a port with the chamber filled with nitrogen. This effect illustrates the ability of the chromatic sensor to give rapid information on irregularities within the plasma.

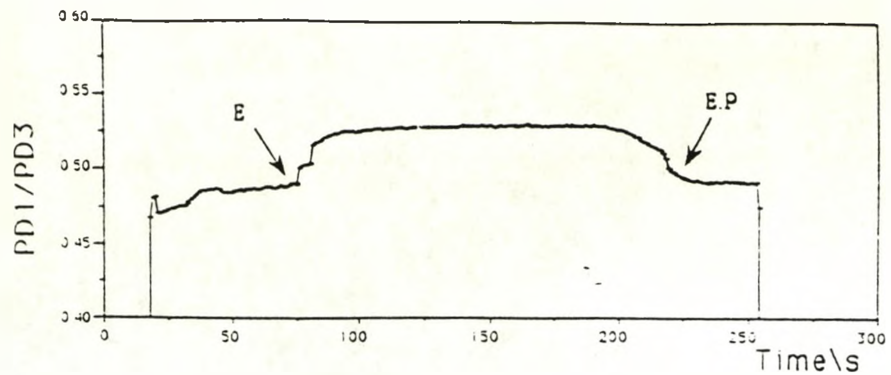

Figure 3 Chromatic monitors have been used to detect the onset (E) and end point (E.P.) of an etching process.

5 Conclusions

Optical sensors based on chromatic modulation have been successfully developed for monitoring plasma emissions. A software simulation package has been developed to allow these sensors to be optimized for any plasma which has optical emissions in the visible and near infrared wavelength range.

The inherent simplicity of these sensors ensures that changes occurring in the optical emissions of the plasma can be identified rapidly, over a wide wavelength range, giving a significant advantage over optical spectrometer techniques. Despite their simplicity they are capable of discriminating changes in optical spectral signatures as low as 0.01nm in wavelength.

These chromatic sensors have identified faults in the radio frequency power supply of a plasma system, indicated changes in the plasma parameters and have been used to give indications of etch end point.

6 References

[1] Cox T.I. et al, "The use of Langmuir probes and optical emission spectroscopy to measure electron energy distribution functions in R.F. generated Argon plasmas", J. Phys. D:Appl. Phys., 20, 1987, 820-831

[2] Thomas D.J. et al, "An investigation of the roughening of Si(100) surfaces in Cl_2/CCl_4 reactive ion etching plasmas by in-situ ellipsometry and quadrupole mass spectrometry: The role of CCl_4", J.Vac.Sci.Technol.B 8 (3), May/Jun 1990

[3] CIE publications 15, "Colorimetry" (1971)

[4] Jones G.R. et al "Optical fibre based sensing using chromatic modulation", Optics and Laser Technol., 19 (6), 1987, 297-303

[5] Kwan S, Beavan C.M. and Jones G.R. "Displacement measurement using a focusing chromatic modulator", Meas. Sci. Technol., 1, 1990, 207-215

Meas. Sci. Technol. 4 (1993) 608–613. Printed in the UK

A fibre-optic oil condition monitor based on chromatic modulation

I I Khandaker, E Glavas and G R Jones

Department of Electrical and Electronic Engineering, University of Liverpool, Brownlow Hill, Liverpool L69 3BX, UK

Received 15 June 1992, in final form 10 February 1993, accepted for publication 11 February 1993

Abstract. A novel optical fibre sensor has been developed for on-line monitoring of oil quality within industrial equipment. The monitoring is based on chromatic modulation because of the inherent self-referencing demonstrated by this technique. The sensor is shown to exhibit long-term stability and is capable of operating up to a temperature of 120 °C. Several industrial oils have been examined using the sensor, and typical modulation depths of 20% were obtained with resolutions in the range of 0.1%. This is sufficient to record some interesting physical and chemical changes related to the reaction kinetics of oil degradation. The sensor is also capable of detecting oil leaks within a system since it can distinguish between the chromaticities of oil and air.

1. Introduction

One of the major factors determining the performance and longevity of industrial machinery is the quality of its lubricating oil. Since the degradation of machine oil is a slow process, commonly taking months, it has become standard practice to replace the oil at regular intervals regardless of its condition. Obviously this procedure fails to allow for varying machine loads and so might lead to oil being replaced when still in good condition or, more seriously, lead to a delay in replacing poor quality oil. The colour of pure oils normally ranges from clear yellow to deep amber, impure oils are of a much deeper shade ranging from dark brown to black. Visual inspection constitutes an inefficient use of manpower, and at best gives only a qualitative indication of oil condition. In an industrial environment, where any down-time may prove costly, an automatic oil-diagnostic system has obvious attractions.

Although a sensor to detect the oil content in water based on laser diffractometry has been reported [1] there is little indication in the literature of a general oil condition monitor.

Fibre-optic sensors demonstrate a number of well-known advantages over conventional electrical sensing techniques. These include their ability to operate in hostile environments and their immunity to stray electric and magnetic fields. Since optical fibre sensors isolate the electronics from the point of detection, they may be used in potentially explosive environments, where electronic sensors might constitute a hazard.

Several methods of optical fibre sensing have been considered as candidates for oil monitoring. These include intensity modulation, interferometry, polarization modulation, diffractometry, wavelength modulation [2, 3] and chromatic modulation [4]. The prerequisites for an industrial oil monitor are low long-term drift, temperature stability, inexpensive instrumentation, high resolution and high optical efficiency. Few sensors can excel in all the above characteristics but chromatic sensing was found to exhibit a balance of performance best suited to an industrial oil monitor.

2. Theory of chromatic modulation

Chromatic modulation refers to the utilization of polychromatic light for sensing changes in a physical system. It relies upon the detection of changes in the total spectral profile of an optical signal and can be considered to be an unusual form of wavelength modulation.

The chromatic modulation technique detects a change in a measurand not by detecting intensity changes at particular wavelengths but by monitoring the sum of the contributions of relative changes at all wavelengths within a spectral power distribution. As such it is an integrated form of spectral monitoring as opposed to the differential (dispersive) nature of most wavelength modulated systems.

Chromatic changes can be monitored by using three photodetectors with overlapping spectral profiles $R_x(\lambda)$, $R_y(\lambda)$ and $R_z(\lambda)$. When addressing an optical signal with spectral power distribution $P(\lambda)$ the output currents of

0957-0233/93/050608+06 $07.50 © 1993 IOP Publishing Ltd

the photodetectors will be

$$I_x = K_x \int P(\lambda)R_x(\lambda)\,d\lambda$$
$$I_y = K_y \int P(\lambda)R_y(\lambda)\,d\lambda$$
$$I_z = K_z \int P(\lambda)R_z(\lambda)\,d\lambda \qquad (1)$$

where K_x, K_y and K_z are constants of proportionality and λ is the wavelength. Equations (1) may be normalized with respect to the effective optical power according to

$$x = I_x/(I_x + I_y + I_z)$$
$$y = I_y/(I_x + I_y + I_z)$$
$$z = I_z/(I_x + I_y + I_z). \qquad (2)$$

If the parameters x, y and z are calculated from a standard set of idealized detectors, a plot of x against y results in a diagram which forms the basis of colour science, according to a convention agreed by the Commission Internationale de l'Eclairage (CIE) [4]. A similar slightly distorted diagram results (figure 1(*a*)) if a non-standard photodetector triplet is used. An entire spectrum is represented by a single point on a CIE diagram and any changes in hue can be represented as changes in the angle θ. If non-standard detectors are used a parameter analogous to hue (referred to as chromaticity) can be measured. Commercial considerations dictated the use of a non-standard detector triplet, the spectral profiles of which are shown in figure 1(*b*).

The normalization of x, y and z has an important implication for optical sensing, namely that chromatic detection techniques are independent of intensity. The inherent intensity compensation renders the chromatic sensor immune to changes in the intensity transmitted through the optical system although it remains vulnerable to changes in the transmission spectrum of the optical system.

This advantage is still apparent if only two detectors are used but in this case it is not possible to distinguish between colours of different saturation since the CIE or chromatic regions collapse to the line $x + y = 1$. If hue is the feature of interest then this simpler distimulus technique can be used in place of the full chromatic approach. Selection of photodetectors with appropriate spectral responses reduces the angle of convergence (φ) between the distimulus line (figure 1(*a*)) and the line of chromatic shift, thus increasing sensor resolution by a factor proportional to cos φ.

In this simplified distimulus form, chromatic modulation utilizes two photodetectors to address the region of spectral overlap and equations (2) reduce to

$$x = I_x/(I_x + I_y) \qquad y = I_y/(I_x + I_y). \qquad (3)$$

Because of the linear relationship between x and y, either parameter may be used to represent distimulus chromaticity. The simplified response of the distimulus system can be estimated by approximating the spectral profiles of the photodetectors to Gaussian curves, when the spectral sensitivities of the photodiodes, R_x and R_y become

$$R_x(\lambda) = A_x e^{-b_x(\lambda - \lambda_{p1})^2}$$
$$R_y(\lambda) = A_y e^{-b_y(\lambda - \lambda_{p2})^2} \qquad (4)$$

and upon substitution of these spectral profiles, first into equations (1) and subsequently into equation (3), we have

$$x = \frac{K_x \int P(\lambda)A_x e^{-b_x(\lambda - \lambda_{p1})^2}\,d\lambda}{K_x \int P(\lambda)A_x e^{-b_x(\lambda - \lambda_{p1})^2}\,d\lambda + K_y \int P(\lambda)A_y e^{-b_y(\lambda - \lambda_{p2})^2}\,d\lambda}. \qquad (5)$$

To illustrate the operation of the technique, equation (5) can be simplified by characterizing the spectrum $P(\lambda)$ by a single dominant wavelength (λ_d) in the region of spectral overlap:

$$x = \text{constant}\ \frac{K_x A_x e^{-b_x(\lambda_d - \lambda_{p1})^2}}{K_x A_x e^{-b_x(\lambda_d - \lambda_{p1})^2} + K_y A_y e^{-b_y(\lambda_d - \lambda_{p2})^2}}. \qquad (6)$$

This analysis of the chromatic variation as a function of wavelength λ_d yields a sigmoid curve. Equation (6) only expresses the variation of chromaticity with a monochromatic signal but, since broad spectral signals can be represented by changes in a single dominant wavelength as defined by the CIE colour system [4], changes in this wavelength are equivalent to a shift in the wavelength of a monochromatic source. Since the dominant wavelength is a function of the oil purity, equation (6) can be used to relate oil chromaticity to oil purity as shown in figure 6 later.

Despite the approximation made in equations (4), the final equation shows a good fit to the data considering that factors such as differential absorption and scattering have been ignored. In order to account for effects of differential absorption and scattering, the equations for complex subtractive mixing would be required. Since these equations commonly have no analytical solutions and demand considerable processing power [5] they were not considered essential to the description of an instrument which is empirically calibrated.

3. Sensor design

Preliminary experiments conducted with a simple transmissive system were satisfactory but since the degree of

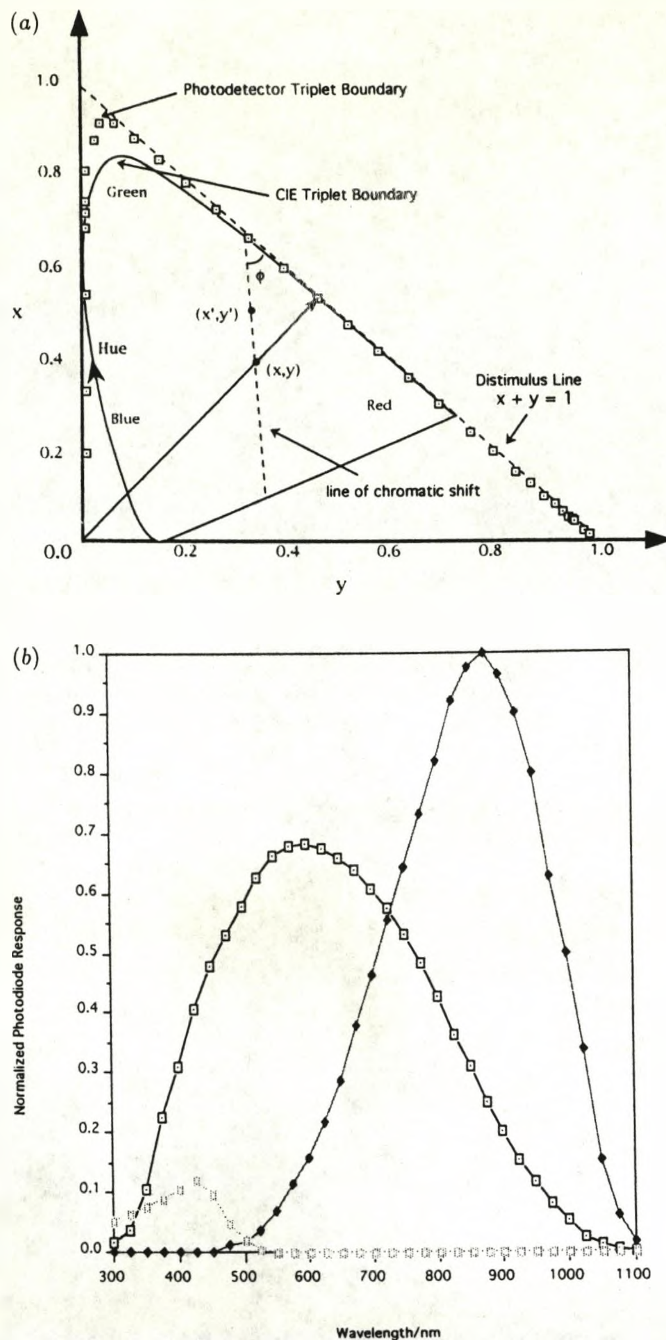

Figure 1. (*a*) CIE chromaticity diagram. *x* and *y* represent normalized photodetector outputs. (*b*) Normalized spectral responses from the photodiode triplet used in the chromatic sensor.

access to the oil sump can vary greatly from machine to machine, the probe was redesigned to operate in a reflective mode so as to be minimally invasive. A reflective probe eliminates the need for two access ports to the sump as well as avoiding the need to bridge the oil sump. Two forms of reflective probe were constructed: one using total internal reflection in a prism, and the other using a spherical lens and plane mirror combination.

The prismatic approach was an attempt to avoid the problems of silvered surfaces. An equilateral prism was drilled longitudinally to provide a path of entry for the oil. Optical access to the oil was obtained by butting the emitter and receiver fibre to the side of the prism. Collimating lenses were used to reduce the divergence of the input and output beams. The performance of this design was similar to that of the spherical lens and plane mirror assembly, but it was rejected on the grounds of cost and probe size.

In the probe incorporating the plane mirror, a collimating lens was used in order to reduce beam divergence. In order to be minimally invasive, the probe length was restricted by selecting a lens with as short a focal length as possible. The spherical soda glass lens chosen had a

focal length of just 2.5 mm. The oil cavity should be illuminated by collimated light in order to eliminate chromatic aberration caused by the refractive index of the oil. This is best achieved by placing the emitter/receiver fibre at the focus of a biconvex lens; the emergent light is then parallel. A four-tailed silica fibre bundle was used, each tail having 1 mm diameter and the head 4 mm diameter.

A probe was made to this design and engineered to survive industrial conditions (figure 2). The optical system described above was encapsulated in a $\frac{3}{8}''$ BSP machine screw for protection and ease of access. Separation between the optical components was maintained by annular nylon spacers. Six holes each of 3 mm radius were drilled into the optical cavity, these were sufficient to provide good drainage for the optical cell. A glass sphere of radius 5 mm was placed 2.5 mm from the fibre bundle and a glass window was placed between the sphere and the plane mirror to create the optical cell. A cavity length of 6 mm was found to give the highest signal : noise ratio.

A white light source, with the spectral characteristics shown in figure 3, was used to couple 120 μW of optical power into the sensor. Following losses due to transmission, reflection and coupling, 10 μW of optical power was converted into an electrical signal by the photodiodes and subsequently amplified by a standard gain stage constructed from a transimpedance amplifier. The resulting photocurrent was recorded onto a computer via a 12-bit ADC and subsequently processed by software described elsewhere [6].

The probe was fitted to the sump of an AEI Metrovac Type GS 10 rotary vacuum pump to investigate the sensor performance.

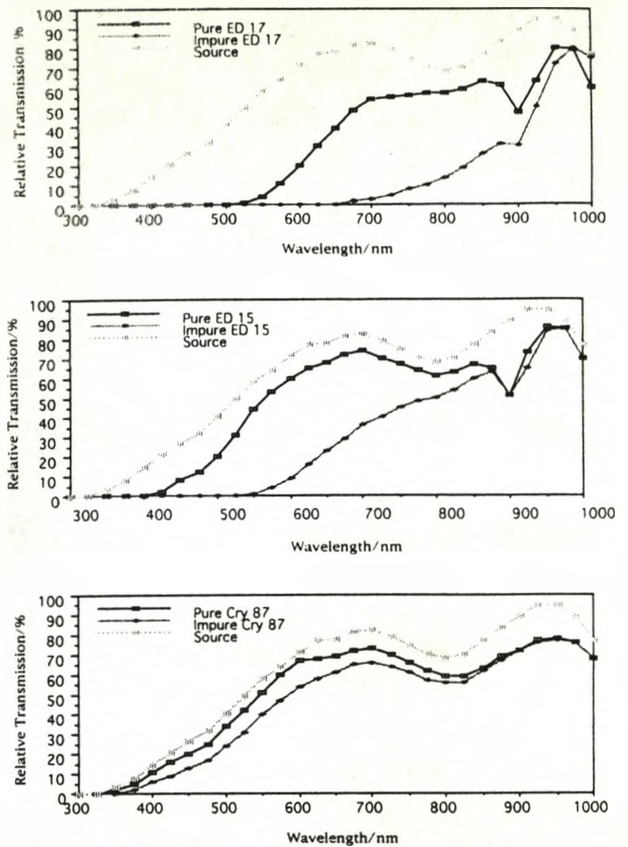

Figure 3. Transmission spectra for pure and impure oils.

4. Results

4.1. Modulation

Although the difference in hue between pure and impure oils is sometimes apparent to the naked eye, the eye is known to be very sensitive in discriminating between hues; hence it was necessary to ensure that a combination of commercially available photodetectors would be capable of discriminating between the pure and impure oil samples. Transmission spectra of these samples were recorded whilst within the probe (figure 3) and digitized to allow a computer program [6] to calculate the distimulus chromaticity. These values were then compared with the experimental results. On examination of these spectra, the decision was taken to ignore the

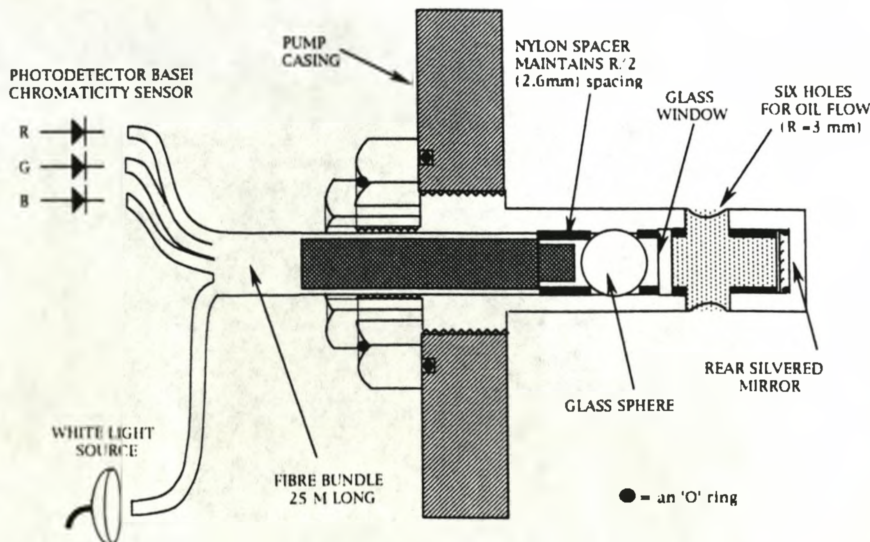

Figure 2. Schematic diagram of the oil condition probe.

blue photodiode and concentrate on the red and IR photodiodes.

Three industrial pump oils were examined for their chromatic modulation depth, a parameter defined by

$$\frac{\text{chromaticity of pure sample} - \text{chromaticity of impure sample}}{\text{chromaticity of pure sample}} \times 100\%.$$

These oils were Edwards 15, Edwards 17 and Crylin 87; the pure and impure oil chromaticities are shown in figure 4. Edwards 15 shows a chromatic modulation depth approximately 20% of signal, Edwards 17 shows a modulation depth 20% of signal but one of the more specialist oils, Crylin 87, shows a modulation depth of only 5%, although this is not surprising as both pure and impure samples are clear to the eye. These experimental values correlate well with the computer predictions of a 26% modulation depth for Edwards 15, 24% for Edwards 17 and 7% for Crylin 87. The discrepancy between the predicted and measured values is in part due to the sensitivity of the photodetectors in IR regions where spectral information was unavailable for use in the simulation software.

A resolution of approximately 0.1% was attained for the chromatic changes in the two Edwards oils, and a resolution of approximately 0.5% for Crylin 87. Even for Crylin 87 the modulation depth and precision obtained are more than sufficient for industrial oil monitoring. However, guided by software simulations [6], it was possible to find a photodetector pair that gave a 12% modulation depth for Crylin 87, with a commensurate improvement in resolution.

4.2. Stability

Having established that it is possible to detect the difference between pure and impure oils, the next step was to examine the stability of the colour output. The chromatic stability of the white light source used to illuminate the oil is a critical factor determining the overall chromatic stability of the instrument. To minimize this limitation a specially designed, stabilized white light source [7] with a chromatic drift of approximately 0.1% was used.

In order to test the temperature stability of the probe, the sensor head was heated from room temperature to 120 °C whilst inside the pump containing pure Edwards 17. The temperature change caused a 0.5% chromatic drift on a 20% modulation depth, whereas the intensity shows a five-fold drift over a comparable modulation depth. Figure 5 shows the light intensity fluctuating strongly as the temperature rises, whilst the colour remains remarkably constant, vindicating the preference for a chromatic sensor over an intensity sensor.

A further noise component may arise from mechanical changes in the probe. Chromaticity values from a probe in an operational (and hence vibrating) pump were compared with values from the pump when switched off and no measurable differences were observed.

4.3. Repeatability

The repeatability of the chromatic signal obtained from Edwards 15 was checked by filling and draining the probe in cycles. Oil colour showed repeatability within 1% of the modulation depth, air colour showed a far poorer repeatability of the order of 4%. The implications of this for the system viability as an oil condition level are not as serious as they first appear after a period of 5 min the different air colours tend to converge to within 1% of each other.

The origin of this chromatic instability proved to be the formation of oil films which exhibit thin film interference, so giving rise to large chromatic changes. These effects are most pronounced when observing the edges of an oil meniscus where light and dark interference fringes are visible to the naked eye. The formation of these films may explain why the oil colour repeatability is limited to 1%.

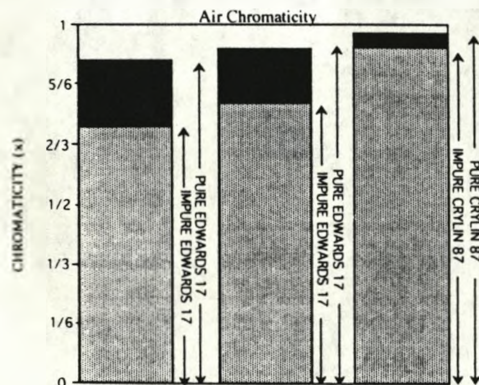

Figure 4. Modulation depth for three pump oils with air as a reference.

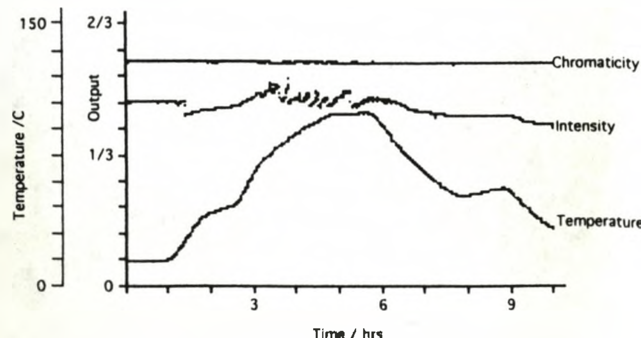

Figure 5. Temperature stability of a chromatic sensor compared with that of an intensity sensor.

The effects of rotating the fibre bundle within the probe head was also examined. Initially a segmented fibre bundle was used, in which the fibres were arranged in quadrants. The bundle was rotated through two complete circles and the chromatic changes recorded. The changes were large (20%) and demonstrated that the system lacked rotational symmetry. When this bundle was replaced by a randomized fibre bundle this source of noise was reduced to a level below that of source noise.

4.4. Linearity

Pure and impure oils have different chromaticities and on progressive mixing or progressive degradation of pure oil the chromaticity varies as a smooth function of oil purity. When two coloured lights are mixed (additive colour mixing) the chromaticity is a linear function of mixture; however, when two oils are mixed (subtractive colour mixing) the situation is complicated by self-absorption and scattering which result in chromaticity showing a sigmoid response to changes in mixture. Figure 6 is a graph showing the variation of chromatic output from Edwards 17 oil as a function of purity, where pure oil is represented as 100% purity and impure oil by 0% purity. The line labelled experimental chromaticity displays values obtained using the distimulus sensor whereas the line labelled theoretical chromaticity displays values calculated from oil spectra. They demonstrate that the chromatic variation displays a pronounced sigmoid characteristic, as predicted by theory (equation (6)). It might be argued that, for the purpose of instrument design, a linear response characteristic would be preferable, but since the sensor described is intended as a warning system for an industrial end-user, the low sensitivities for small deviations from complete oil purity might be seen as an advantage.

5. Conclusions

The on-line fibre-optic oil condition monitor is capable of measuring the state of purity of machine oils in an industrial environment. The mode of operation, chromatic modulation, mimics the method used by maintenance technicians who judge the appropriate time for an oil change by observing the colour of the oil. The sensor displays sufficient resolution and stability to predict the optimum time for a system oil change. Furthermore its simplicity and relatively low cost has generated commercial interest in addition to the obvious transport-related applications. The instrument appears to have potential in monitoring the degradation of transformer oils widely used in the electrical supply industry and it may have applications in measuring rates of reaction in liquids of interest to the chemical industry; further work is envisaged in these directions.

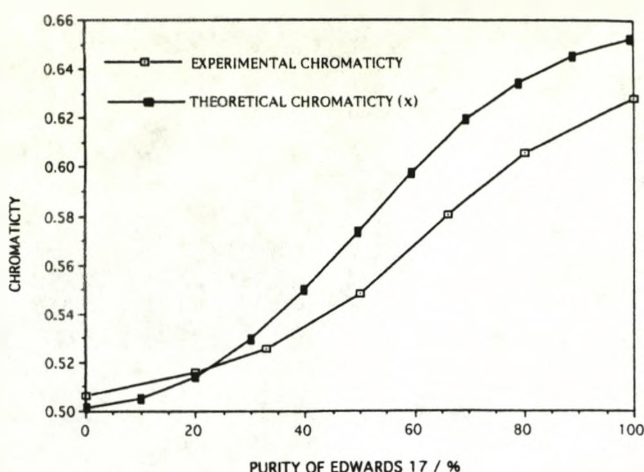

Figure 6. Chromaticity of Edwards 17 as a function of purity.

Acknowledgments

The authors are indebted to the DTI, Chell Instruments and Lucas Applied Technology for their financial support. We are grateful to Dr R Jones, B Taylor and R Miller for enlightening discussions and to A Edwards for his assistance in the optoelectronic circuit design. We are also indebted to P Hale for his help in the design of the sensor head. Finally we wish to thank Dr P J Henderson for his valuable advice.

References

[1] Snell D and Pitt G D 1983 *Proc. Int. Conf. on Optical Techniques in Process Control* (Cranfield: BHRA Fluid Engineering Publications) pp 27–41
[2] Giallorenzi T D *et al* 1982 Optical fibre sensor technology *IEEE J. Quant. Electron.* **18** 626–65
[3] Pitt G D *et al* 1985 Optical-fibre sensors *IEE Proc.* Pt J **132** 214–48
[4] Jones G R, Kwan S, Beavan C, Henderson P and Lewis E 1987 Optical fibre based sensing using chromatic modulation *Optics Laser Technol.* **19** 297–303
[5] Billmeyer F W and Saltzmann M 1966 *Principles of Colour Technology* (New York: Wiley) pp 11–124
[6] Russell P C, Morse K, Khandaker I, Glavas E and Jones G R 1990 Computer aided design of an optical fibre sensor based upon chromatic modulation, poster presentation *Applied Optics and Opto-electronics, 17–20 September 1990, Nottingham* (Bristol: IOP) pp 159–60
[7] Lucas Product Reference OSL-00513.

Vacuum/volume 45/number 1/pages 109 to 113/1994
Printed in Great Britain

0042-207X/94$6.00+.00
© 1993 Pergamon Press Ltd

Chromatic modulation as an on-line plasma monitoring technique

I I Khandaker, E Glavas, K Morse, S Moruzzi and G R Jones, *Department of Electrical and Electronic Engineering, University of Liverpool, Brownlow Hill, Liverpool L69 3BX, UK*

received for publication 22 September 1992

A novel fibre-optic sensor has been designed to function as a real-time plasma diagnostic tool. Plasma composition and discharge power have been monitored by recording the chromaticity of the glow discharge. The chromatic sensor operates in a manner analogous to the human eye and consists of three photodiodes with overlapping spectral responses. When used in conjunction, the three photodiodes are capable of measuring the hue and saturation of a plasma emission spectrum, in addition to the intensity measured by traditional photodiode sensors. Hue and saturation can be mapped onto a chromatic plane, each point of which corresponds to a set of spectra. Although many spectra can be mapped onto a single point on the chromatic plane, the degree of degeneracy is less than that of intensity sensors where spectra map into points restricted to a line. Chromatic sensing is shown to retain the cost and sampling rate advantages of intensity sensors whilst demonstrating an ability to detect spectral shifts, more often associated with spectrometry.

1. Introduction

The implantation of nitrogen is an established commercial method for enhancing the surface hardness and corrosion resistance of finished metal components. advantages conferred by plasma nitriding as opposed to thermal nitriding arise from the nonequilibrium distribution of internal energy within the plasma, which results in electron temperatures typically two orders of magnitude greater than the ion temperature. This nonthermal energy distribution permits strongly endothermic reactions to occur and allows the formation of metastable or thermally unstable end products. In addition the increase in reaction rate at a given 'temperature' allows nitriding to occur at commercially viable rates without causing thermal damage to the workpiece[1]. Current practice is to set the plasma process parameters to empirically obtained 'optimum' values and maintain these values throughout a production run; but such open-loop control systems are sensitive to disturbances in the process.

Since electrons and ions are the reactants in a plasma, closed-loop control of a nitriding process can be achieved by monitoring the density and temperature of these reactants. Such a control system can be implemented using the feedback from a Langmuir probe but as these probes distort the plasma potential, non-invasive diagnostic techniques are preferred. Mass spectrometers and optical spectrometers are the standard research tools. However these instruments are not only too bulky and expensive for production-line monitoring, they also lack the kilohertz sampling frequencies that may be required for closed-loop control. For inexpensive monitoring at high sampling rates an alternative optical diagnostic technique is necessary.

Several optical sensing techniques have been considered for plasma monitoring. These include interferometry, intensity modulation[2], wavelength modulation[3] and chromatic modulation[4]. Interferometry is capable of generating information on the spatial distribution of the plasma density but not capable of identifying emitting species. In addition the cost and complexity of the technique reduce its applicability in an industrial environment. Intensity modulation can provide an estimate of the overall density of emitting species but it fails to discriminate between the emitting species. This technique can be tailored to monitor a specific process by the use of interference filters which transmit wavelengths that correspond to particular electronic transitions. However the technique is specific to one transition and requires modification to study a range of processes.

Chromatic modulation refers to the utilization of polychromatic light for sensing changes in a physical system. It relies upon the detection of changes in the total spectral profile of an optical signal and can be considered to be an integrated form of wavelength modulation. Potentially this technique can monitor the spectral shifts required for closed-loop control without the gathering and processing of superfluous data that adds cost and complexity to spectrometric methods.

2. Theory of chromatic modulation

The characteristic difference between chromatic detection and wavelength detection is that chromatic detection involves monitoring spectral changes over a broad band of wavelengths, whilst wavelength detection involves monitoring only a limited number of specific wavelengths. The chromatic modulation technique detects a change in a measurand not by detecting intensity changes at particular wavelengths but by monitoring the sum of the contributions of relative changes at all wavelengths within a spectral power distribution. As such it is an integrated form of spectral monitoring as opposed to the differential (dispersive) nature of wavelength modulated systems.

Chromatic changes can be monitored by using three photodetectors with overlapping spectral profiles $R_x(\lambda)$, $R_y(\lambda)$, $R_z(\lambda)$. When addressing an optical signal with spectral power distribution $P(\lambda)$ the output currents of the photodetectors will be:

$$I_x = K_x \int P(\lambda) R_x(\lambda)\, \mathrm{d}\lambda,$$

$$I_y = K_y \int P(\lambda) R_y(\lambda)\, \mathrm{d}\lambda,$$

$$I_z = K_z \int P(\lambda) R_z(\lambda)\, \mathrm{d}\lambda, \qquad (1)$$

where K_x, K_y and K_z are constants of proportionality and λ is the wavelength. These equations (1) may be normalized with respect to the effective optical power according to:

$$x = I_x/(I_x + I_y + I_z),$$

$$y = I_y/(I_x + I_y + I_z),$$

$$z = I_x/(I_x + I_y + I_z). \qquad (2)$$

If the parameters x, y, z are calculated from a standard set of idealized detectors, a plot of x against y results in the CIE diagram which forms the basis of colour science[5] [Figure 1(a)]. An entire spectrum is represented by a single point on a CIE diagram; any changes in hue can be represented as changes in the angle θ whilst changes in saturation are represented by changes in r. The use of real detectors results in a similar diagram [dotted line on Figure 1(a)] which is distorted because of the mismatch between their spectral responses [Figure 1(b)] and those of the idealized CIE detectors[5]; this is referred to as the chromatic plane.

Hue and saturation can be mapped onto a chromatic plane, each point of which corresponds to a set of spectra. Although many spectra can be mapped onto a single point on the chromatic plane the degree of degeneracy is less than that of intensity sensors where spectra map onto points restricted to a line. Hence chromatic analysis permits discrimination between spectra which could not be distinguished by measuring the intensity alone. The normalization of x, y and z has another important implication for optical sensing, namely that chromatic detection techniques are independent of intensity. The inherent intensity compensation renders the chromatic sensor immune to changes in source intensity and fluctuations in transmission along the optical path.

Whilst the chromatic analysis of dyes requires the theory of complex subtractive mixing, self-luminant plasmas can be analysed using the simpler theory of additive mixing. It has been shown[5] that in the case of additive colour mixing the tristimulus values can be obtained by a simple linear superposition of the transmitted energy at each wavelength:

$$x = \sum_{\lambda} P(\lambda) R_x(\lambda),$$

$$y = \sum_{\lambda} P(\lambda) R_y(\lambda),$$

$$z = \sum_{\lambda} P(\lambda) R_z(\lambda), \qquad (3)$$

where x, y, z refer to the partial sums over all wavelengths of the product of the energy $P(\lambda)$ at each wavelength and the spectral response of the photodetector $R(\lambda)$. Equation (3) predicts that when two coloured lights are mixed in varying degrees, the resulting points on the chromatic plane all lie on the same straight line.

Of course a spectrometer can provide the profile $P(\lambda)$ with a resolution limited only by the dispersive power of its optics. For many sensing applications this additional information is spurious

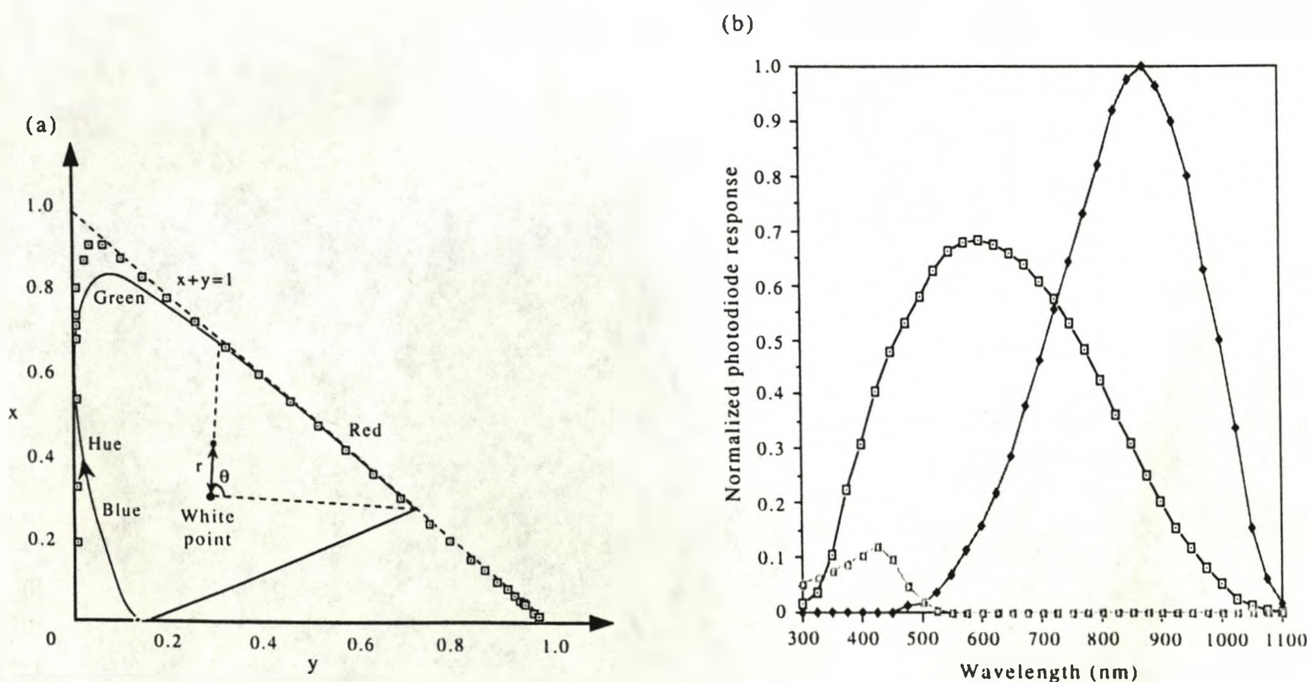

Figure 1. (a) CIE chromaticity diagram: x and y represent normalized photodetector outputs; r and θ represent the saturation and hue. (b) Normalized spectral responses from the photodiode triplet used in the chromatic sensor.

since it is processed to give a single value, which can be easily related to changes in a measurand. Thus chromatic modulation is an analogue spectral processing technique that transforms the 6899 data points, in each of the spectra taken below, into two data points representing the chromatic coordinates of that spectrum[6]. The extent of this spectral data compression makes chromatic sensing particularly attractive for on-line plasma monitoring.

3. Apparatus

The sensing technique was tested using a high current dc plasma chamber (Figure 2). The main chamber was a 24 litre stainless steel cylinder which acted as the anode; safety considerations dictated that the chamber be grounded. An axial spindle acted as the cathode, on which the titanium samples were supported. Power to hold the cathode at a negative potential was obtained from a switched-mode power supply capable of generating up to 3 kV at 150 mA although working plasmas could be generated with 0.8 kV at 15 mA. A 5 H inductor was connected in series with the power supply to store enough energy to sustain the high transient-current arcing that occurred at points of contamination.

Gas pressures were measured using an MKS 310 Baratron capacitance manometer which measures pressures up to 1333.22 Pa, an MKS 220 Baratron for pressures up to atmospheric and an ion gauge for pump-down pressures around 10^{-4} Pa. An MKS 270 gauge head unit was used as a driver for both the Baratron and an MKS 252 exhaust flow controller; this unit also provided a digital pressure readout. Flow rates were measured and regulated using MKS 1259 mass flow controllers which operated by recording the amount of energy required to sustain a fixed thermal gradient along the gas lines.

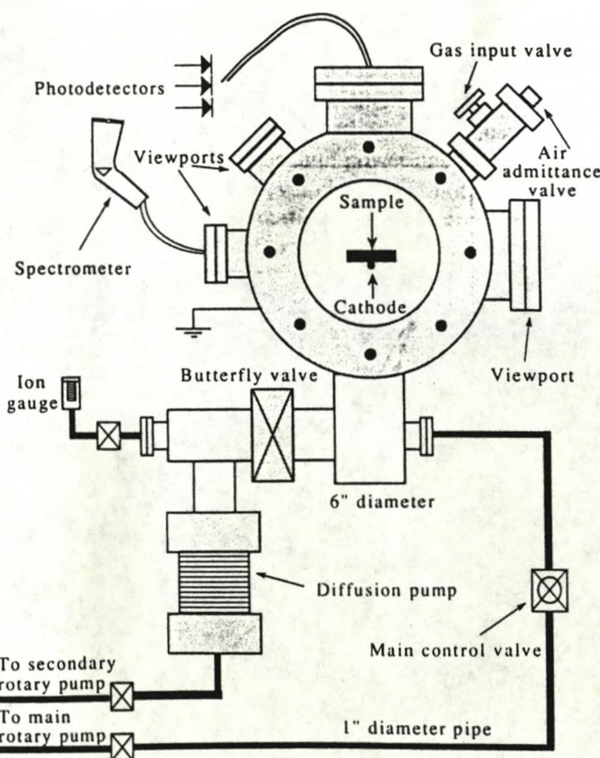

Figure 2. Schematic of dc plasma chamber.

Chromatic characteristics of the emission spectrum were measured by recording the output voltages of three photodiodes on a PC via a 12-bit ADC card. These photodiodes were selected for their sensitivity and coverage of the appropriate spectral range. A combination of these diodes have been shown to discriminate 0.04 nm spectral shifts[4]. Plasma spectra were obtained by the concurrent use of a Hilger–Watts 0000 spectrograph modified into a spectrometer by the addition of a stepper-motor driven exit slit which illuminated a photomultiplier. Spectral resolutions of 0.1 nm were obtained but the slow scan rate of this instrument dictated a four minute scan periodicity. A Keithley Instruments 417 picoammeter was used to measure the photomultiplier output currents; these values were logged on a PC via an ADC card. Both sets of optical data were obtained through a set of glass fibre bundles with high transmission in the visible and near uv.

4. Experimental results

Knowledge of plasma composition is particularly important in the detection of leaks. A typical leakage condition might be the gradual introduction of atmospheric nitrogen into the process chamber so this event was staged to test the chromatic monitor. The power discharged in a plasma can determine the rate at which a deposition process occurs. These two parameters were investigated in an effort to determine whether chromatic techniques were capable of distinguishing between the spectral changes caused by varying either parameter. Conventional spectra were obtained to ensure that the three photodiodes had spectral responses appropriate to the changes in emission.

4.1. Plasma composition. Pure hydrogen was introduced into the process chamber at a pressure of 20 kPa and a 20 W plasma discharge was initiated, the flow rate was kept at 0.6667 $cm^3 s^{-1}$. Nitrogen was then introduced into the chamber in a sequence of controlled releases in which its flow rate was ramped by 0.1667 $cm^3 s^{-1}$ with a corresponding decrease in hydrogen flow; thus increasing the relative concentration of nitrogen in steps of 20%. Figure 3 shows the spectra of pure hydrogen and pure nitrogen. Figure 4 shows the change in chromaticity as a function of increasing hydrogen concentration; the change in plasma intensity is shown for reference. When applied to the monitoring of gas mixture, the pure gas plasmas show significant deviations from linearity. The sensitivity to mixture as calculated from the linear region is 0.5 mV per 1% H in N with a 0.5 mV noise component corresponding to a resolution of 1% H in N.

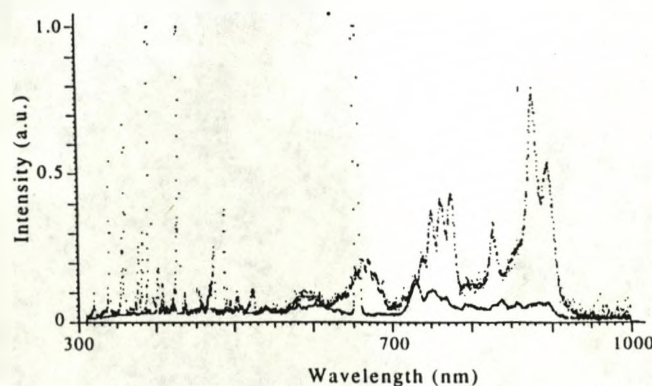

Figure 3. Emission spectra of pure hydrogen (lower trace) and nitrogen (upper trace).

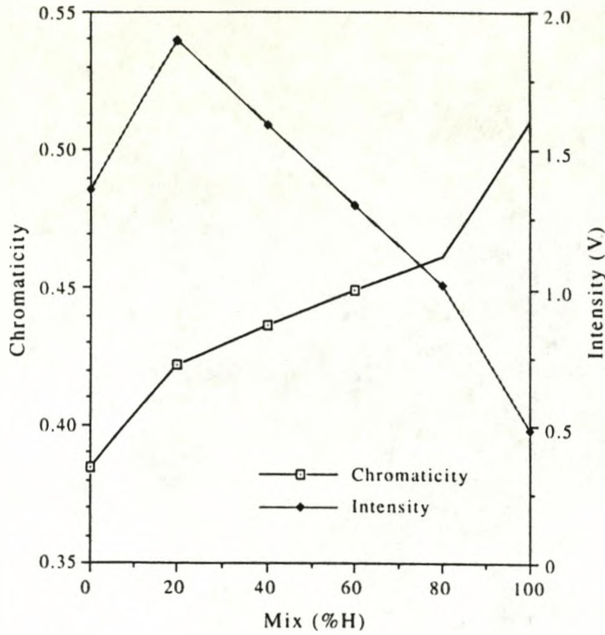

Figure 4. Plasma chromaticity and intensity as a function of hydrogen concentration.

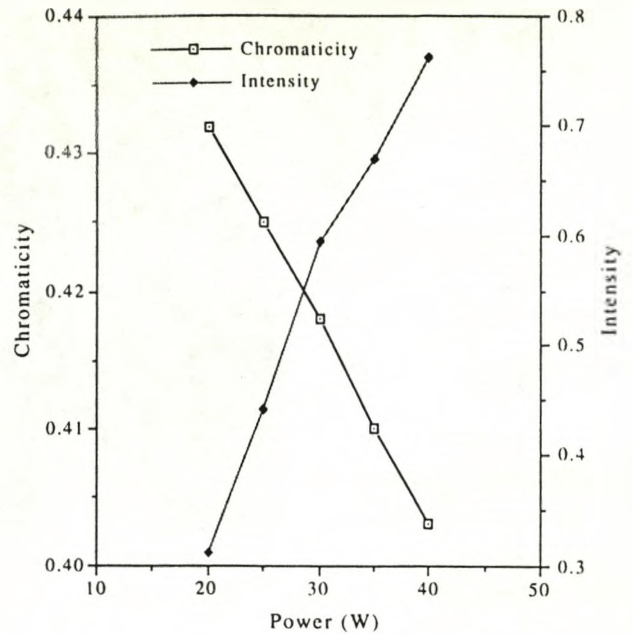

Figure 6. Plasma chromaticity and intensity as a function of power.

4.2. Discharge power. Nitrogen was introduced into the plasma chamber at a flow rate of 0.6667 $cm^3 s^{-1}$ and pressure of 20 kPa. The power deposited by a constant current was ramped from 20 W to 40 W in 5 W steps by appropriate increases in voltage. Figure 5 shows the spectra of pure nitrogen plasmas at 20 W and 40 W. Figure 6 shows the change in chromaticity as a function of increasing discharge power with the change in plasma intensity for reference. When applied to the monitoring of plasma power the chromatic sensor demonstrates a linear response. The sensitivity to power is 1.6 $mV W^{-1}$ with a 0.5 mV noise component corresponding to a resolution of 0.3 W. It should be noted the responses for both nitrogen (1.6 $mV W^{-1}$) and hydrogen (1.7 $mV W^{-1}$) are very similar.

4.3. Flow rate. Pure nitrogen was introduced into the process chamber at a pressure of 20 kPa and a 20 W plasma discharge was initiated. The flow rate of nitrogen into the chamber was ramped from 0.6667 $cm^3 s^{-1}$ to 2 $cm^3 s^{-1}$ in steps of 0.1667 $cm^3 s^{-1}$, chromatic and spectral emission from the plasma was recorded. Neither the chromatic emission nor the spectral emission demonstrated any dependence on flow rate.

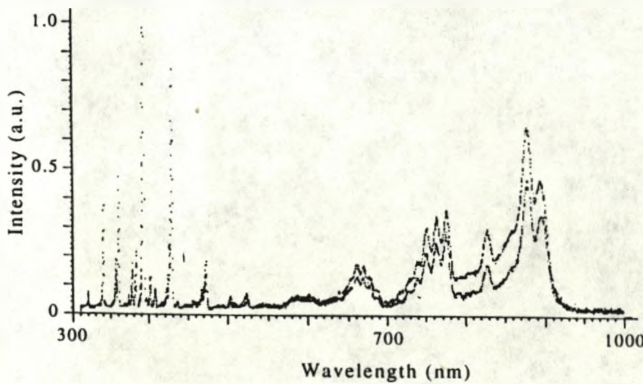

Figure 5. Emission spectra of pure nitrogen at 20 W (lower trace) and 40 W (upper trace).

5. Discussion

Figure 7 displays the experimental data on the chromatic plane.

A linear chromatic response to a change in plasma parameter has two implications; that the conditions for additive colour mixing are satisfied and that the parameter change causes a linear

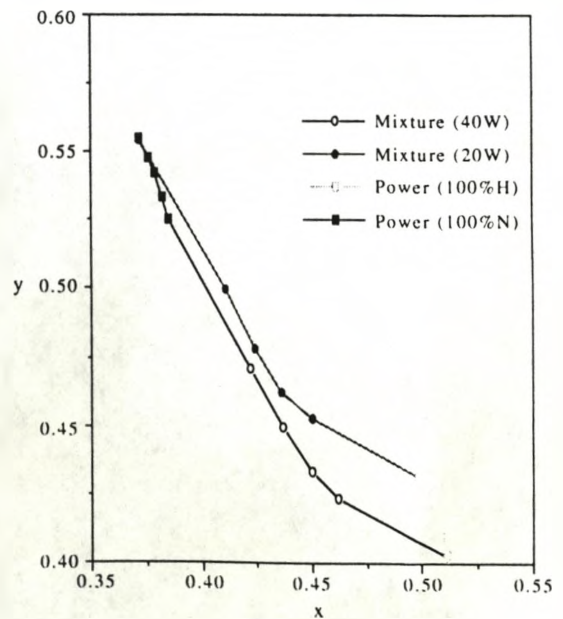

Figure 7. Experimental data summarized on the chromatic plane.

shift in the plasma emission spectrum. Additive colour mixing is only valid if the plasma has minimal self-absorption and scattering; an additional requirement is that the excited species are non-interacting. The advantage of chromatic self-referencing is emphasized in Figure 4 which shows that the intensitiy is a double valued function of mixture whereas the chromaticity is a single valued function.

One possible mechanism for the observed linear chromatic response to power is a shift in the black body radiation generated by electrical heating. An increase in temperature is known to cause a linear decrease in the wavelength of the black body emission peak (Wiens displacement law). Although the peak wavelength shows a linear downshift with temperature, the accompanying change in spectral profile causes the chromaticity of black body radiation to describe a curve on the chromatic plane[5]. However the curvature is only noticeable over a large temperature range so the linear results are still consistent with this explanation. Attempts were made to confirm this idea by recording the plasma temperature using a thermocouple, but they proved unsuccessful because of repeated arcing, despite attempts to sheath the junction in quartz.

The linearity of chromatic response to changes in gas mixture holds over the range 20% H/80% N to 80% H/20% N but significant deviations are observed for the pure gases. In this case the chromatic shift originates from the different intensities of the emission spectra of the two gases but the assumption that the excited species are non-interacting must be questioned. Figure 4 illustrates the anomalous changes in intensity and chromaticity that occur at the transition between pure gas and mixture. These changes may indicate that hydrogen and nitrogen react to create excited radicals which contribute to the intensity and chromaticity of the plasma discharge.

The chromatic responses to power and mixture trace out a contour map of the parameter value on the chromatic plane. If these contour lines were orthogonal it would be possible to measure both parameters independently simply by using the contour lines as a set of coordinate axes. Figure 7 illustrates the chromatic power and mixture responses the gradients of which are -2.31 and -1.23 respectively. The lack of orthogonality means that it is not possible to deduce the absolute power and mixture from an absolute chromaticity. However changes in both power and mixture would result in a chromatic shift with a gradient that is the weighted mean of the two extreme gradients. The value of the weightings then yield the relative contributions of power and mixture fluctuations.

6. Conclusion

The chromatic sensor has been shown to function as a real-time plasma diagnostic tool. Changes in plasma power and mixture have been shown to generate chromatic shifts of differing gradients. This result confirms that the chromatic sensor has the capability of discriminating between those changes in optical emission due to power fluctuations and those due to mixture fluctuations; something that is beyond the capability of intensity sensors. Chromatic modulation has been shown to function as an analogue spectral processing technique that transforms the thousands of data points in a spectrum into two data points representing the chromatic coordinates of that spectrum. Whilst this data 'compression' discards much of the fine chemical detail the compressed data is sufficient to close the control loop. In conjunction with the cost and sampling rate advantages over spectrometric techniques[7], these characteristics make chromatic sensing a viable diagnostic tool.

Acknowledgements

The authors are indebted to the DTI, Chell Instruments and Lucas Applied Technology for their financial support. We are grateful to Dr R Jones, B Taylor and R Miller for enlightening discussions and to A Edwards for his assistance in the opto-electronic circuit design. Finally we wish to thank Dr P J Henderson for his valuable advice.

References

[1] S Veprek, *Plasma Chem Process*, **9**, 29S–54S (1989).
[2] T D Giallorenzi, J A Bucaro, A Dandridge, G H Siegel Jr, J H Cole and S C Rashleigh, *IEEE J Quant Electron*, **QE-18**, 626–665 (1982).
[3] G D Pitt, P Extance, R C Neat, D N Batchelder, R E Jones, J A Barnett and R H Pratt, *IEE Proc*, **132**, Pt J, 214–248 (1985).
[4] G R Jones, S Kwan, C Beavan, P Henderson and E Lewis, *Optics Laser Tech*, **19**, 297–303 (1987).
[5] F W Billmeyer and M Saltzmann, *Principles of Colour Technology*. John Wiley, New York (1981).
[6] P C Russell, K Morse, I I Khandaker, E Glavas and G R Jones, Computer aided design of an optical fibre sensor based upon chromatic modulation, Poster presentation, *Applied Optics and Opto-electronics*, 17–20 September 1990, Nottingham, pp 159–160 (1990).
[7] S Kwan, C Beavan and G R Jones, *Measmt Sci Tech*, **1**, 207–215 (1990).

Chromatic monitoring for the processing of materials with plasmas

P.C. Russell
I. Khandaker
E. Glavas
D. Alston
R.V. Smith
G.R. Jones

Indexing terms: Plasmas, Material processing, Monitoring

Abstract: A non-invasive monitoring system for material-processing plasmas has been developed based on chromatic modulation. The monitor consists of two parts, one for monitoring the emission spectra of plasmas and the second for monitoring the thickness of films on semiconductors during etching or deposition. These chromatic systems offer significant speed advantages over equivalent spectroscopic techniques. Both systems have been tested on a variety of plasma chambers and typical results from both systems are presented. Chromatic monitoring provides rapid feedback on the state of a plasma and on film thickness, providing the possibility for real-time monitoring and control of the plasma state. Further enhancement of the chromatic techique allows two-dimensional monitoring of the plasma, providing information on its uniformity.

1 Introduction

Plasma processes are now widely used in industry, especially for surface modification and for semiconductor processing, but the complex nature of the plasma state makes it difficult to accurately predict the behaviour of a plasma processing system, leading to problems in setting up a stable process. Currently, plasma systems have to be individually characterised to produce a system-specific operating recipe. Having established a stable operating point, further problems arise due to variations between runs. Many semiconductor processes are sensitive to variations, and this leads to changes in the resulting device characteristics.

A number of techniques have been used to monitor and characterise plasmas. These conventional monitoring systems are either intrusive, like the Langmuire probe [1], or rely on spectroscpic analysis of the plasma, either optical [1] or mass spectrometry [2]. The Langmuir probes can give useful information on the state of the plasma and have been successfully used in the transferral of processes between chambers [3]. However, because of their intrusive nature, Langmuir probes would not be acceptable as continuous monitors: the probe tends to cause a local disturbance in the plasma that affects uniformity across the processing system.

Optical and mass spectrometry have both been used to provide a range of detailed diagnostic information on plasma processes [1, 2]; both can be used on a run-by-run basis and can indicate variations in the plasma environment. However, the instruments required for these techniques are expensive and produce excessive amounts of data that are not easily interpreted.

In this paper we describe a noninvasive monitoring system based upon chromatic modulation [4]. Optical systems have been developed to measure optical emissions from the plasma and to monitor the chromaticity of thin insulating films on a semiconductor substrate. The plasma-emission monitor produces a rapid output which indicates the current state of the plasma. The thin-film monitor gives rapid feedback on the instantaneous thickness of a film. The outputs from these systems have been used as inputs to an intelligent control system, which can identify variations between runs, diagnose problems and send control actions to improve the operation.

2 Chromatic sensing

2.1 Basic principles

Chromatic sensing is the utilisation of polychromatic light for sensing changes within a physical system [5]. Chromatic detection involves an array of photodetectors with overlapping wavelength-dependent responses $C(\lambda)$; an example of typical detector relative responsivities used for such purposes is shown in Fig. 1*a*. The output from each detector, when used to monitor an optical signal having a spectral power distribution $P(\lambda)$, will be

$$V = \int_{\lambda} P(\lambda)C(\lambda)\, d\lambda \qquad (1)$$

For many applications the optimum combination involves three detectors, with responses $C_x(\lambda)$, $C_y(\lambda)$ and

© IEE, 1994

Paper 9850A (S3), first received 27th April and in revised form 28th July 1993

The authors are with the Department of Electrical Engineering and Electronics, University of Liverpool, Brownlow Hill, P.O. Box 147, Liverpool L69 3BX, United Kingdom

The authors wish to thank Chell Instruments, GEC Marconi Materials Technology and the DTI for funding this work and for supplying essential information.

$C_z(\lambda)$, giving three outputs:

$$V_x = \int_\lambda P(\lambda)C_x(\lambda)\,d\lambda$$
$$V_y = \int_\lambda P(\lambda)C_y(\lambda)\,d\lambda$$
$$V_z = \int_\lambda P(\lambda)C_z(\lambda)\,d\lambda \qquad (2)$$

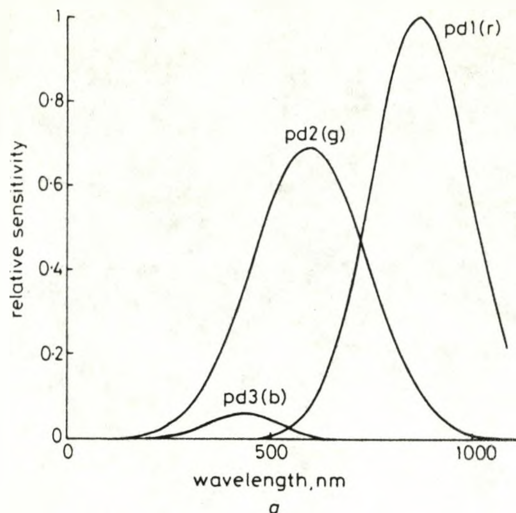

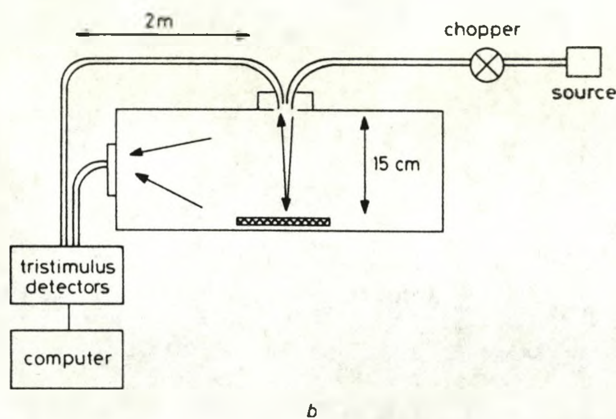

Fig. 1 *Tristimulus systems*

a The responsivities of the detectors plotted relative to the peak responsivity of detector pd1

b The experimental arrangement around the plasma chamber

Two tristimulus systems were used, one observing the film thickness through a viewport at the top of the chamber and the second observing the plasma through a side-mounted viewport

which can be light-intensity normalised according to

$$x = \frac{V_x}{(V_x + V_y + V_z)}$$
$$y = \frac{V_y}{(V_x + V_y + V_z)}$$
$$z = \frac{V_z}{(V_x + V_y + V_z)} \qquad (3)$$

The resulting parameters x, y and z form chromaticity coordinates which quantify the spectral signature $P(\lambda)$.

The state of any one of the chromaticity coordinates can be obtained from a knowledge of the other two, as $x + y + z = 1$. If the detector responses c_x, c_y and c_z were made to correspond to the detectors in a standard human observer, as laid down by the International Commission on Illumination (CIE), then the resulting x, y plot would form the CIE chromaticity diagram, which is well known in the field of colour science [6]. In this representation, saturated or pure colours reside around the periphery of the chromaticity curve, whereas composite spectral signatures reside within the area enclosed by the chromaticity boundary.

These considerations have importance in relation to optical sensing because the implication is that even complicated spectral signatures can be quantified in terms of only two parameters, x and y. Changes in the spectral signature can therefore be quantified in terms of a change in these two parameters.

As the chromaticity coordinates x, y and z are light-intensity normalised, a chromatic sensing system is inherently insensitive to intensity variations caused by changes in the transmissivity of the optical path. For instance, changes in intensity due to a build-up of deposit on a plasma chamber window would have little effect on the chromatic signal, provided the deposit had no spectrum-modifying properties and none of the photodetector signals approached the noise threshold. Indeed, it has been demonstrated [5] that an error in dominant wavelength determination of less than 0.00013 nm per percentage change in signal intensity is achievable above the detector noise threshold.

It should be noted that chromatic sensing differs from colorimetry in a number of important ways:

(*a*) Unlike colorimetry, chromatic sensing is concerned with changes in spectral signatures rather than monitoring of absolute colour values.

(*b*) For chromatic sensing the detector responsivities C_x, C_y and C_z may be varied to modify the resolution, dynamic range and spectral location of the detection system. The relationship between responsivity changes and the measurement quantification was investigated by Beavan [5], and is reported by Jones and Russell [4]. In colorimetric terms the implication is that responsivity changes modify the form of the chromaticity diagram, of which the CIE diagram is but a special case.

(*c*) The range and resolution of a chromatic sensing system may be varied online using software to control the processing of signals from each detector [7]. For instance, with a distimulus system the chromaticity may be defined as the ratio of the photodetector outputs. The linearity of the output can be improved by using a difference-over-sum relationship:

$$v = G\left(\frac{V_x - \alpha V_y}{V_x + \beta V_y}\right) \qquad (4)$$

The range and resolution can be adjusted by varying G, α and β. This enables the tracking or detailed location of spectral signature variations to be implemented [8]. Similar algorithms may be used with tristimulus systems.

Chromatic sensing has been successfully developed for a number of industrial and medical monitoring applications [9, 10]; in this paper its use for monitoring plasma processes is considered.

2.2 Plasma chromaticity

To illustrate the capabilities of the technique, Figs. 2*a* and 2*b* show the spectra of two different glow plasmas: pure hydrogen and pure nitrogen. When addressed chromatically with detectors of appropriate responsivities,

giving the chromatic envelope shown in Fig. 2*c*, the spectra of Figs. 2*a* and 2*b* may be located at points A and B, respectively. If the relative concentrations of the individual species in the plasma are varied, the plasma chromaticity varies along a locus connecting A and B. The precise locus will be governed by conditions within the plasma, such as impurity levels, gas flows and the emissions produced by radicals and species generated in reactions between the gases. Chromatic sensing provides a means of tracking these changes in plasma conditions relatively simply, and with the potential for very high time resolution. As a result it is attractive for online monitoring on industrial plasma processing systems.

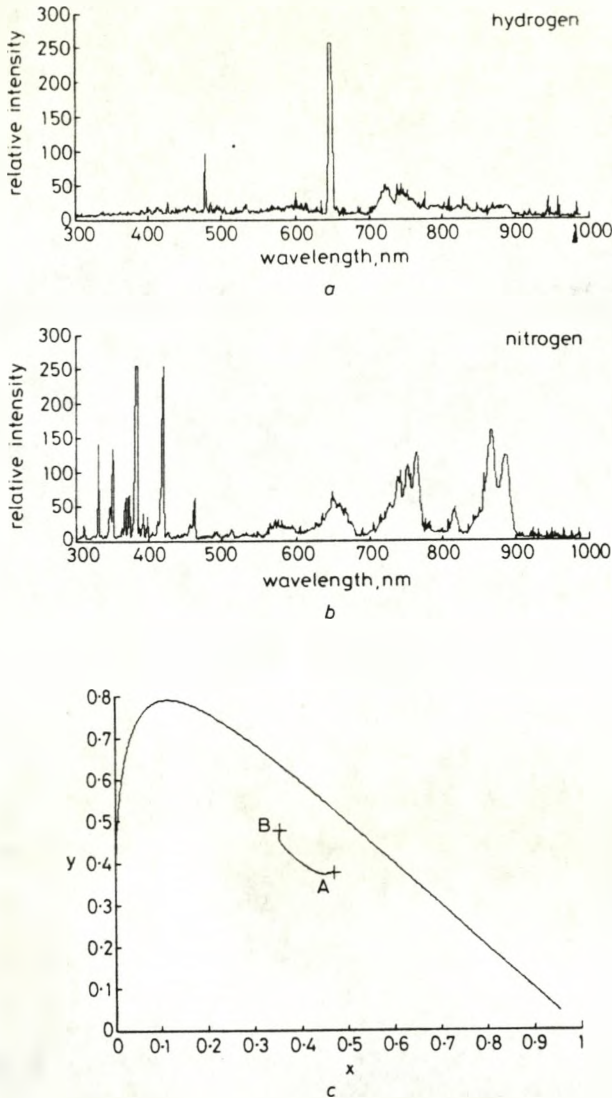

Fig. 2 *Chromaticity of plasmas*

a The optical emission spectrum of a pure hydrogen plasma
b The emission spectrum of a pure nitrogen plasma
c A chromaticity diagram. Points A and B represent the chromaticity values for the spectra shown in *a* and *b*, respectively

2.3 Chromaticity of thin semiconductor films

The thickness d of thin films may be determined in principle if the refractive index of the film is known, from cyclical intensity variations of a monochromatic light source (wavelength λ) due to well known interference effects [11] governed by the condition for destructive interference:

$$nd \cos \theta = \frac{m\lambda}{2} \quad (5)$$

where m is an integer, n is the refractive index of the film and θ is the angle of incidence. The problems with such an approach are that other spurious effects can cause intensity variations that confuse the thickness monitoring, and that the cyclical intensity variations make it difficult to extract an absolute thickness value, as opposed to relative changes.

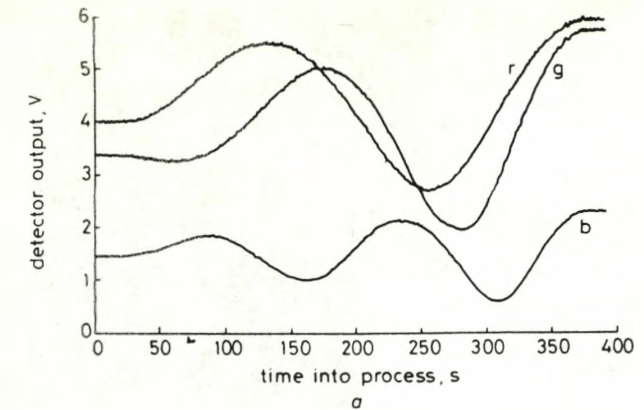

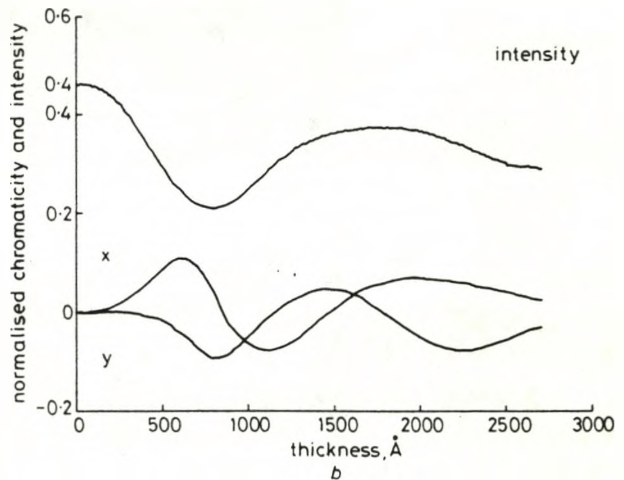

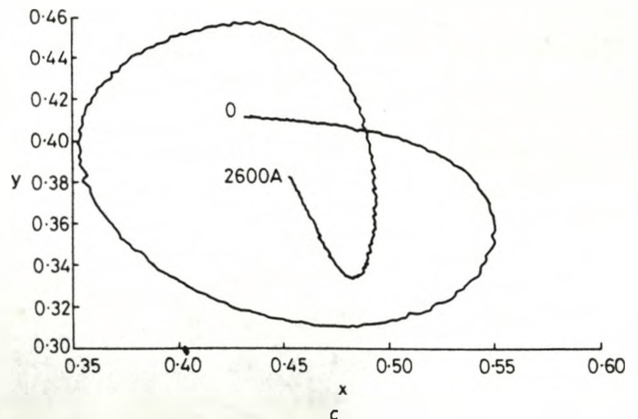

Fig. 3 *Output from the thin-film monitor during an etching run*

a The voltage output from the three detectors (r is C_x, g is C_y and b is C_z)
b The chromaticity and intensity variation calibrated against film thickness
c The corresponding chromaticity variation

However, by extending the thin-film interference approach to the use of polychromatic light, such difficulties can be overcome using chromatic detection. Under such conditions the optical power spectral distribution of eqn. 1 becomes

$$P(\lambda) = P_o(\lambda) \sin^2\left(\frac{\delta}{2}\right) \quad (6)$$

where $\delta = (2\pi/\lambda)n(\lambda)d$, λ is the optical wavelength $n(\lambda)$ is the refractive index and d is the path length. Thus, when the thickness of a film is monitored during an etching run, with three detectors of different responsivities C_x, C_y and C_z (covering the wavelength range 300–1100 nm), the signals recorded as a function of time are of the form shown in Fig. 3*a*. Fig. 3*b* shows the chromatic variation plotted as a function of thickness. Translating these into a two-dimensional chromaticity plot leads to the variation shown in Fig. 3*c*. Each point on the chromaticity diagram can be mapped on to a thickness value. There is now only one ambiguous point and, by using the gradients of the curve, this ambiguity can be resolved.

3 System implementation

Systems based on the above chromatic principle have been implemented for online testing for both plasma condition and film thickness during the etching of silicon nitride off GaAs substrates using a reactive ion etching (RIE) system. An arrangement typical of those used for such investigations is shown in Fig. 1*b*.

3.1 Plasma emission

Plasma emission has been monitored using a photodiode-based tristimulus system covering a wavelength window extending from 300 to 1100 nm. Suitable detector responsivities, of the type shown in Fig. 1*a*, were chosen using a specially constituted CAD package [8] which enabled the detection system to be matched to the plasma emissions. Optical access to the plasma was obtained via a quartz viewing port and optical fibre transmission to allow the optoelectronic processing to be situated remote from the radiofrequency environment required for plasma production.

3.2 Thin-film monitoring

The film thickness-monitoring system consists of a stable, unpolarised white light source (Optical sensing department of Lucas Engineering Systems, Part No. OSL00513), optical fibres and a tristimulus chromatic detection system. One fibre guides the light on to the substrate and the second collects the reflected light and guides it back to the detectors. The fibres are placed at a predetermined angle to the normal

The thickness-monitoring system was used in a calibrated rather than an absolute measurement mode. This means that the system output (film thickness relationship) was determined beforehand using a series of films preetched to different thicknesses. A typical calibration curve is shown in Fig. 3*c*, and this provides film thickness values to a resolution of ± 0.5 nm under ideal conditions. The calibrated approach also avoids complications associated with light polarisation effects, provided the system configuration remains fixed and the calibration examples established.

To allow in-situ monitoring of film growth, in the presence of the plasma emission as background, the white light source was chopped with a rotating shutter and the output from the detectors measured using a lock-in amplifier.

The monitoring system has been tested on several systems, but most tests have been performed on an RIE system. The input and output fibres were situated outside a quartz window in the upper nonpowered electrode (Fig. 1*b*). A GaAs wafer coated with silicon nitride was placed under this window and the output from the detector monitored.

4 Assessment of monitoring systems

The two monitoring systems, for plasma emission and film thickness, have been tested on a number of plasma processing systems, including research and commercial systems.

4.1 Types of plasma system

The plasma-emission monitor has been tested on a plasma-oxidation system, a DC plasma-nitriding system, a plasma-deposition/etching system and a reactive ion-etching system. The plasma-oxidation system consisted of an inductively coupled oxygen plasma excited by an external RF coil at a frequency of 13.56 MHz at a power of 1 kW and an oxygen pressure of 0.15 Torr. Oxide growth was induced using a 100 V DC bias to an Si wafer.

The nitriding system consisted of a glow initiated by using 1–3 kV DC voltages and was used for nitriding titanium discs. Experiments were performed over a range of processing conditions and using a variety of gas mixtures. Processing pressure was in the range 2–6 T. The sample was maintained at a temperature of 270°C. The discharge current was maintained at 137 mA by varying the applied voltage.

The RIE system consisted of a 60 cm diameter chamber and an RF supply at 13.56 MHz frequency. The system was used for etching silicon nitride layers on semiconductor substrates using a CF_4/O_2 plasma. A gas flow of 50 sccm was used, consisting of 18.3% CF_4, 1.7% O_2 and 80% N_2. The chamber pressure was maintained at 70 mT and the plasma was maintained using a power of 60 W.

The plasma deposition/etching system used consisted of a standard Plasma Technology μp800 running a custom etching process.

The film thickness-monitoring system has been tested on the plasma-oxidation and the RIE systems described above. The signal levels obtained from the photodiode detectors during plasma-emission tests were between 0.5 and 25 nA, which were above the detector noise level, which is typically 0.1 nA. During the thin-film monitoring the signal strength can be adjusted via the intensity of the white light source: signals of the order of 10 nA were normally utilised.

4.2 Typical test results

A range of test results has been obtained with the chromatic monitors using the various plasma systems described above. The results have shown that the monitoring systems operate well under the various conditions existing within the different plasma processing systems. These results have confirmed the following performance capabilities.

Experimentally, for the RIE system described above, the plasma-emission monitor was able to distinguish changes in gas pressure of 2 mT, in plasma sustaining power levels of 1 W and in a gas mixture of 0.5%. Faulty operating conditions (e.g. variations in the plasma–gas mixtures caused by a faulty gas regulator, faulty plasma-energising power systems and faulty vacuum system behaviour) have been shown to be easily detectable.

Examples of the results obtained are shown in Fig. 2*c* and Fig. 4. Fig. 2*c* has already been described, and shows how the correct composition of the plasma can be checked via the values of the chromaticity coordinates x and y. Fig. 4 shows the chromaticity variation during an etching run with the RIE system, using the standard

etching conditions described above. Clear and abrupt changes in chromaticity are apparent at both the beginning and end of the etch process, so enabling the etch

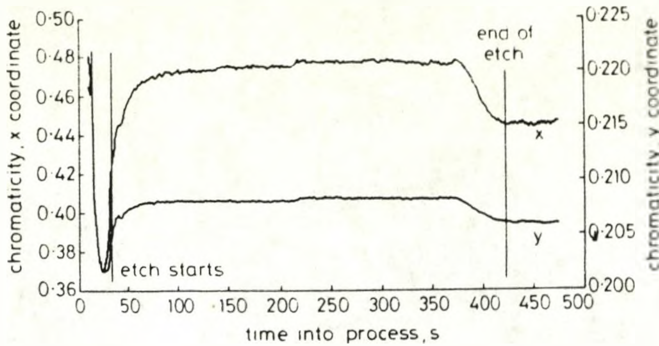

Fig. 4 *Output from the plasma emission monitor. The chromaticity coordinates x and y are plotted individually against time*

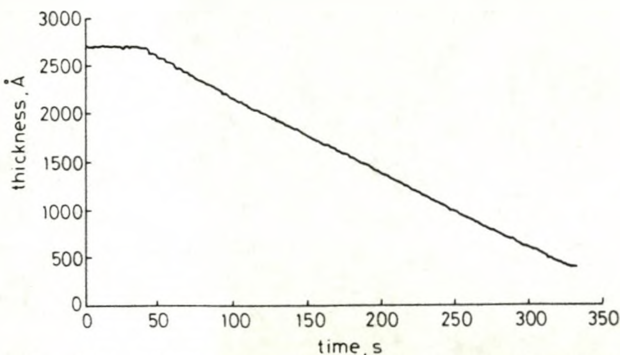

Fig. 5 *Calibrated output from the thin-film monitor against process time for an etching process*

period and end point to be clearly identified. In this case the chromaticity changes are produced by the presence of the etching byproducts in the plasma, which affect the plasma composition and optical emissions. Thus the plasma emission monitor allows overetching to be avoided.

An example of the results obtained with the film-thickness monitor was given in Fig. 3. The chromaticity variation is a complex spiral, indicating that the chromaticity progresses through a number of spectral signature cycles. The cases shown in Fig. 3*c* corresponds to cycles of 1.5 orders, implying a thickness change of about 0.25 μm. For thicker films the chromaticity varies through a greater number of fringe orders, leading to additional loops on the chromaticity diagram.

For such chromatic signals to be of direct value for film-thickness monitoring it is advantageous to deconvolute the chromaticity spiral to give a linear calibration curve in terms of film thickness. Such calibration has been achieved by performing a number of partial etches of different final thicknesses. Accurate measurement of these partially etched wafers allowed a calibration table of chromaticity against thickness to be produced. The lookup table algorithm matches the chromaticity values read from the monitor to the nearest values in the calibration table, to allow for the effect of noise. To produce a definitive thickness value at the crossover points in the chromaticity diagram, the lookup table algorithm makes use of previous data to determine the direction of change. These calibration data allow real-time monitoring of the thickness during the etching process. A typical example of such a result is shown in Fig. 5. The thickness data from the thin-film monitor have been used to confirm the end-point data obtained using the plasma-emission monitor (e.g. Fig. 4).

Initial etching runs with the RIE system were diagnosed with the plasma-emission monitor to be of variable

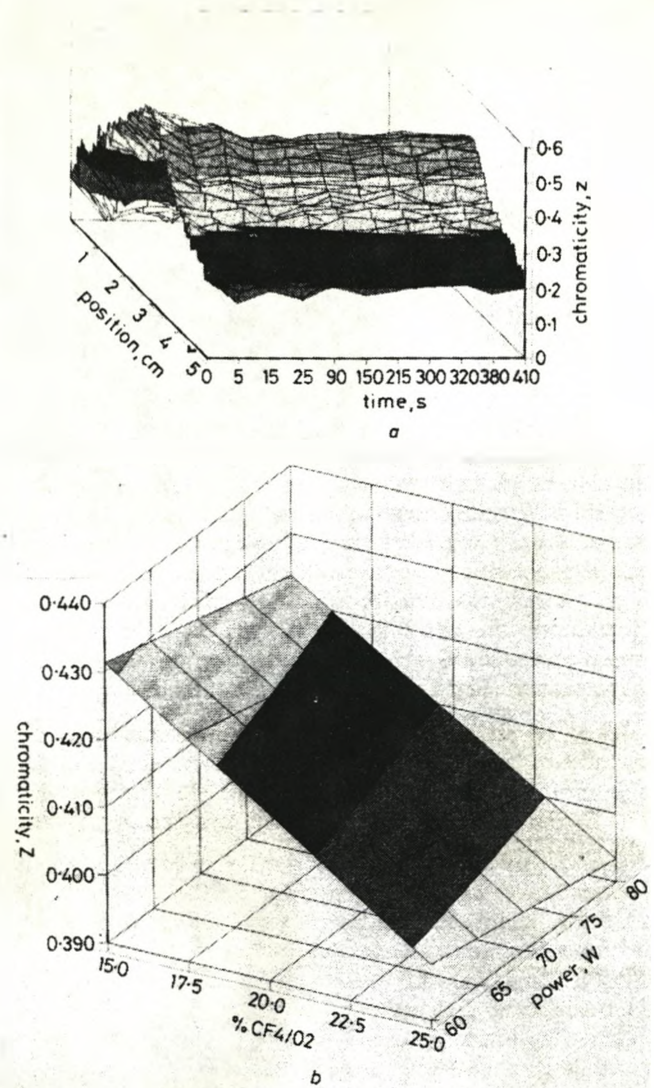

Fig. 6 *Use of chromacity in plasma control*

a Chromaticity variation with time and position across a section of the plasma, as seen through a 5 cm viewport

b The chromaticity surface as a function of plasma composition (as governed by the input gas mixture) and power

duration. Simultaneous monitoring with both plasma-emission and film-thickness systems indicated that the correlation between the commencement of etching and the plasma-emission response was good. These results assisted in identifying the variability in etch commencement as being associated with condensation induced on the chamber walls during sample loading.

5 Conclusions

Despite its inherent simplicity, chromatic monitoring enables changes in spectral signatures to be rapidly identified over a wide wavelength range. To allow flexibility, the monitoring systems are usually coupled to the chamber via a quartz viewport; fibre feedthroughs can be used if no viewport is available.

The chromatic systems can comfortably discriminate wavelength changes as low as 0.01 nm [5]. In terms of measured parameters, the plasma monitor can discriminate changes of 0.5% in the gas composition, 2 mT in

pressure and 1 W of power. The resolution of the thin-film monitor is currently limited more by the calibration procedures than by the resolving power of the optics. Worst-case film thickness estimates of ± 2 nm have been achieved, with estimates of ± 0.5 nm possible over most of the thickness range.

There are two further important implications which ensue from such chromaticity monitoring.

(*a*) Two-dimensional monitoring of plasma and film thickness is easily accommodated through the use of an array of tristimulus photodetectors, such as a CCD array. Such an array consists of 768 × 512 pixels, providing a spatial resolution of approximately 20 μm. Fig. 6*a* shows an example of the results of such two-dimensional monitoring of plasma emission chromaticity, which enables the uniformity of the plasma conditions (important for a uniform etch) to be checked.

(*b*) Chromatic monitoring forms a convenient and natural part of an intelligent knowledge-based system (IKBS) because of its ability to compress experimental information without sacrificing discrimination. The output from such systems may be used to define volumes in multidimensional space, within which plasma processing systems need to operate to ensure an optimum yield of processed material. As an example of this capability, we present results in three-dimensional space which define the chromaticity surface as a function of plasma composition and radiofrequency power sustaining the plasma (Fig. 6*b*).

An IKBS based upon such chromatic inputs has already been assembled [12]. This system compares the chromatic inputs with a chromatic model yielding optimal yield. Deviations between the model and the monitored inputs results in the IKBS issuing adjustment instructions about the process variables to bring the process back on target. Experience with this system to date indicates its performance to be extremely reliable.

6 References

1 DESHMUKH, V.G.I., and COX, T.I.: 'Physical characterisation of dry etching plasmas', *Plasma Phys. Cont. Fusion*, 1988, **30**, pp. 21–33

2 THOMAS, D.J., SOUTHWORTH, P., FLOWERS, M.C., and GREEF, R.: 'An investigation of the roughening of Si(100) surfaces in Cl_2/CCl_4 in reactive ion etching plasmas by in-situ ellipsometry and quadrupole mass spectrometry: the role of CCl_4', *J. Vac. Sci. Technol. B*, 1990, **8**, (3), pp. 516–522

3 COX, T.I., DESHMUKH, V.G.I., HOPE, D.A.O., HYDES, A.J., BRAITHWAITE, N.StJ., and BENJAMIN, N.M.P.: 'The use of Langmuir probes and optical emission spectroscopy to measure electron energy distribution functions in RF generated argon plasmas', *J. Phys. D: Appl. Phys.*, 1987, **20**, pp. 820–831

4 JONES, G.R., and RUSSELL, P.C.: 'Chromatic modulation based metrology', *Pure Appl. Optics*, 1993, **2**, pp. 87–110

5 BEAVAN, C.M.: 'Colour measurement in optical metrology' (PhD Thesis, Liverpool University, 1989)

6 ROSSOTTI, H.: 'Colour' (Princeton University Press, New Jersey, 1983)

7 KERSHAW, D.: 'Chromatic signal processing for optical metrology' (PhD Thesis, Liverpool University, 1991)

8 MORSE, K.: 'Multi-wavelength analysis of plasma processes' (PhD Thesis, University of Liverpool, 1991)

9 JONES, G.R., KWAN, S., BEAVAN, C., HENDERSON, P., and LEWIS, E.: 'Optical fibre based sensing using chromatic modulation', *Optics Laser Tech.*, 1987, **19**, (6), pp. 297–303

10 KWAN, S., BEAVAN, C.M., and JONES, G.R.: 'Displacement measurement using a focusing chromatic modulator', *Meas. Sci. Tech.*, 1990, **1**, pp. 207–215

11 JENKINS, F.A., and WHITE, H.E.: 'Fundamentals of optics' 4th edn (McGraw Hill, Kogakusha, 1976)

12 SMITH, R.V.: 'An interactive IKBS for plasma processing' (MSc Thesis, University of Liverpool, 1993)

Meas. Sci. Technol. **5** (1994) 639–647. Printed in the UK

Chromatic interferometry for an intelligent plasma processing system

G R Jones, P Russell and I Khandaker

Department of Electrical Engineering and Electronics, The University of Liverpool, Liverpool L69 3BX, UK

Received 2 November 1993, in final form 4 February 1994, accepted for publication 11 February 1994

Abstract. A thin film measuring system for the online monitoring of semiconductor films during processing with a radio frequency plasma is described. The method is based upon the use of chromatic processing of polychromatic interference signals produced by the thin semiconductor film when illuminated with white light. A description is given of the interpretation of the polychromatic signals produced by interference effects and some typical experimental results are presented to illustrate the capabilities of the technique. The approach utilizes cost effective instrumentation with acceptable time response for real time process control via optical fibre transmission. It is currently being incorporated as part of an intelligent knowledge based system for such process control.

1. Introduction

A hierarchial approach to the monitoring of electrical plasma systems used for the processing of semiconductor materials is showing promise for improving sample yield. Two components of this system which are essential to close the monitoring loop rely upon remotely addressing the plasma emission and the material film being processed by optical methods.

With regard to the optical monitoring, the requirement is not so much for measuring fundamental plasma and substrate properties, but rather for identifying unsatisfactory operating conditions followed by an indication of their cause so that appropriate control action can be rapidly implemented. An implication of such requirements is that economic optical information acquisition and instrument commonality and flexibility are paramount in order to preserve acceptable online control response and to ensure industrial compatibility.

An optical technique which meets these requirements relies upon the chromatic monitoring of spectral signatures (Jones and Russell 1993). The basis of the approach involves identifying a spectral signature by using a number N photodetectors, each having a different wavelength responsivity, for locating the spectral signature in an (N-1) dimensional chromatic space. Spectral signature variations are then identifiable as changes in the (N-1) coordinates of the signature in chromatic space and the nature of these changes may be correlated with different causes.

The approach has been used to track changes in both the plasma and substrate conditions and has been successfully incorporated as part of an intelligent knowledge based system for controlling processing plasma. Figure 1 indicates the monitoring requirements of a typical plasma processing system. Conventional control systems maintain the pressure, flow rate of reactive gases and radio frequency (RF) power at pre-set levels. Optical measurement of the plasma emissions can be performed through a side mounted view port and observation of the material film through a viewport in the top electrode. This paper is restricted to the description of the chromatic technique as applied to monitoring the substrate thickness via white light interferometry.

2. Theory

2.1. Optical interference in the wavelength domain

The *in situ* measurement of thin films within a processing plasma is conventionally performed using ellipsometric (see e.g. Hazebroek and Visser 1983) or laser interferometric (Yu *et al* 1992) techniques. These monochromatic techniques give good resolution but interpretation of the results can be difficult, requiring intensive computing power. In this work an alternative solution is described based on white light interferometry. A theoretical description of white light interference in thin films has been given by Musilova and Ohlidal (1990). Here we adapt the theoretical approach for incorporation into a chromaticity analysis.

For a single layer film of a non-absorbing medium, as shown in figure 2(*a*), the amplitude of the reflected light is given by (see e.g. Heavens (1965))

$$R=\frac{r_1+r_2e^{-2i\delta}}{1+r_1r_2e^{-2i\delta}} \quad (1)$$

where r_1 and r_2 are the Fresnel reflection coefficients at the first and second interface respectively and δ is the

0957-0233/94/060639+09 $19.50 © 1994 IOP Publishing Ltd

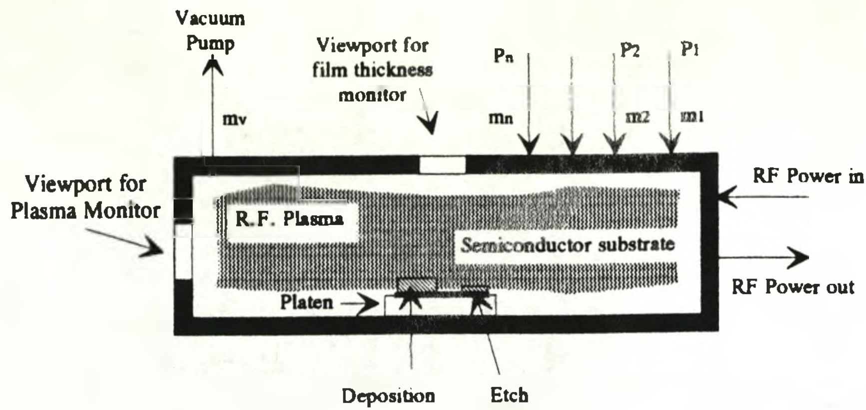

Figure 1. Schematic diagram of the monitoring requirements for a plasma processing system. P_1 to P_n represent the partial pressure of the reactive gases, m_1 to m_n are the measured flow rates. m_v represents the measured chamber pressure.

phase difference introduced to the light traversing the film, which is given by

$$\delta = \frac{2\pi}{\lambda\gamma} n_1 d \cos\phi \tag{2}$$

n_1 is the refractive index of the film, d is the thickness of the film, ϕ is the angle of refraction, and λ is the wavelength of the incident light.

In cases where these reflection coefficients are small compared with unity this equation reduces to

$$R = r_1 + r_2 e^{-2i\delta}. \tag{3}$$

Assuming that the path difference nd is less than the coherence length of the light, the intensity P of the reflected light from such a system is approximately that produced by the interference of two light beams of intensity P_1 and P_2.

$$P = P_1 + P_2 + 2\sqrt{(P_1 P_2)} \cos 2\delta \tag{4}$$

where $P_1 = r_1^2$ and $P_2 = r_2^2$.

The values of the Fresnel reflection coefficients, and hence the intensity of the reflected beams, depend on the polarization of the incident light and on the angle of incidence. At normal incidence polarization has no effect on the reflection coefficients which are given by

$$r_1 = \frac{n_0 - n_1}{n_0 + n_1} \qquad r_2 = \frac{n_1 - n_2}{n_1 + n_2} \tag{5}$$

where n_0 and n_1 are the refractive indices either side of the first interface and n_1, n_2 are the refractive indices either side of the second interface. The reflected intensities, for incident light of unit intensity, are given by r_1^2 and r_2^2. The results presented here are for a system using unpolarized light at normal incidence. The system has, however, also been used successfully with higher angles of incidence.

A graphical representation of equation (4) shows the well known periodic variation of intensity which constitutes the formation of interference fringes (curve λ_1 figure 2(*b*)). The depth of modulation depends of course on the relative intensities of the two beams P_1, P_2.

Equation (4) applies to the interference of light reflected from the front and back of a thin film (figure 2(*a*)) provided the optical path length nd is less than the coherence length of the optical source and with polarization and multiple reflection effects neglected. Furthermore, according to equation (4), the periodicity of the fringes with respect to optical path length increases with the optical wavelength λ so that the graphical representation of the interference at progressively longer wavelengths (λ_2, λ_3) appears as shown in figure 2(*b*) (curves λ_2, λ_3). The implication of this representation is that there is a phase difference between fringes at different wavelengths. Consequently if a transformation is made to view the interference of polychromatic light at a series of discrete optical path lengths in the wavelength domain then the spectral signature variations (shown as shaded regions in figure 2(*c*)) are observed. The pattern corresponding to the spectral signature variations is composed of a series of variations with wavelength dependent periodicities.

2.2. Polychromatic interference in chromatic space

The spectral signatures of the form shown in figure 2(*c*) produced by polychromatic interference may be addressed via chromatic monitoring methods. The chromaticity of an electromagnetic field can in general be defined by (N-1) parameters of the form (Smith *et al* 1992)

$$x_\mu = \frac{\int P(\lambda) R_\mu(\lambda)\, d\lambda}{\sum_{\mu=1}^{N} \int P(\lambda) R_\mu(\lambda)\, d\lambda} \tag{6}$$

where $P(\lambda)$ = electromagnetic field power

$R_\mu(\lambda)$ = responsivity of the photodetector μ

$i_\mu = \int P(\lambda) R_\mu(\lambda) d\lambda$

= output signal from detector μ

$$\sum_{\mu=1}^{N} \int P(\lambda) R_\mu(\lambda) d\lambda \tag{7}$$

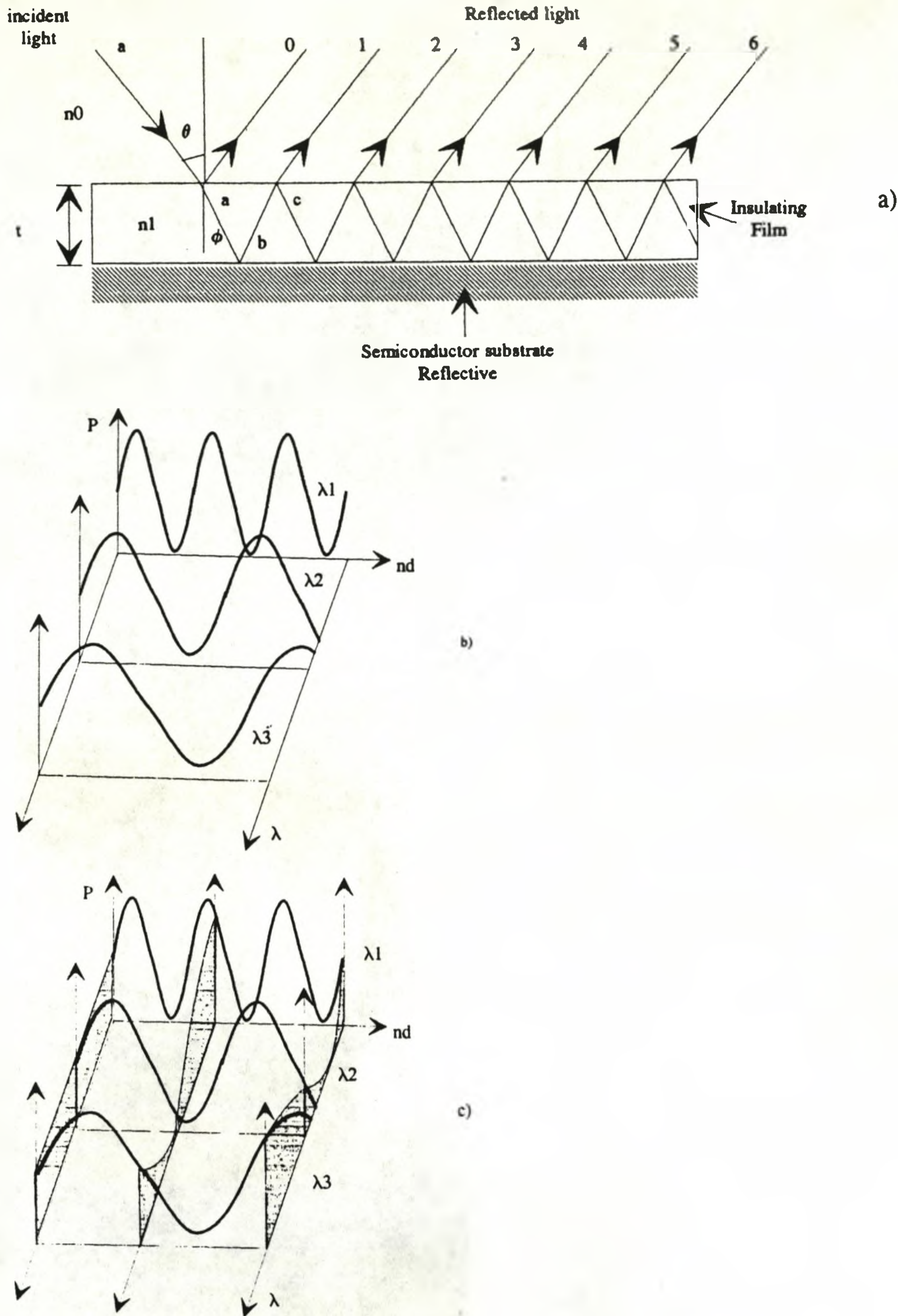

Figure 2. (*a*) Light incident on a thin film undergoes multiple reflections which produce interference effects. (*b*) Interference fringes at three wavelengths (λ_1, λ_2, λ_3) for increasing optical thickness of a thin film. (*c*) The interference of polychromatic light at a series of discrete optical path lengths.

= Intensity of the electromagnetic wave

As a consequence of equation (6)

$$\sum_{\mu=1}^{N} x_\mu = 1 \qquad 0 \leqslant x_\mu \leqslant 1 . \tag{8}$$

In practice, $N=3$ provides an optimum arrangement for most purposes whilst $N=2$ is a good compromise for many purposes.

In order to appreciate the implications of equation (6) we consider the case $N=3$. It follows from equation (8) that a two-dimensional chromaticity space is defined by x_1, x_2 (at any point in this chromaticity space the state of the third variable x_3 is totally defined by a

knowledge of the values of x_1, x_2 according to equation (8)). If, for example, three detector responsivities of the form shown in figure 3(*a*) are used then the resulting operating chromatic boundary within this two-dimensional space appears as shown in figure 3(*b*). Purely monochromatic signals lie along the curved boundary of figure 3(*b*) (so that this boundary provides a wavelength scale) whilst departures from monochromaticity are registered by increasing displacements from the boundary towards the centre of the enclosed space.

The implication is that a spectral signature may be quantified in terms of two coordinates x_1, x_2 so that changes in spectral signatures may be traced as a locus in the chromaticity space. The nature of the change may then be defined in terms of the considerations given above.

The spectral signature variations produced by polychromatic interference (figure 2(*c*)) may be incorporated into the chromatic description by substituting for $P(\lambda)$ in equation (6) by P given by equation (4). Thus the chromatic variations produced by changes in optical path length (nd) may then be determined from the resulting relationship by numerical computation to yield for $N=3$ values of x_1, x_2 as a function of optical path length. A typical example of the results of such a calculation is shown in figure 4. These results assume that the refractive index is independent of wavelength, a valid assumption for the materials used in this work.

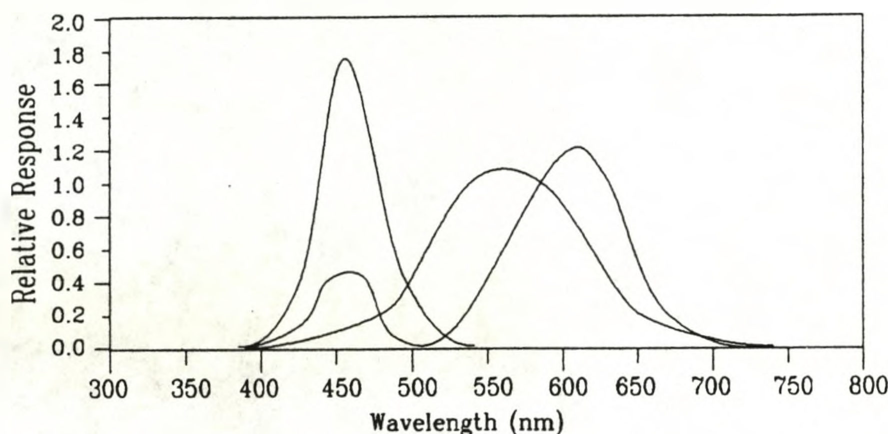

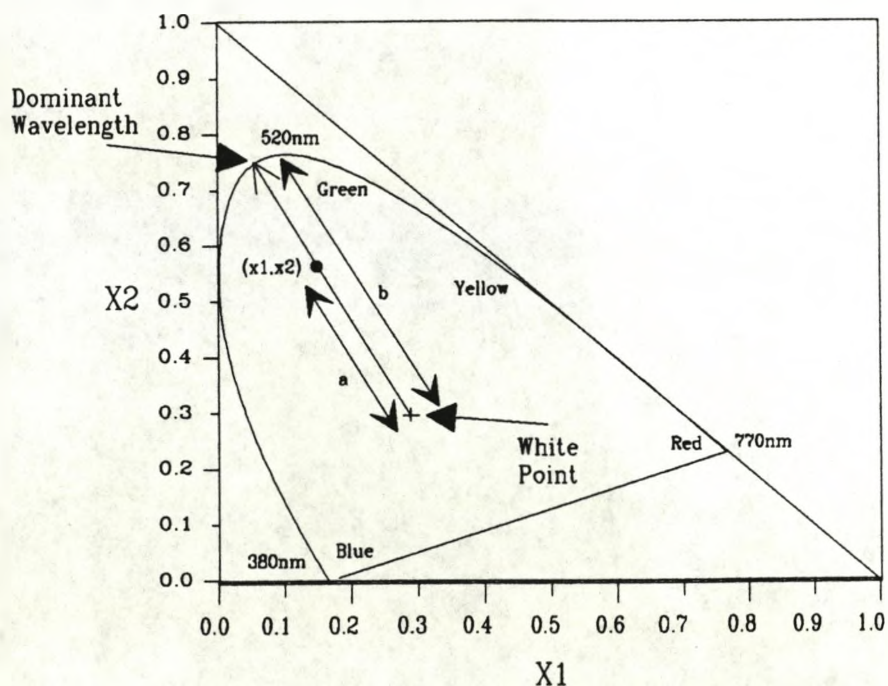

Figure 3. The three detector responses shown in (*a*) produce the chromaticity diagram shown in (*b*). Using these detectors, white light has coordinates (0.3,0.3) as indicated in (*b*). A coloured source may have coordinates (x_1, x_2). The dominant wavelength of this source is shown in (*b*). The saturation of the source is calculated from the ratio of the lengths *a*/*b*.

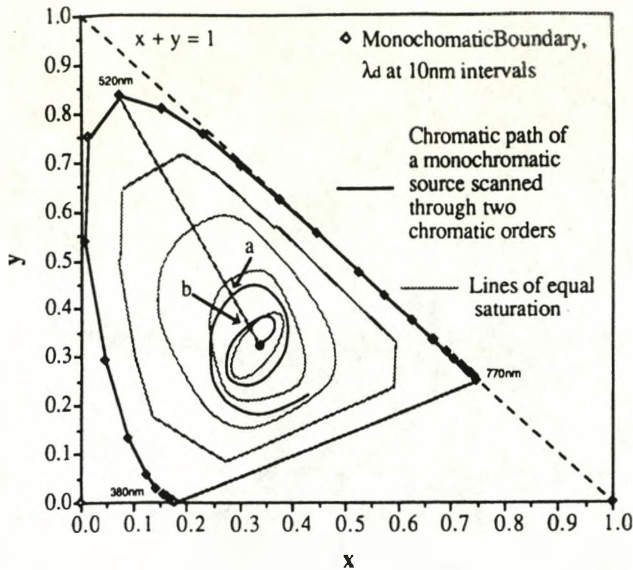

Figure 4. The helical locus represents the interference colours seen in thin films.

Such calculations reflect the periodicity of the spectral signature changes as a helical locus in chromatic space with the interference fringe order given by the extremities of the loops of the helix.

If the responsivities of the photodetectors ($R_\mu(\lambda)$) are made to coincide with those of the human eye, the helical locus of figure 4 represents the well known interference colours seen in thin films (Lipson and Lipson 1991). However the broader implications of full chromatic monitoring are that the chromatic range and resolution may be optimized for particular applications by choosing an appropriate combination of detector responsivities (see e.g. Jones and Russell 1993). Furthermore, if additional weighting factors are introduced via electronic signal processing the chromaticity coordinates may be written as (Jones (1991)).

$$x_1 = \frac{A[ai_1 - (i_1 + i_2 + i_3)]}{(i_1 + i_2 + i_3)} \tag{9}$$

$$x_2 = \frac{B[bi_2 - (i_1 + i_2 + i_3)]}{(i_1 + i_2 + i_3)} \tag{10}$$

where i_μ is defined by equations (4) and (7) and A, B, a, b are weighting factors which may be controlled either in software or hardware (amplifier gains). The implication of such a procedure is that the chromatic area addressed and the sensitivity to specified spectral signature changes may be controlled on line if required.

3. Experiments

3.1. Experimental apparatus

A schematic of the experimental system developed for the chromatic monitoring of plasma processed thin films is shown in figure 5. The polychromatic source used to produce the addressing light was a tungsten halogen

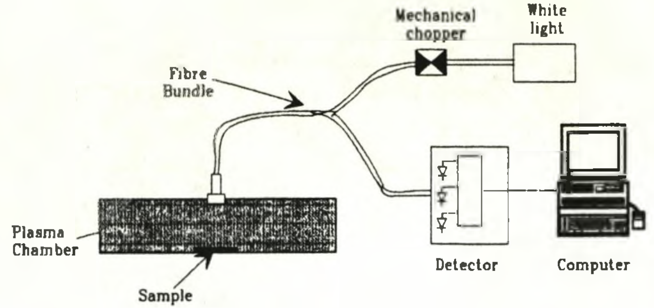

Figure 5. The experimental system used for monitoring film thickness online.

source incorporated in a Lucas Control Systems Products power unit and stabilized to drifts of no more than 0.1 nm in its spectral output. Light from this source was delivered to the plasma chamber via optical fibres and the signal reflected from the film being processed was also received via similar fibres. By suitable optical focusing the light from the fibres could be collimated, allowing the film to be addressed remotely over a distance of about 10 cm. In this manner invasion of the RF plasma volume and possible effects upon the processing could be avoided.

The interference signal produced by the thin film was detected by three photodiodes—a sharp PD150 (containing two detectors) and a Hamamatsu G1961 (figure 6). In order to eliminate the effect of the background optical emission of the RF plasma the polychromatic source was repetitively chopped with a rotating slot shutter in conjunction with a lock-in amplifier incorporated in the detection system.

3.2. Experimental procedures

The chromatic system was tested with a RF plasma processing system operating at 13.56 MHz and a power

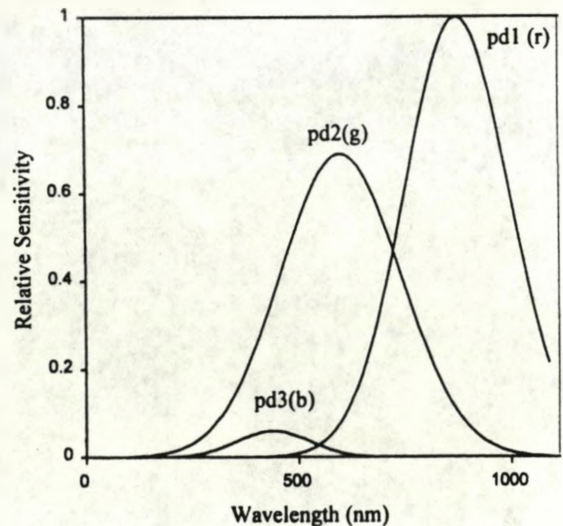

Figure 6. The response characteristics of the detectors used in the thin film monitor.

of 60 W. The process used in these tests was the etching of a SiN_3 film on a Si or GaAs substrate using reactant gases of CF_4 and 0_2 diluted with N_2. The flows and pressures of these gases were set using MKS Brooks 5850 flow controllers and vacuum general capacitance monometers.

Because of the complexity and uncertainties in attempting to derive film thickness theoretically from the equations given in section 2, a calibration procedure was preferred. This involved preparing a series of thin films of different thicknesses and constant refractive index. Thickness was measured with a standard polarimetric technique and the chromaticity of the reflected light from each sample was measured with the experimental system described in section 3.1 above.

The results of these calibration measurements are given in figure 7 in terms of the variation of $P_1/(P_1+P_2+P_3)=x$ and $P_2/(P_1+P_2+P_3))=y$ as a function of the physical thickness of the film. The phase difference between these two curves enables the ambiguity produced by their periodicity to be removed in principle. In practice, two methods of interpreting these nonlinear curves have been used—look-up tables and artificial neural networks. A look-up table, consisting of three columns (x, y and thickness), can be set up directly from the calibration graph. The thickness of a sample can be found by determining the nearest chromaticity coordinate x, y to that measured.

Artificial neural networks are now being used extensively for interpreting complex data (e.g. Zurada 1992), the most widely used configuration being the multilayer perceptron, trained using back propagation. In this work we have used a perceptron with one hidden layer to map the measured chromaticity onto thickness. The network was trained using the calibration curves of figure 7 and was then used to provide thickness values in real time. .

Online testing of the chromatic system was undertaken by etching a 260 nm thick SiN_3 film and measuring the output of each of the three photodiodes continuously as a function of time. The chromaticity was calculated from these values as described in section 2 and the chromaticites translated into thicknesses using the calibration curve of figure 7.

3.3. Experimental results

The output of each of the three photodetectors during an etching process is shown as a function of time in figure 8(*a*). Each output is cyclical in nature, consistent with equation (1) (although because of the finite optical bandwidth of each detector the signals are not purely monochromatic). The number of fringes decreases from three for the short wavelength detector to 1.25 for the long wavelength detector (of figure 2(*a*)). The results cover a time period during which a SiN_3 film of thickness 260 nm was totally removed from the substrate so that the final signal recorded is that for zero film thickness ($d=0$).

When presented in chromaticity space these results appear as the convolution shown on figure 8(*b*) with time increasing as indicated by the arrow. This gives approximately a 1.75 cycle variation for this particular film thickness etch with a crossover point about half a cycle after etch commencement. The maximum x and y excursions are 0.35–0.54 and 0.38–0.458 respectively with a resolution of 0.005.

Using the calibration curve of figure 7 the results of figure 8(*b*) may be transformed, using one of the techniques described earlier, into a film thickness: time

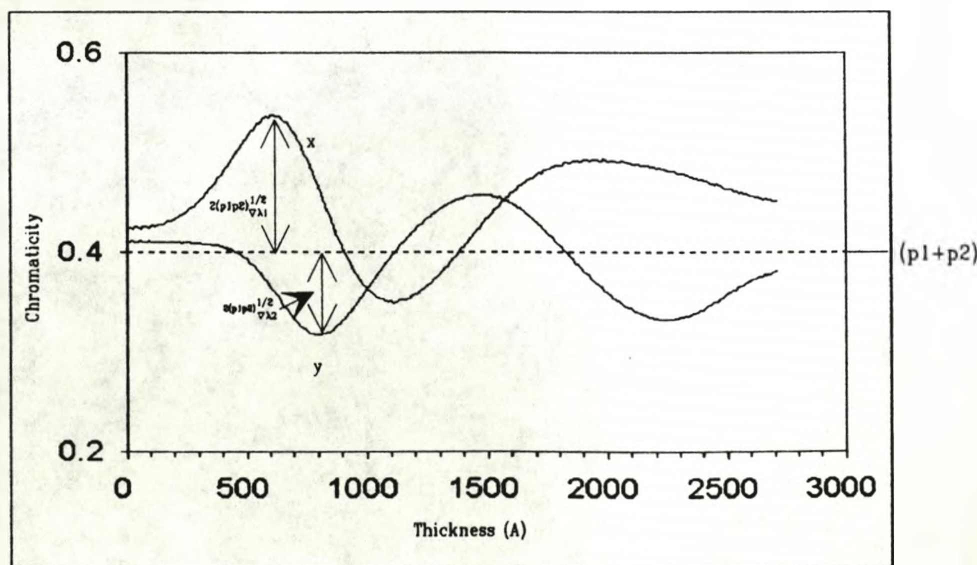

Figure 7. The calibration curve used to convert chromaticity into thickness. Traces $x=P_1/P_1+P_2+P_3)$ and $y=P_2/(P_1+P_2+P_3)$ are the chromaticity coordinates. P_1, P_2 and P_3 are the intensity of reflected light measured by the three detectors.

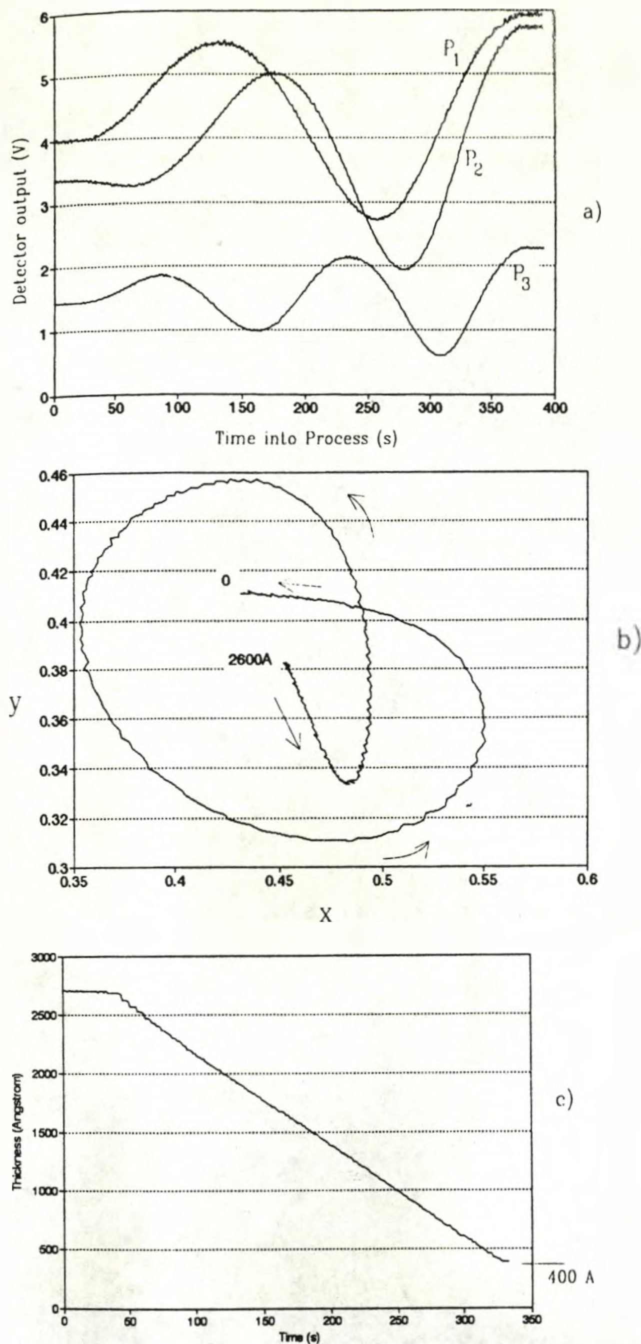

Figure 8. (*a*) The output of the three detectors (P_1, P_2 and P_3) in the film monitor during an etching process. A 260 nm thick film of SiN_3 was totally removed. (*b*) The variation in chromaticity of a film observed during an etching run. Again the SiN_3 film was completely removed. The arrows represent increasing time. (*c*) The output of the thickness calibration routine for an etching run. In this run the etch was deliberately stopped before the film was completely removed, leaving a 40 nm thick film.

characteristic as shown on figure 8(*c*). This indicates a fairly linear variation of film thickness with time corresponding to an etch rate of about 0.7 nm s^{-1}. The estimated resolution is 2 nm, being governed predominantly by the accuracy of the calibration curves of figure 7.

The crossover points in the chromaticity graph, figure 8(*b*), can prove problematic for both the look-up table and neural network. Two methods were used to remove the uncertainty at these crossover points; the gradient of the chromaticity curves at each point and the overall intensity of the reflected light were taken into account. Taking account of both of these effects allowed unambiguous values of optical thickness to be obtained over the entire etching operation.

4. Discussion

4.1. Physical interpretation

According to equation (4) the monochromatic intensity should vary periodically with film thickness with a period of $\lambda/2$ and an amplitude $2(P_1P_2)^{1/2}$ superimposed upon a mean level of (P_1+P_2). The implication of equation (4) is that the amplitude of the fringe intensity variations should be independent of film thickness whereas the experimental results for the short, medium and long wavelengths all show the amplitude decreasing as the film thickness increases. In order to explain this deviation the experimental results of figure 8(*a*) have been analysed to determine the precise nature of path length dependent amplitude decrease which are as shown in figure 9.

The decremental decrease in amplitude every period was measured for both positive and negative half cycles. The level $2(P_1P_2)^{1/2}$ at zero interference level ($d=0$) was taken as a reference so that the decremental decreases for the positive amplitudes were unambiguously determined relative to this reference (see figure 9). It was then assumed that the decremental decrease of the first negative amplitude would be approximately half of that of the first positive amplitude. This enables a reference level for the negative going half cycles to be established. Additional positive and negative amplitudes at intermediate half periods were established to assist curve fitting by reflecting the negative half cycle decrements on the positive excursions and vice versa as shown in figure 9. Since figure 8(*c*) establishes that the etch rate is constant throughout the process duration, the time increments in figure 9 are therefore proportional to film thickness, consistent with each half cycle peak being equally spaced in time and representing a half wavelength ($\lambda_0/2$) change (λ_0 in this case is a weighted wavelength representing the optical bandwidth across the detector responsivity range). As a result the amplitude envelopes for the short, medium and long wavelength cases could be established as shown in figure 9. Approximate extrapolations were made in each case to find the point of intersection of the positive and negative going envelopes. This enabled the zero level for the oscillatory optical signals to be approximately established. A cross check on the validity of this procedure is provided by comparing the amplitudes of the positive and negative reference levels with respect to this zero level. These values for the short, medium and long wavelength results were (+2.3), (−2.3); (+6.7), (−6.3);

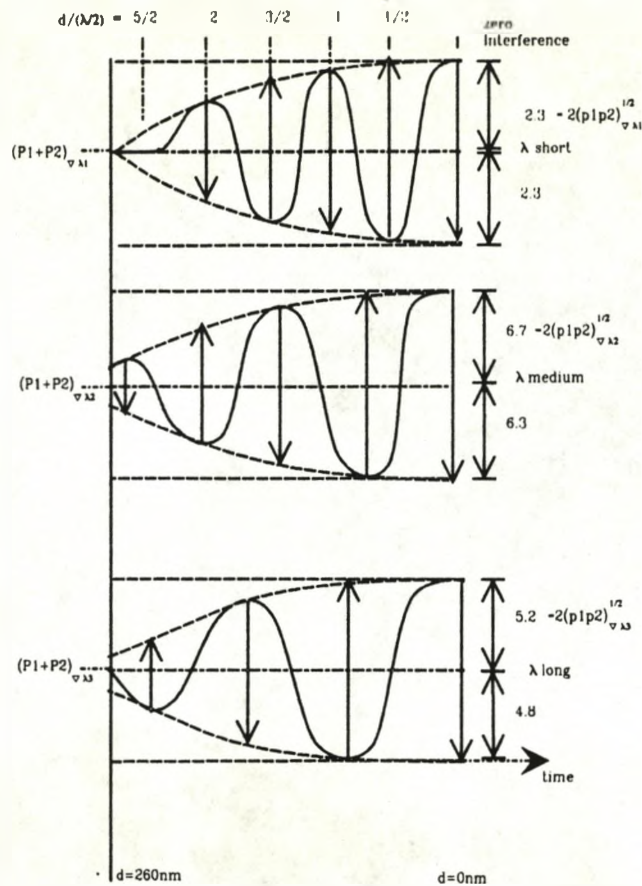

Figure 9. As the thickness of the film increases the amplitude of the detector outputs are observed to decrease. The envelope of the detector outputs can be extrapolated to indicate the maximum measurable thickness.

(+5.2), (−4.8) respectively so confirming the validity of the approach.

Two possible reasons for the amplitude decrease may be postulated as follows.

(a) A reduction in the intensity of the light penetrating the thin film (P_2) which increases with penetration depth d according to $e^{-\alpha d}$ (α is the attenuation coefficient) so that the amplitude term $2(P_1P_2)^{1/2}$ (equation (1)) also decreases. This would also produce a decrease in the non-oscillatory term (P_1+P_2) (equation (4)) implying that the zero level of the oscillatory component should increase as the film thickness tends to zero. The derived results shown in figure 9 along with the discussion above show no such substantial trend so implying that any attenuation in the thin film is negligibly small.

(b) The formation of interference fringes is only feasible for path length differences less than the coherence length of the light. The visibility of the fringes produced by the interference of two beams of non-monochromatic light (with a spectral half width Δ) is known to decrease with path difference in a similar manner to the envelopes shown in figure 9. The visibility of the fringes is reduced by a factor of two when the path difference $= 2\pi c/\Delta$ (Lipson & Lipson 1981). The coherence length is approximately determined by the optical bandwidth of the light detected which, because of the requirements of chromatic monitoring, is relatively wide for the present work and governed by the responsivity of each detector (figure 6). For instance, for the short wavelength detector the optical bandwidth $\Delta\lambda$ is approximately 200 nm and the mean wavelength λ_0 is about 450 nm. The coherence length $k=\lambda_0^2/\Delta\lambda$ (Halg 1991) is 1.01 μm. Inspection of the short wavelength results of figure 8 indicates that a maximum optical path difference of about $(5/2)\lambda_0$ existed between the front and back reflected signals. If λ_0 is assumed to be about 450 nm then the total optical path difference is 1.12 μm indicating that the signal decay observed experimentally is due to the limited coherence length of the optical signal detected by each detector.

The implication of the coherence length limit for the present application is that the maximum optical thickness which may be monitored by this short wavelength detector is about 500 nm which, for a film with refractive index of two, gives a maximum physical film thickness of 250 nm. Repeating this calculation for the long wavelength detector gives a maximum physical film thickness of 650 nm. From the aspect of monitoring the approach to complete etching, these maximum values are not a serious limitation.

For a film deposition (as opposed to etching) process it would also be of interest to check the quality of the film as reflected by its refractive index. In principle it should be possible to extract refractive index by a modification to the technique described.

The reflection coefficients for a light polarized parallel and perpendicular to the film surface are (e.g. Heavens 1965):

$$r_p=\frac{n_0\cos\phi_1-n_1\cos\phi_0}{n_0\cos\phi_1+n_1\cos\phi_0}$$

and

$$r_s=\frac{n_0\cos\phi_0-n_1\cos\phi_1}{n_0\cos\phi_0+n_1\cos\phi_1}$$

respectively (where ϕ_0 is the angle of incidence and ϕ_1 is the angle of refraction). For light incident at angles between 20° and 80° the values of r_p and r_s are not equal. Although complicated by reflection from the substrate, by using the chromatic system to measure the reflected signals for both polarization states it should be possible to extract both physical film thickness and refractive index.

4.2. Knowledge based monitoring and control

The chromatic technique for film thickness monitoring described above has been implemented in conjunction

with plasma emission monitoring also using a chromatic approach as part of a knowledge based system for plasma process control.

The first level of the hierarchial approach involves checking the chromatic signals from the processing plasma. The second level utilizes the above chromatic monitoring of film thickness. Utilized in this mode the signals from the three photodetectors are processed via either a look-up table or a neural network to yield a film thickness: time characteristic of the form shown in figure 8(*c*) which in turn gives a rapid online indication of etch progress.

The neural network is capable of overcoming the ambiguity of the crossover point in figure 8(*c*) by adequate training. Thus the second level in the hierarchial approach is to check for the anticipated maintenance of etch rate and to predict the imminence of complete etching to prevent substrate damage by overexposure to the RF plasma. The economic data utilization and processing offered by the chromatic approach allows this to be achieved sufficiently rapidly for on line control.

The third level in the hierarchial approach relates to the possibility of checking film quality from estimates to refractive index n_1 as described in section 4.1.

For the etch process described in this paper the first level of monitoring has been sufficient and the second level of film thickness monitoring has been used as a valuable cross check. The third level (film quality) is of less consequence for etching but is expected to be useful for processing involving deposition.

5. Conclusions

A system has been described which utilizes white light interferometry to measure the optical thickness of a thin film. The system is based on the technique of chromatic modulation and is capable of providing a rapid, online, indication of the optical thickness of a film in a processing plasma environment.

The output from this thin film monitor can be used, in conjunction with the output from a chromatic modulation based plasma emission monitor, to provide input to an intelligent system which can provide real time control of the plasma equipment.

The film measurement system could be modified to provide both physical film thickness and refractive index by measuring the components of the reflected signals polarized parallel and perpendicular to the film.

The generic nature of chromatic monitoring provides the opportunity for a cost effective, integrated sensing system for plasma system control.

Acknowledgments

We acknowledge the efforts of several colleagues who have contributed to the work described in this contribution. The financial support provided by the DTI and Chell Instruments is appreciated as is the interaction with GEC–Marconi and Lucas Engineering Systems.

References

Halg B 1991 A silicon pressure sensor with an interferometric optical readout *Transducers '91, Int. Conf. on Solid State Sensors and Actuators (San Francisco) 24–27 June 1991* 682–4

Hazebroek H F and Visser W M 1983 Automated laser interferometric ellipsometry and precision reflectometry *J. Phys. E: Sci. Instrum.* **16** 654–61

Heavens O S 1965 *Optical Properties of Thin Solid Films* (New York: Dover)

Jones R E 1991 *Private communication* Lucas Control System Products

Jones G R and Russell P C 1993 Chromatic modulation based metrology *Pure Appl. Opt.* **2** 87–110

Lipson S G and Lipson H 1981 *Optical Physics* 2nd edn (Cambridge: Cambridge University Press)

Mayer-Arendt J R 1984 *Introduction to Classical and Modern Optics* 2nd edn (Englewood Cliffs, NJ: Prentice Hall)

Musilova J and Ohlidal I 1990 Possibilities and limitations of the film thickness determination method based on white light interference *J. Phys. D: Appl. Phys.* **23** 1227–38

Smith R, Ahmed S, Vourdas A, Spencer J, Russell P C and Jones G R 1992 Chromatic modulation for optical fibre sensing electromagnetic and speckle noise analysis *J. Mod. Opt.* **39** (11) 2301–14

Yu F, Zhou Z H, Stout P and Rafael R 1992 *In-situ* monitoring of epitaxial film thickness by IEMI *IEEE Trans. Semicond. Manuf.* **5** (1) 34–40

Zurada J M 1992 *Introduction to Artificial Neural Systems* (St Paul: West Publishing)

Chell

PlasmaChrom

Process diagnostics and control

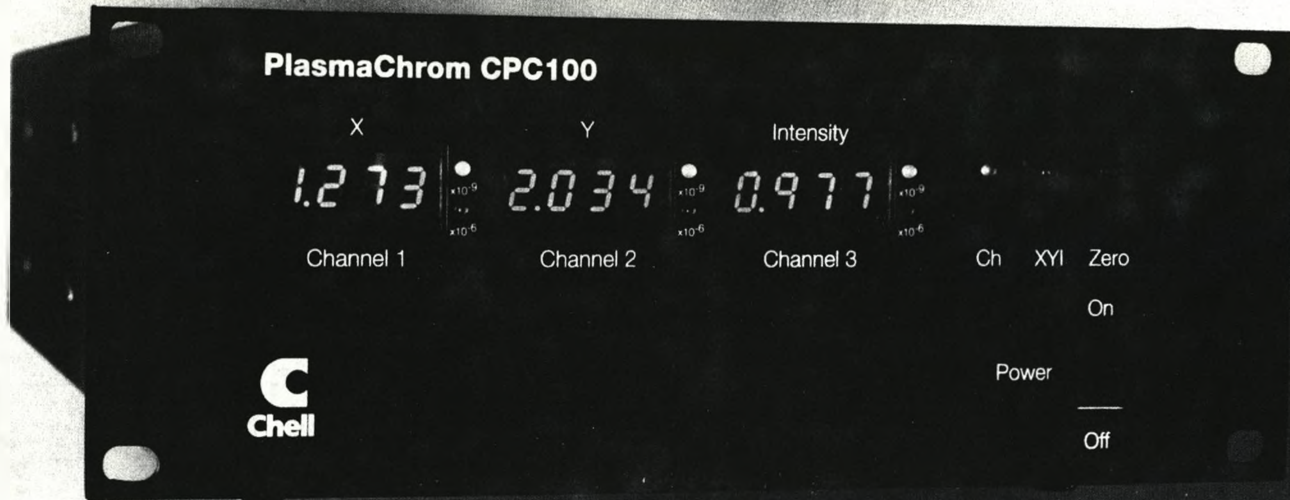

PlasmaChrom™ uses highly sensitive proprietary techniques to quantify colour and luminosity variations. These variations can then be used for diagnostics, decision making or closed loop control. Furthermore, because the technique is continuously sensitive throughout the spectrum, changes are detected which are beyond the sensitivity and speed of dispersive instruments such as grating monochromators.

As a diagnostic instrument

The CPC 100 is linked via a standard RS232 port to a PC where the data can be displayed, stored and manipulated using PlasmaWare™ proprietary software. This can be used for fault diagnosis, process transfer or process qualification in plasma etch and deposition.

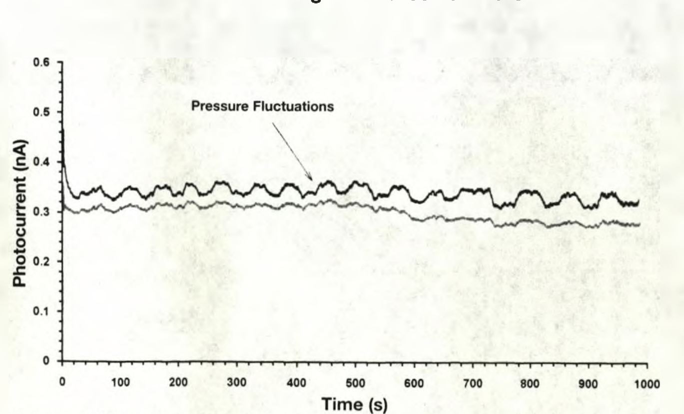

Figure 1: Raw optical data

Figure 1 shows that the optical data is sensitive to a 1 x 10^{-3} Torr pressure fluctuation with a possible end point indicated at 5-600sec.

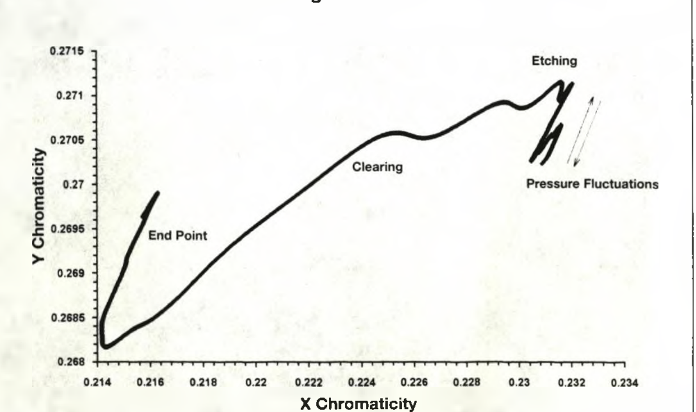

Figure 2: Chromatic representation showing end point

Figure 2 is a chromaticity plot of figure 1 and shows the pressure fluctuation, the process taking place and then a clear, unequivocal end point.

The chromatic technique is sensitive to gas flow changes below 0.1% FS and one user reports diagnosis of MFC overshoot.

PlasmaChrom™ - Specifications & Prices

CPC100 Chromatic sensing system for process condition monitoring - includes Plasmaware software package for analysis and display of data on user's P.C. £9,400.00

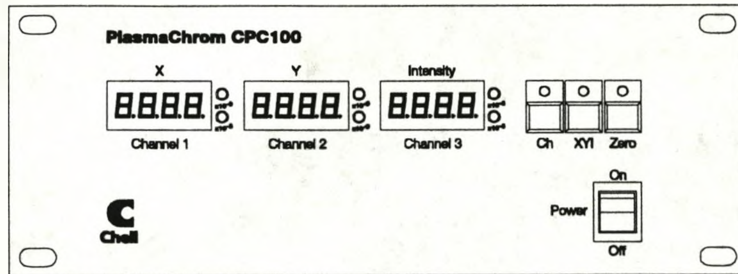

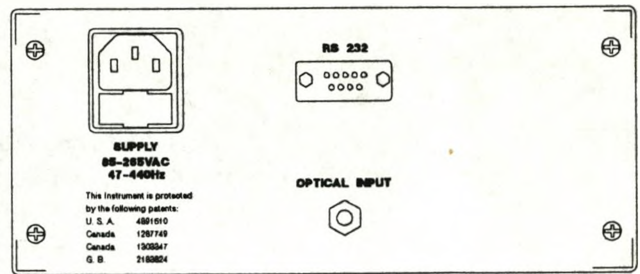

Front

Rear

CPC101 Phase sensitive detector, ac chromatic sensing system - for use in applications using differential measurements such as etch or deposition rate monitoring - includes PlasmaWare - also requires CPC201 for illumination. £11,500.00

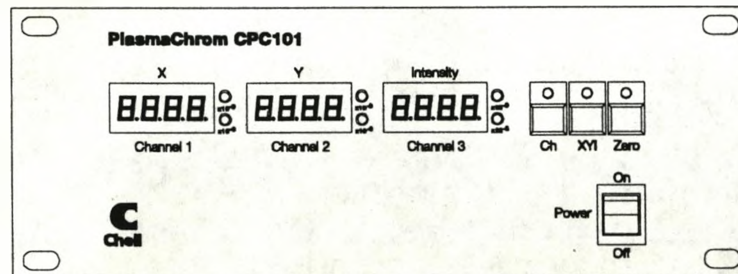

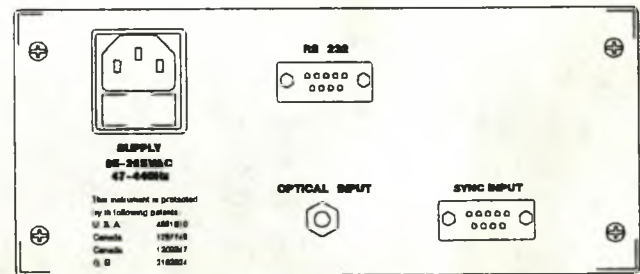

Front

Rear

CPC201 High stability fully compensated white light source and chopper for use with CPC101 and CPC301. £3,500.00

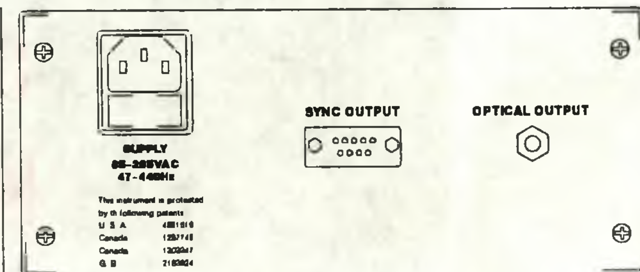

Front

Rear